COMPUTATION OF COMPLEX CEPSTRUM

by

Bir Bhanu

B.Sc. (Eng.), Banaras Hindu University, India
(1972)

M.E., Birla Institute of Technology and Science,
Pilani, India
(1974)

SUBMITTED IN PARTIAL FULFILLMENT OF THE REQUIREMENTS

FOR THE DEGREES OF

MASTER OF SCIENCE

AND

ELECTRICAL ENGINEER

at the

MASSACHUSETTS INSTITUTE OF TECHNOLOGY

September, 1977
(i.e. February, 1978)

Signature of Author _____
Department of Electrical Engineering
and Computer Science
September 23, 1977

Certified by _____
Thesis Supervisor

Accepted by _____
Chairman
Departmental Committee on Graduate Students

COMPUTATION OF COMPLEX CEPSTRUM

by

BIR BHANU

Submitted to the Department of Electrical Engineering and Computer Science on September 23, 1977 in partial fulfillment of the requirements for the Degrees of Master of Science and Electrical Engineer.

ABSTRACT

The principal computational step in using homomorphic signal processing is the computation of the complex cepstrum which requires phase unwrapping. A technique based on fitting the splines to the phase derivative curve is proposed and analyzed in one and two dimensions. It is shown that the use of splines leads to a very reliable phase unwrapping algorithm.

In one dimension an analysis is made, under the assumption that the zeroes of the finite length sequence are known, to relate the closeness of the zeroes to the required frequency sampling rate. The minimum FFT size and the thresholds of the phase unwrapping are analyzed as a function of the radii of the zeroes. These results are useful if we have some idea about the order of closeness of zeroes relative to the unit circle for the specific type signal under consideration.

An application of complex cepstrum in testing the stability of one and two dimensional recursive digital filters is considered. This method of checking the stability is compared with the existing methods on the basis of computational complexity, programming, and efficiency.

THESIS SUPERVISOR: James H. McClellan
TITLE: Assistant Professor of Electrical Engineering

ACKNOWLEDGEMENT

I wish to express my sincere gratitude to my advisor Professor J. H. McClellan for his guidance, suggestions and understanding throughout the course of this thesis.

Discussions with José Tribolet are appreciated and thanks are due him and Dave Harris for sharing with me their plotting routines.

I also wish to acknowledge the support from the Government of India in the form of a national scholarship.

Finally, I thank Sheila Parker for the excellent typing of the manuscript.

TABLE OF CONTENTS

LIST OF FIGURES

TABLES

CHAPTER I

INTRODUCTION

I.1 Introduction

Homomorphic signal processing, a class of nonlinear filtering techniques, based on linear filtering operations, has been applied to a variety of problems in image processing, speech analysis-synthesis, seismology, EEG data processing etc.

The main computational step in using this technique is the computation of complex cepstrum. For minimum or maximum phase sequences, there exist a set of recursive equations which can be used for its computation. However, the application of these recursive equations to a mixed phase sequence does not make any sense. Furthermore, the use of these equations is inefficient. So in general for a sequence of data, we need a direct method of computation.

The complex cepstrum is defined as the inverse z-transform of the complex logarithm of the z-transform of a signal. Since the complex logarithm is a multi-valued function, the condition of uniqueness and analyticity require that the phase function associated with the signal be defined so that it is continuous, odd and periodic. An inverse tangent routine will typically compute a phase value, called the principal value, between $-\pi$ and π. Thus the phase is obtained modulo 2π and must be "unwrapped" to satisfy the continuity

requirement. This process is known as phase unwrapping.

I.2 Previous Work

In the past phase unwrapping in one dimension has been done using the following three techniques:

(i) Processing of the principal value of the phase [1] (Schafer's Algorithm)

(ii) Numerical integration of phase derivative

(iii) Adaptive numerical integration scheme [2] (Tribolet's Algorithm).

In Schafer's algorithm it is essential to correctly identify the jumps of 2π for successful phase unwrapping and it has been shown that the principal value alone is not sufficient for successful phase unwrapping [2]. Numerical integration requires a perfect integration rule so that, while integrating the phase derivative, the truncation error will be small. The adaptive numerical integration scheme combines the first two approaches. It requires a considerable amount of computation time because of the step interval adaption, the global estimate of the linear phase and the simple trapezoidal rule for integration used.

The two-dimensional (2-D) cepstrum is a straightforward extension from the one-dimensional (1-D) definition. Dudgeon [3] has given the necessary and sufficient conditions (which are similar to the 1-D case) for its existence. There have been two attempts [4, 22] for the computation of the 2-D cep-

strum. Both are based on processing the principal value of the phase and therefore, they are not reliable for the same reasons as mentioned in the 1-D case. Moreover, until now no analysis has been made relating the frequency sampling rate to changes in the phase derivative curve or to the locations of zeroes of a finite length sequence relative to the unit circle.

I.3 Main Purpose

The main purpose of this dissertation is to make a comprehensive study of the complex cepstrum and its application for testing the stability of 1-D and 2-D recursive digital filters.

An investigation of piecewise interpolation methods for integration, viz., cubic spline, Bessel and Hermite interpolation has been carried out. It is shown that the use of splines leads to a very reliable phase unwrapping algorithm.

This approach to phase unwrapping has also been implemented in two dimensions, where a number of computational strategies have been considered. In one dimension an analysis is presented to relate the closeness of the zeroes of a finite length sequence and the frequency sampling rate in order to answer the question of what the minimum FFT size should be if the zeroes are very close to the unit circle. Other issues such as the need for double precision, efficient computation of DFT at a single frequency which is not on the DFT raster and a more

reasonable estimate for the linear phase component are considered.

Finally, the use of the complex cepstrum for checking the stability of 1-D and 2-D recursive digital filters is explored. In 1-D we make use of the fact that the number of zeroes outside the unit circle is equal to the slope of the linear phase. In 2-D this concept does not apply because there is no factorization theorem. But in 2-D we make use of the fact that if the system is stable, then the cepstrum is non-zero only where impulse response is non-zero. The comparison of this method with the existing methods is also considered.

In Chapter II we review the basic theory of one-dimensional homomorphic systems. In Chapter III we present the existing methods for phase unwrapping, introduce the use of piecewise polynomial interpolation and discuss in detail the computational problems encountered and their solutions for phase unwrapping in one dimension. Chapter IV presents an analysis of various theoretical and practical questions associated with phase unwrapping in one dimension. Chapter V discusses the properties and computation of the two-dimensional complex cepstrum. In Chapter VI we consider the use of the complex cepstrum for checking the stability of filters in one and two dimensions. Finally, Chapter VII gives a summary and suggestions for further work that can be carried out.

CHAPTER II

ONE DIMENSIONAL HOMOMORPHIC SYSTEMS

II.1 Introduction

Generally a linear filter is used when one is faced with the problem of separating two signals which have been added. The linear filters are easy to analyze and are convenient in filtering such signals. This is a consequence of the superposition property, according to which the behavior of a linear system L for the sum of signals $x_1[n]$ and $x_2[n]$ is the sum of responses $y_1[n]$ and $y_2[n]$, that is,

$$L(ax_1[n] + bx_2[n]) = aL(x_1[n] + bL(x_2[n]) = ay_1[n] + by_1[n] \tag{2.1}$$

for arbitrary constants a and b.

However, in many situations, we encounter signals which are combined by a rule other than addition, e.g., multiplication or convolution. In such cases linear systems may be quite ineffective in separating or independently modifying the component signals. However, it is desired to filter the signals through systems that are matched to such rules (multiplication, convolution etc.) in the same way that linear systems are matched to addition. This leads to the consideration of classes of nonlinear systems that obey a generalized principle of superposition. An approach to characterizing such

nonlinear systems based on linear algebra was originally proposed by Oppenheim [6]. In this approach signals are regarded as vectors in vector spaces. Since such systems are represented by algebraically linear transformations between input and output vector spaces, they have been called homomorphic systems. Two classes of homomorphic systems viz., multiplicative homomorphic system and homomorphic system for convolution have been used in a wide variety of applications [7].

In this chapter we review the basic theory of one-dimensional homomorphic systems. This will establish the necessary notations and background for the following chapters. Two dimensional counterpart is considered in Chapter V.

II.2 Generalized Principle of Superposition

Let M be a system transformation between signal vector spaces and let us denote by $\square$ and : the rules of vector addition and scalar multiplication in the input vector space for H. Similarly, $\oplus$ and $\boxdot$ correspond to vector addition and scalar multiplication in the output vector space for H. Then the system H is said to obey a generalized principle of superposition, if

$$H[(c:x_1[n])\square(d:x_2[n])] = [c\boxdot H(x_1[n])]\oplus[d\boxdot H(x_2[n])] \quad (2.2)$$

A homomorphic system which obeys eq. (2.2) can be represented as shown in Fig. 2.1.

Fig. 2.1 Representation of a Homomorphic System

II.3 Canonic Representation of Homomorphic System

It has been shown [6] that all homomorphic systems have a canonic representation as the cascade of a non-linear system followed by a linear system and then another non-linear system. Using the notations of earlier section, such a canonic representation is shown in fig. 2.2.

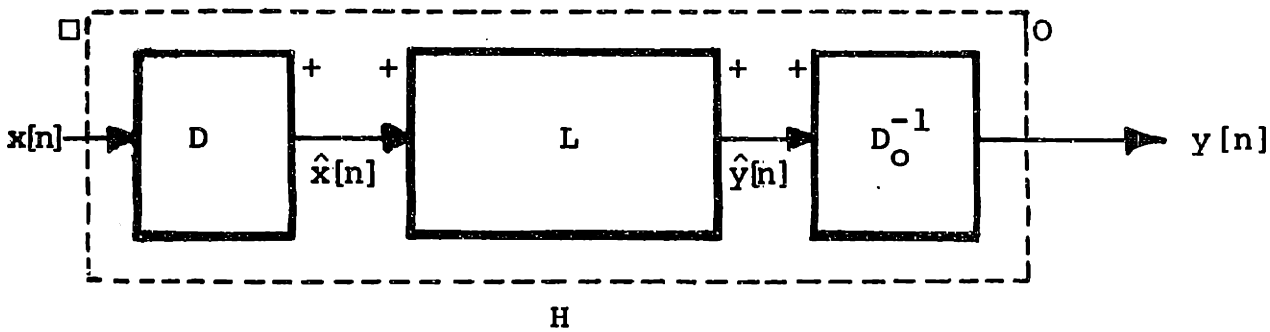

Fig. 2.2 Canonic Representation of Homomorphic Systems

The system $D_{\square}$ is a homomorphic transformation from □ to addition space so that $D_{\square}$ has the property

$$D_{\square}[(c:x_1[n])\square(d:x_2[n])] = cD_{\square}(x_1[n]) + dD_{\square}(x_2[n])$$

$$= c\hat{x}_1[n] + d\hat{x}_2[n] \qquad (2.3)$$

and thus obeys a generalized principle of superposition. System L is a linear system in the conventional sense of eq. (2.1). The homomorphic system D_o^{-1} serves to transform from addition to O, so

$$D_o^{-1}\left(c\hat{y}_1[n]+d\hat{y}_2[n]\right) = [c \,\tilde{\downarrow}\, D_o^{-1}(\hat{y}_1[n])] \,O\, [d \,\tilde{\downarrow}\, D_o^{-1}(\hat{y}_2[n])]$$

$$= (c \,\tilde{\downarrow}\, y_1[n]) \,O\, (d \,\tilde{\downarrow}\, y_2[n]) \qquad (2.4)$$

$$= y[n] \qquad (2.5)$$

The systems $D_\square$ and D_o depend entirely on the specific operation for combining signals and have been termed as characteristic systems for $\square$ and O respectively. It is to be noted that all the filtering ability of a homomorphic system specified in the canonic form lies in the choice of the linear system. The canonic homomorphic system may also be used in the synthesis of more general classes of homomorphic system when preceded by appropriate non-canonic normalization mappings [8].

II.4 Homomorphic Systems for Multiplication and Convolution

Multiplicative Homomorphic System -- In general a multiplicative homomorphic system in which the operations $\square$ and O are multiplication and the operations : and $\tilde{\downarrow}$ are exponentiation involves complex log and all the sequences $\hat{x}[n]$, $x[n]$, $\hat{y}[n]$ and $y[n]$ are complex. The formal representation of such a canonic

system for multiplication is shown in Fig. 2.3. It has been successfully used in image enhancement.

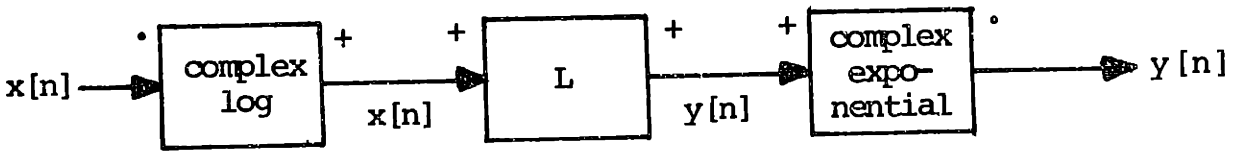

Fig. 2.3 Multiplicative Homomorphic System

Since the complex log is a multivalued function, the representation shown in Fig. 2.3 is not unique unless the ambiguity in the imaginary part of the complex log is resolved. These problems are thoroughly treated in the following discussion of homomorphic system for convolution.

Homomorphic Systems for Convolution -- The homomorphic system for convolution has been used in a wide variety of applications such as in image processing, speech analysis, echo removal and detection, speech vocoding, system identification, EEG analysis and seismic signal processing. The formal representation of the canonic system for convolution as the input and output operation is shown in Fig. 2.4,

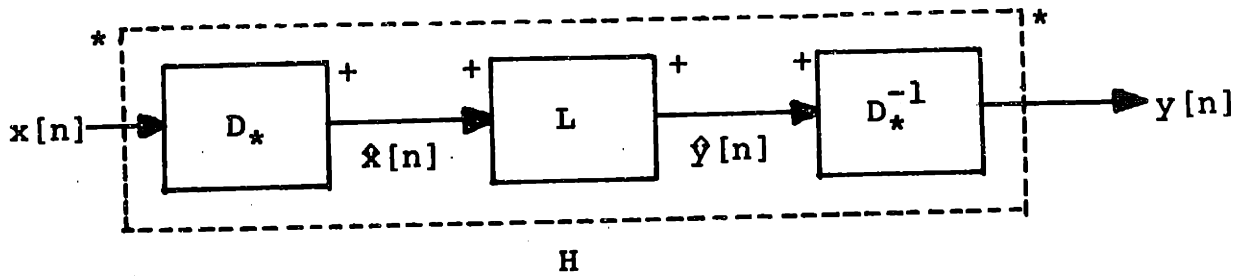

Fig. 2.4 Canonic Representation of Homomorphic System for Convolution

where the characteristic system D_* is such that the z-transform of its output is equal to the complex log of the z-transform of its input, i.e., if

$$\hat{x}[n] = D_*\Big[x[n]\Big] \tag{2.6a}$$

Then,

$$\hat{X}(z) = \text{Log } X(z) \tag{2.6b}$$

Recently [8] the representation of Fig. 2.4 has been called a full band homomorphic system to emphasize the fact that it is not appropriate for the processing of band-pass filtered signals. A new class of systems referred to as band-pass homomorphic systems was suggested which is suited to band pass signals. These systems are defined as the cascade of a band-pass mapping system with a full band homomorphic system followed by the inverse band-pass mapping system. The characteristic system of these band pass homomorphic systems is essentially a logarithmic mapping whose domain is restricted to encompass only the pass-band of the input. In this thesis we shall restrict our attention to the full band homomorphic system of Fig. 2.4.

II.5 The Characteristic System

The key to the mathematical representation of the characteristic system D_* shown in Fig. 2.5 (or equation (2.6)), is

that the z-transform of a convolution of two sequences is equal to the product of the z-transforms of each of the signal sequences, i.e.,

$$\text{If} \qquad x[n] = x_1[n] * x_2[n]$$

$$\text{then} \qquad X(z) = X_1(z) \cdot X_2(z) \tag{2.7}$$

Then, the z-transform operation can be viewed as a homomorphic transformation with convolution as the input operation and multiplication as the output operation. However, the z-transforms are also linear transformations in the conventional sense. Therefore, we may represent the characteristic system D_* in terms of a cascade of three homomorphic systems as shown in Fig. 2.5.

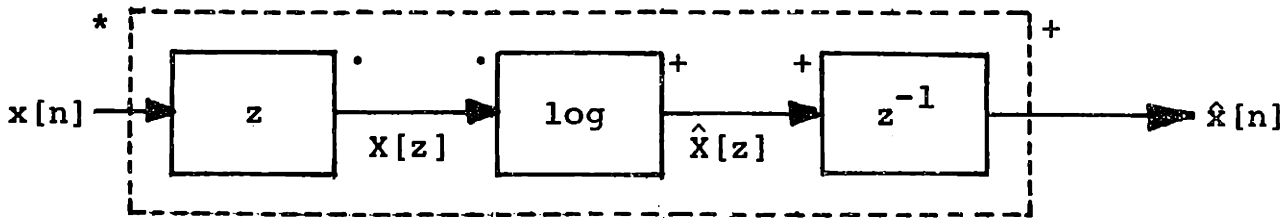

Fig. 2.5 Representation of Characteristic Systems D_*

It is noted that in this representation, it is not necessary to include the z^{-1} block since at its input signals are already additively combined, however, doing so has the advantage that the output of D_* is now a sequence.

Implicit in the representation of Fig. 2.5 is the assumption that both $X(z)$ and $\hat{X}(z)$ converge in some annular region in the z-plane. We require the region of convergence of $\hat{X}(z)$ to include the unit circle, thus restricting the sequences $\hat{x}[n]$ to be stable which is a very reasonable practical requirement. The most important implication of analyticity of $\hat{X}(z)$ on the unit circle is that $\hat{X}(e^{j\omega})$ must be a continuous function of ω.

If $x[n] \leftrightarrow X(e^{j\omega})$ and $\hat{x}[n] \leftrightarrow \hat{X}(e^{j\omega})$,

$$X(e^{j\omega}) = X_R(e^{j\omega}) + jX_I(e^{j\omega}) \tag{2.8a}$$

$$= |X(e^{j\omega})|\, e^{j \arg[X(e^{j\omega})]} \tag{2.8b}$$

and

$$\hat{X}(e^{j\omega}) = \hat{X}_R(e^{j\omega}) + j\hat{X}_I(e^{j\omega}) \tag{2.9a}$$

$$= \log |X(e^{j\omega})| + j \arg [X(e^{j\omega})] \tag{2.9b}$$

Then comparing eqs. (2.9), we get

$$\hat{X}_R(e^{j\omega}) = \log |X(e^{j\omega})| \tag{2.10a}$$

and

$$\hat{X}_I(e^{j\omega}) = \arg [X(e^{j\omega})] \tag{2.10b}$$

Therefore, $\log |X(e^{j\omega})|$ and $\arg [X(e^{j\omega})]$ must be continuous functions of ω.

Continuity of log $|X(e^{j\omega})|$ -- The log magnitude function is continuous on the unit circle if $X(z)$ and its inverse $X^{-1}(z)$ are both analytic on the unit circle. So we cannot take arbitrary signals as inputs to this homomorphic system. In particular, low-pass, high-pass and band-pass signals are not allowable. Thus the set of signals to which we are restricted is the class of stable sequences with stable inverses.

Continuity of arg $[X(e^{j\omega})]$ -- The continuity of arg $[X(e^{j\omega})]$ is the most stringent requirement which makes the efficient and reliable computation of complex cepstrum a challenging task. Since the complex logarithm is a multivalued function, the continuity of arg $[X(e^{j\omega})]$ depends not only on the specific properties of the signal $x[n]$ but also on the definition of complex logarithm. One approach to such a definition is to assume that the continuous complex logarithm is obtained by the integration of its derivative. Assuming a single-valued differentiable complex logarithm, we have

$$\frac{d}{dz}\hat{X}(z) = \frac{d}{dz}\log[X(z)] = \frac{1}{X(z)}\frac{d}{dz}X(z) \qquad (2.11)$$

Evaluating this logarithmic derivative on the unit circle, we get

$$\hat{X}'(e^{j\omega}) = \hat{X}'_R(e^{j\omega}) + j\hat{X}'_I(e^{j\omega}) = \frac{X'(e^{j\omega})}{X(e^{j\omega})} \qquad (2.12)$$

where the prime denotes differentiation with respect to ω. Equating imaginary parts on both sides in the above equation, we obtain the phase derivative as

$$\hat{X}_I'(e^{j\omega}) = \frac{d}{d\omega} \arg\ [X(e^{j\omega})]$$

$$= \frac{X_R(e^{j\omega})X_I'(e^{j\omega}) - X_I(e^{j\omega})X_R'(e^{j\omega})}{|X(e^{j\omega})|^2} \tag{2.13}$$

It can be shown easily that the phase derivative is bounded on the unit circle whenever the signal sequence x[n] and its inverse are stable. The phase derivative is an even function of ω, whenever x[n] is a real sequence. Furthermore, using the linearity of derivative operator, it can be shown that,

$$\frac{d}{d\omega} \arg\ [X_1(e^{j\omega})X_2(e^{j\omega})] = \frac{d}{d\omega} \arg\ [X_1(e^{j\omega})] + \frac{d}{d\omega} \arg\ [X_2(e^{j\omega})] \tag{2.14}$$

Definition of the phase function by the integration of its derivative (eq. 2.13) is unique to within an integration constant. This integration constant is determined according to the requirement that the logarithm be a homomorphic mapping between multiplication and addition, as represented in Fig. 2.5. Therefore, we require that

$$\arg\,[X_1(e^{j\omega})X_2(e^{j\omega})] = \arg\,[X_1(e^{j\omega})] + \arg\,[X_2(e^{j\omega})] \quad (2.15)$$

The above equation for real x[n] can only be satisfied if the integration constant is chosen such that:

$$\arg\,[X(e^{j\omega})]\Big|_{\omega=0} = 0 \quad (2.16)$$

Since
$$X(e^{j\omega})\Big|_{\omega=0} = \sum_{n=-\infty}^{\infty} x[n] \quad (2.17)$$

it follows that only signals with a positive DC component will satisfy this requirement. Finally, arg $[X(e^{j\omega})]$ must be, of course, periodic in ω with a period 2π. Being odd due to eq. (2.16) and continuous, the phase must satisfy:

$$\arg\,[X(e^{j\omega})]\Big|_{\omega=\pi} = 0 \quad (2.18)$$

Since
$$\arg\,[X(e^{j\omega})]\Big|_{\omega=\pi} = \int_0^{\pi} \frac{d}{d\omega} \arg\,[X(e^{j\omega})]\, d\omega \quad (2.19)$$

and since the phase derivative is an even function of ω, we conclude that only signals with zero mean phase derivative are compatible with the above requirement.

The inverse characteristic system, D_*^{-1}, is shown in fig. 2.6.

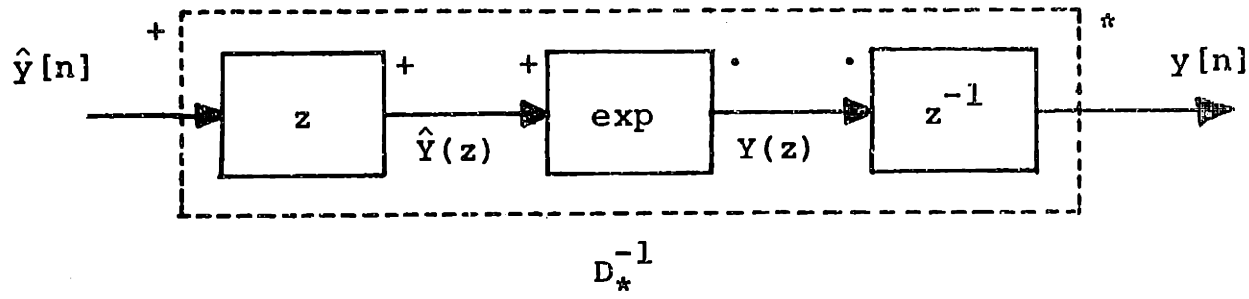

Fig. 2.6 Representation of Inverse Characteristic System D_*^{-1}

II.6 Input Normalization

We have seen that the input space to the characteristic system D_* is formed by all stable sequences with stable inverses having positive D.C. component and zero mean phase derivative. In general, however, we might be interested in analyzing sequences which do not satisfy these conditions. Let us look at how restrictive the above attributes are and then describe the modifications to be used in analyzing general sequences.

For a real sequence x[n], the most general rational z-transform can be written as,

$$X(z) = s_x A_x z^{r_x} \frac{\prod_{k=1}^{m_i} (1-a_k z^{-1}) \prod_{k=1}^{m_o} (1-b_k z)}{\prod_{k=1}^{p_i} (1-c_k z^{-1}) \prod_{k=1}^{p_o} (1-d_k z)} \qquad (2.20)$$

where s_x is equal to +1 or -1, A_x is a positive real value, r_x is an integer and $|a_k|$, $|b_k|$, $|c_k|$ and $|d_k|$ are less than unity.

It can be shown [7] that

$$s_x = \text{sgn} \left(\sum_{n=-\infty}^{\infty} x[n] \right) \tag{2.21}$$

where sgn denotes the signum function and that

$$r_x = \frac{1}{2\pi} \int_{-\pi}^{\pi} \frac{d}{d\omega} \left[\arg \left[X(e^{j\omega}) \right] \right] d\omega \tag{2.22}$$

s_x is known as the polarity of x[n] and r_x as the lag of x[n].

Thus in order to handle any stable signal with stable inverse having arbitrary polarity and lag, we need a transformation N, called the normalization transformation defined by

$$N(x[n]) = r_x \, x[n+r_x] \tag{2.23}$$

The normalization N corresponds to a sign reversal for sequences with negative polarity and to a time shift by an amount equal to the signal lag. N is well defined from a theoretical point of view, and in the z-transform domain it can be represented in a simple analytic form as,

$$X(z) \xrightarrow{N} s_x z^{-r_x} X(z) \tag{2.24}$$

N also satisfies the conditions required for it to be cascaded with a canonic homomorphic system for convolution, leading to the synthesis of a general homomorphic system for convolution [8]

From a practical point of view, and in the context of deconvolution by homomorphic signal processing, the normalization amounts to the normalization of the signal components. Thus their true polarities and lags cannot be determined by this technique. This is analogous in linear system theory to the situation in which two signals, each with nonzero DC label have been added. Using linear filtering on the sum of the signals, the true DC labels of the components can never be determined.

For most deconvolution problems, however, the loss of polarity and lag information does not represent a serious problem, since such information can often be measured by other means.

II.7 The Complex Cepstrum

Having discussed the characteristic system D_*, we concentrate on its output.

The output x[n] of the system D_* is referred to as the complex cepstrum of the signal x[n]. This terminology is motivated by the relationship between this transformation and the cepstrum as proposed by Bogert, Healy and Tukey [9] for the detection of echoes. Specifically, the real cepstrum c[n] of a signal x[n] was defined as the power spectrum of the logarithm of the power spectrum of x[n]. Since the cepstrum was directed toward echo detection rather than deconvolution, phas information was not important. Thus it does not utilize phase

information and involve the logarithm of real, positive values.

By contrast the output of the system D_* is referred to as the complex cepstrum to emphasize the fact that it requires the use of a complex logarithm. It is to be noted that the complex cepstrum of a real sequence is a real valued sequence.

Defining the even and odd components of the complex cepstrum $\hat{x}_e[n]$ and $\hat{x}_o[n]$, as,

$$\hat{x}[n] = \hat{x}_e[n] + \hat{x}_o[n] \tag{2.25a}$$

where
$$\hat{x}_e[n] = \frac{\hat{x}[n] + \hat{x}[-n]}{2} = \hat{x}_e[-n] \tag{2.25b}$$

and

$$\hat{x}_o[n] = \frac{\hat{x}[n] - \hat{x}[-n]}{2} = -\hat{x}_o[-n] \tag{2.25c}$$

it follows that:

$$\hat{x}_e[n] = \frac{1}{2} \text{ IFT } \{\log |X(e^{j\omega})|^2\} \tag{2.26a}$$

and

$$\hat{x}_o[n] = \text{IFT } \{\arg [X(e^{j\omega})]\} \tag{2.26b}$$

Thus, the cepstrum c[n] as defined by Bogert, Healy and Tukey is proportional to the even part of the complex cepstrum. The sequence $\hat{x}_e[n]$ is also referred to as the real cepstrum. The sequences $\hat{x}_e^2[n]$ and $\hat{x}_o^2[n]$ have been referred as the power and phase cepstrum, respectively.

II.8 Properties of Complex Cepstrum

In order to investigate the properties of the complex cepstrum, we consider the rational z-transform of a signal x[n] given by eq. (2.20) with m_i zeroes and p_i poles inside the unit circle and m_o zeroes and p_o poles outside it. The sequence x[n] is thus, in general, mixed phase.

We group all the poles and zeroes inside the unit circle in a single factor, defining a normalized minimum phase sequence $x_{min}[n]$, where z-transform is,

$$X_{min}(z) = \frac{\prod_{k=1}^{m_i} (1-a_k z^{-1})}{\prod_{k=1}^{p_i} (1-c_k z^{-1})} \tag{2.27}$$

Similarly, we define a normalized maximum-phase sequence $x_{max}[n]$, whose z-transform is,

$$X_{max}(z) = \frac{\prod_{k=1}^{m_o} (1-b_k z)}{\prod_{k=1}^{p_o} (1-d_k z)} \tag{2.28}$$

Thus the sequence x[n] satisfies

$$x[n+r_x] = s_x A_x \left(x_{min}[n] * x_{max}[n] \right) \tag{2.29}$$

where $x_{min}[n] = 0$, $n < 0$ and $x_{max}[n] = 0$, $n > 0$.

The normalized sequence N(x[n]) is then given by,

$$N(x[n]) = A_x\left(x_{min}[n] * x_{max}[n]\right) \tag{2.30}$$

and it follows that,

$$\hat{X}(z) = \log A_x + \log X_{min}(z) + \log X_{max}(z) \tag{2.31}$$

and consequently,

$$\hat{x}[n] = \log A_x \delta[n] + \hat{x}_{min}[n] + \hat{x}_{max}[n] \tag{2.32}$$

Now using the power series expansion for log it follows that

$$\log (1-az^{-1}) = - \sum_{n=1}^{\infty} \frac{a^n}{n} z^{-1} \qquad |z| > |a| \tag{2.33}$$

and

$$\log (1-az) = - \sum_{n=1}^{\infty} \frac{a^n}{n} z^{n} \qquad |z| < |a^{-1}| \tag{2.34}$$

It follows that

$$\hat{x}_{min}[n] = \left(- \sum_{k=1}^{m_i} \frac{a_k^n}{n} + \sum_{k=1}^{p_i} \frac{c_k^n}{n}\right) u[n-1] \tag{2.35}$$

and

$$x_{max}[n] = \left(+ \sum_{k=1}^{m_o} \frac{b_k^{-n}}{n} - \sum_{k=1}^{p_o} \frac{d_k^{-n}}{n}\right) u[-n-1] \tag{2.36}$$

From the above equations, we observe the following properties of the complex cepstrum:

Property 1 The complex cepstrum decays at least as fast as 1/n. Specifically

$$|\hat{x}[n]| < c\left|\frac{\alpha^n}{n}\right|, \quad -\infty < n < \infty$$

where c is a constant and α equals the maximum $|a_k|$, $|b_k|$, $|c_k|$ and $|d_k|$.

Property 2 If x[n] is of finite duration ($p_i = p_o = 0$), $\hat{x}[n]$ will nevertheless have infinite duration.

Property 3 The complex cepstrum of a minimum phase sequence is zero for $n < 0$. The complex cepstrum of a maximum phase sequence is zero for $n > 0$.

The complex cepstrum was derived above in terms of the poles and zeroes of X(z). It is also possible to obtain an expression relating x[n] with $\hat{x}[n]$, which in certain cases reduces to a very useful recursion formula. This relation may be derived as follows:

Assuming x[n] to be normalized, then

$$-z \frac{d}{dz} \hat{X}(z) = \frac{1}{X(z)} \cdot \left(-z \frac{d}{dz} X(z)\right) \tag{2.37a}$$

and it follows that

$$n\hat{x}[n] * x[n] = nx[n] \tag{2.37b}$$

Since for (normalized) mixed-phase signals, both $x[n]$ and $\hat{x}[n]$ are two sided sequences, the above relation cannot be rearranged into a recursion formula for the computation of $\hat{x}[n]$ from $x[n]$, or vice versa.

However, both $x_{min}[n]$ and $\hat{x}_{min}[n]$ are causal sequences. Similarly, both $x_{max}[n]$ and $\hat{x}_{max}[n]$ are anti-causal sequences. In these cases equation (2.37b) can be used to derive recursive formulas which are valid for the class of minimum and maximum-phase sequences.

Property 4 The complex cepstrum of a minimum phase sequence satisfies:

$$\hat{x}_{min}[n] = x_{min}[n] - \sum_{k=1}^{n-1} \frac{k}{n} \hat{x}_{min}[k]\, x_{min}[n-k] \qquad (2.38)$$

Property 5 The complex cepstrum of a maximum phase sequence satisfies

$$\hat{x}_{max}[n] = x_{max}[n] - \sum_{k=n+1}^{-1} \frac{k}{n} \hat{x}_{max}[k]\, x_{max}[n-k] \qquad (2.39)$$

The above two relations can be used to compute complex cepstrum, if the signal is known to be minimum or maximum phase. However, for a mixed phase sequence their use does not make any sense.

Also we mention that exponential weighting of the signal can be used to move the zeroes which are outside the unit circle

to inside. Exponential weighting has the effect of scaling the poles and zeroes of the z-transform of the inputs. Thus a mixed phase signal can be converted to a minimum phase signal. Now the complex cepstrum of this sequence can be easily determined. However, it has certain limitations [8].

In this chapter we have reviewed the basic theory of homomorphic systems and carefully treated the problems associated with the complex log. In the next chapter we consider the existing methods of phase unwrapping together with the methods based on piecewise polynomial interpolation. Various computational strategies are considered to make the computation of the one dimensional complex cepstrum more efficient and reliable. Some of the examples are also presented.

CHAPTER III

COMPUTATION OF ONE-DIMENSIONAL COMPLEX CEPSTRUM

III.1 Introduction

In the last chapter we have discussed the basic theory of homomorphic systems and observed that a class of homomorphic system (Fig. 3.1) for convolution can be defined using a complex logarithmic characteristic system D_* whose output is known as the complex cepstrum of the input signal. In this chapter we are concerned with the problems associated with the implementation of this homomorphic system in one dimension. First we critically examine the existing methods of phase unwrapping and then investigate the use of piecewise polynomial interpolation such as spline, Bessel and Hermite interpolations for phase unwrapping. Our objective is to consider all those features which may lead to the most efficient and reliable computation of the 1-D cepstrum. Therefore, we consider the various issues such as improvement of the integration routine, efficient computation of DFT at a single frequency which is not on the DFT raster, need for double precision, selection of thresholds, linear phase, etc.

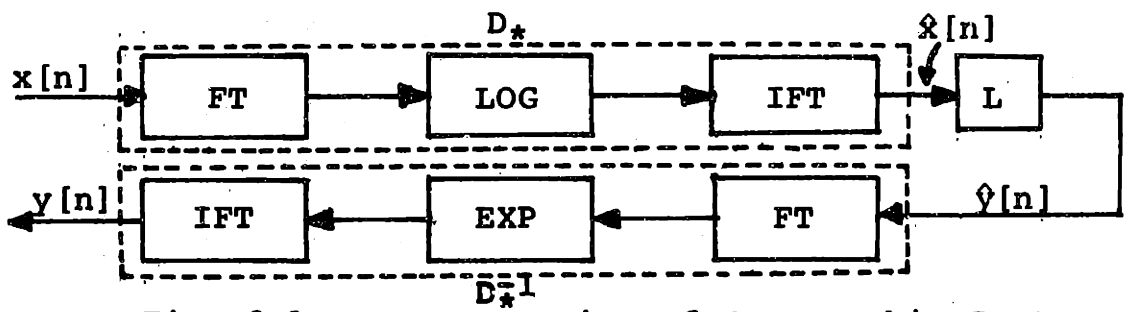

Fig. 3.1 Representation of Homomorphic System

III.2 DFT Implementation of Homomorphic System for Convolution

Our discussion in the last chapter was based on the use of the Fourier transform and accordingly the characteristic system D_* (Fig. 3.1) is represented by the equations

$$X(e^{j\omega}) = \sum_{n=-\infty}^{\infty} x[n]\, e^{-j\omega n} \tag{3.1a}$$

$$\hat{X}(e^{j\omega}) = \log\,[X(e^{j\omega})] \tag{3.1b}$$

$$\hat{x}[n] = \frac{1}{2\pi}\int_{-\pi}^{\pi} \hat{X}(e^{j\omega})\, e^{j\omega n}\, d\omega \tag{3.1c}$$

However, since digital computers perform finite computation, we are limited to finite length input sequences and we can compute the Fourier transform at only a finite number of points. So we need to use the discrete Fourier transform instead of the Fourier transform for the actual implementation of homomorphic systems.

Let the finite length sequence x[n] exist in the interval $0 \leq n \leq N-1$. Thus, for N-point DFT instead of eq. (3.1), we have the computational realization

$$\hat{x}_p[n] = \frac{1}{N}\sum_{k=0}^{N-1} \hat{X}(e^{j\frac{2\pi k}{N}})\, e^{+j\frac{2\pi k}{N}} \tag{3.2a}$$

where $\hat{X}(e^{j\frac{2\pi k}{N}})$ is the sampled complex logarithm:

$$\hat{X}(e^{j\frac{2\pi k}{N}}) = \log \{s_x e^{j\frac{2\pi k}{N} r_x} \sum_{n=0}^{N-1} x[n] e^{-j\frac{2\pi kn}{N}}\} \qquad (3.2b)$$

and s_x and r_x are signal polarity and signal lag as defined in Chapter II.

Since the complex cepstrum is computed from samples of its Fourier transform, time aliasing of the complex cepstrum occurs. That is,

$$\hat{x}_p[n] = \sum_{k=-\infty}^{\infty} \hat{x}(n+kN) \qquad (3.3)$$

The complex cepstrum $\hat{x}[n]$ in general has infinite duration, so a certain amount of time aliasing will always occur. However, as has been shown, $\hat{x}[n]$ decays faster than an exponential sequence, so it is to be expected that the aliasing can be reduced by appending zeroes to the data x[n] before computing the DFT, in order to increase the total length N. This corresponds to a finer spectral sampling of $\hat{X}(e^{j\omega})$.

The selection of a particular transform size is dependent on how much cepstral aliasing one is willing to tolerate. As with all problems involving aliasing phenomenon, such judgement is very much application dependent.

The DFT implementation of the inverse cepstral mapping yields:

$$y_p[n] = \frac{1}{N} \sum_{k=0}^{N-1} Y(e^{j\frac{2\pi k}{N}}) e^{j\frac{2\pi kn}{N}} \qquad (3.4)$$

where $Y(e^{j\frac{2\pi k}{N}})$ is the sampled complex exponential.

$$Y(e^{j\frac{2\pi k}{N}}) = \exp\left[\sum_{n=0}^{N-1} \hat{y}[n]\, e^{-j\frac{2\pi kn}{N}}\right] \qquad (3.5)$$

where $y_p[n]$ is an aliased version of $y[n]$ with period N, which might accurately represent $y[n]$ to the extent that $y[n]$ is a finite sequence of length not greater than N.

III.3 Unwrapped Phase -- From eq. (3.2b) it can be noticed that we need to evaluate the samples of the continuous complex logarithm. In particular, we need to determine the samples of the continuous phase function of the normalized input.

As we discussed in Chapter II, the input normalization is associated with the proper definition of the continuous phase. Normalization of the signal polarity can be easily done by observing the sign of $X(0) = \sum_n x[n]$. If it happens to be negative, then we change its sign and take care of it in determining the principal value. The signal lag or the slope of the linear phase at $\omega = \pi$ is, in general, not known a priori (If the location of the zeroes of the finite length sequence is known, then the signal lag is equal to the number of zeroes outside the unit circle.) In practice the required input normalization is done in the process of evaluating the continuous phase. Thus, using arguments similar to those of Chapter II, we define a phase function $\arg_u [X(e^{j\omega})]$ associated with the non-normalized input $x[n]$ as an integral of the form:

$$\arg_u [X(e^{j\omega})] = \int_0^{\omega} \left(\frac{d}{dy} \arg_u' [X(e^{jy})] \, dy \right), \quad 0 \leq \omega \leq \pi \tag{3.6a}$$

where $$\arg_u [X(e^{j0})] = 0 \tag{3.6b}$$

and the phase derivative is given by

$$\arg_u' [X(e^{j\omega})] = \frac{X_R(e^{j\omega}) X_I'(e^{j\omega}) - X_I(e^{j\omega}) X_R'(e^{j\omega})}{|X(e^{j\omega})|^2} \tag{3.7}$$

and $$X'(e^{j\omega}) = X_R'(e^{j\omega}) + jX_I'(e^{j\omega}) = -j \text{ F.T.}[nx[n]] \tag{3.8}$$

The phase function $\arg_u [X(e^{j\omega})]$ is commonly called the unwrapped phase of x[n].

As has been shown in Chapter II, the signal lag r_x is simply the mean of the phase derivative. Thus, in general, the unwrapped phase will exhibit a linear phase component due to r_x, which may be computed as,

$$r_x = \frac{\arg_u [X(e^{j\pi})]}{\pi} \tag{3.9}$$

Therefore, the continuous phase of the normalized input satisfies,

$$\arg [s_x e^{j\omega r_x} X(e^{j\omega})] = \arg_u [X(e^{j\omega})] - \omega r_x \tag{3.10}$$

In spite of the fact that the unwrapped phase is very precisely defined by eqs. (3.6) to (3.8), such equations can never be exactly implemented on a digital computer because of the finite amount of computation. It is therefore, of interest to investigate alternative methods of evaluating the unwrapped phase. Such methods have been referred to as phase unwrapping methods. In the following section we carefully examine the existing methods of phase unwrapping.

III.4 Existing Methods of Phase Unwrapping

Following are the techniques that have been used for phase unwrapping in one diemnsion.

(i) Numerical integration of phase derivative

The most straightforward approach to phase unwrapping is to do numerical integration of the phase derivative using the trapezoidal rule for integration. Samples of $\arg_u' [X(e^{j\frac{2\pi k}{N}})]$, $k = 0, 1, \ldots, N-1$ can be evaluated very efficiently by computing the DFT's of x[n] and nx[n] using FFT algorithm and combining the results according to eqs. (3.7) and (3.8). The method depends very critically on the frequency sampling interval. It does not give good results even with reasonably large size FFT's [2]. The reason being that the truncation error can not be brought down to zero. However, if a better integration rule is used, the truncation error can be made small. But all this is not satisfactory, because whatever error is made, is carried over throughout.

(ii) Processing the principal value of the phase (Schafer's Algorithm) [1]

The idea of phase unwrapping based on this approach is to compute the principal value of the unwrapped phase

$$ARG_u\ [X(e^{j\frac{2\pi k}{N}})] = \left[arg_u\ [X(e^{j\frac{2\pi k}{N}})]\right]_{mod\ 2\pi},\ k = 0,\ldots,N-1 \quad (3.11)$$

using inverse tangent routines on $X(e^{j\omega})$. Discontinuities introduced by the modulo 2π operation are then detected and finally unwrapping is done by appropriately adding multiples of 2π to the principal value until the discontinuities introduced by the modulo 2π operation are removed. Specifically,

(a) whenever a jump of -2π is detected while unwrapping along the positive ω axis, a constant 2π is added to the principal value at that point, and

(b) whenever a jump of $+2\pi$ is detected while unwrapping along the positive ω axis, a constant -2π is added to the principal value at that point, where the jump is defined as the difference between the new and old principal value.

An example is shown in Fig. 3.2. Phase unwrapping as illustrated in this figure appears quite simple, however, in practice the problem becomes complicated by the fact that we have only the samples of the principal value curve and it is possible to miss a jump of $\pm 2\pi$. Once we have missed even a single jump, we shall obtain a completely erroneous result. This is

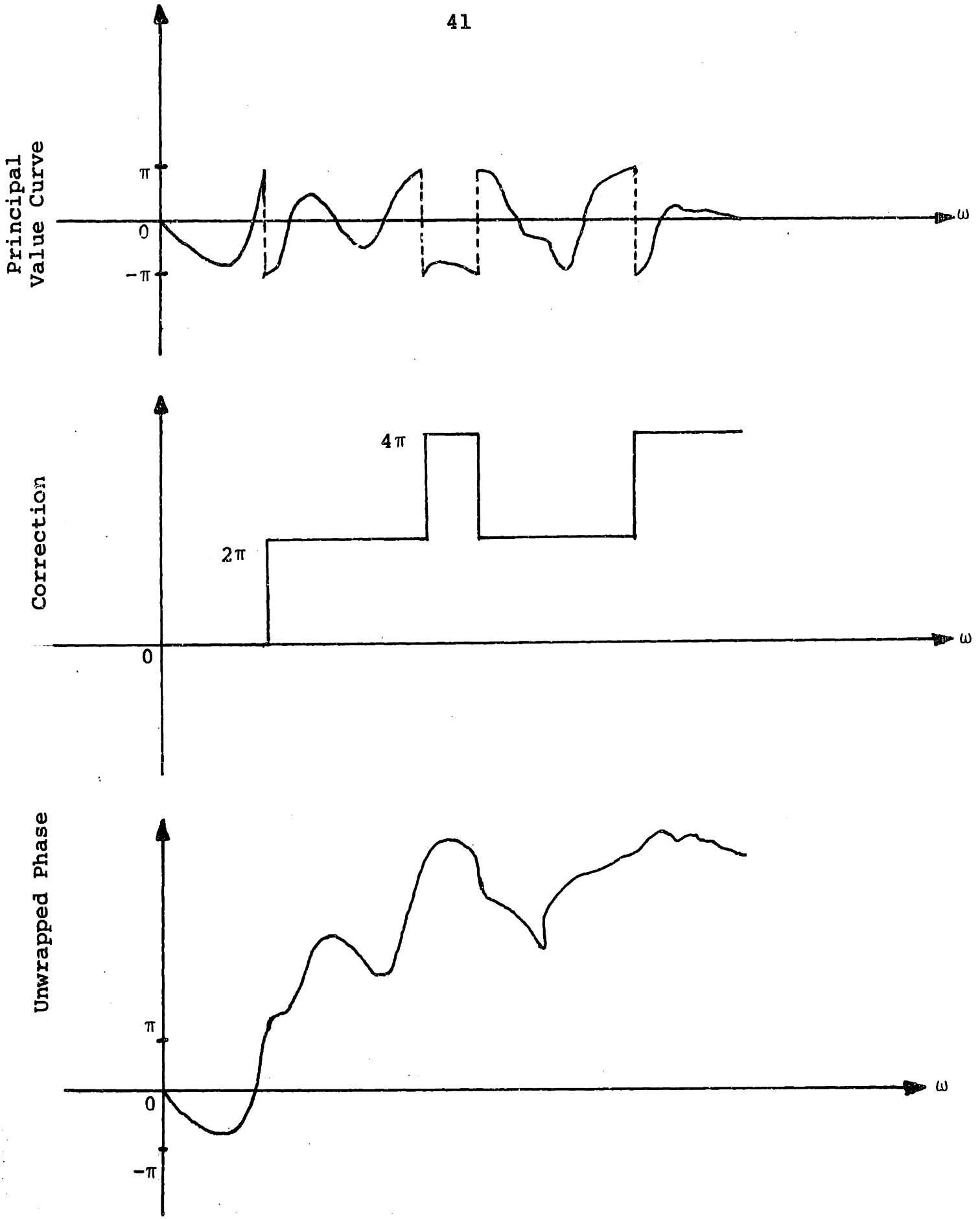
Principal
Value Curve
π
0
-π
ω
Correction
4π
2π
0
ω
Unwrapped Phase
π
0
-π
ω

Fig. 3.2

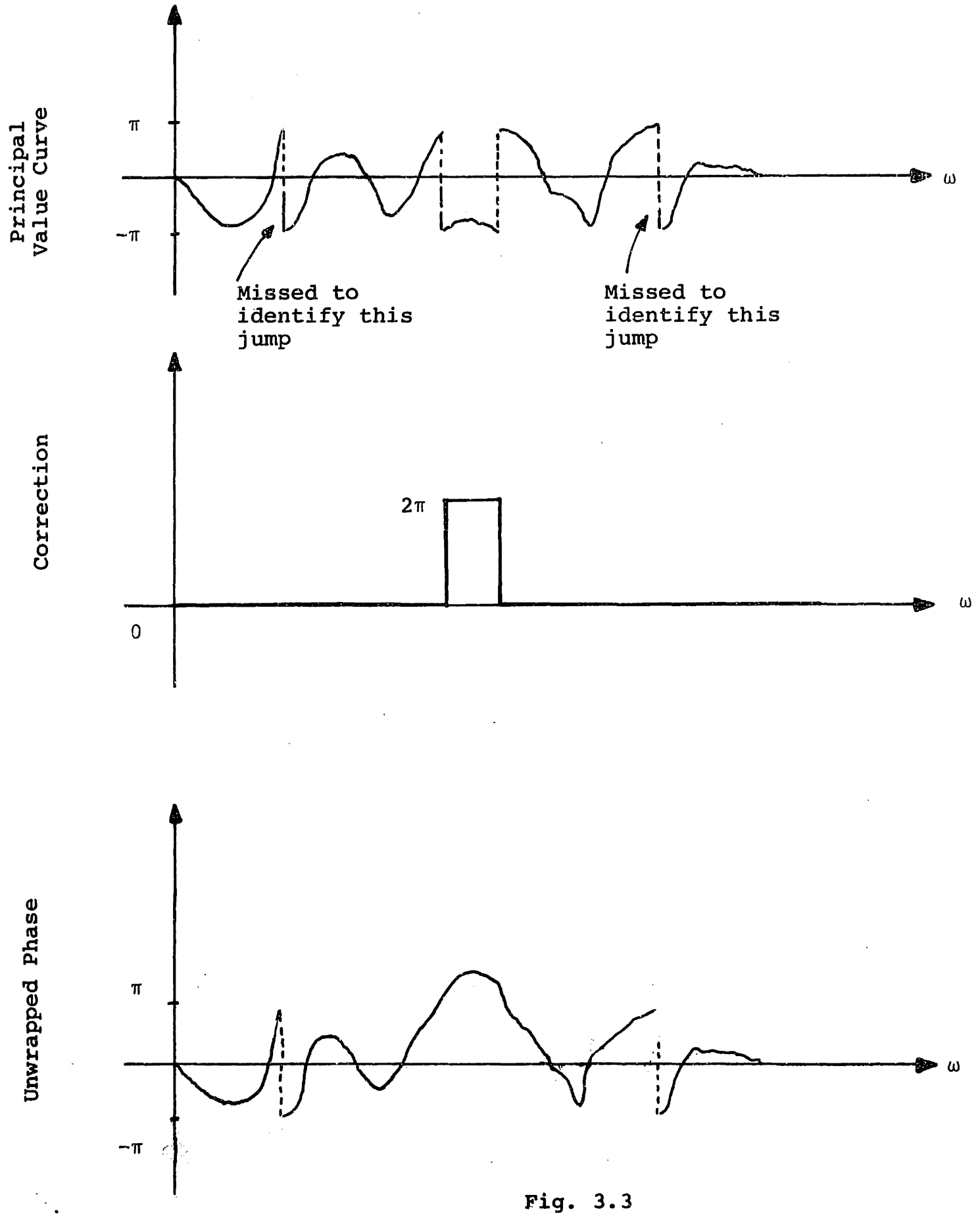
Principal Value Curve
π
−π
ω
Missed to identify this jump
Missed to identify this jump
Correction
2π
0
ω
Unwrapped Phase
π
−π
ω

Fig. 3.3

illustrated in Fig. 3.3. Thus any error made at any point along ω axis while unwrapping the phase tends to propagate undiminished. Therefore, in this method, a jump is said to exist when the difference between the two principal values at adjacent frequencies is greater than a threshold (a fraction of 2π). This threshold depends to some extent on the sampling frequency. However, this involves a tradeoff, because if it is too small, we shall be missing jumps, and if it is too large, we shall be identifying a jump when there was none. In short

(a) This method requires that the frequency sampling be fine enough so that the difference in the principal values of two adjacent samples be always less than the prescribed threshold.

(b) It has been shown [2] that in spite of a very high sampling rate, the method may not work even when a single zero is close to the unit circle lying between two samples of DFT. The principal value alone is not sufficient to allow a reliable operation [2,4].

(iii) Adaptive numerical integration scheme (Tribolet's Algorithm) [2]

This method of phase unwrapping combines the numerical integration and the information about the principal value of the phase. At each frequency, a set of permissible phase values is defined by adding integer multiples of 2π to the principal value of the phase. The selection of one of these

values is done with the help of phase estimate formed by trapezoidal integration of the phase derivative with a given step interval. This step interval is adapted until the phase estimate becomes arbitrarily close to one of the permissible phase values.

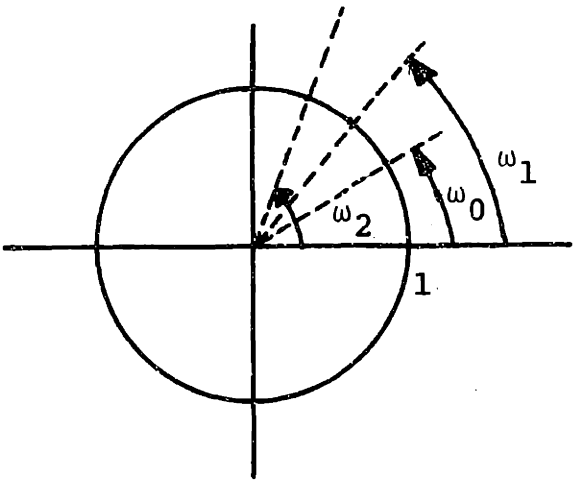

Fig. 3.4

Let us now formulate the equations. Let ω_1 be an arbitrary frequency value (refer to Fig. 3.4) and $ARG_u\ [X(e^{j\omega_1})]$ be the principal value of the phase at ω_1. The set of permissible phase values at ω_1 is given by

$$ARG_u\ [X(e^{j\omega_1})] + 2\pi k, \quad k \text{ integer} \tag{3.12}$$

The whole problem of phase unwrapping is to find the correct integer value of $k_c(\omega_1)$ such that

$$arg_u\ [X(e^{j\omega_1})] = ARG\ [X(e^{j\omega_1})] + 2\pi k_c(\omega_1) \tag{3.13}$$

This is done through the use of numerical integration of

the phase derivative using the trapezoidal rule for integration. Let the unwrapped phase be known at a frequency $\omega_o < \omega_1$. Then the phase estimate at ω_1 is given by

$$\tilde{\arg}\left[X(e^{j\omega_1})\Big|_{\omega_o}\right] = \arg\left[X(e^{j\omega_o})\right] + \left(\frac{\omega_1-\omega_o}{2}\right)\left[\arg_u'\left[X(e^{j\omega_o})\right] + \arg_u'\left[X(e^{j\omega_1})\right]\right] \tag{3.14}$$

where the step interval is $\Delta\omega = \omega_1 - \omega_o$. Clearly the estimate of the unwrapped phase at ω_1 improves as $\Delta\omega$ becomes smaller. The phase estimate at ω_1 is said to be consistent, if it lies within a predefined threshold θ_2, called the consistency threshold, of one of the permissible phase value at ω_1, that is, if there exists $k_c(\omega_1)$ such that

$$\left|\tilde{\arg}\left[X(e^{j\omega_1})\Big|_{\omega_o}\right] - \text{ARG}\left[X(e^{j\omega_1})\right] - 2\pi k_c(\omega_1)\right| < \theta_2 < \pi \tag{3.15}$$

The basic idea of this algorithm is to adapt the step interval $\Delta\omega$ until a consistent estimate is found. The value $k_c(\omega_1)$ so obtained is then used to form the unwrapped phase at ω_1, which in turn is used to estimate the unwrapped phase at ω_2 ($\omega_2 > \omega_1$) and so on.

In the implementation of the above approach we must determine the phase derivative and the principal value of the phase at a set of uniformly spaced frequencies with interval

$\frac{2\pi}{N}$ using FFT's of size N to evaluate the DFT's of x[n] and nx[n] for $0 \leq \omega \leq \pi$ (using the fact that we are computing the DFT of a real sequence and the phase is an odd function). At each ω_k, a phase estimate is initially formed by one-step trapezoidal integration at ω_{k-1}. If the resultant estimate is not consistent, the adaptive integration scheme is applied within the interval $[\omega_{k-1}, \omega_k]$. The search for consistency is done by consecutively splitting the step interval in half. The phase derivative and the phase principal values are computed at these intermediate points and are stored in a stack fashion (Note that for each splitting of the step interval we must take 2 DFTs at an intermediate frequency and then compute the phase derivative, the phase principal value, form the phase estimate and check the consistency). As soon as a consistent estimate is found, the corresponding data is moved out of the stack to a register that holds the most recent consistent estimate of the phase at some frequency within $[\omega_{k-1}, \omega_k]$. New estimates are always found by integrating from the most recent estimate to the frequency corresponding to the top of the stack.

Besides the check for consistency two more checks are used in this implementation to increase the reliability of phase unwrapping.

(1) We compute the phase increment using the linear phase estimate (obtained by summing the phase derivative values and then dividing by the total number of points). If the phase increment so obtained differs from the

increment obtained using the trapezoidal rule for integration in the interval $[\omega_{k-1}, \omega_k]$ by a certain threshold, θ_1, called the incremental threshold, then the algorithm will adapt.

(2) Having computed the unwrapped phase at ω_1, we check whether the difference between the unwrapped phase at ω_1 and ω_o is greater than π. If yes, then again the algorithm will adapt.

We shall elaborate more on these checks in the following sections.

This method of phase unwrapping works reasonably well. However, it takes a considerable amount of time for phase unwrapping because of the step interval adaption, and the simple rule for integration used. Direct computation of DFT at a single frequency which is not on the DFT raster, global estimate of the linear phase (signal lag), and the high precision requirement for certain variables also affect the phase unwrapping algorithm.

The cases where the phase unwrapping is difficult are those in which the zeroes of the sequence are close to the unit circle and such situations exhibit large narrow peaks in the phase derivative curve. In such instances, use of the trapezoidal rule for integration results in large truncation errors (refer to fig. 3.5) and the execution of the program takes a rather long time due to the step interval adaption. So we consider the use of other piecewise polynomian inter-

polation methods such as spline, Bessel and Hermite interpolations since they give rise to better rules for integration [11,13,16,17] and can be easily incorporated into a phase unwrapping algorithm.

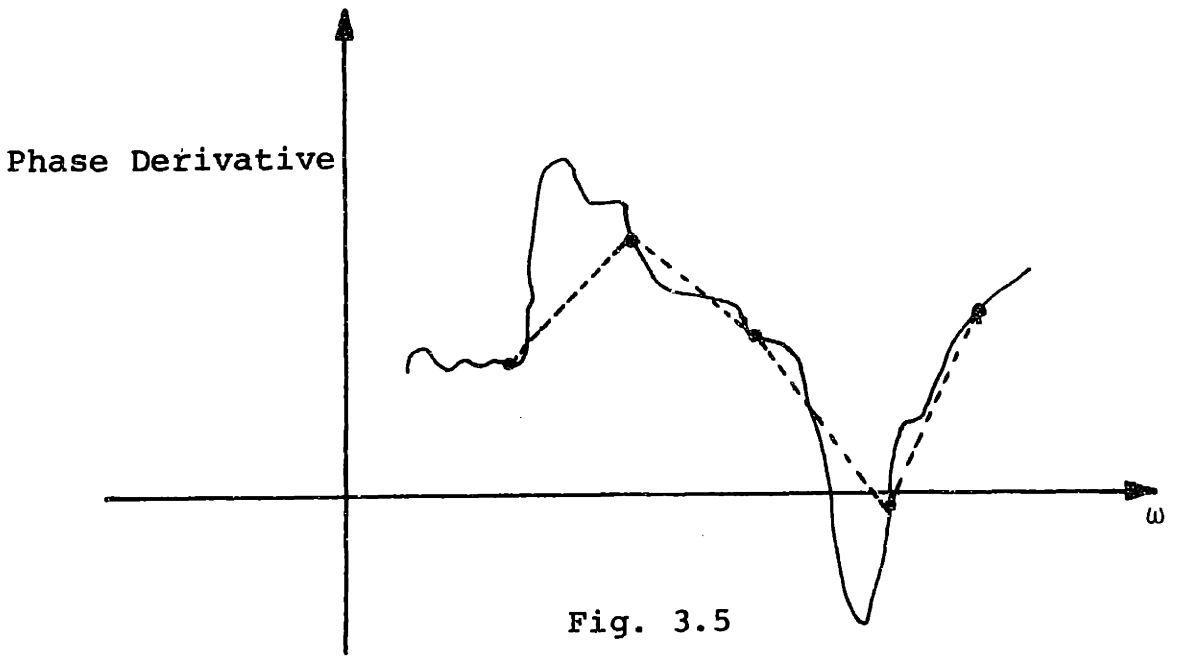

Fig. 3.5

Tribolet's phase unwrapping algorithm based on adaptive numerical integration computes the DFT at intermediate frequencies directly, which requires 4N real multiplications and 4N-2 real additions to compute the DFT at a single frequency where N is the length of the sequence. However, a more efficient algorithm that can be used for computing the DFT at a single frequency is Goertzel's algorithm [7]. It requires 2N + 4 real multiplications and 4N + 1 real additions to compute the DFT at a single frequency. However, the straightforward use of Goertzel's algorithm to find the DFT at inter-

mediate frequencies yields the correct amplitude, but the phase is wrong. Bonzanigo [10] shows that the phase correction term can be easily obtained by using an identity. Such a method to compute the DFT will be referred to as modified Goertzel algorithm. It requires 2N + 8 real multiplications and 4N + 6 real additions to compute the DFT at a single frequency. Details of this will be given in the following sections.

The linear phase estimate obtained as the mean of the phase derivative in Tribolet's algorithm is a global estimate in the sense that the value of the estimate depends upon the values of the phase derivative at all the DFT points. This estimate is erroneous if a DFT sampling point happened to the one at which the phase derivative is very large (zero close to the unit circle) and the FFT size is not very high. In such situations the method requires adaption because the incremental constraint mentioned earlier is not satisfied and it takes excessive amount of time. Our interest is to find an efficient estimate (which is local) for the linear phase in order to make the computation faster.

Tribolet [2] uses a stack size of 13 for storing variables such as phase derivative, phase principal value at the intermediate frequencies. Thus the adaptive feature of the algorithm is able to divide any interval between two DFT points by a factor of 4096. For example, 1024 points FFT corresponds

to the frequency spacing of 0.00613923 radians. Now dividing this frequency spacing by 4096, we get the minimum frequency spacing of about 4.98×10^{-7} radians. Because in single precision the machine used (Digital Equipment Corporation PDP 11/50 with a floating point processor and 32K words of core memory) has only a precision of about 6 digits of real arithmetic, we see that the computation at intermediate frequencies becomes susceptible to numerical errors. The FFT computation and hence the evaluation of phase derivative is very much susceptible to numerical errors when the zeroes are close to the unit circle. We shall point out which variables should be computed in double precision to maintain accuracy. Also we shall consider the selection of the incremental and consistency threshold for Tribolet's implementation.

III.5 Use of Piecewise Polynomial Interpolation

In the last section we carefully considered the existing methods of phase unwrapping and pointed out the various features which should be incorporated in the phase unwrapping method based on the adaptive numerical integration so as to make it more efficient and reliable. In this section we shall consider the use of piecewise polynomial interpolation methods such as cubic spline, Bessel and Hermite interpolations as they give rise to better rules of integration and can be easily included in the phase unwrapping algorithm.

Spline interpolation - Here the problem of phase unwrapping is viewed as fitting a curve to a finite set of known values of the phase derivative in order to perform numerical integration utilizing the extremal properties of spline functions in numerical quadrature [16]. The integration alone is not sufficient since whatever error is committed is carried over throughout. So the adaptive nature of the algorithms will be used to relate the density of the data to the local smoothness of the phase derivative.

Throughout this discussion when we say splines, we mean cubic splines. Consider the fitting of splines $s(\omega)$, having continuous first and second derivatives, to the phase derivative between $\omega = 0$ and $\omega = \pi$ at N given points. The spline approximation is the smoothest in the sense that the mean square value of its second derivative is minimal [13]. Moreover, the solution is unique and consists of different cubics in each interval. Also the cubic arcs that make up $s(\omega)$ join smoothly in the sense that the two polynomials that represent $s(\omega)$ to the left and to the right of ω_i have the same ordinate and the same values of first and second order derivatives.

Symbols used - We refer to the phase derivative as the function, denoted by y (refer to fig. 3.6), to which we want to fit the splines. The values of the function, y_i, are known at discrete points ω_i $(1 \leq i \leq N)$. Derivatives of the function

will be denoted by y', y'', y''',... $s(\omega)$ denotes the spline; its derivatives are s', s'',... When a subscript is used, it means that the derivative is computed at the point (ω_i, y_i).

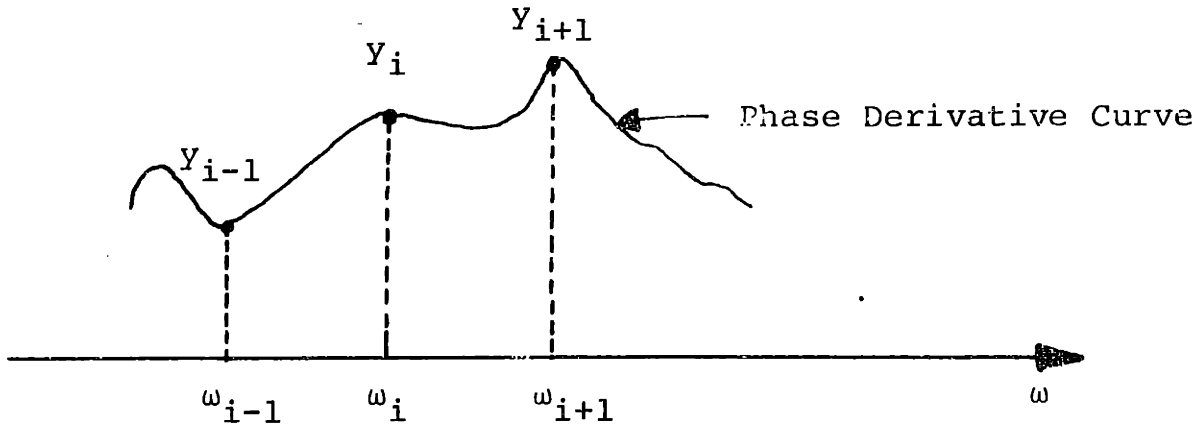

Fig. 3.6 Notations used in the Discussion of Piecewise Polynomial Interpolation

Basic Spline Equation - The condition for a cubic spline fit are that we pass a set of cubics through the points y_i of the function using a new cubic in each interval. We require that the slope and curvature be the same for the pair of cubics that join at each point (curvature is approximated by second derivative). The equation [11] satisfying the above constraints is,

$$\frac{1}{h_{i-1}} s'_{i-1} + 2\left(\frac{1}{h_{i-1}} + \frac{1}{h_i}\right) s'_i + \frac{1}{h_i} s'_{i+1} =$$

$$3\left(\frac{y_i - y_{i-1}}{h^2_{i-1}}\right) + 3\left(\frac{y_{i+1} - y_i}{h_i^2}\right) \qquad (3.16)$$

where, $h_i = \omega_{i+1} - \omega_i$

This equation applies at each interval point from i = 2 to N-1, N being the total number of points. Thus we obtain N-2 equations relating the N values of s'_i. Two additional equations involving s'_1 and S'_N are obtained when we specify end conditions.

<u>End Conditions</u> - setting $s'_1 = y'_1$, $s'_N = y'_N$ (3.17)

we mean that the first derivative of the spline (interpolating curve) at the two boundary points is equal to the actual value of the first derivative of the function (or second derivative of the phase) that we want to approximate. The expression for the phase second derivative can be obtained from eq. (3.7) as

$$\arg''_u [X(e^{j\omega})] = \frac{1}{|X|^4} [|X|^2 \{X_R X_I'' - X_I X_R''\} +$$

$$2X_R X_I \{(X_R')^2 - (X_I')^2\} + 2X_R' X_I' \{X_I^2 - X_R^2\}] \quad (3.18)$$

where we have avoided the argument notation for the sake of simplicity

From this equation it is easy to conclude that the phase second derivative at $\omega_1 = 0$ and $\omega_N = \pi$ is always zero irrespective of the presence or absence of the linear phase component in the unwrapped phase. So our end conditions become

$$s'_1 = s'_N = 0 \tag{3.19}$$

Once we have computed s'_i (for i = 2 to N-1) we know the equation of the spline in each interval [15,16] and now our interest is to integrate it so as to obtain an estimate of the phase. Integrating this eq. of spline, it is easy to obtain [11],

$$\int_{\omega_i}^{\omega_{i+1}} s(\omega)d\omega = \frac{h_i}{2}(y_i+y_{i+1}) - \frac{h_i^2}{12}(s'_{i+1}-s'_i) \tag{3.20}$$

$$\text{for } 1 \leq i \leq N-1$$

Since we are using the FFT to compute the phase derivative, our data points are equally spaced. (Note that for this reason quadrature formulae which give an optimal distribution of abscissa could not be used.) Thus

$$h_i \equiv \omega_{i+1} - \omega_i = h \text{ (i = 1 to N-1) and} \tag{3.21}$$

eq. (3.16) simplifies to

$$s'_{i-1} + 4s'_i + s'_{i+1} = 6\left(\frac{y_{i+1}-y_{i-1}}{2h}\right), \text{ i=2 to N-1} \tag{3.22}$$

where the bracketed term in the above equation is the mean central difference. Specifying the boundary conditions (3.19), the above equation can be written in matrix form as

$$\begin{bmatrix} 4 & 1 & 0 & 0 & & & 0 \\ 1 & 4 & 1 & 0 & & & 0 \\ 0 & 1 & 4 & 1 & & & 0 \\ & & & & & & \\ & & & & 1 & 4 & 1 \\ 0 & 0 & 0 & & 0 & 1 & 4 \end{bmatrix} \begin{bmatrix} s'_2 \\ s'_3 \\ s'_4 \\ \\ s'_{N-2} \\ s'_{N-1} \end{bmatrix} = \frac{3}{h} \begin{bmatrix} y_3-y_1 \\ y_4-y_2 \\ y_5-y_3 \\ \\ y_{n-1}-y_{n-3} \\ y_n-y_{n-2} \end{bmatrix} \qquad (3.23)$$

So the N-2 unknowns s'_2 to s'_{N-1} are obtained by solving the above nonsingular matrix, which is diagonally dominant.

Before looking into the efficient method of solving the above matrix, let us look at the integration rule for equal interval case. For equal intervals, eq. (3.20) becomes,

$$\int_{\omega_i}^{\omega_{i+1}} s(\omega)d\omega = \frac{h}{2}(y_i+y_{i+1}) - \frac{h^2}{12}(s'_{i+1}-s'_i) \qquad (3.24)$$

$$i=1 \text{ to } N-1$$

Note that the first term of the above equation is the trapezoidal integration term and second term is similar to the truncation term in the trapezoidal rule, usually given by $\frac{-h^3}{12} f''(\theta)$, $\omega_i \leq \theta \leq \omega_{i+1}$.

Note that if the phase derivative curve happens to be a cubic between each subinterval, the integration rule given by eq. (3.24) is exact.

To use eq. (3.24), it is necessary to know the values of s'_i for i = 2 to N-1. There can be two approaches:

(1) Compute the exact values of s'_i (i=2 to N-1) from

eq. (3.18).

(2) Solve the tridiagonal matrix eq. (3.23) using Gaussian elimination specifically suited to it. This will give an approximate computation of the phase second derivative [12,15].

It can be shown that Eq. (3.23) can be solved more efficiently from computations and memory requirement points of view than using Eq. (3.18) which requires the DFT's of x[n], nx[n] and n^2 x[n]. However, in spite of all the advantages of second approach, it is shown below that it is essential to compute the second derivative exactly using Eq. (3.18), when the zeroes are quite close ($\leq 10^{-3}$) to the unit circle.

The spline approximation is global in the sense that the value of $s(\omega)$ in any interval $[\omega_i, \omega_{i+1}]$ depends on all s_i's without exception. So if the phase derivative happens to be irregular even at just one sampling point, the effect of irregularity propagates throughout, but fortunately diminishes by a factor of 0.268 in each subinterval [5,14].

Bessel's interpolation - Bessel's method of cubic interpolation has an advantage over spline interpolation. In local cubic interpolation, the s'_i (i=2 to N-1) are calculated from

$$(\Delta\omega_{i-1}+\Delta\omega_i)s'_i = [\Delta\omega_i \frac{\Delta Y_{i-1}}{\Delta\omega_{i-1}} + \Delta\omega_{i-1} \frac{\Delta Y_i}{\Delta\omega_i}] \qquad (3.25)$$

where $\Delta\omega_i = \omega_{i+1} - \omega_i$, $\Delta Y_i = Y_{i+1}-Y_i$ (3.26)

or, for equal intervals,

$$(\omega_{i+1}-\omega_{i-1})\ s'_i = (y_{i+1}-y_{i-1}) \tag{3.27}$$

Hermite interpolation is then used to compute $s(\omega)$ in each interval. From this we obtain a piecewise cubic polynomial having continuous first derivative. It gives the integration formula

$$\int_{\omega_i}^{\omega_{i+1}} s(\omega)d\omega = \frac{h}{2}(y_i+y_{i+1}) - \frac{h^2}{12}(s'_{i+1}-s'_i) + \frac{h^5}{720}y^{iv}(\xi)$$
$$\omega_i \leq \xi \leq \omega_{i+1} \tag{3.28}$$

This equation is similar to eq. (3.23) except for the last term. Also it follows that spline approximation differs from the cubic Hermite interpolation only by the terms which are small, of order h^5 in interior subintervals.

III.6 Computational Strategies

In this section we consider the various features to be incorporated in a phase unwrapping technique based on the adaptive numerical integration scheme. The next section will include various examples.

Modification of Integration Routine - In the last section we obtained the integration formula (eq. (3.24)) for splines, which in terms of more explicit notation, is

$$\int_{\omega_i}^{\omega_{i+1}} \arg'[X(e^{j\omega})]d\omega = \frac{\Delta\omega}{2}[\arg'[X(e^{j\omega_{i+1}})]+\arg'[X(e^{j\omega_i})] - \frac{(\Delta\omega)^2}{12}[\arg''[X(e^{j\omega_{i+1}})] - \arg''[X(e^{j\omega_i})]] \tag{3.29}$$

where $\Delta\omega = \omega_{i+1} - \omega_i$, and $1 \leq i \leq N-1$.

In order to use the above equations as the integration routine in the phase unwrapping algorithm, we need to compute the phase first and second derivatives at the DFT points. Formulae for these derivatives are given by eqs. (3.7) and (3.18) respectively. The evaluation of the phase second derivative (eq. (3.18)) requires the FFT's of X[n], nx[n] and $n^2x[n]$, where

$$X_R(e^{j\omega}) = \text{Re(F.T. } x[n]), \quad X_I(e^{j\omega}) = \text{Im(F.T. } x[n]),$$
$$X'_R(e^{j\omega}) = \text{Im(F.T.}nx[n]), \quad X'_I(e^{j\omega}) = -\text{Re(F.T.}nx[n]),$$
and $$X''_R(e^{j\omega}) = -\text{Re(F.T.}n^2x[n]), \quad X''_I(e^{j\omega}) = -\text{Im(F.T.}n^2x[n]).$$

So now we take 3 FFT's instead of 2 as in Tribolet's phase unwrapping algorithm based on adaptive numerical integration. Thus we increase the amount of computations while hoping to reduce the number of times that the algorithm must adapt. Also when adaptation is required, we must compute 3 DFT's. Thus a tradeoff is involved.

The modification of the integration routine reduced the number of times that the algorithm must adapt by a factor of up to 20%. One such example is presented in the next section (Example 3.1). However, on the basis of computation time it does not provide a significant saving. The computation time required using this feature is comparable to that of Tribolet's (refer to table 3.1). However, the biggest advantage of using

this modification is the significant increase in the reliability and precision of phase unwrapping technique. In the next section we shall present an example (refer to example 3.2) where the Tribolet algorithm fails and the phase unwrapping employing the modified integration routine is successful due to the improved integration.

Modification for computing the DFT at a single frequency -

By definition, the discrete Fourier transform is,

$$X(K) = \sum_{n=0}^{N-1} x[n]\, W_N^{nk} \tag{3.30}$$

where $W_N = e^{\frac{-j2\pi}{N}}$, K = 0,1,...,N-1 and N is the length of the sequence = length of the DFT. However, we need not evaluate all the N different values of X(K). We are interested in evaluating X(K) for one value of K. In the adaptive part of the phase unwrapping we want to compute the DFT at a frequency K/M for M>N. Then,

$$X(K) = \sum_{n=0}^{N-1} x(n)\, e^{-j2\pi\frac{K}{M}n} \tag{3.31}$$

Using the identity [10],

$$1 = e^{j2\pi\frac{K}{M}(N-N)} = W_M^{-K(N-N)}, \text{ we have}$$

$$X(K) = (e^{-j2\pi\frac{KN}{M}}) \sum_{n=0}^{N-1} x[n]\, e^{j2\pi\frac{K}{M}(N-n)} \tag{3.32}$$

The term outside the square bracket is the phase correction term. Eq. (3.32) can be implemented using Goertzel's algorithm

[7] to calculate the term inside the square bracket and the result so obtained can be multiplied by the phase correction term. Thus we can efficiently compute the DFT at a single frequency, K/M, which does not lie on the DFT raster. It requires 2N+8 real multiplications and 4N+6 real additions per DFT point. Thus whenever the length of the sequence is greater than 4 or 5 the modified Goertzel algorithm is more efficient to use than the direct computation. Its extension to the two dimensional case is discussed in Chapter 5. Table 3.1 illustrates the improvement provided by this technique of computing the DFT at a single frequency. Also it has been found that the modified Goertzel algorithm is more susceptible to numerical errors than the direct DFT when considering zeroes close to the unit circle because of the precision (6 digits in real arithmetic) involved.

Need for Double Precision - We need double precision for certain variables in the phase unwrapping algorithm because of the following two reasons.

1) The computation of DFT in single precision is subject to errors, and

2) When the algorithm adapts, the computation is very sensitive to the value of the intermediate frequency at which we compute the DFT's of x[n], nx[n] and n^2x[n] and, therefore, the computation of phase derivatives and principal value is affected. In the next section we shall present examples for

[7] to calculate the term inside the square bracket and the result so obtained can be multiplied by the phase correction term. Thus we can efficiently compute the DFT at a single frequency, K/M, which does not lie on the DFT raster. It requires 2N+8 real multiplications and 4N+6 real additions per DFT point. Thus whenever the length of the sequence is greater than 4 or 5 the modified Goertzel algorithm is more efficient to use than the direct computation. Its extension to the two dimensional case is discussed in Chapter 5. Table 3.1 illustrates the improvement provided by this technique of computing the DFT at a single frequency. Also it has been found that the modified Goertzel algorithm is more susceptible to numerical errors than the direct DFT when considering zeroes close to the unit circle because of the precision (6 digits in real arithmetic) involved.

Need for Double Precision - We need double precision for certain variables in the phase unwrapping algorithm because of the following two reasons.

1) The computation of DFT in single precision is subject to errors, and

2) When the algorithm adapts, the computation is very sensitive to the value of the intermediate frequency at which we compute the DFT's of x[n], nx[n] and $n^2x[n]$ and, therefore, the computation of phase derivatives and principal value is affected. In the next section we shall present examples for

the above two cases. In the second case the lack of double precision leads to the failure of the algorithm (Example 3.3 and Table 3.2, 3.3).

The variables which are to be used in double precision are π, the intermediate frequency when the algorithm requires adaption and the computation of DFT's of x[n], nx[n] and $n^2x[n]$. In single precision the problem occurs because of rounding in the DO loop implementation of computing the DFT at a single frequency where we are multiplying numbers and summing them up.

Linear Phase Estimate - Since in practice we may encounter signals having strong linear phase components associated with them, our interest is to find an efficient estimate (which is local) for the linear phase in order to make the computation faster. Tribolet [2] uses the mean of the phase derivative which works alright when the FFT size is of the order of 1024. However, it gives an erroneous estimate when the FFT size is not very high and if a derivative point happens to be the one at which phase derivative is very large. In such situations the linear phase estimate is quite large compared to the number of signal points, which is certainly unrealistic. If it is less than the sequence length we make use of it otherwise we don't make use of it in the incremental criterion. Example 4 given in the next section illustrates this point.

Also the algorithm based on adaptive numerical integra-

tions [2] assumes the thresholds arbitrary. They may be fine for one set of data, but may not be suited to the other type of data. Table 3.1 shows how the computation time varies for various values of these thresholds. In Chapter 4 we discuss in detail the relations between these two thresholds. However, there is a difference in the incremental threshold definition of Chapter 4, and the one that has been used here. In this chapter, we evaluate the phase increment from the linear phase estimate and the area criterion. If the absolute value of the difference between these two values is greater than a certain number, called the incremental threshold, then the algorithm requires adaption. In the analysis presented in Chapter 4, we don't make use of the linear phase and hence we simply check whether the absolute value of the phase increment obtained from area criterion is greater than a certain number called the incremental threshold. So the results obtained in Chapter 4 will be more conservative.

III.7 Examples and Comments

In this section we consider various examples in support of the arguments presented in the last section.

Example 3.1 - 256 points synthetic signal shown in Fig. 3.7 requires 16% fewer adaptions compared to the algorithm which uses trapezoidal integration. FFT size selected was 1024. Fig. 3.8 shows the phase first and second derivatives,

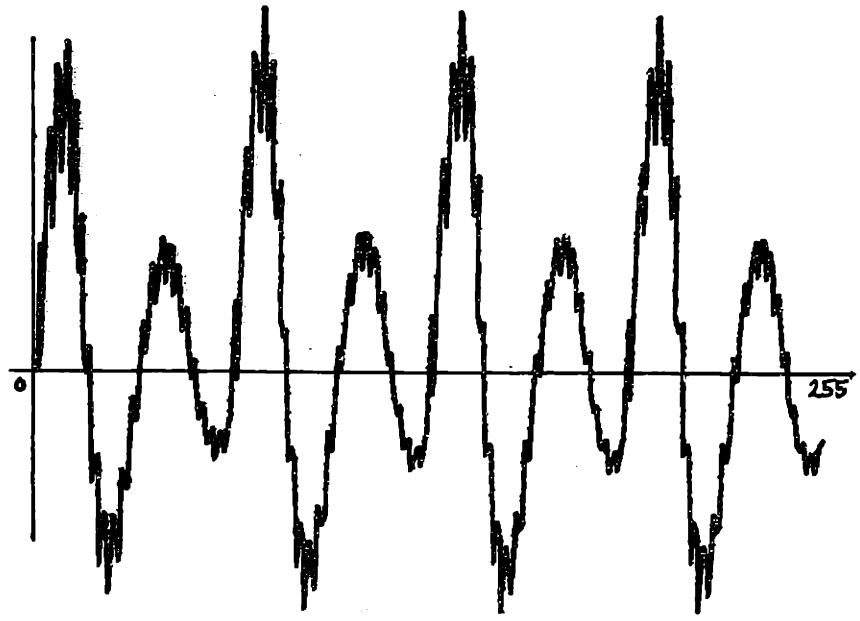

Fig. 3.7 256 Points Synthetic Signal

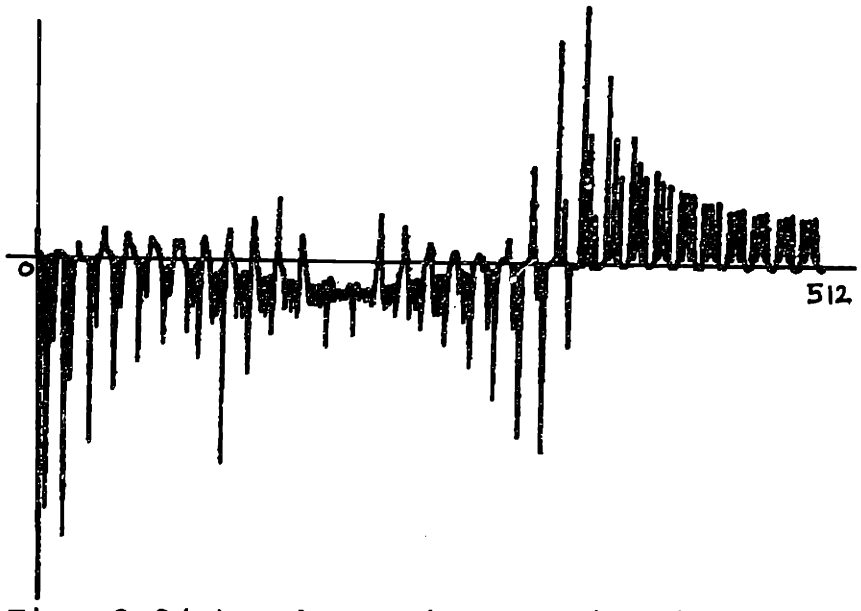

Fig. 3.8(a) Phase First Derivative

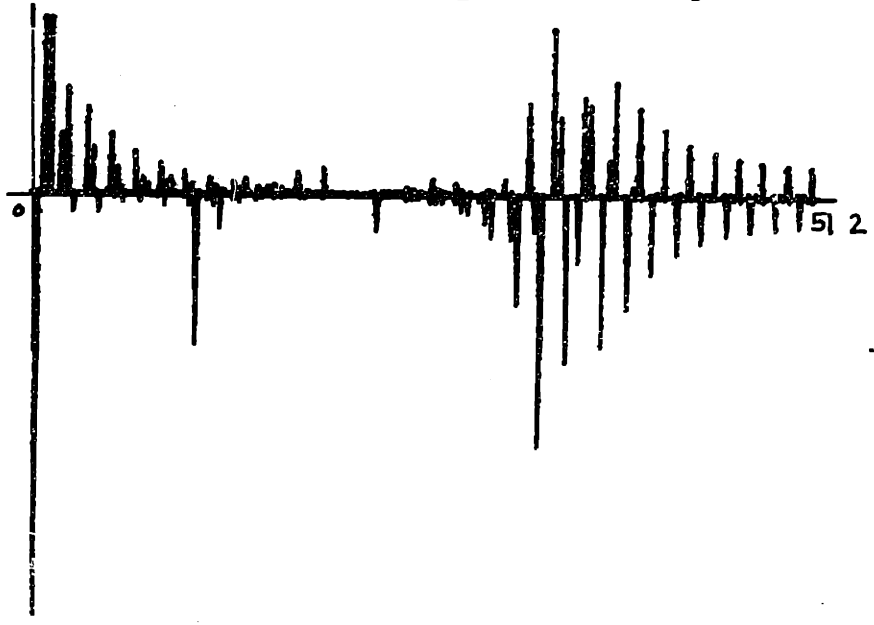

Fig. 3.8(b) Phase Second Derivative

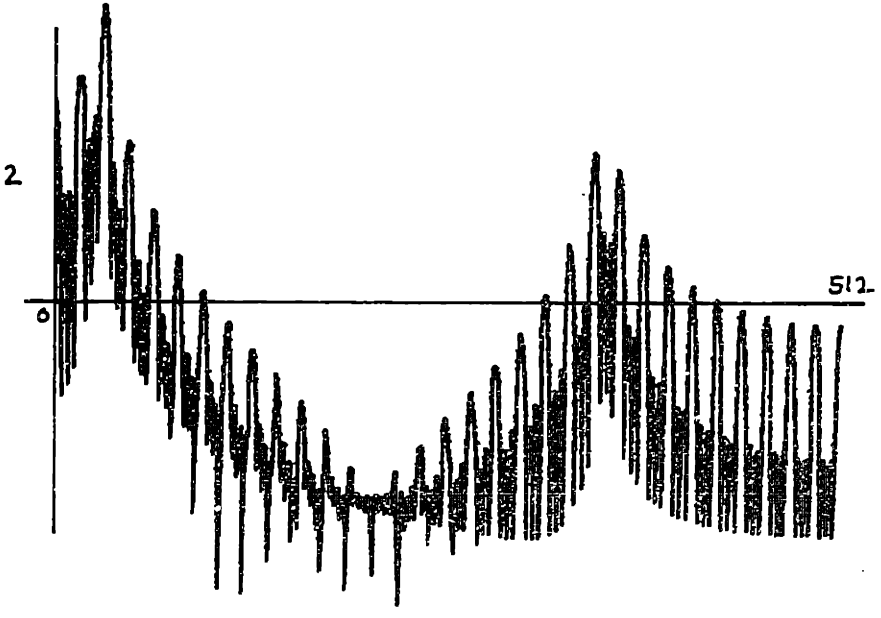

Fig. 3.9 Log Magnitude of the Frequency Response

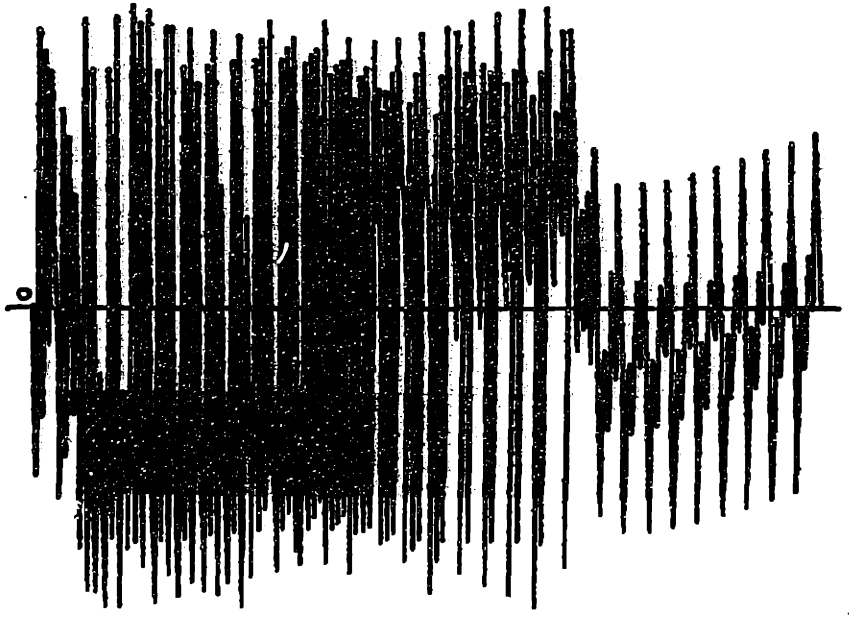

Fig. 3.10 Phase Principal Value

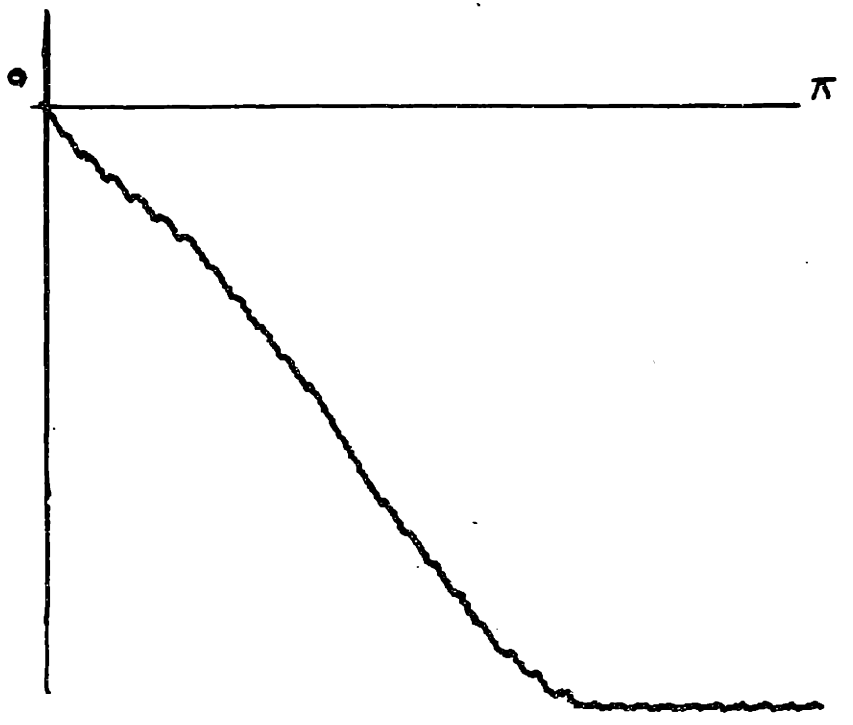

Fig. 3.11 Unwrapped Phase before Removal of Linear Phase

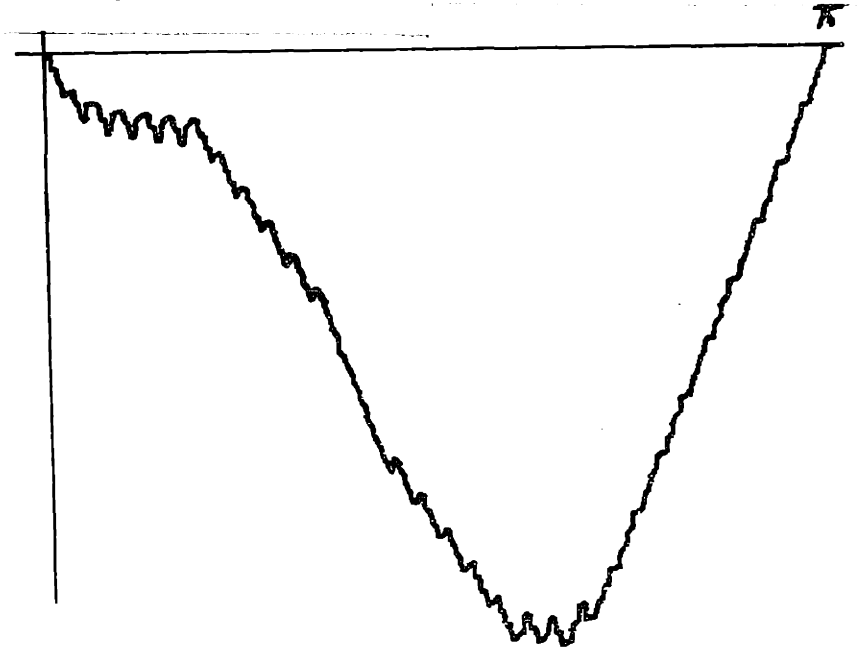

Fig. 3.12 Unwrapped Phase after Removal of Linear Phase

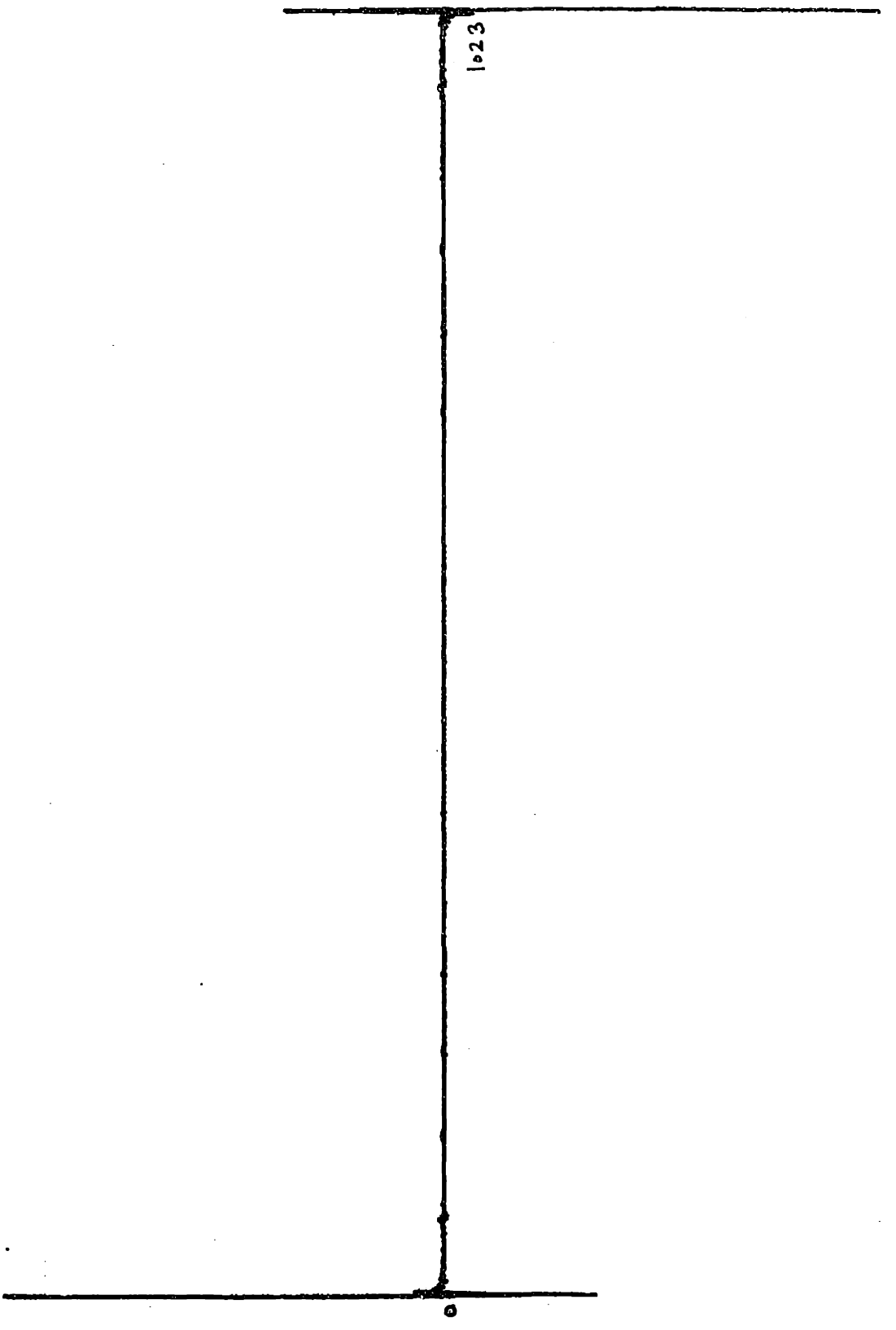

Fig. 3.13 Complex Cepstrum

Fig. 3.10 shows the principal value plot. From this it can be seen that it has a large number of jumps at $\pm\pi$. Fig. 3.9 is the log magnitude of the frequency response. Figs. 3.11 and 3.12 show the unwrapped phase before and after the removal of linear phase. From Fig. 3.11, it can be seen that the phase unwrapping has worked successfully and the jumps in the principal value plot (Fig. 3.10) have been removed. Finally Fig. 3.13 shows the complex cepstrum. The linear phase was -120 and the estimated linear phase was -131.6 which is quite close to -120.

Table 3.1 illustrates the time required by the phase unwrapping algorithm based on adaptive numerical integration scheme when the various features are added to it and for the various values of thresholds. The signal used in Table 3.1 is the same as has been shown in Fig. 3.7. The FFT size was 1024 and the sequence length is 256. Table 3.1 illustrates that how the arbitrary selection of thresholds affect the computation time. Issues pertaining to thresholds are discussed in more detail in the next chapter. Also, the computation time in the algorithm using the modified integration obtained from the splines criterion is comparable to the case where it is not used. Now we present an example which shows the need for improving the integration routine.

Example 3.2 - This is the example in which Tribolet's algorithm (signal is shown in Fig. 3.14b) fails to do success-

FFT size = 1024, Sequence length = 256

C01 = Same as Tribolet's (using Direct DFT implementation)

C02 = Tribolet's + Modified Goertzel

C03 = Tribolet's + Modified Goertzel + Double Precision

C04 = Modified integration + Modified Goertzel

C05 = Modified integration + Modified Goertzel + Double Precision

TIME IN SECONDS					Increment Threshold	Consistency Threshold	Comments
C01	C02	C03	C04	C05			
38.3	33.6	33.1	35.4	37.1	3	2	1)Timing includes 2I/O operations
47	33.3	32.3	36.1	40.1	2.5	1.5	
47.9	41.4	41.3	42.2	48.7	2	1	2)Time is accurate to within -2 secs.
57	42.5	52.2	49.6	57.9	1.5	1	
90.6	56.0	70.4	75.6	96.2	1	0.5	3)Unwrapping was alright for all the values of both thresholds except the last pair of values.
135.2	76.8	100.7	101.4	128.6	0.75	0.4	
190.8	108.8	144.4	155.1	192.7	0.5	0.25	
411.5	215.	294.7	314.	412.5	0.25	0.1	
1052.3	559.9	777.4	858.4	1148.1	0.1	0.05	
Failed	Failed	Failed	Failed	Failed	0.01	0.005	

Effect of Thresholds on Phase Unwrapping

Table 3.1

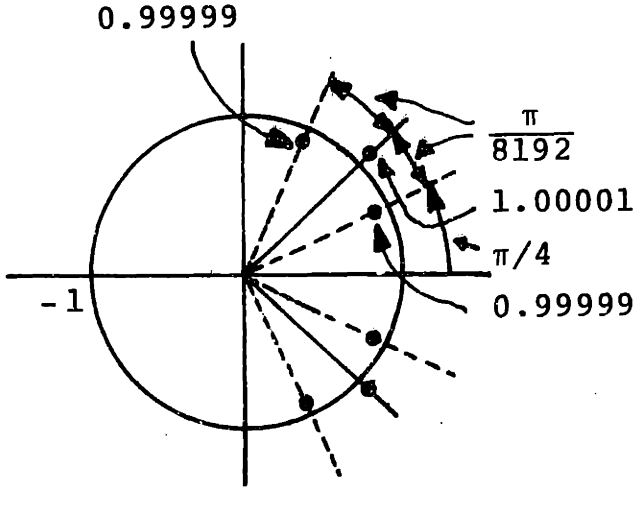

Fig. 3.14(a)

Diagram not to Scale

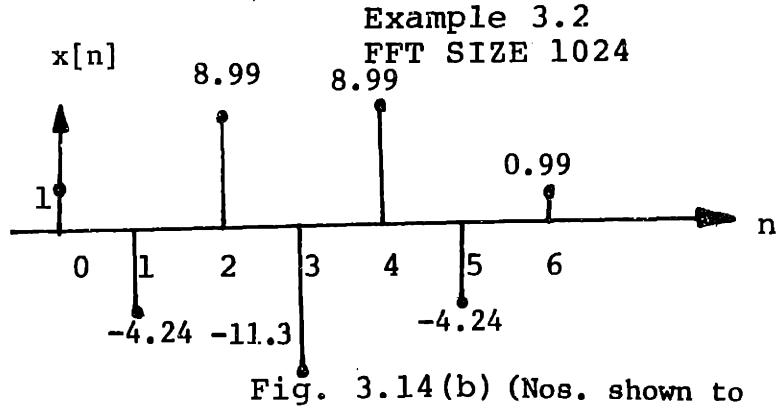

Fig. 3.14(b) (Nos. shown to two places of decimal)

ful phase unwrapping as a result of the poor integration of the trapezoidal rule. The sequence shown in Fig. 3.14(b) is generated corresponding to the pole-zero plot shown in Fig. 3.14(a). The FFT size used was 1024. Figs.3.15 and 3.16 show the two phase derivatives. Fig. 3.17 shows the principal value plot. Figs. 3.18 and 3.19 show the unwrapped phase before and after the removal of the linear phase. Fig. 3.20 shows the log magnitude of the frequency response and finally Fig. 3.21 shows the cepstrum. Note that the cepstrum is mixed phase and also the plot of unwrapped phase in Fig. 3.18 can be verified from the selected geometry of pole-zero in Fig. 3.14(a). The value of increment threshold used was 2 and that of consistency threshold 1. Theoretical details about the values of cepstrum are given below.

Z_1, Z_1^* zeroes at $\pm\pi/4 \rightarrow 0.707099 \pm j\ 0.707099$

Z_2, Z_2^* zeroes at $\pm(\frac{\pi}{4}+\frac{\pi}{8192}) \rightarrow 0.706842 \pm j\ 0.707384$

Z_3, Z_3^* zeroes at $\pm(\frac{\pi}{4}+\frac{2\pi}{8192}) \rightarrow 0.70655 \pm j\ 0.707634$

$$X(Z) = \frac{Z_2 Z_2^* (1-Z_1 Z^{-1})(1-Z_1^* Z^{-1})(1-Z_3 Z^{-1})(1-Z_3^* Z^{-1})(1-\frac{1}{Z_2})(1-\frac{1}{Z_2^*}Z)}{Z^2}$$

$$\hat{X}(0) = \text{Log}[Z_2 Z_2^*] = \log[1.00001] \simeq 0$$

$$\hat{X}[n] = -[\frac{Z_1^n}{n} + (\frac{Z_1^*}{n})^n + \frac{Z_3^n}{n} + \frac{(Z_3^*)^n}{n} \qquad n>0$$

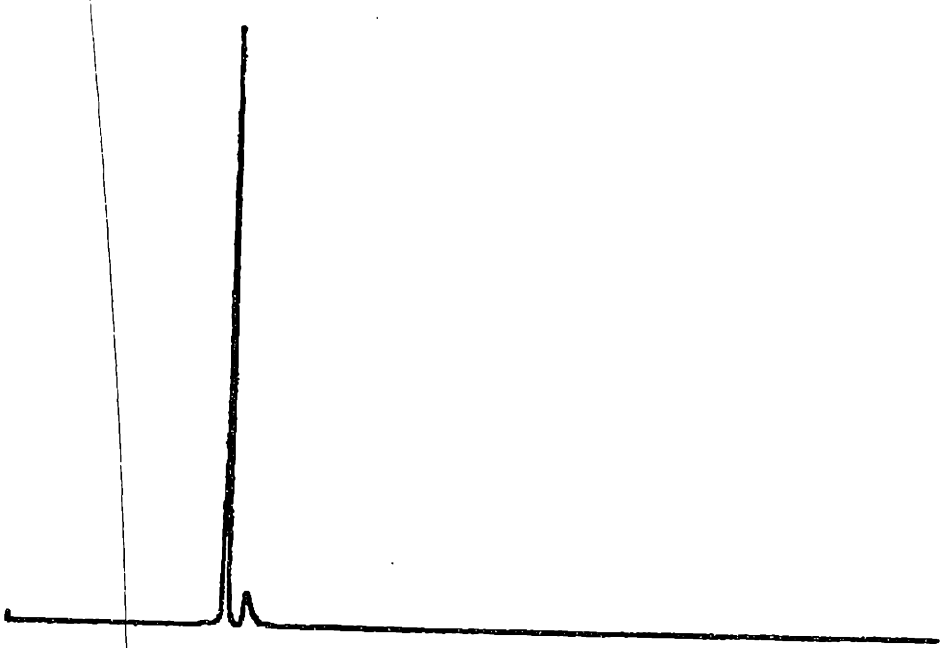

Fig. 3.15 Phase First Derivative

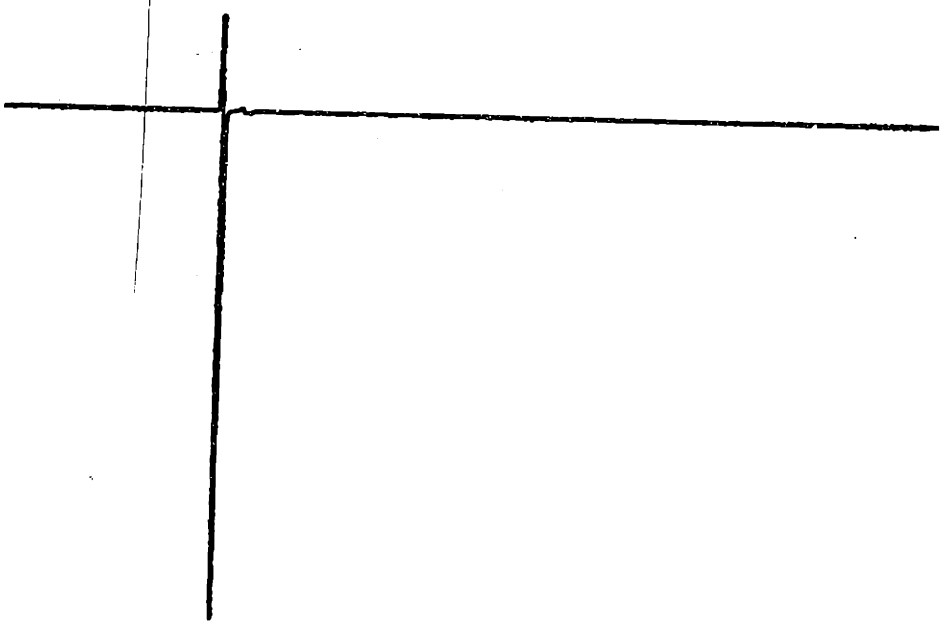

Fig. 3.16 Phase Second Derivative

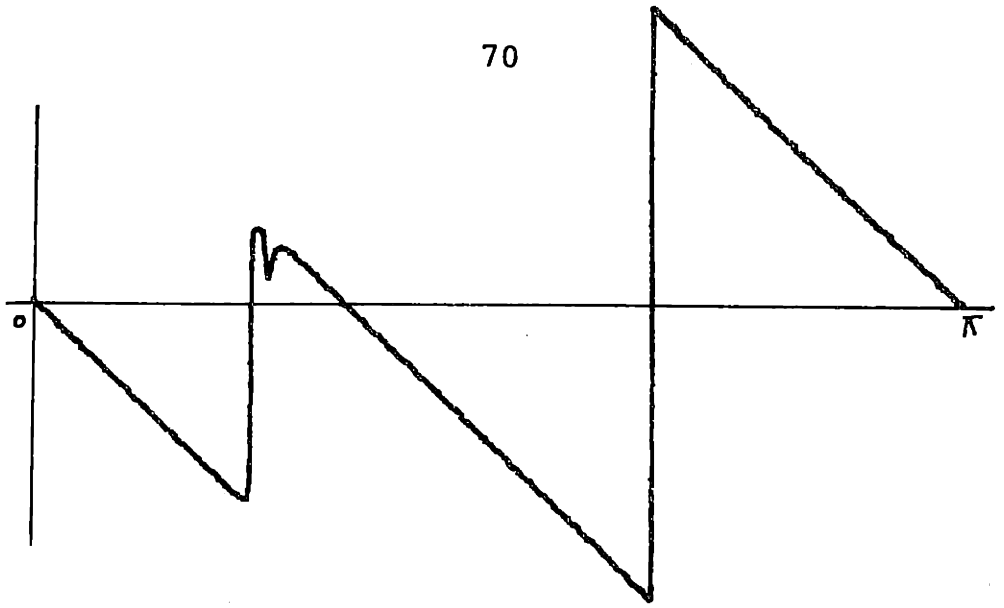

Fig. 3.17 Phase Principal Value

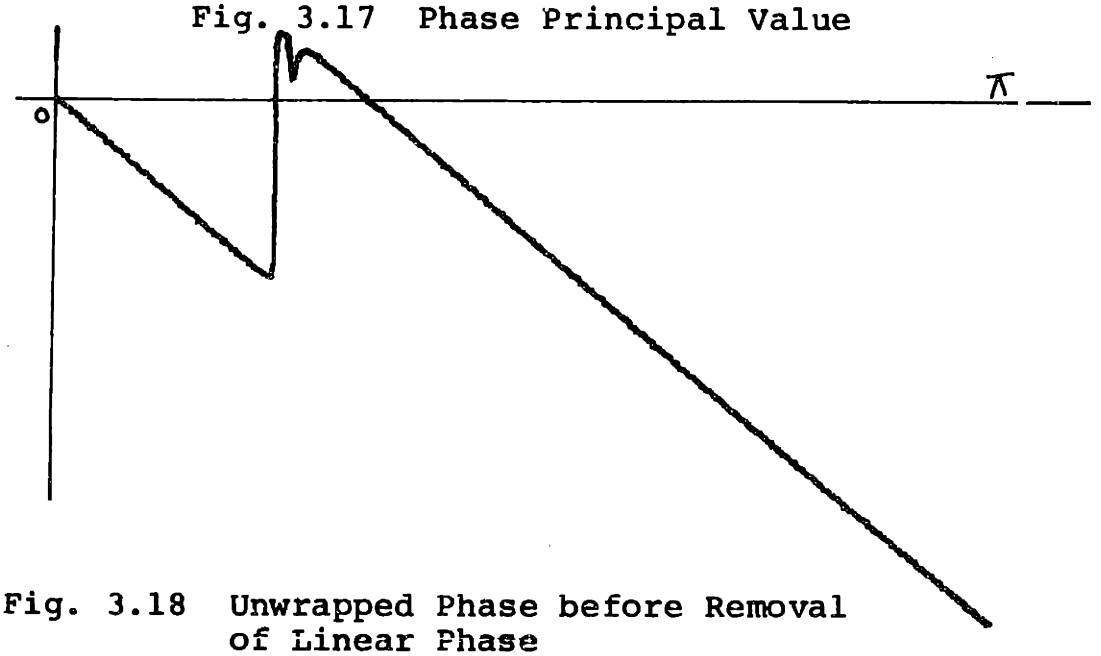

Fig. 3.18 Unwrapped Phase before Removal of Linear Phase

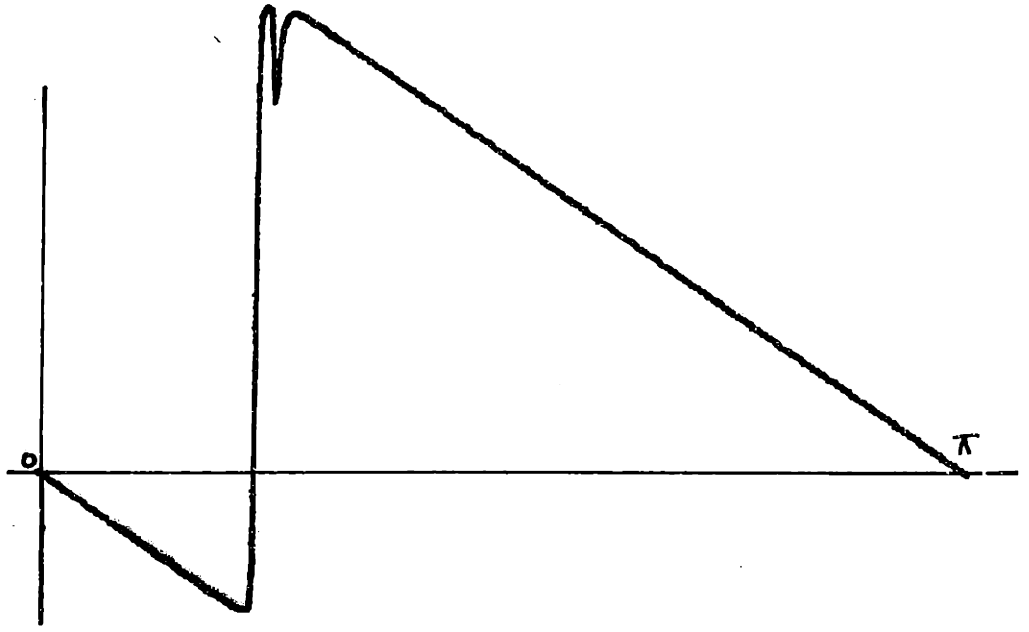

Fig. 3.19 Unwrapped Phase after Removal of Linear Phase

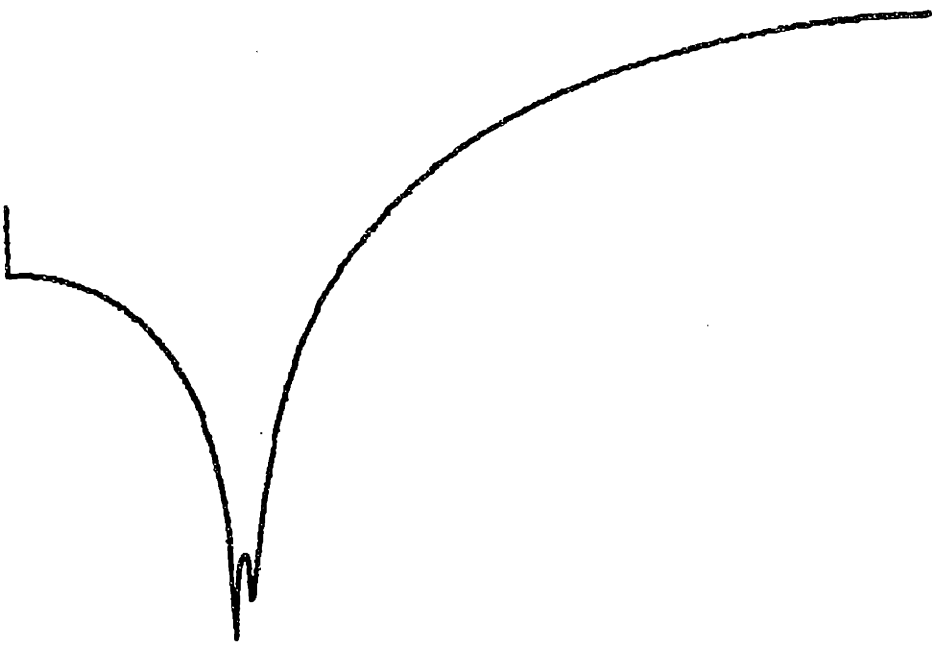

Fig. 3.20 Log Magnitude of the Frequency Response

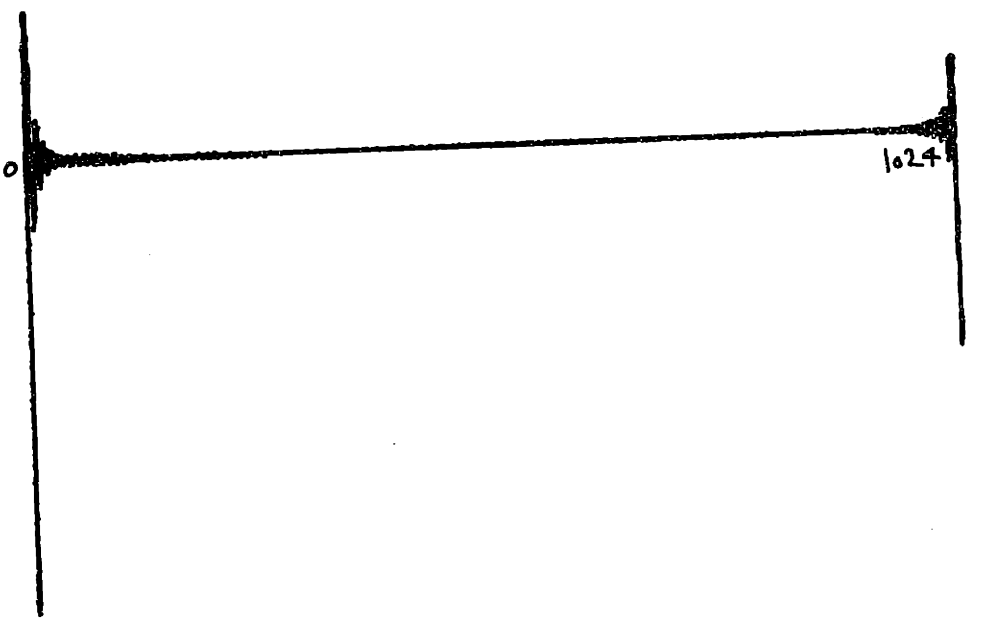

Fig. 3.21 Complex Cepstrum

$$\hat{X}(1) = -2.827298$$

$$\hat{X}(2) = 0.00153$$

$$\hat{X}(3) = 0.94384$$

$$\hat{X}(4) = 0.999934$$

$$\hat{X}(5) = 0.48$$

$$\hat{X}(6) = -0.050$$

$$\vdots$$

and, $\hat{X}[n] = \frac{1}{n}\left[\frac{1}{(z_3)^{-n}} + \frac{1}{(z_3^*)^{-n}}\right] \quad n<0$

$$\hat{X}(-1) = -1.413684$$

$$\hat{X}(-2) = 0.000766$$

$$\hat{X}(-3) = 0.471958$$

$$\hat{X}(-4) = 0.500017150$$

$$\hat{X}(-5) = 0.24116150$$

$$\hat{X}(-6) = -0.0024$$

$$\vdots$$

Now using Table 3.2 we illustrate how the computation of DFT is susceptible to errors when the zeroes are very close to the unit circle and single precision is used. The example considered is shown in Fig. 3.14. We took the 128 pt. FFT. We show the phase derivative and principal value obtained in the neighborhood of $\pi/4$ (17th DFT point) where the complex pair of zeroes occur.

It can be noted from Table 3.2 that in the immediate neighborhood of $\pi/4$, the computation of the DFT in single

DFT Point	Values with Single Precision		Values obtained with a 12 digit accuracy on a HP 9830 calculator	
	Phase Der.	Phase Principal val.	Phase Der.	Phase Principal val.
14	-2.989718	-1.912977	-2.999536	-1.914346
15	-2.972331	-2.056977	-2.998973	-2.061574
16	-2.859446	-2.175950	-2.9960430	-2.208737
17	-0.9343479	-0.2880554	-1022.008	1.239700
18	-2.421185	0.6192901	-2.996019	0.637929
19	-1.813523	0.4890796	-2.998962	0.490767
20	-2.946232	0.3432840	-2.999553	0.343539
21	-2.994130	0.1962455	-2.999735	0.196294

Table 3.2
Susceptibility of the DFT Computation to Errors

precision is susceptible to errors and because of this the phase unwrapping may not be correct, so we need double precision for the values mentioned in the earlier section, while adaption is needed.

Now we present an example in which if we don't use double precision for the computation at intermediate frequencies, then the phase unwrapping breaks down.

Example 3.3 - The real speech example used to illustrate the need for double precision is shown in Fig. 3.22. The sequence length is 200 and the FFT size is 1024. The incre-

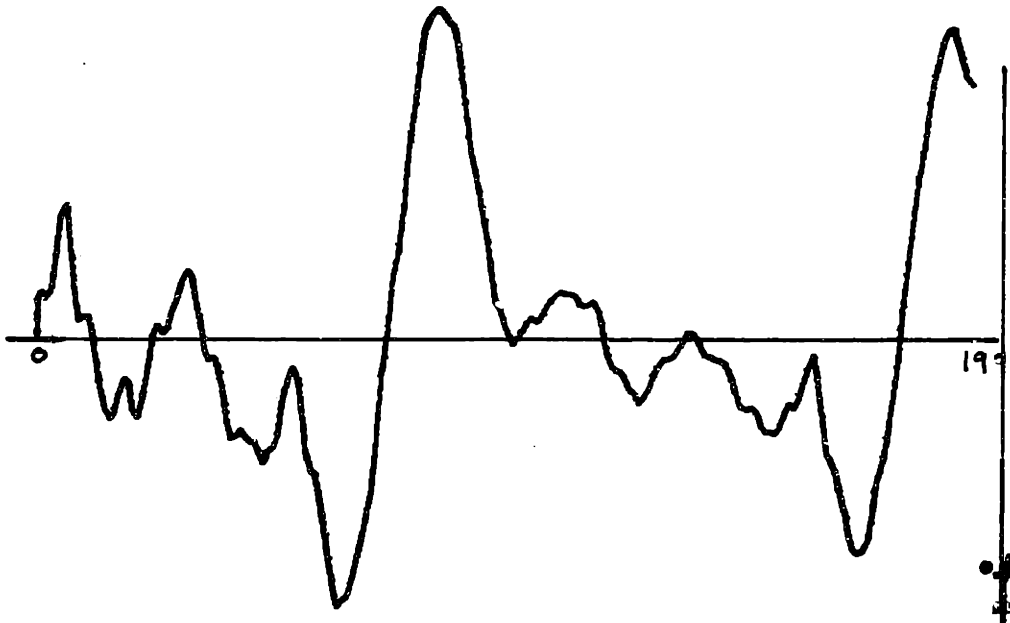

Fig. 3.22 Real Speech Signal

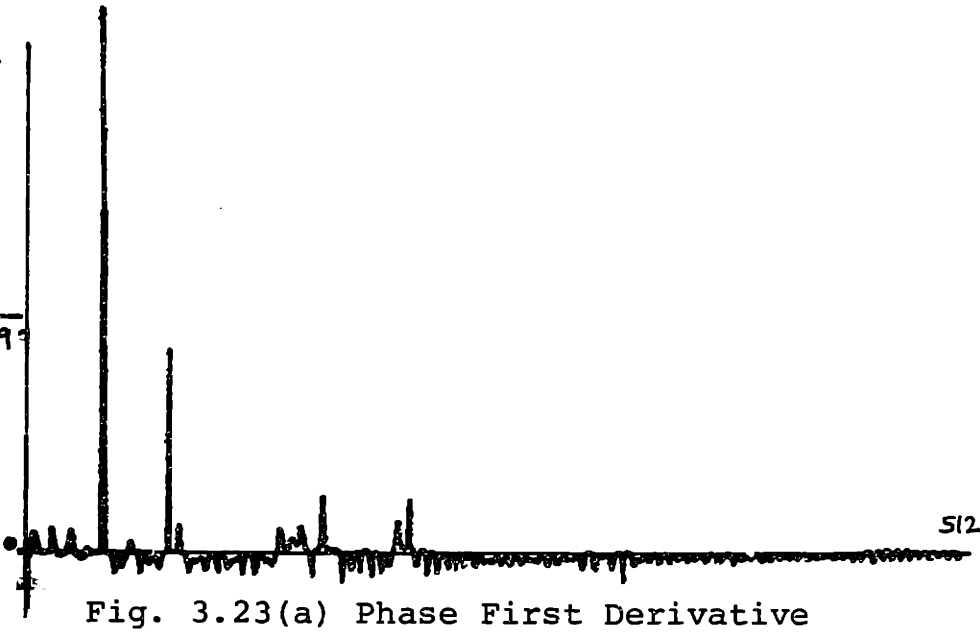

Fig. 3.23(a) Phase First Derivative

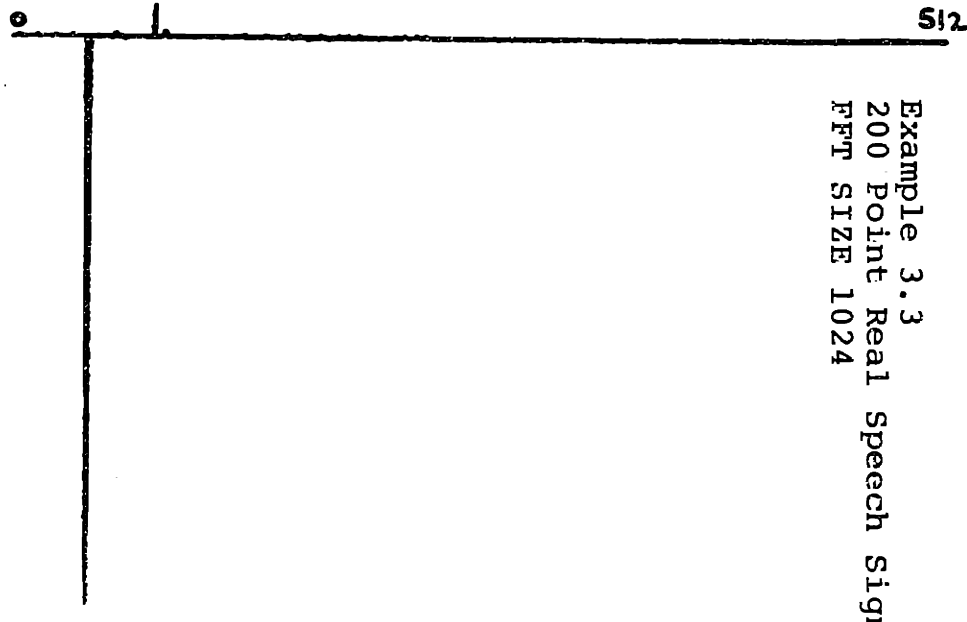

Fig. 3.23(b) Phase Second Derivative

Example 3.3
200 Point Real Speech Signal
FFT SIZE 1024

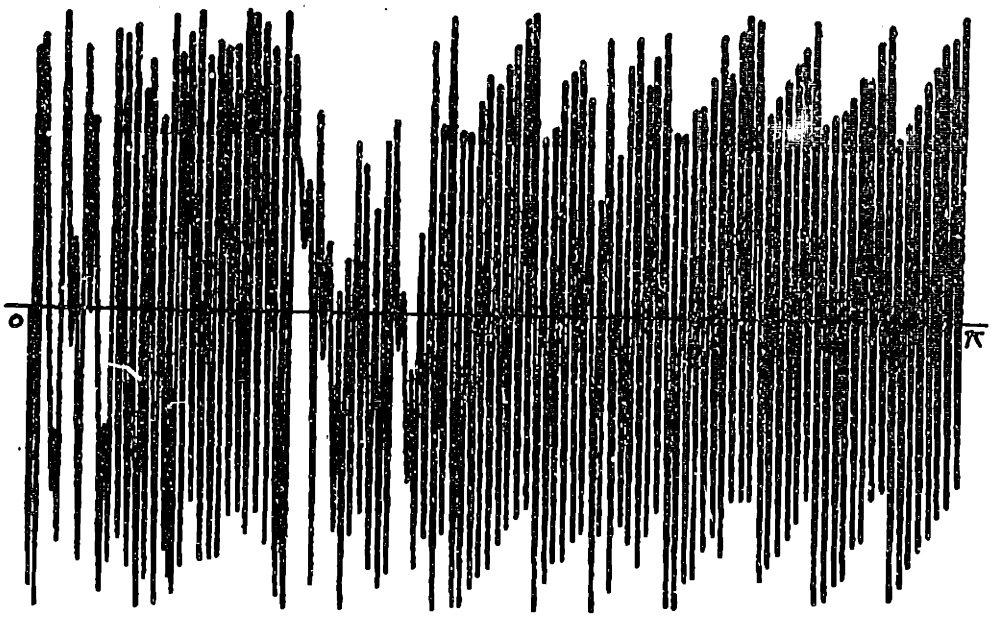

Phase Principal Value

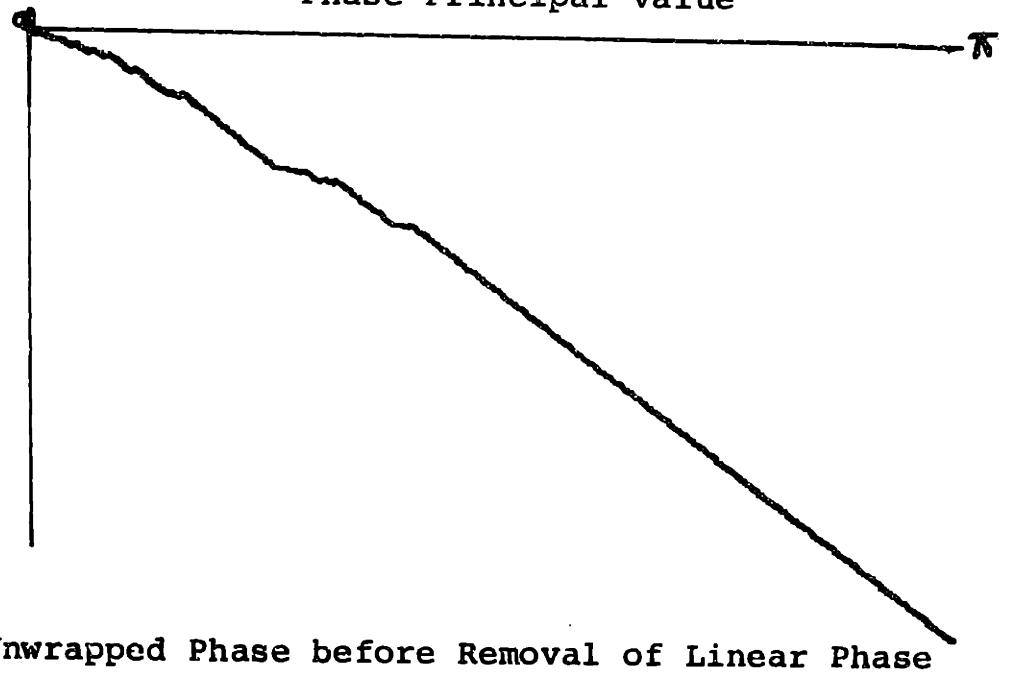

Unwrapped Phase before Removal of Linear Phase

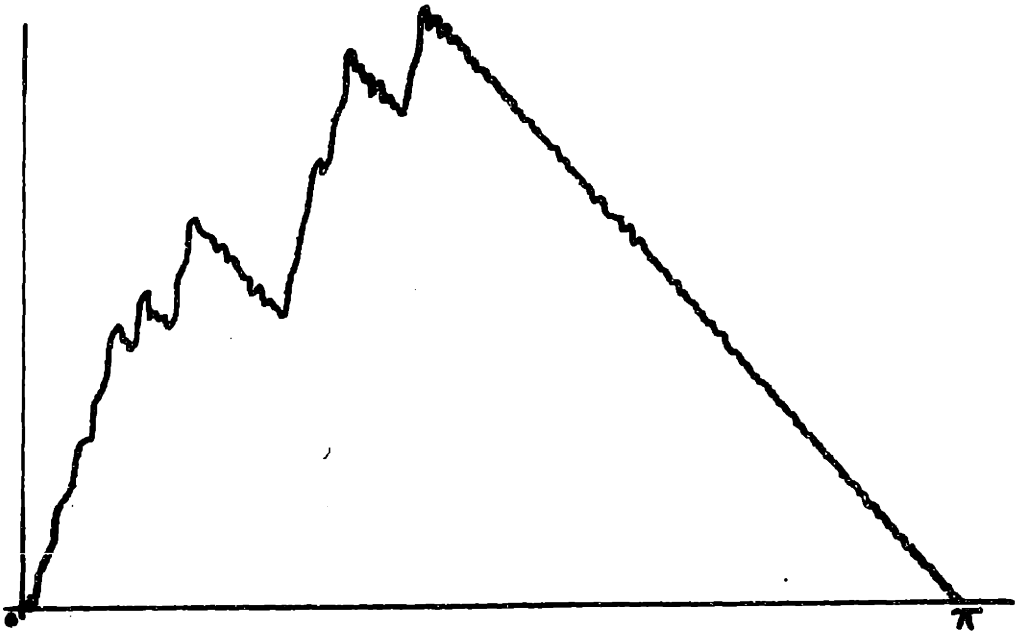

Unwrapped Phase after Removal of Linear Phase

Fig. 3.24

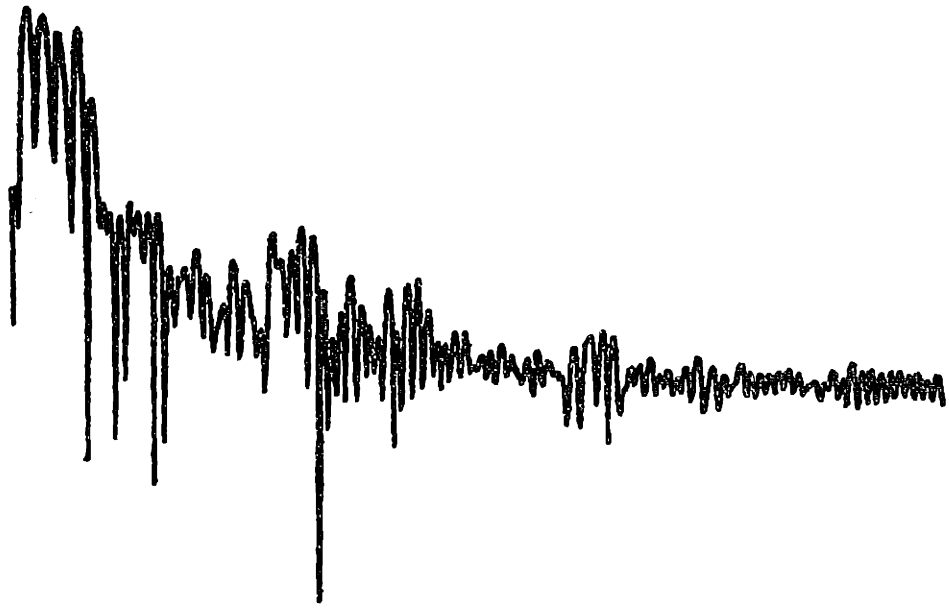

Fig. 3.25 Log Magnitude of the Frequency Response

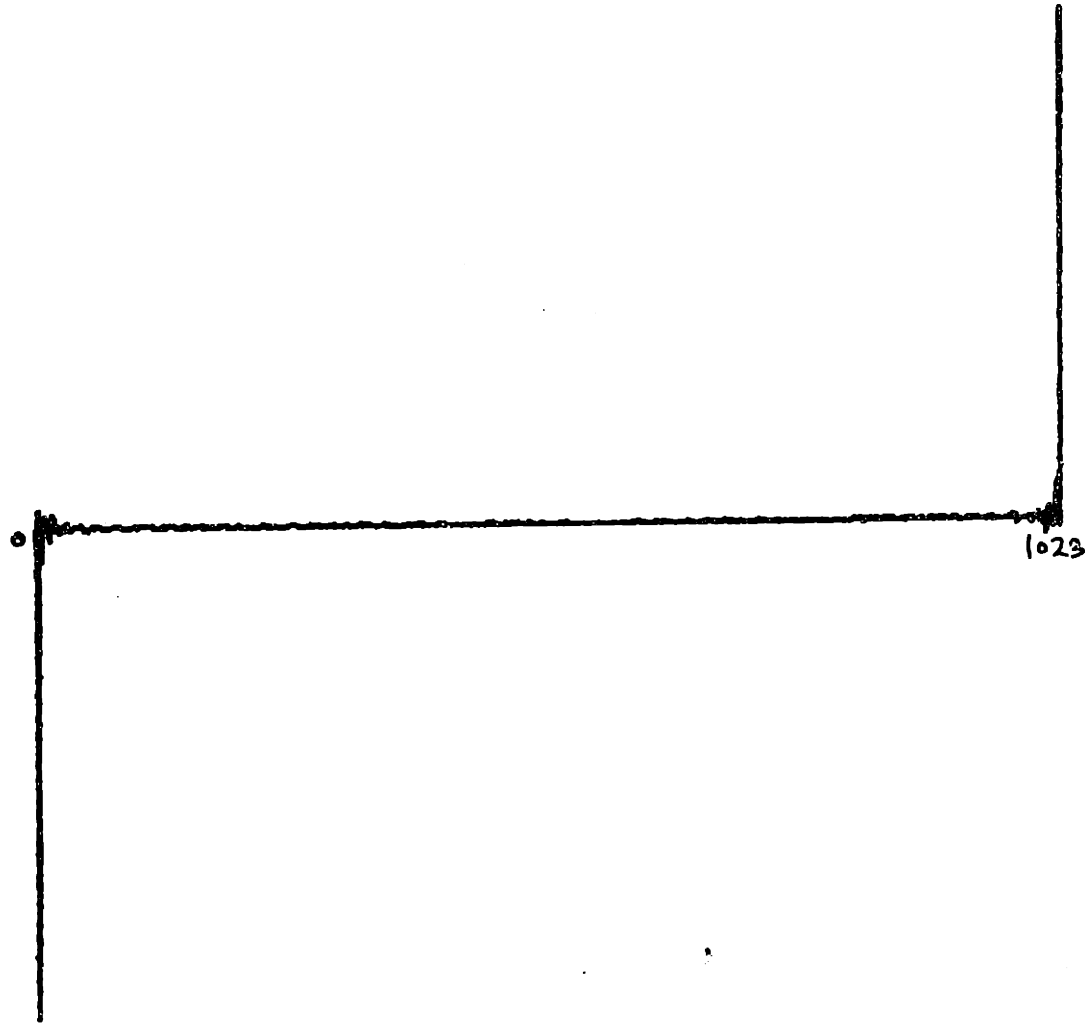

Fig. 3.26 Complex Cepstrum

ment and consistency thresholds were 2.5 and 1.5, respectively. Fig. 3.23 shows the phase 1st & 2nd derivatives. Fig. 3.25 shows the log magnitude of the frequency response. Fig. 3.24 shows the principal value and the unwrapped phase before and after the removal of the linear phase. Finally Fig. 3.26 shows the complex cepstrum.

Table 3.3 shows the values of phase derivative and principal values obtained with and without using double precision.

	Double Precision		Single Precision	
	Phase Der.	Phase Principal Val.	Phase Der.	Phase Principal Val.
I=170	- 99.35	-2.2827	- 99.35	-2.2827
K=2049	-105.777	0.533904	-105.776	0.533885
1025	-105.349	0.695856	-105.346	0.695842
513	-104.687	0.776484	-104.676	0.776464
257	- 97.402	0.816018	96.997	0.815943
129	- 23.843	-0.230057	- 19.312	-0.230037
193	- 39.72	0.823937	- 38.490	0.823888
161	24556.11	0.768034	26378.48	0.7639676
145	260.846	-2.298963	263.361	-2.29887
153	1791.73	-2.290237	1838.64	-2.28965
157	14372.07	-2.259461	14331.08	-2.258796
159	897333.6	-1.911259	669723.1	-1.96540
160	---	---	150562.2	0.670899
I=171	-106.587	.208161	---	---

Table 3.3

From the Table 3.3 it can be observed that when the frequency spacing becomes very small, double precision helps. In this table I corresponds to the DFT point and K corresponds to the division of the frequency spacing between I = 170 and 171. For example, K = 2049 means we are at the midpoint of the interval. Details about K can be seen in [2].

Now finally we present an example which illustrates the linear phase computation.

Example 3.4 - Consider a complex pair of zeroes located at $\pm\pi/4$ as shown in Fig. 3.27

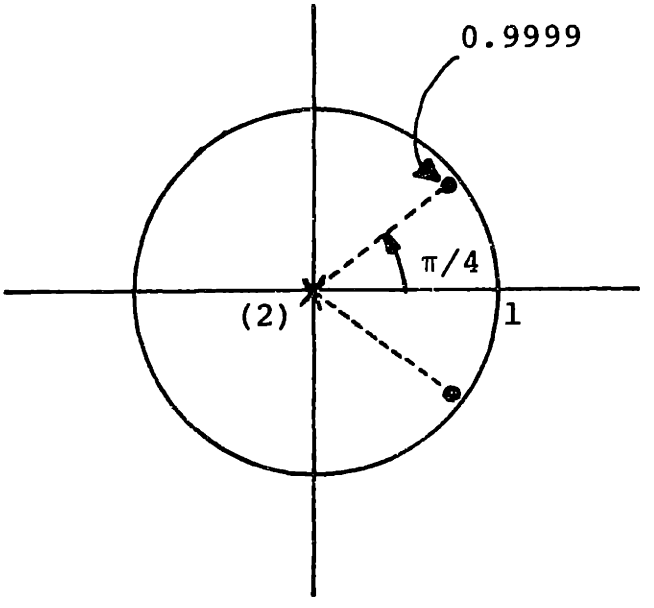

Fig. 3.27

An FFT size of 32 was used with increment and consistency thresholds of 2.5 and 1.5. The linear phase estimated by Tribolet's algorithm was found to be -122.5, which is com-

pletely unrealistic and because of this incorrect estimate adaption was required 1001 times. However, we note that the linear phase estimate is greater than the length of the sequence which is 3. So making use of this fact reduced the number of adaptions to 18.

In this chapter we considered the various issues related to the computation of the one-dimensional complex cepstrum. We have shown that the incorporation of the added features such as using the integration routine obtained from splines consideration, efficient computation of DFT at a single frequency, double precision for certain variables, and linear phase in the phase unwrapping method based on adaptive numerical integration becomes very reliable and more efficient. In the next chapter we discuss the theoretical and practical issues such as the relation between the min. FFT size and closeness to the unit circle, relation between the thresholds of phase unwrapping are thoroughly discussed.

CHAPTER IV

THEORETICAL ISSUES RELATED TO THE COMPUTATION OF ONE DIMENSIONAL COMPLEX CEPSTRUM

IV.1 Introduction

In the last chapter we described the existing methods for phase unwrapping in one dimension and critically examined their shortcomings and relative advantages. We also considered the use of piecewise polynomial interpolation such as spline, Bessel and Hermite interpolation for this purpose. However, the following questions remain unanswered for all these methods of phase unwrapping:

(1) How do we know a priori the minimum FFT size to be used for successful phase unwrapping. In other words we want to know what is that value of maximum frequency spacing which leads to successful phase unwrapping.

(2) How do we choose the increment and consistency threshold for different types of signals such as for speech, seismic, image etc.

(3) How does the minimum FFT size vary for successful phase unwrapping when we move zeroes of the finite length sequence closer to the unit circle.

(4) How much two zeroes inside or outside or one inside and the other outside the unit circle can be close together as well as the extent of their closeness to the unit circle for successful phase unwrapping using real arithmetic

or even using extended precision.

In practice for a given sequence, we select a particular FFT size depending upon the length and type of the signal and the amount of aliasing tolerated. If the phase unwrapping algorithm breaks down because the allocated stack size is not sufficiently large then we use a longer FFT. In this chapter we develop analytical relations in order to answer the above questions in the special case when the location of the zeroes is known. Then we consider the case of arbitrary signals. Examples are presented where we show how the minimum FFT size varies with the location of the zeroes relative to the unit circle and their generalization is suggested.

The way the actual values of the incremental and consistency thresholds are presently taken is arbitrary, but there is a relationship between them for a particular FFT size. The problem with this arbitrary selection is that we may have a particular value of incremental and consistency thresholds that work fine for a certain set of data, whereas they may be quite unreasonable for some other set of data. Also if the values of these thresholds is made too small, the algorithm may break down, and even if it works, it may take a large amount of time. On the other hand if these thresholds are made larger, we may not be sure about the computed values of the unwrapped phase. The approach discussed here makes it possible to know the values of these thresholds and to select their values in relation with each other.

IV.2 Integral Relations for the Exact Computation of Unwrapped Phase

In this section we derive the exact formulae for the unwrapped phase in the case of a real zero and for the case of a complex pair of zeroes. These two relations allow us to compute theoretically (as opposed to using the phase unwrapping algorithms) the unwrapped phase for any given combination of real or complex pair of zeroes. It is to be noted that we are carrying out our present discussion in terms of zeroes, because for a finite length sequence all the poles are located at the center of the unit circle.

There are two methods to obtain the required relationships. In the first method we obtain the results geometrically. This, however, has certain limitations. In the other method we actually integrate the phase derivative.

Case 1 Real Zero

Fig. 4.1 shows the sequence for a real zero and the corresponding pole-zero plot.

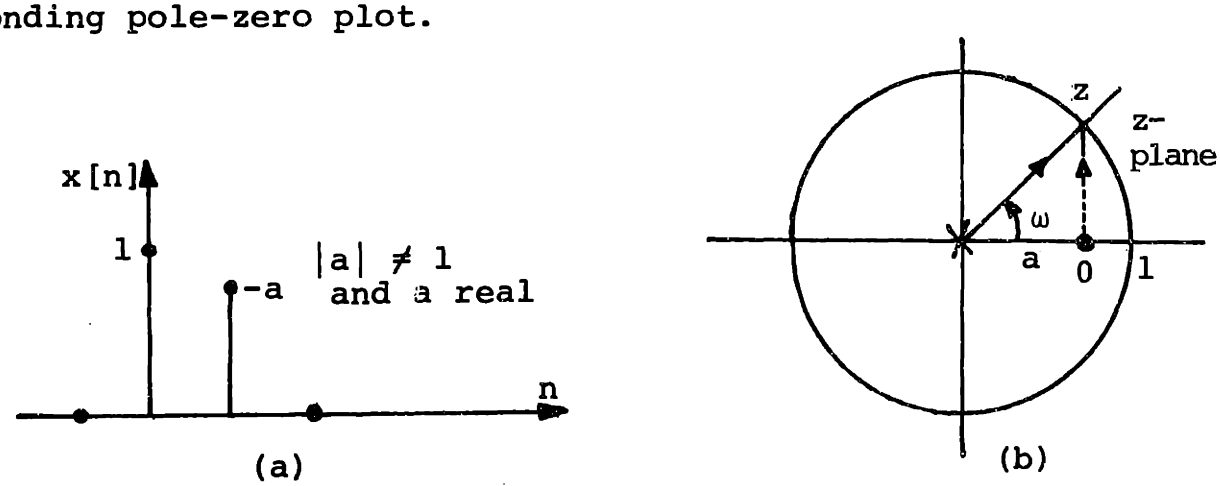

Fig. 4.1 Two Point Sequence and Its Pole-Zero Plot

From the pole-zero plot shown in Fig. 4.1(b) it is easy to obtain the unwrapped phase using geometry as

$$\arg\,[X(e^{j\omega})] = -\omega + \tan^{-1}\left[\frac{\sin\omega}{-a+\cos\omega}\right] \qquad (4.1)$$

In the above expression $-\pi < \tan^{-1}[\cdot] \leq \pi$ depending on the sign of the numerator and denominator. However, this expression cannot be used for all values of a without some restrictions. Specifically, for $a > 1$ evaluating eq. (4.1) for $\omega = 0$ and $\omega = \pi$, we get

$$\arg\left[X(e^{j\omega})\Big|_{\omega=0}\right] = 0 + \pi = \pi$$

and

$$\arg\left[X(e^{j\omega})\Big|_{\omega=\pi}\right] = -\pi + \pi = 0$$

which is contrary to our requirements,

$$\arg\left[X(e^{j\omega})\Big|_{\omega=0}\right] = 0$$

and

$$\arg\left[X(e^{j\omega})\Big|_{\omega=\pi}\right] = -\pi$$

giving a linear phase of -1. So eq. (4.1) cannot be used as a general formula for all values of a.

In the second method we obtain the unwrapped phase using integration. The unwrapped phase has been defined as the integral of phase derivative, i.e.,

$$\arg\left[X(e^{j\omega_1})\right] = \int_0^{\omega_1} [\arg' [X(e^{j\omega})]\, d\omega \qquad (4.2a)$$

and

$$\arg\left[X(e^{j\omega})\Big|_{\omega=0}\right] = 0 \qquad (4.2b)$$

to ensure that arg $[X(e^{j\omega})]$ is an odd and continuous function of ω. The z-transform of the signal shown in Fig. 4.1(a) is,

$$X(z) = 1-az^{-1} \qquad (4.3)$$

or the Fourier transform,

$$X(e^{j\omega}) = X(z)\Big|_{z=e^{j\omega}} = 1-ae^{-j\omega}$$

or,

$$X(e^{j\omega}) = 1 - a\cos\omega + ja\sin\omega \qquad (4.4a)$$

The Fourier transform of the signal nx[n] is,

$$X_1(e^{j\omega}) = -a\cos\omega + ja\sin\omega \qquad (4.4b)$$

From eq. (2.13) the phase derivative, is

$$\arg' [X(e^{j\omega})] = - \frac{Re(F.T.x[n]) \cdot Re(F.T.nx[n]) + Im(F.T.x[n]) \cdot Im(F.T.nx[n])}{[Re(F.T.x[n])]^2 + [Im(F.T.x[n])]^2} \tag{4.5a}$$

$$= - \frac{(1 - a \cos \omega)(-a \cos \omega) + a^2 \sin^2 \omega}{(1 - a \cos \omega)^2 + a^2 \sin^2 \omega} \tag{4.5b}$$

Simplifying, we get,

$$\arg' [X(e^{j\omega})] = \frac{a \cos \omega - a^2}{(1+a^2) - 2a \cos \omega} \tag{4.6}$$

Now using eqs. (4.1) and (4.2), the unwrapped phase at $\omega = \omega_1$ is,

$$\arg [X(e^{j\omega_1})] = \int_0^{\omega_1} \frac{a \cos \omega - a^2}{(1+a^2) - 2a \cos \omega} d\omega \tag{4.7}$$

$$\text{or, } \arg [X(e^{j\omega_1})] = a \int_0^{\omega_1} \frac{\cos \omega \, d\omega}{(1+a^2) - 2a \cos \omega} - a^2 \int_0^{\omega_1} \frac{d\omega}{(1+a^2) - 2a \cos \omega} \tag{4.8}$$

Make use of the following substitution

$$y = \tan \frac{\omega}{2} \tag{4.9}$$

Then
$$d\omega = \frac{2dy}{1+y^2} \tag{4.10}$$

and
$$\cos \omega = \frac{1-y^2}{1+y^2} \tag{4.11}$$

Using eqs. (4.9), (4.10) and (4.11), eq. (4.8) becomes

$$\arg\,[X(e^{j\omega_1})] = 2a \int_0^{\tan\frac{\omega_1}{2}} \frac{(1-y^2)\,dy}{(1+y^2)\,[(1+y^2)(1+a^2)-2a(1-y^2)]}$$

$$- 2a^2 \int_0^{\tan\frac{\omega_1}{2}} \frac{dy}{(1+a^2)(1+y^2)-2a(1-y^2)}$$

After making partial fractions and simplifying, the above expression can be written as

$$\arg\,[X(e^{j\omega_1})] = 2a \int_0^{\tan\frac{\omega_1}{2}} \frac{\frac{(1+a^2)}{2a}\,dy}{(1-a)^2+(1+a)^2y^2} - \int_0^{\tan\frac{\omega_1}{2}} \frac{dy}{1+y^2}$$

$$- 2a^2 \int_0^{\tan\frac{\omega_1}{2}} \frac{dy}{(1-a)^2+(1+a)^2y^2}$$

$$= (1-a^2) \int_0^{\tan\frac{\omega_1}{2}} \frac{dy}{(1-a)^2+(1+a)^2y^2} - \int_0^{\tan\frac{\omega_1}{2}} \frac{dy}{1+y^2}$$

$$= \frac{1-a^2}{(1+a)^2} \int_0^{\tan\frac{\omega_1}{2}} \frac{dy}{\left(\frac{1-a}{1+a}\right)^2+y^2} - \int_0^{\tan\frac{\omega_1}{2}} \frac{dy}{1+y^2}$$

Now using standard integral formulae, we get

$$\arg\,[X(e^{j\omega_1})] = \left[\tan^{-1}\,(\tfrac{1+a}{1-a})y\right]_0^{\tan\frac{\omega_1}{2}} - \left[\tan^{-1}\,y\right]_0^{\tan\frac{\omega_1}{2}}$$

$$= \tan^{-1}\left[(\tfrac{1+a}{1-a})\,\tan\tfrac{\omega_1}{2}\right] - \tan^{-1}\left[\tan\tfrac{\omega_1}{2}\right]$$

or, $$\arg\,[X(e^{j\omega_1}) = -\tfrac{\omega_1}{2} + \tan^{-1}\left[(\tfrac{1+a}{1-a})\,\tan\tfrac{\omega_1}{2}\right] \qquad (4.12)$$

or, in general

$$\arg\,[X(e^{j\omega})] = -\tfrac{\omega}{2} + \tan^{-1}\left[(\tfrac{1+a}{1-a})\,\tan\tfrac{\omega}{2}\right] \qquad (4.13)$$

If a > 1, then the two point sequence shown in Fig. 4.1 is maximum phase and we expect a linear phase of -1. Evaluating eq. (4.13) we see that

$$\arg\,[X(e^{j\omega})]\Big|_{\omega=\pi} = -\tfrac{\omega}{2} + \tan^{-1}[-\infty] = -\tfrac{\pi}{2} - \tfrac{\pi}{2} = -\pi,$$

which gives a linear phase of -1.

Thus eq. (4.13) allows us to compute the unwrapped phase in the case of a single real zero for all values of a. Now we are interested in the case of a complex pair of zeroes.

Case 2 Complex Pair of Zeroes

Fig. 4.2 shows a sequence for the complex pair of zeroes and corresponding pole-zero plot.

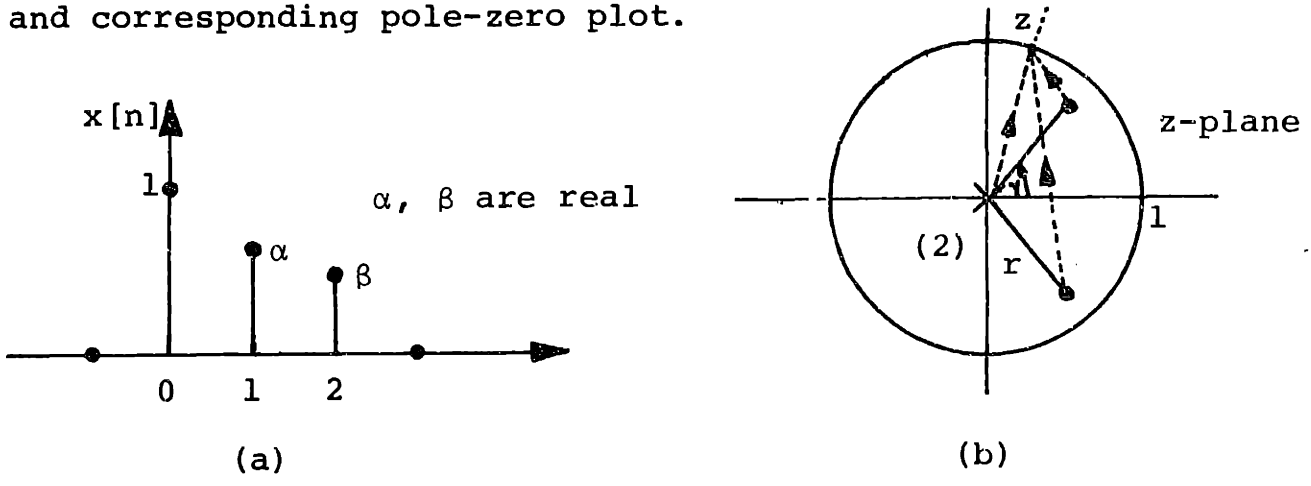

Fig. 4.2 Three Point Sequence and Its Pole-Zero Plot

Using geometry shown in 4.2(b) the unwrapped phase can be easily obtained as,

$$\arg\,[X(e^{j\omega})] = -2\omega + \tan^{-1}\left[\frac{\sin\omega - r\sin\gamma}{-r\cos\gamma + \cos\omega}\right]$$

$$+ \tan^{-1}\left[\frac{\sin\omega + r\sin\gamma}{-r\cos\gamma + \cos\omega}\right] \qquad (4.14)$$

However, for the reasons similar to those mentioned before while deriving the expression for unwrapped phase using Fig. 4.1(b), the eq. (4.14) cannot be used as a general formula for the unwrapped phase for a complex pair of zeroes. So we use integration.

The z-transform of the signal shown in Fig. 5.2(a) is

$$X(z) = 1 + \alpha z^{-1} + \beta z^{-2}$$

and the Fourier transform,

$$X(e^{j\omega}) = X(z)\Big|_{z=e^{j\omega}} = 1 + \alpha e^{-j\omega} + \beta e^{-j\,2\omega}$$

or, $X(e^{j\omega}) = 1 + \alpha \cos \omega + \beta \cos 2\omega - j[\alpha \sin \omega + \beta \sin 2\omega]$

The Fourier transform of the sequence $nx[n]$ is

$$X_1(e^{j\omega}) = \alpha \cos \omega + \beta \cos 2\omega - j[\alpha \sin \omega + \beta \sin 2\omega]$$

The phase derivative is given by

$$\arg' [X(e^{j\omega})] = \frac{-[\alpha^2+2\beta^2+\alpha(1+3\beta) \cos \omega + 2\beta \cos 2\omega]}{(1-\beta)^2+\alpha^2+2\alpha(1+\beta) \cos \omega + 4\beta \cos^2 \omega}$$

Therefore, unwrapped phase at $\omega = \omega_1$ is

$$\arg [X(e^{j\omega_1})] = -\int_0^{\omega_1} \frac{[\alpha^2+2\beta^2+\alpha(1+3\beta) \cos \omega + 2\beta \cos 2\omega]}{(1-\beta)^2+\alpha^2+2\alpha(1+\beta) \cos \omega + 4\beta \cos^2 \omega} \, d\omega$$

Using the only possible substitution $y = \tan \frac{\omega}{2}$, the evaluation of the above integral in terms of the general notation α and β becomes quite complicated as the integrand involves quartic polynomial in y. Therefore, an alternative idea is used.

Consider the figure shown in 4.3. If we can evaluate

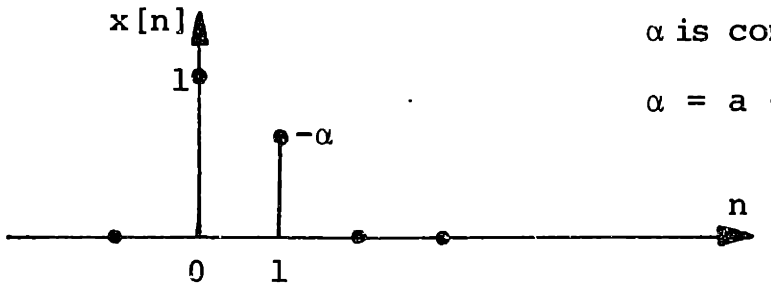

Fig. 4.3 Two Point Complex Sequence

the unwrapped phase for this case, then the unwrapped phase for the complex pair of zeroes can be easily determined. We are interested in the real sequence for which a real cepstrum exists and for which all complex zeroes must occur in conjugate pairs.

Looking at Fig. 4.3 it may appear that if α is complex then we may substitute α for a in eq. (4.13) to get the unwrapped phase in this case since arctan of a complex number is a well defined operation in terms of complex log which however, is multivalued. But it is to be noted that the expression for the phase derivative of the signal in Fig. 4.3 cannot be obtained just by replacing a by its complex value in eq. (4.5b) since its derivation involves the separation of real and imaginary parts.

Now considering the signal of Fig. 4.3, we find that the phase derivative of the signal is

$$\arg' [X(e^{j\omega})] = \frac{-(a^2+b^2)+a\cos\omega + b\sin\omega}{1+a^2+b^2-2a\cos\omega - 2b\sin\omega}$$

So, the unwrapped phase at $\omega = \omega_1$ is

$$\arg\,[X(e^{j\omega_1})] = \int_0^{\omega_1} \frac{-(a^2+b^2)+a\cos\omega + b\sin\omega}{1+a^2+b^2-2a\cos\omega - 2b\sin\omega} \qquad (4.15)$$

The evaluation of eq. (4.15) is somewhat complicated and its proof is given in Appendix A. The integral of eq. (4.15) or the unwrapped phase is given by

$$\arg\,[X(e^{j\omega_1})] = \frac{-\omega_1}{2} - \tan^{-1}\left(\frac{-2b+[(1+a)^2+b^2]\tan\frac{\omega_1}{2}}{a^2+b^2-1}\right)$$

$$+ \tan^{-1}\left(\frac{-2b}{a^2+b^2-1}\right),\quad a^2+b^2 \neq 1 \qquad (4.16)$$

and, therefore, for a complex pair of zeroes at $a \pm jb$, the unwrapped phase in general is given by

$$\arg_c\,[X(e^{j\omega})] = -\omega - \tan^{-1}\left(\frac{-2b+[(1+a)^2+b^2]\tan\frac{\omega}{2}}{a^2+b^2-1}\right)$$

$$- \tan^{-1}\left(\frac{2b+[(1+a)^2+b^2]\tan\frac{\omega}{2}}{a^2+b^2-1}\right)$$

$$a^2+b^2 \neq 1 \qquad (4.17)$$

When $\omega = \pi$ and complex zero pair lies inside the unit circle ($a^2+b^2 < 1$), then

$$\arg_c [X(e^{j\omega})]\Big|_{\omega=\pi} = -\pi - \tan^{-1}[-\infty] - \tan^{-1}[-\infty]$$

$$= -\pi + \frac{\pi}{2} + \frac{\pi}{2} = 0$$

and, when the complex zero pair lies outside the unit circle ($a^2+b^2 > 1$), then

$$\arg_c [X(e^{j\omega})]\Big|_{\omega=\pi} = -\pi - \tan^{-1}[\infty] - \tan^{-1}[\infty]$$

$$= -\pi - \frac{\pi}{2} - \frac{\pi}{2} = -2\pi$$

so then the value of linar phase is -2 as expected as two zeroes lie outside the unit circle.

Eqs. (4.13) and (4.17) represent the unwrapped phase for the case of a real and a complex pair of zeroes respectively. These two equations can be used to compute the unwrapped phase for any given combination of simple and complex pairs of zeroes. The total unwrapped phase will be the sum of unwrapped phase for each simple and complex pair of zeroes. It should be noted that eqs. (4.13) and (4.17) are the result of a definite integral and the value of arctan in these equations will always be between $\pm\frac{\pi}{2}$.

IV.3 Analysis of Unwrapped Phase

In this section we present an approach which may be useful to answer the various questions related to phase unwrapping mentioned at the beginning of this chapter. We restrict ourselves to the special case in which the zeroes of the finite length sequence under consideration are known a priori. In the following section we make a generalization of these results.

Approach

From the given pole-zero plot, we determine the sequence. Having obtained the phase derivative of the signal, we consider the following question.

Given analytic expression of the phase derivative, what should be the maximum value of frequency spacing $\Delta\omega$ (which corresponds to the minimum size of FFT to be used) such that the following two constraints are satisfied.

(1) The approximate area between the two sampling points given by

$$\frac{\Delta\omega_i}{2}\left[\arg'\,[X(e^{j\omega_{i+1}})] + \arg'\,[X(e^{j\omega_i})]\right]$$

$$-\frac{(\Delta\omega_i)^2}{12}\left[\arg''\,[X(e^{j\omega_{i+1}})] - \arg''\,[X(e^{j\omega_i})]\right] \qquad (4.18)$$

be less than or equal to a certain threshold θ_1, called the incremental threshold. It is to be noted

here that we are using the integration rule obtained from spline interpolation.

(2) The value of the approximated integral differs from the true value by less than a certain threshold θ_2, called the consistency threshold (Fig. 4.4), i.e.,

$$\left.\begin{aligned} A3 &= |A1 - \arg_a [X(e^{j\omega_{i+1}})]| \leqslant \theta_2 \\ \text{or} \\ A4 &= |A2 - \arg_a [X(e^{j\omega_{i+1}})]| \leqslant \theta_2 \end{aligned}\right\} \qquad (4.19)$$

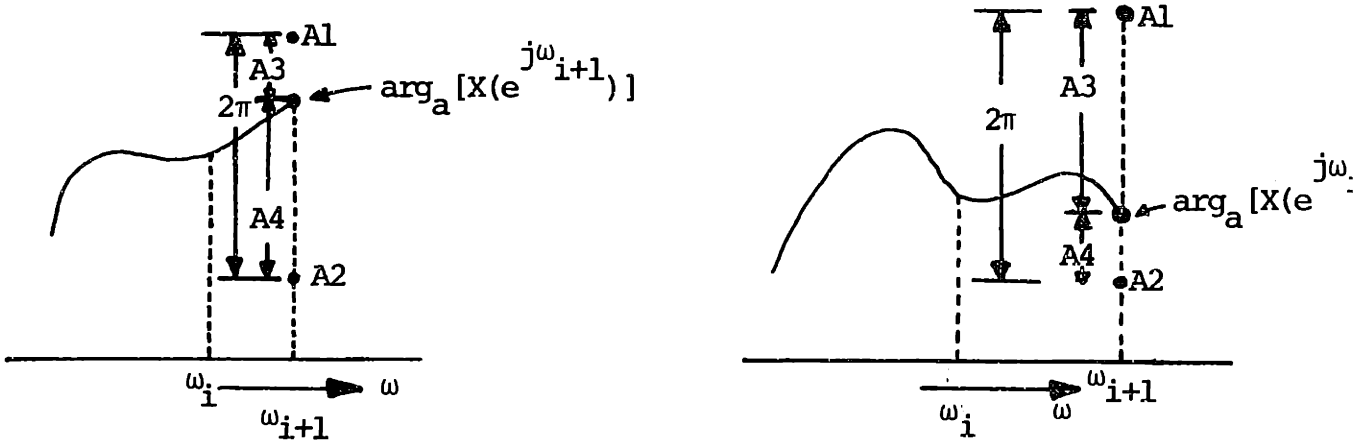

(a) A3 < A4 (b) A3 > A4

Fig. 4.4 Illustration of Consistency Criterion

where

$\Delta\omega_i = \omega_{i+1} - \omega_i$, frequency spacing in radians between the two samples of phase derivative.

$$A1 = \text{IFIX}\left[\frac{\arg_a[X(e^{j\omega_{i+1}})]-\text{ARG}[X(e^{j\omega_{i+1}})]}{2\pi}\right] \cdot 2\pi + \text{ARG}\,[X(e^{j\omega_{i+1}})] \tag{4.20}$$

IFIX[x] = (sign of x) · M, where M is the largest integer $\leq |x|$.

$$A2 = A1 + 2\pi \cdot \text{Sgn}\ \frac{\arg_a[X(e^{j\omega_{i+1}})]-\text{ARG}[X(e^{j\omega_{i+1}})}{2\pi} \tag{4.21}$$

$$\text{Sgn}\ (x) = 1,\ x \geq 0$$

$$= -1,\ x < 0$$

$\arg'\,[X(e^{j\omega_{i+1}})]$ = Phase derivative of the given signal at ω_{i+1}

$\arg'\,[X(e^{j\omega_i})]$ = Phase derivative of the given signal at ω_i

$\arg''\,[X(e^{j\omega_{i+1}})]$ = Phase second derivative of the given signal at ω_{i+1}

$\arg''\,[X(e^{j\omega_i})]$ = Phase second derivative of the given signal at ω_i

$\text{ARG}\ [X(e^{j\omega_{i+1}})]$ = Principal value of $X(e^{j\omega})$ at $\omega = \omega_{i+1}$ and such that $-\pi < \text{ARG}\ [X(e^{j\omega_{i+1}})] \leq \pi$.

$\arg_a [X(e^{j\omega_{i+1}})]$ = Exact value of the unwrapped phase up to ω_i + approximated phase increment between ω_i and ω_{i+1} given by eq. (4.18).

By the exact value above we mean that the phase unwrapping has been done successfully up to $\omega = \omega_i$. Also we mention that in the course of finding the maximum value of frequency spacing $\Delta\omega$, we shall also be answering some of the questions posed at the beginning of this chapter.

Before we delve into more details, we want to make the second constraint more clear.

By definition the complex log is

$$\log X(e^{j\omega_{i+1}}) = \log |X(e^{j\omega_{i+1}})| + j \arg [X(e^{j\omega_{i+1}})] \quad (4.22)$$

$$\text{or, } \log [X(e^{j\omega_{i+1}})] = \log |X(e^{j\omega_{i+1}})| + j [\text{ARG } (X(e^{j\omega_{i+1}}) + 2\pi k] \quad (4.23)$$

where k is an integer.

As we have mentioned the whole problem of phase unwrapping is to find the right value of k in eq. (4.23) so that the complex log can be unambiguously defined and be made continuous.

Let k_a = an integer which is within ±1 of the integer k and is obtained as (referring to eqs. 4.22 and 4.23),

$$k_a = \text{IFIX}\left\{\frac{\arg_a\,[X(e^{j\omega_{i+1}})] - \text{ARG}\,[X(e^{j\omega_{i+1}})]}{2\pi}\right\}$$

So the exact value of the unwrapped phase,

$$\arg_e\,[X(e^{j\omega_{i+1}})] = \begin{cases} \text{ARG}\,[X(e^{j\omega_{i+1}})] + k_a \cdot 2\pi = A1 \\ \\ A1 + 2\pi \cdot \text{Sgn}\,[k_a] = A2 \end{cases}$$

depending upon whether A3 = |A1 - P| or A4 = |A2 - P| is smaller, i.e., the integrated value which lies between A1 and A2 is within θ_2 to either A1 or A2. Fig. 4.4 illustrates the two possible cases, A3 < A4 or A3 > A4.

Now we give examples, one is for the case of a real zero and the other one is for a complex pair of zeroes. These two will allow us to formalize the procedure in general for finding the maximum value of frequency spacing or the minimum FFT size needed for successful phase unwrapping for a finite length sequence which may have any combination of zeroes.

Example 4.1 Real Zero Case

A pole-zero plot is shown in Fig. 4.5(a) and the signal is shown in Fig. 4.5(b).

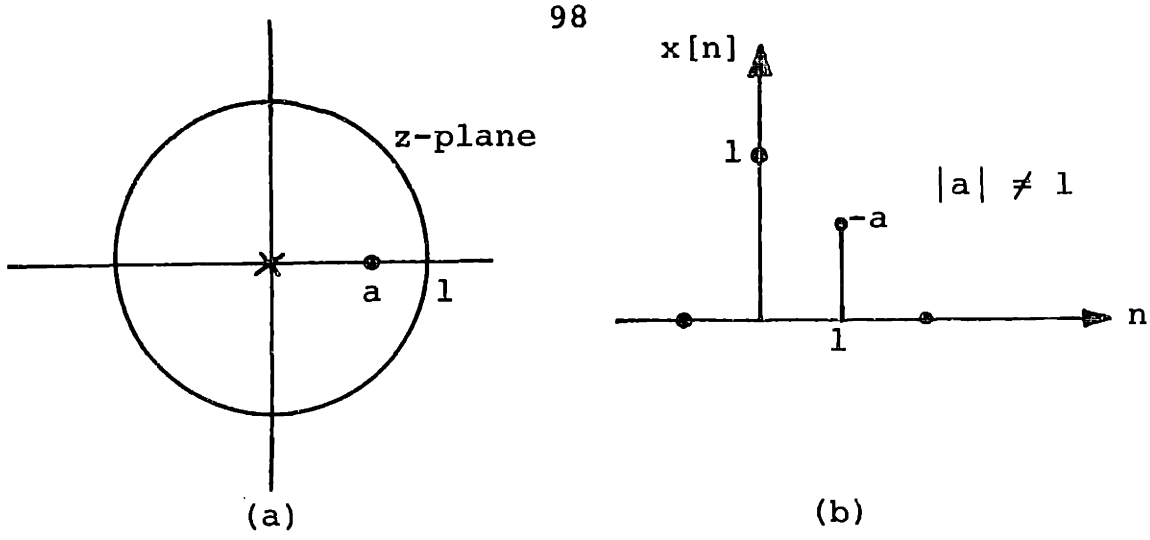

Fig. 4.5 Pole-Zero Plot and Corresponding Sequence for a Real Zero Case

We follow the stepwise procedure given below to answer the various questions related to phase unwrapping in this case.

(a) Obtain the expression for the phase derivative (even, periodic and continuous) of the signal in Fig. 4.5(b).

$$\arg' [X(e^{j\omega})] = \frac{a \cos \omega - a^2}{(1+a^2) - 2a \cos \omega} \qquad (4.24)$$

Obtain the expression for the phase second derivative (odd, periodic and continuous),

$$\arg'' [X(e^{j\omega})] = \frac{d}{d\omega} [\arg' [X(e^{j\omega})]$$

$$= \frac{-a(1-a^2) \sin \omega}{(1+a^2-2a \cos \omega)^2} \qquad (4.25)$$

(b) Obtain the expression for the unwrapped phase,

$$\arg\,[X(e^{j\omega})] = -\frac{\omega}{2} + \tan^{-1}\,[(\frac{1+a}{1-a})\,\tan\frac{\omega}{2}]$$

$$\arg\,[X(e^{j\omega})]\Big|_{\omega=\pi} = \begin{cases} 0, & \text{if } a < 1 \\ -\pi & \text{if } a > 1 \end{cases} \qquad (4.26)$$

(c) Setting the phase second derivative to zero in eq. (4.25), we find that the absolute maxima or minima is going to occur at $\omega = 0$ or $\omega = \pi$. Table 4.1 shows the location and values of maxima and minima for various ranges of a.

Value of a	Location of Max. of Phase Der. in radians	Location of Min. of Phase Der. in radians	Max. Value of Phase Der.	Min. Value of Phase Der.
$0 < a < 1$	0	π	$\frac{a}{1-a}$	$\frac{-a}{1+a}$
$1 < a < \infty$	π	0	$\frac{-a}{1+a}$	$\frac{a}{1-a}$
$-1 < a < 0$	π	0	$\frac{-a}{1+a}$	$\frac{-a}{1-a}$
$-\infty < a < -1$	0	π	$\frac{a}{1-a}$	$\frac{-a}{1+a}$

Table 4.1 Maxima, Minima Values for Real Zero Case

In the illustration presently under investigation we concentrate on the values of a between $0 < a < 1$. The same procedure applies for the other three cases. For $0 < a < 1$, the absolute maxima occurs at $\omega = 0$ and the absolute minima at

$\omega = \pi$. The value of maximum derivative is $\frac{a}{1-a}$ and the value of minimum phase derivative is $\frac{-a}{1+a}$.

(d) Fig. 4.6 shows the phase derivative curves and unwrapped phase curves for several values of a. From this we observe that the maximum area under the peak is in the neighborhood of $\omega = 0$. Referring to eqs. (4.2) and (4.18), the area under $\Delta\omega$ (see Fig. 4.6(a)) is given by

$$\arg_a [X(e^{j\omega})\Big|_{\omega=\Delta\omega}] = \frac{\Delta\omega}{2} [\arg' [X(e^{j\omega})]\Big|_{\omega=0} + \arg' [X(e^{j\omega})]\Big|_{\omega=\Delta\omega}] - \frac{(\Delta\omega)^2}{12} [\arg'' [X(e^{j\omega})]\Big|_{\omega=\Delta\omega} - \arg'' [X(e^{j\omega})\Big|_{\omega=0}] \quad (4.27)$$

Substituting values from eqs. (4.24) and (4.25), we get

$$\arg_a [X(e^{j\omega})\Big|_{\omega=\Delta\omega}] = \frac{\Delta\omega}{2} [\frac{a}{1-a} + (\frac{a\cos\omega - a^2}{1+a^2-2a\cos\omega})\Big|_{\omega=\Delta\omega}] - \frac{(\Delta\omega)^2}{12} [(\frac{-a(1-a^2)\sin\omega}{(1+a^2-2a\cos\omega)^2})\Big|_{\omega=\Delta\omega}] \quad (4.28a)$$

$$\text{ARG } [X(e^{j\omega})\Big|_{\omega=\Delta\omega}] = \text{Principal value of } X(e^{j\omega}) \text{ at } \Delta\omega = \tan^{-1} [\frac{a\sin\omega}{1-a\cos\omega}]\Big|_{\omega=\Delta\omega} \quad (4.28b)$$

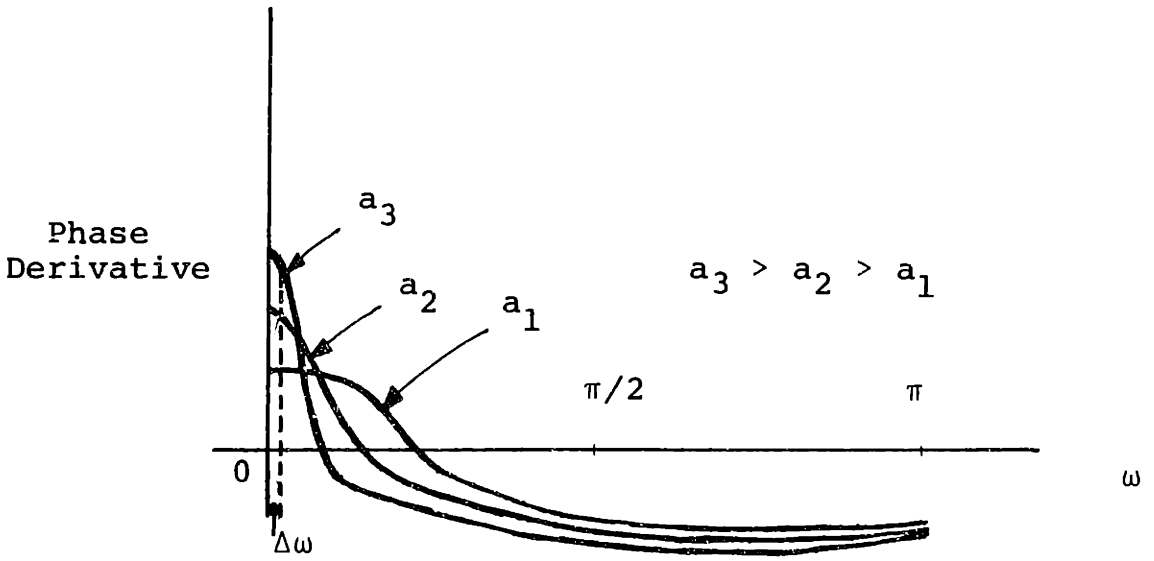

Fig. 4.6(a) Phase Derivative for Several Values of a; a_1, a_2, a_3

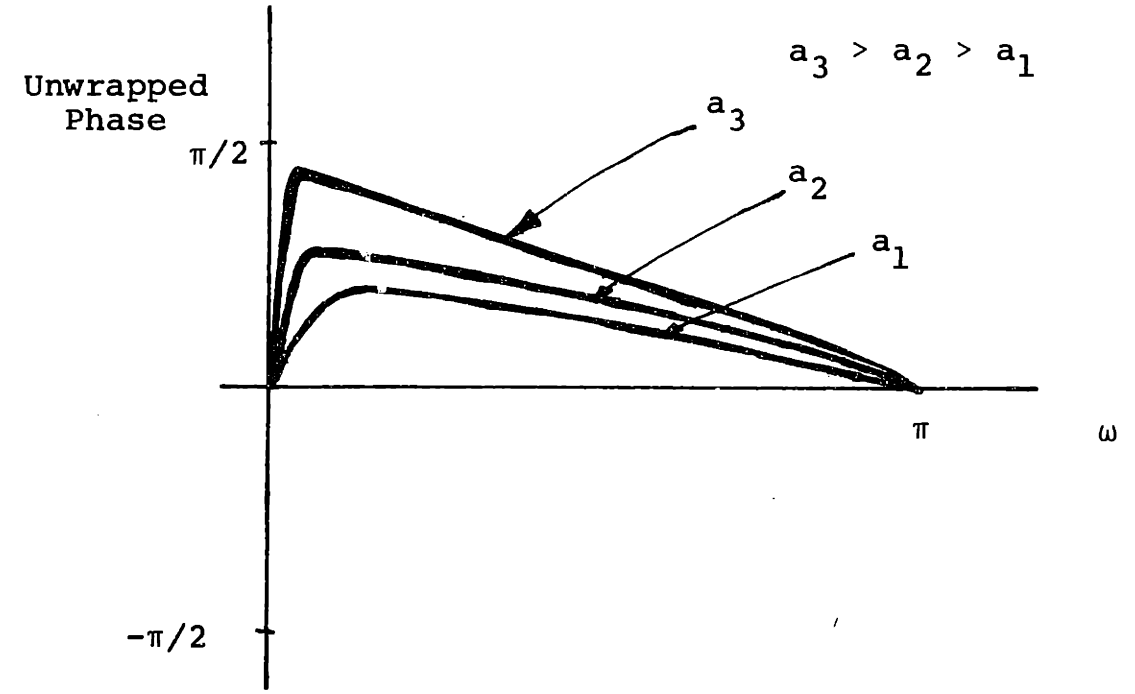

Fig. 4.6(b) Unwrapped Phase for Various Values of a; a_1, a_2, a_3

Now using eqs. (4.19), (4.26) and (4.26) we conducted an experiment in the following way: we selected a particular value of a and found the maximum value of $\Delta\omega$ such that the calculated value of the unwrapped phase obtained after satisfying the consistency criterion matches the theoretical value given by eq. (4.26). This we carried out for values of a from a = 0.05 to 0.999999. These results are shown in Table 4.2.

In Table 4.3 we show the maximum derivative for various values of a and the product of $\Delta\omega_{max}$ and maximum derivative which helps to find the value of the incremental threshold. Also in this table we show the minimum FFT size needed, when the real zero is located at a certain value of z = a.

Discussion of Tables 4.2 and 4.3

Column 1 of Table 4.2 shows the values of a varying from a = 0.05 to 0.999999 i.e., we move more and more close to the unit circle. In column 2 we have shown only the maximum value of frequency spacing at which the theoretical value of the unwrapped phase as obtained by using the exact integration formula and the calculated value of the unwrapped phase obtained after applying the consistency criterion are in agreement. For example, for a = 0.9 the theoretical and calculated value of the unwrapped phase are in agreement for $\Delta\omega \leq 0.37$. If we set $\Delta\omega = 0.375$, the two values are not in agreement as there happens to be a jump of 2π in the value of Al

a	$\Delta\omega_{max}$	A1	A2	A3	A4	Theoretical or calculated unwrapped phase at $\Delta\omega_{max}$
0.05	1.5	$5x10^{-2}$	-6.23	$3.41x10^{-4}$	6.282	$5x10^{-2}$
0.1	1.5	0.1	-6.18	$3.24x10^{-4}$	6.282	0.1
0.2	1.5	0.199	6.48	$3.75x10^{-3}$	6.279	0.199
0.3	1.5	0.296	6.57	$2.2x10^{-2}$	6.261	0.296
0.4	1.5	0.389	6.67	$7.2x10^{-2}$	6.210	0.389
0.5	1.5	0.477	6.76	0.186	6.096	0.477
0.6	1.5	0.558	6.84	0.423	5.85	0.558
0.7	1.0	0.758	7.04	0.378	5.90	0.758
0.8	0.78	0.916	7.19	0.628	5.65	0.916
0.9	0.37	1.111	7.39	0.63	5.648	1.111
0.95	0.18	1.200	7.48	0.633	5.649	1.20
0.99	0.035	1.273	7.556	0.623	5.65	1.273
0.995	0.017	1.275	7.558	0.588	5.69	1.275
0.999	0.0035	1.290	7.573	0.629	5.65	1.290
0.9995	0.0017	1.283	7.567	0.591	5.691	1.283
0.9999	0.00035	1.292	7.575	0.630	5.652	1.2923
0.99995	0.00017	1.284	7.5678	0.592	5.691	1.284
0.99999	0.000035	1.292	7.5756	0.630	5.6529	1.2924
0.999995	0.000017	1.2849	7.579	0.630	5.691	1.2849
0.999999	0.0000035	1.2924	7.5756	0.630	5.6529	1.2925

Table 4.2 Real Zero, Example 4.1

a	$\Delta\omega_{max}$	Max. Der. $= \frac{a}{1-a}$	$\Delta\omega_{max} \cdot$ Max. Der.	1-a	$\frac{2\pi}{\Delta\omega_{max}}$	Min. FFT Size, N	N as Power of 2
0.05	1.5	0.0526	0.080	0.95	4.18	8	2^3
0.1	1.5	0.1111	0.16	0.9	4.18	8	2^3
0.2	1.5	0.25	0.375	0.8	4.18	8	2^3
0.3	1.5	0.428	0.65	0.7	4.18	8	2^3
0.4	1.5	0.666	1.0	0.6	4.18	8	2^3
0.5	1.5	1.00	1.5	0.5	4.18	8	2^3
0.6	1.5	1.5	2.25	0.4	4.18	8	2^3
0.7	1	2.33	3.5	0.3	6.28	8	2^3
0.8	0.78	4	3.12	0.2	8.05	16	2^4
0.9	0.37	9	3.33	0.1	16.98	32	2^5
0.95	0.18	19	3.42	0.05	34.9	64	2^6
0.99	0.035	99	3.46	10^{-2}	179.5	256	2^8
0.995	0.017	199	3.38	5×10^{-3}	369.5	512	2^9
0.999	0.0035	999	3.49	10^{-3}	1795.1	2048	2^{11}
0.9995	0.0017	1999	3.39	5×10^{-4}	3695.99	4096	2^{12}
0.9999	0.00035	9999	3.49	10^{-4}	17951.95	32768	2^{15}
0.99995	0.00017	19999	3.39	5×10^{-5}	36959.9	65536	2^{16}
0.99999	0.000035	99999	3.49	10^{-5}	179519.5	262144	2^{18}
0.999995	0.000025	199999	3.39	5×10^{-6}	369599.1	524288	2^{19}
0.999999	0.0000035	999999	3.49	10^{-6}	1795195.8	2097152	2^{21}

Table 4.3 Real Zero, Example 4.1

and A2.

In Table 4.3, the third column shows the maximum value of phase derivative which is given by $\frac{a}{1-a}$ for $0 < a < 1$. In the next column we have multiplied $\Delta\omega$ by the maximum value of phase derivative. This gives a reasonable estimate of incremental threshold θ_1, that is,

Incremental threshold $\theta_1 \approx \Delta\omega_{max}$ x Maximum value of phase der.

It is observed from this table that for $0.7 \leqslant a \leqslant 0.999999$, the value of incremental threshold θ_1 becomes approximately constant. Also from Table 4.2 we observe that the value of A3 (= value of consistency threshold θ_2) becomes constant at a value of 0.7 for $0.7 \leqslant a \leqslant 0.999999$. So we conclude that the reasonable value of consistency threshold to be used in conjunction with the incremental threshold of 3.5 is 0.7. Thus the approach that has been used above allows us to find the matching values of two thresholds and thus we need not select them arbitrarily. Also from this table it is noted that as the value of a tends towards 1 say from 0.999 to 0.9999, the maximum $\Delta\omega$ for successful phase unwrapping decreases by a factor of 10.

Table 4.3 also shows how the minimum FFT size varies when the real zero is moved towards the unit circle. These results have been verified separately using the phase unwrapping algorithm discussed in Chapter III. The minimum FFT size tells us

that if the zero is close to the unit circle, say a = 0.9999, then the minimum FFT size to be used for successful phase unwrapping is 2^{15}. This analysis assumes no use of the phase adaption feature. This does not mean that in practice we have to use such a large size FFT, because we can always reduce the FFT size by providing the adaptive feature of the phase unwrapping algorithm. For example, in this case we can have 2^{10} = 1024 point FFT with minimum stack size of 6 or 2^{9} = 512 point FFT with minimum stack size of 7. So, the phase unwrapping algorithm with 1024 point FFT and a stack size of 13 is able to handle zeroes as close to the unit circle as 10^{-6} provided we use double precision as has been concluded in Chapter III. All the results obtained in this chapter were obtained using double precision. Fig. 4.7 shows graphically the relation between the minimum FFT size needed and closeness to the unit circle, 1-a for values of $0.05 \leq a \leq 0.9$. For values of $0.05 < a \leq 0.7$, it is possible to use a little larger value of $\Delta\omega_{max}$ and hence slight reduction in the value of $\frac{2\pi}{\Delta\omega_{max}}$. However, we were not interested in this, as we want to keep the size of FFT about 4 times that of the sequence due to cepstral aliasing. Moreover, for this range of a, the FFT size is not critical.

Because of the large range of a, we have plotted the minimum FFT size versus closeness to the unit circle $\varepsilon = 1-a$ on a log-log paper for $0.95 \leq a \leq 0.999995$ (Fig. 4.8). This relationship comes out to be a straight line on the log-log scale.

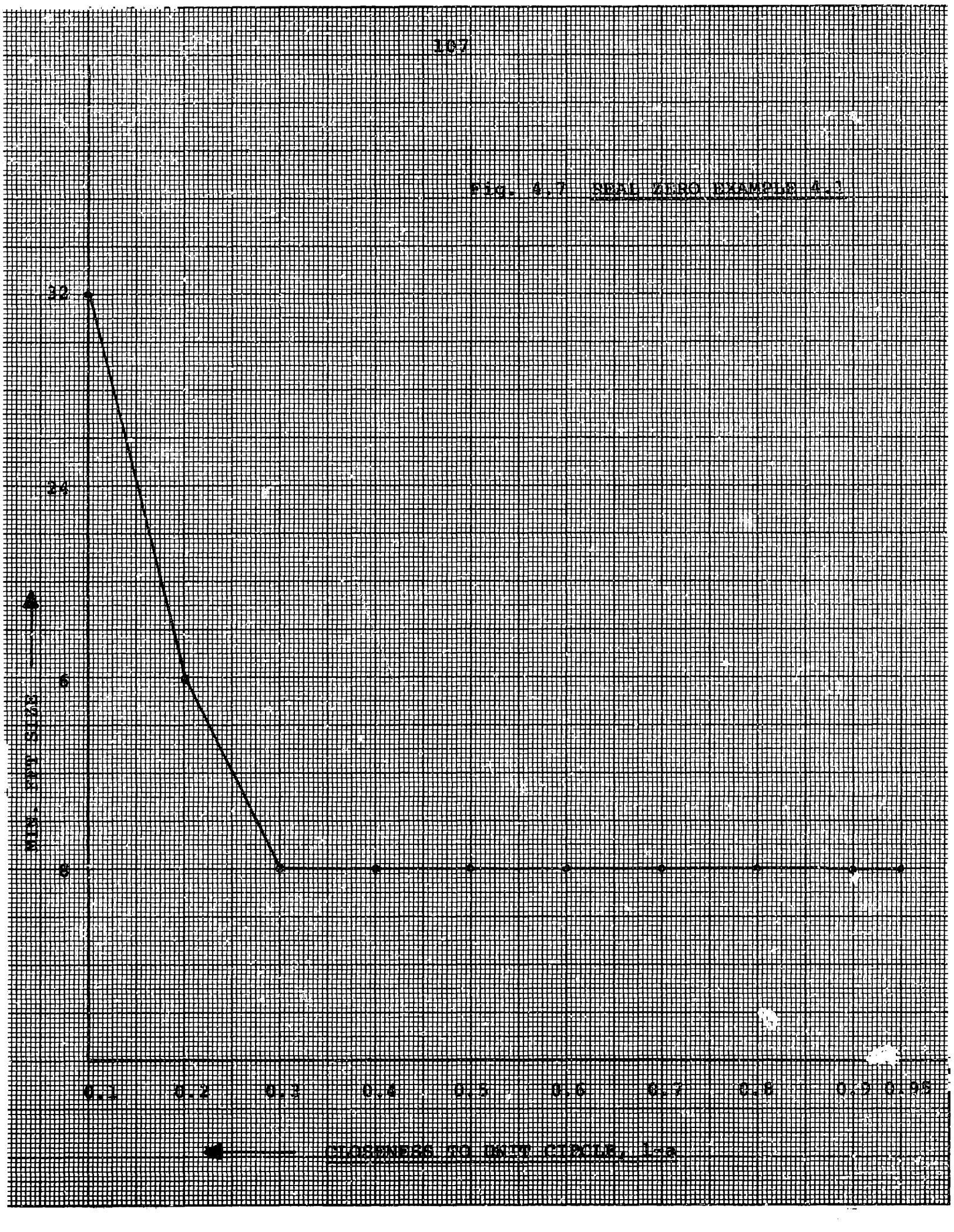

Fig. 4.7 SEAL ZERO EXAMPLE A-3

It has been found that required relation between $\varepsilon = 1-a$ and minimum FFT size N, comes out to be

$$\varepsilon N = 2.45 \tag{4.29}$$

In order to know the minimum FFT size required and the closeness of the two peaks in the phase derivative curve (discussed in detail in the next section) we need to know the width of the peak. In the following we determine the width of the peak in the phase derivative for a zero close to the unit circle (Fig. (4.6a). Note that the phase derivative is an even function.)

The expression for phase derivative as obtained in eq. (4.24) is

$$\arg' [X(e^{j\omega})] = \frac{a \cos \omega - a^2}{(1+a^2) - 2a \cos \omega}$$

Approximating $\cos \omega = 1 - \frac{\omega^2}{2}$, we have

$$\arg' [X(e^{j\omega})] = \frac{a(1-a) - \frac{a\omega^2}{2}}{(1-a)^2 + a\omega^2}$$

For $a \approx 1$, the 3 db frequency,

$$\omega^2 = \frac{(1-a)^2}{a} \approx (1-a)^2$$

or,

$$\omega = 1-a \tag{4.30}$$

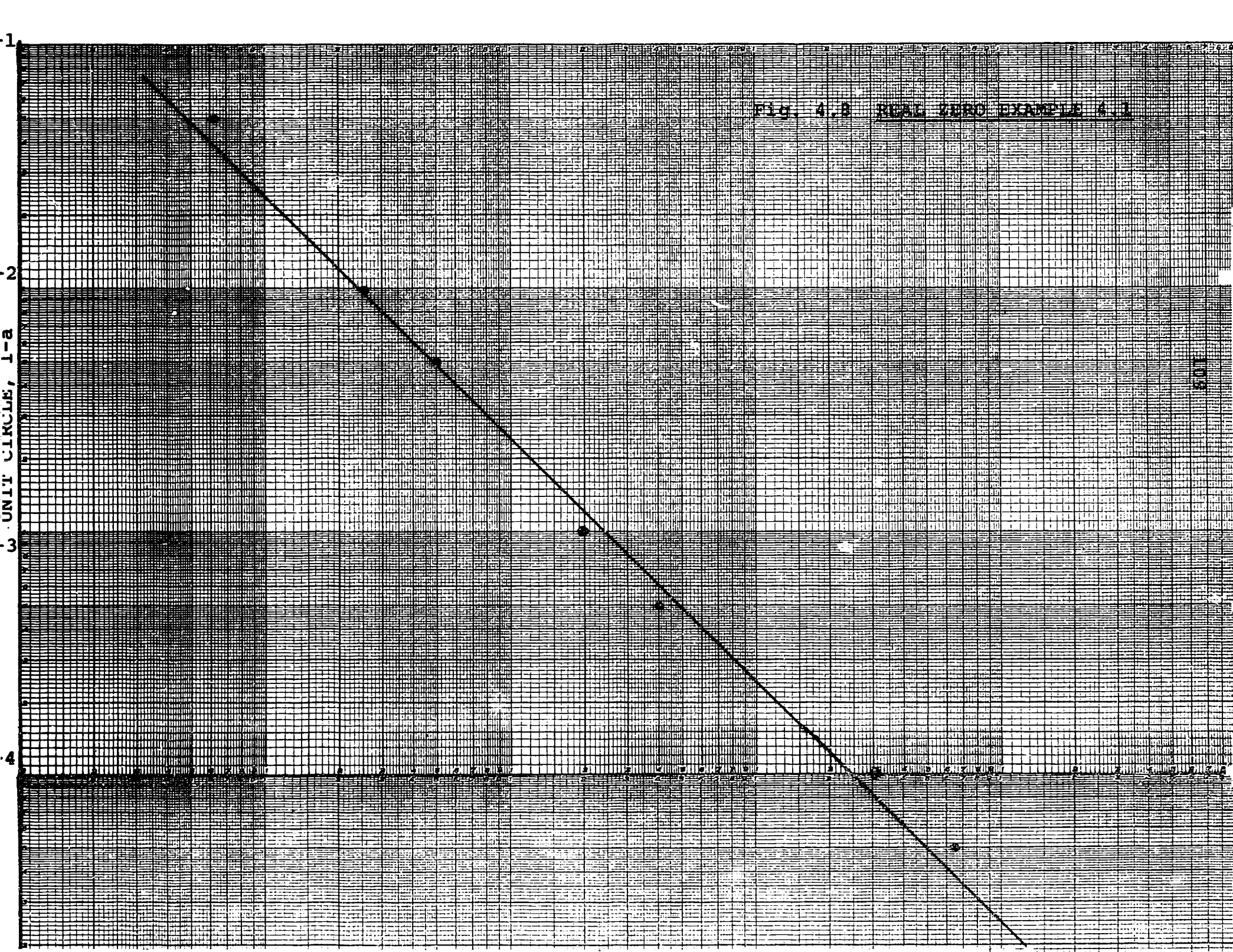
Fig. 4.8 REAL ZERO EXAMPLE 4.1
UNIT CIRCLE, 1-a
SOLN

Corresponding to this value of ω,

$$\arg' [X(e^{j\omega})] \approx \frac{1}{2} \left(\frac{a}{1-a}\right) = \frac{1}{2} \times \text{maximum value of phase derivative}$$

So 3 db frequency is indeed equal to (1-a). Thus we conclude that Example 4.1 illustrates the following points:

(1) There exists a definite relation between the minimum FFT size needed and the closeness of the real zero close to the unit circle. This relationship is $\epsilon N = 2.45$. This has been obtained for $0.05 \leqslant \epsilon \leqslant 5 \times 10^{-6}$.

(2) A definite procedure can be used which allows us to find the incremental and consistency threshold which are in agreement with each other.

(3) Also it has been found that using single precision arithmetic it does not make sense to consider the zeroes which are closer to the unit circle by more than 10^{-5} as the machine used (PDP 11/50) has 6 digits of precision in real arithmetic.

Now we present the example for the case of a complex pair of zeroes, which further reveals some important facts about phase unwrapping.

Example 4.2 Single Complex Pair of Zeroes

A complex pair of zeroes located at radius r and the corresponding signal is shown in Fig. 4.9.

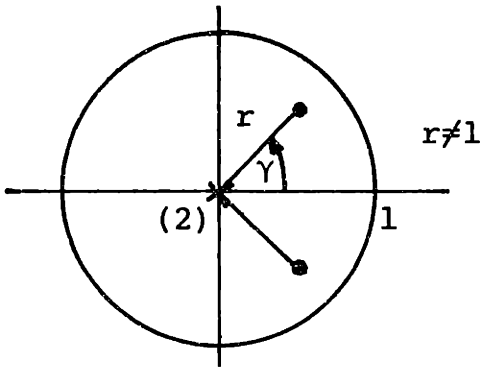

Fig. 4.9(a) Pole-Zero Plot

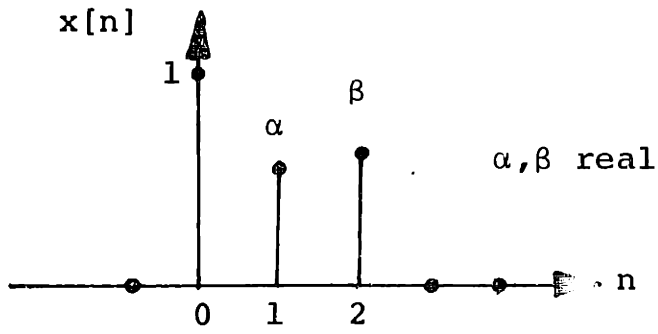

Fig. 4.9(b) Sequence

Fig. 4.9 A Complex Pair of Zeroes, Example 4.2

Let $R1 = r \cos \gamma$

$R2 = r \sin \gamma$

Then the sequence shown in Fig. 4.9(b) is,

$$x[0] = 1,\ x[1] = \alpha = -2R_1,\ x[2] = \beta = R_1^2+R_2^2 = r^2$$

The following stepwise procedure is used to answer the various questions related to phase unwrapping for this example.

(a) Obtain the expression for phase derivative for the signal shown in Fig. 4.9(b),

$$\arg' [X(e^{j\omega})] = \frac{-[\alpha^2+2\beta^2+\alpha(1+3\beta)\cos\omega + 2\beta\cos 2\omega]}{(1-\beta)^2+\alpha^2+2\alpha(1+\beta)\cos\omega + 4\beta\cos^2\omega} \quad (4.31a)$$

Setting

$$k_1 = \alpha^2 + 2\beta^2$$

$$k_2 = (1+3\beta)$$

$$k_3 = (1-\beta)^2 + \alpha^2 \quad (4.31b)$$

$$k_4 = 2\alpha(1+\beta)$$

Phase derivative becomes

$$\arg' [X(e^{j\omega})] = \frac{-[k_1+k_2 \cos \omega + 2\beta \cos 2\omega]}{k_3+k_4 \cos \omega + 4\beta \cos^2 \omega} \qquad (4.32)$$

Differentiating the above expression, we get the expression for phase second derivative,

$$\arg'' [X(e^{j\omega})] =$$

$$\frac{\sin [(k_2+8\beta\cos \omega)(k_3+k_4\cos\omega+4\beta\cos^2\omega)-(k_4+8\beta\cos \omega)(k_1+k_2\cos\omega+2\beta\cos 2\omega)]}{[k_3 + k_4 \cos \omega + 4\beta \cos^2 \omega]^2} \qquad (4.33)$$

(b) The expression for unwrapped phase is given by,

$$\arg [X(e^{j\omega})] = -\omega - \tan^{-1} \left[\frac{-2R_2 + [(1+R_1)^2 + R_2^2]\tan \frac{\omega}{2}}{R_1^2 + R_2^2 - 1}\right]$$

$$- \tan^{-1} \left[\frac{+2R_2 + [(1+R_1)^2 + R_2^2]\tan \frac{\omega}{2}}{R_1^2 + R_2^2 - 1}\right] \qquad (4.34)$$

$$R_1^2+R_2^2 \neq 1$$

(c) Setting the phase second derivative to zero in eq. (4.33) we find that the relative maxima or minima are going to occur at

$$\omega = n\pi, \quad n = 0, \pm 1, \pm 2, \ldots \tag{4.35}$$

or ω given by

$$4\alpha\beta(1-\beta)\cos^2\omega + 8\beta(1-\beta^2)\cos\omega + \alpha - \alpha^3 - 5\alpha\beta^2 + 5\alpha\beta - \alpha\beta^3 + \alpha^3\beta = 0 \tag{4.36}$$

Let a_1 and b_1 be the two roots of eq. (4.36) which are less than or equal to 1, then

$\omega = \omega_1 = \tan^{-1}\left[\left(\sqrt{(1-a_1^2)}\right)/a_1\right]$, similarly corresponding to b_1,

$$\omega = \omega_2 = \tan^{-1}\left[\left(\sqrt{(1-b_1^2)}\right)/b_1\right]$$

Eqs. (4.35) and (4.36) may suggest that there are a total of 4 relative maxima and minima between 0 and π including end points. However, from the nature of the pole-zero plot shown in Fig. 4.9(a), we expect only one relative maxima or minima for $0 < \omega < \pi$ (two exist at $\omega = 0$ and $\omega = \pi$).

In this illustration we concentrate on the values of $0 < r < 1$ and assume that $\gamma = 45°$. However, the same set of ideas apply for any value of $|r| \neq 1$.

For this case, it is found that for $r < 0.3$, the values of cos ω given by eq. (4.36) are both greater than 1 and in that case we conclude that there cannot be any relative maxima or minima between $0 < \omega < \pi$, and the phase derivative should vary linearly between $\omega = 0$ and $\omega = \pi$. However when $r \geq 0.3$,

we find that the one root of cos ω is less than 1 and the other one is greater than 1, so we get a relative maxima between $0 < \omega < \pi$ as expected.

Now our interest is to find the absolute maxima and minima in this case. For $r \geq 0.4$, the absolute maxima occurs for $0 < \omega < \pi$ and tends towards $\pi/4$ as we move closer to the unit circle i.e. $r \to 1$. The absolute minima occurs at $\omega = 0$ and π. (The value of phase derivative at these points is about the same when r is very near to 1 and this value is about -0.9999.) We are interested in the maximum which occurs between $\omega = 0$ or $\omega = \pi$ since in general the absolute maxima or minima which occur at $\omega = 0$ or $\omega = \pi$ can always be handled by the procedure outlined for the case of real zero in example 4.1.

So in this example we answer the various questions related to phase unwrapping when peak in the phase derivative occurs for $0 < \omega < \pi$. Fig. 4.10 shows the phase derivative curves and unwrapped phase curves for various values of r ($r_3 > r_2 > r_1$).

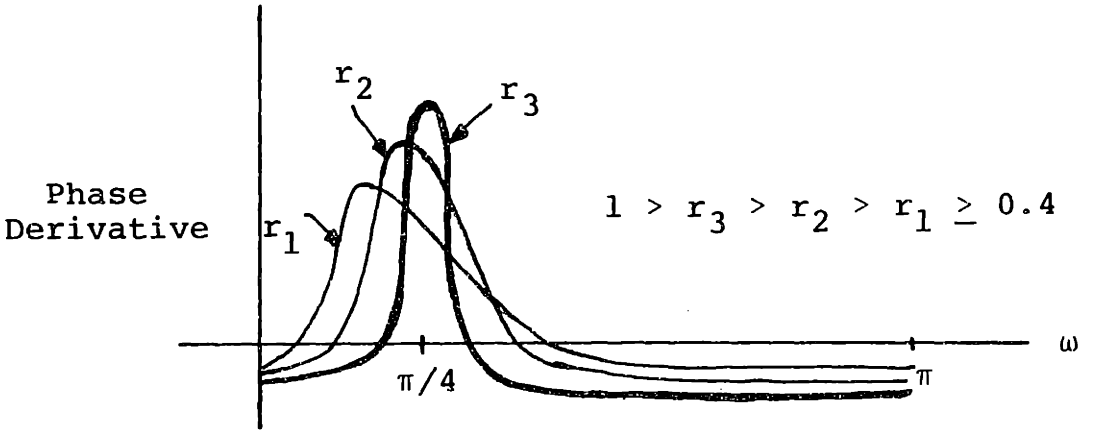

Fig. 4.10(a) Phase Derivative Curves for Various Values of r for Example 4.2

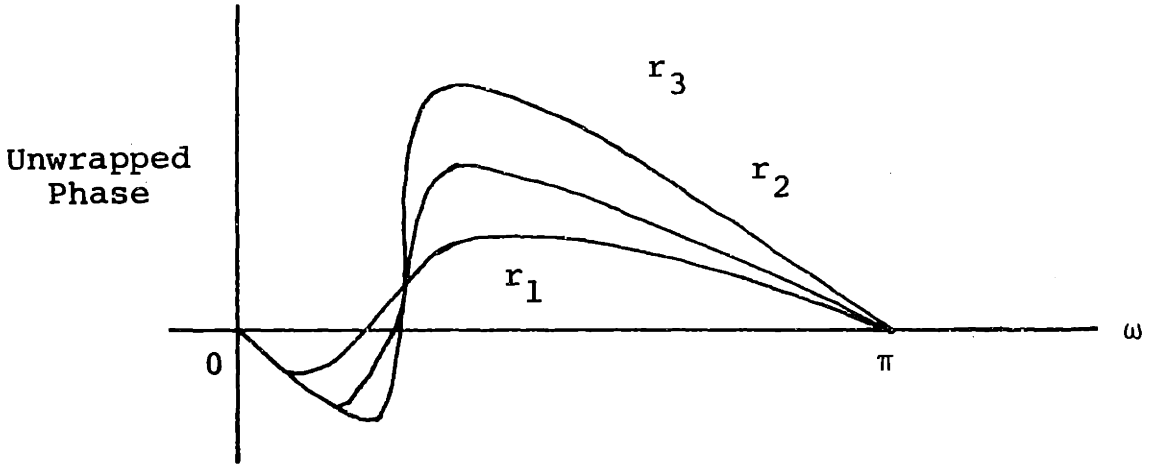

Fig. 4.10(b) Unwrapped Phase

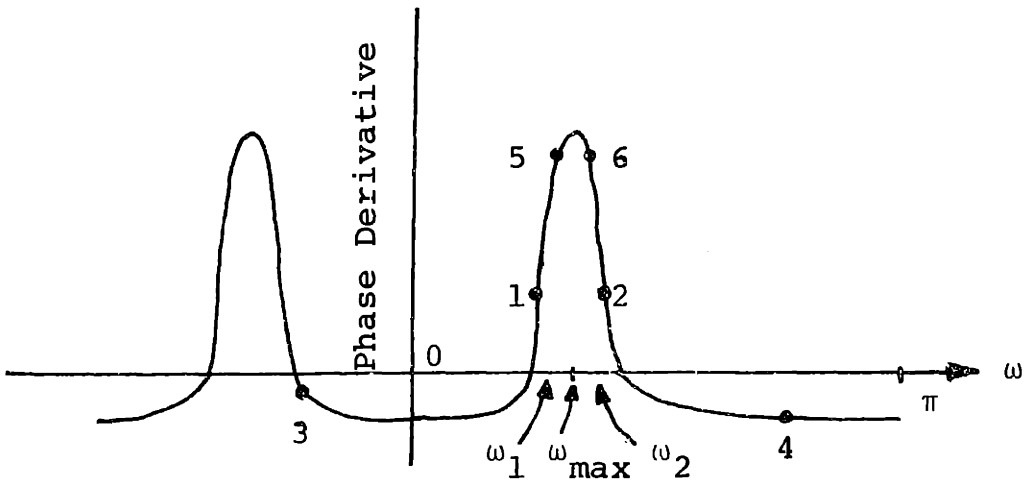

Fig. 4.11 Phase Derivative Curve for Some Typical Value of $0.4 \leqslant r < 1$

(d) Now we find the maximum frequency spacing $\Delta\omega$ for the successful phase unwrapping. We take two points 1 and 2 on the left and right of the peak, and determine the unwrapped phase at ω_2, knowing the value of the unwrapped phase at ω_1, i.e., we compute the theoretical value of the unwrapped phase at ω_1 using eq. (4.34) and add to it the area between ω_1 and ω_2 using eq. (4.18) (with i = 1) to approximate the unwrapped phase at ω_2. At this point it is possible to find the value of $\Delta\omega_{max} = \omega_2 - \omega_1$ such that for $\Delta\omega \leqslant \Delta\omega_{max}$ the calculated value of the unwrapped phase at ω_2 satisfying consistency criterion and the theoretical value of the unwrapped phase at ω_2 obtained using eq. (4.34) are in agreement. But it is not reasonable because the integration may be too bad and we may

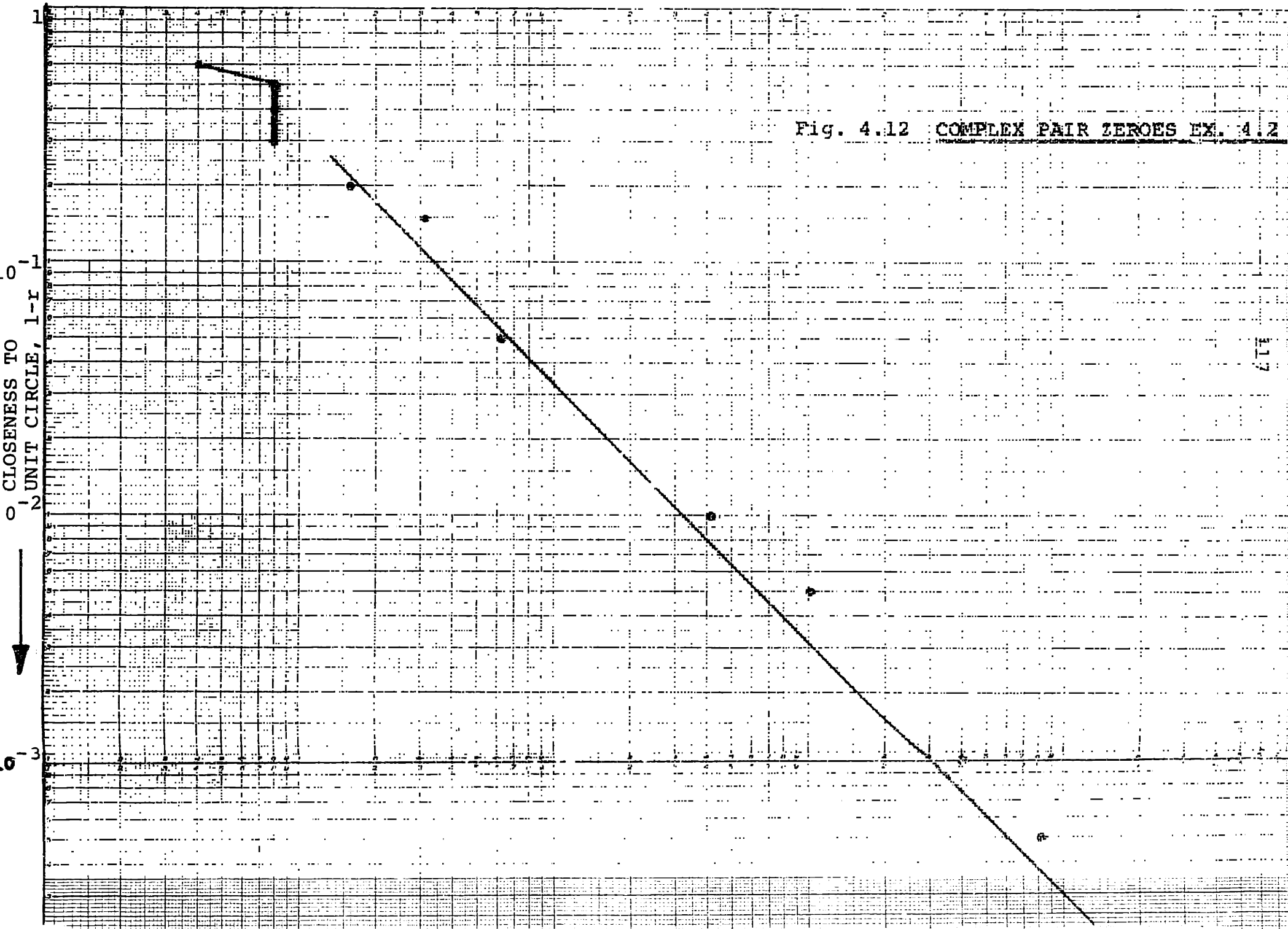

Fig. 4.12 COMPLEX PAIR ZEROES EX. 4.2

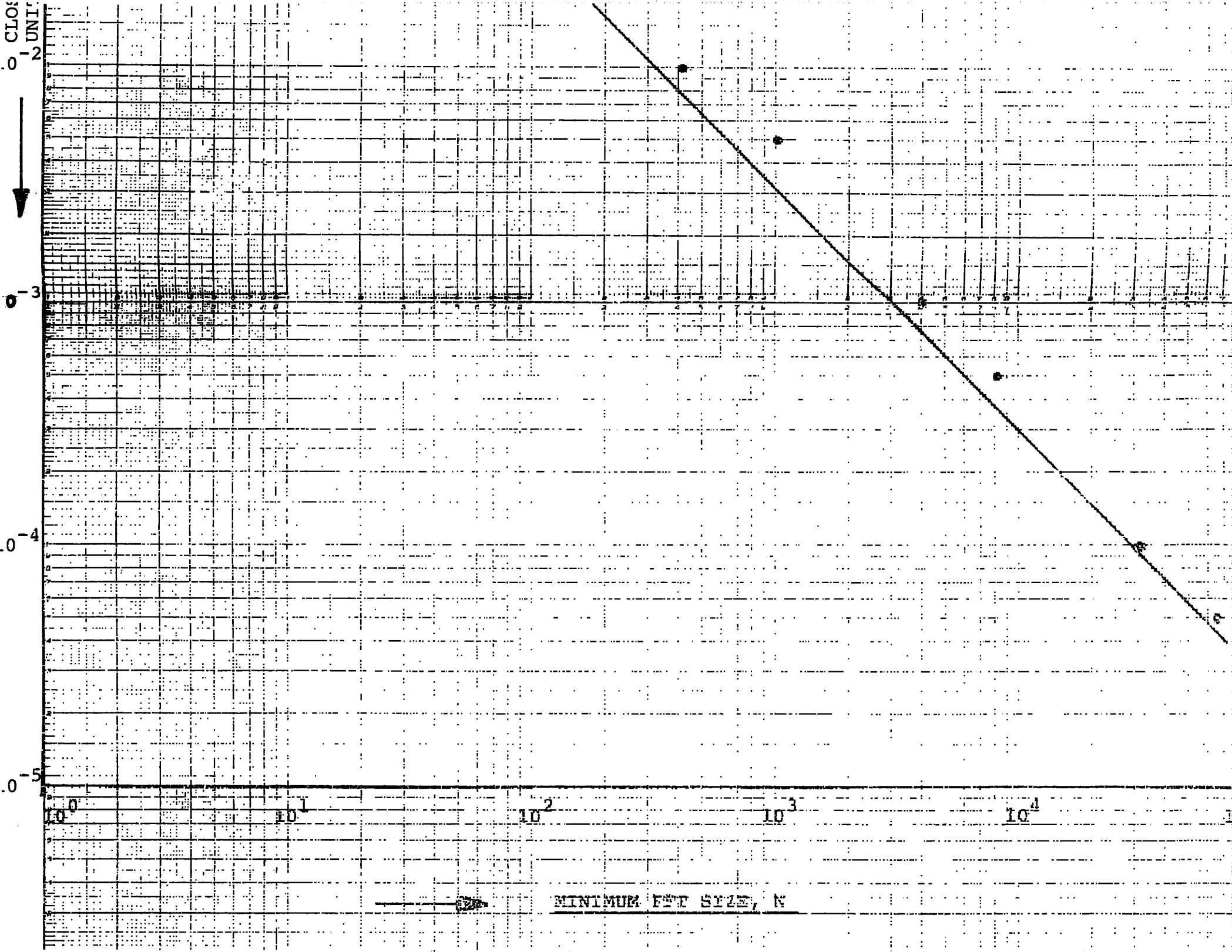
CLOS
UNI
.0^-2
0^-3
.0^-4
.0^-5
10^0
10^1
10^2
10^3
10^4
MINIMUM FIT SIZE, N

be quite far away from ω_{max} such as the points 3 and 4 in Fig. 4.11. With a view to improve the integration and for the approach to work in general, we select the value of consistency threshold, θ_2 as 1 (in principle it can be anything less than π). So now we shall choose two points on the two sides of the peak (Fig. 4.11) such that the consistency threshold $\theta_2 \leqslant 1$. Hence the procedure is

(i) Select a consistency threshold of 1.

(ii) Using eq. (4.34) compute the theoretical value of the unwrapped phase at $\omega = \omega_1$ and use eq. (4.18) to find the area under the phase derivative curve between ω_1 and ω_2. Thus, we obtain

$$\arg_a [X(e^{j\omega_2})] = \arg [X(e^{j\omega_1})] + \left(\frac{\omega_2-\omega_1}{2}\right) \left[\arg' [X(e^{j\omega})]\Big|_{\omega=\omega_1} + \arg' [X(e^{j\omega})]\Big|_{\omega=\omega_2}\right] - \frac{(\omega_2-\omega_1)^2}{12} \left[\arg'' [X(e^{j\omega})]\Big|_{\omega=\omega_2} - \arg'' [X(e^{j\omega})]\Big|_{\omega=\omega_1}\right] \quad (4.37)$$

Radius, r	1 - r	Consistency Threshold	$\Delta\omega_{max}$	Max. Phase Der.	$\Delta\omega_{max}$ * Max. Phase Der.	$\frac{2\pi}{\Delta\omega_{max}}$	Min. FFT Size, N
0.4	0.6	0.42	2x0.79	0.542	0.856	3.977	2^2
0.5	0.5	0.57	2x0.78	0.805	1.256	4.028	2^3
0.6	0.4	0.85	2x0.77	1.236	1.903	4.080	2^3
0.7	0.3	0.9	2x0.6	2.0	2.4	5.236	2^3
0.8	0.2	0.9	2x0.29	3.60	2.088	10.833	2^4
0.9	0.1	0.99	2x0.12	8.55	2.052	26.180	2^5
0.95	$5x10^{-2}$	0.91	2x0.05	18.55	1.855	62.83	2^6
0.99	10^{-2}	0.99	2x0.0103	98.50	2.029	305.009	2^9
0.995	$5x10^{-3}$	0.99	2x0.0051	198.5	2.025	615.999	2^{10}
0.999	10^{-3}	0.98	2x0.001	998.5	1.997	3141.5	2^{12}
0.9995	$5x10^{-5}$	0.98	2x0.0005	1998.5	1.999	6283.1	2^{13}
0.9999	10^{-4}	0.98	2x0.0001	9998.5	2.000	31415.9	2^{15}
0.99995	$5x10^{-5}$	0.98	2x0.00005	19998.5	2.000	62831.8	2^{16}
0.99999	10^{-5}	0.98	2x0.00001	99998.5	2.000	314159.2	2^{19}

Table 4.4 Complex Pair of Zeroes, Example 4.2

where use is made of eqs. (4.32) and (4.33). Principal value at $\omega = \omega_2$ is given by,

$$\text{ARG } [X(e^{j\omega_2})] = \tan^{-1}\left[\frac{-\{\alpha \sin(\omega) + \beta \sin(2\omega)\}}{1 + \alpha \sin(\omega) + \beta \sin(2\omega)}\right]\Bigg|_{\omega=\omega_2} \qquad (4.38)$$

Now using eqs. (4.19), (4.37) and (4.38) we conducted an experiment in the following way:

For a particular value of r we find the maximum $\Delta\omega = \omega_2 - \omega_1$ such that the consistency threshold θ_2 is just less than 1 and the calculated value satisfying consistency criterion and the theoretical value are in agreement. This was carried out for $0.4 \leq r \leq 0.99999$. The results are shown in Table 4.4.

Discussion of Table 4.4

Column 1 shows the radius of location of complex pair of zeroes from the origin. This radius varies from 0.4 to 0.99999. Column 4 shows the maximum value of frequency spacing around ω_{max} for which the consistency threshold is under 1. Column 5 gives the values of maximum phase derivative. It is to be noted that this value of maximum derivative is very close to r/(1-r). Column 6 shows the product of $\Delta\omega_{max}$ and the maximum phase derivative. From this we conclude the value of incremental threshold. It is observed that the value of this threshold becomes constant at 2. Similar to the simple zero case in example 4.1, it is observed here that if we increase the radius from 0.999 to 0.9999, the max $\Delta\omega$ required decreases

by a factor of 10. Finally, the last column of the table shows the minimum FFT size to be used when the complex pair of zeroes is close to the unit circle by a given amount. In an attempt to verify the FFT size given by this table, we used the phase unwrapping algorithm and found that for some cases a FFT size, half of that given in this table work for successful phase unwrapping. This was expected as we have discussed earlier. We conclude that the FFT size given in this table is guaranteed to work if we picked up the incremental and consistency threshold as 2 and 1. But in some cases it may not be the least one.

In Fig. 4.12, a plot is given of the minimum size of FFT versus closeness ($\varepsilon = 1-r$) of zeroes to the unit circle. We observe the same type of behavior as in the example 4.1 (Fig. 4.8) for $0.8 \leqslant r$.

In this case the required relation between $\varepsilon = 1-a$ and the minimum FFT size N comes out to be

$$\varepsilon N = 3.5 \tag{4.39}$$

which is a hyperbola in the ε,N plane.

Using eq. (4.32) and following the approaches similar to that in example 4.1, the determination of the width of the peak in the phase derivative curve becomes extremely complicated. However, we expect an expression for the width of the peak similar to that of example 4.1. (The value of maximum derivative for the two examples can be noted.)

We approximate the width of the peak (occurring in general for $0 < \omega < \pi$) as

$$2(1 - r) \tag{4.40}$$

The factor 2 appears here because in example 4.1 we considered only one side of the peak. In the next section we show that such an approximation is quite reasonable.

In summary, for this example of complex pair of zeroes we have shown

(1) how the minimum FFT size varies as we move the complex pair of zeroes more and more close to the unit circle.

(2) how one can determine the value of incremental threshold for a given value of consistency threshold.

(3) Just as in the case of example 4.1, it has been found that it does not make sense to consider the zeroes which are closer to the unit circle by more than 10^{-5} while using real arithmetic.

IV.4 Generalization

Having discussed the examples for the case of a real zero and a complex pair of zeroes, we wish to extend their results for the case of a finite length signal whose pole-zero plot consists of any arbitrary number of zeroes whose location is known in the z-plane and then to any arbitrary real or synthetic signal for which we do not know the exact

pole-zero plot.

In section IV.3 we did not encounter the problem of how close two zeroes can be together and to the unit circle and still be able to do phase unwrapping. The exact mathematical answer to this question seems to be very difficult. We suggest a procedure in the following and present experimental results.

When two zeroes are close together, following are the three situations which may exist in the phase derivative curve.

(i) two positive peaks (Fig. 4.13(a))

(ii) two negative peaks (Fig. 4.13(b))

(iii) one positive and one negative peak (Fig. 4.13(c)).

A typical phase derivative curve is shown in Fig. 4.14.

If we can handle the above mentioned 3 cases, then we should be able to comment about phase unwrapping for any finite length sequence whose pole-zero plot is known.

Note that for each of the cases (Fig. (4.13)) the expression for the exact unwrapped phase can be obtained using eq. (4.17). In this figure h depends on the angular displacement of the two zeroes and the height of the peak depends upon the closeness of the corresponding complex pair of zeroes to the unit circle. Fig. 4.13(b) is the upside down of Fig. 4.13(a), so we need to concentrate only on Figs. 4.13(a) and 4.13(c). We suggest the following procedure for these situations.

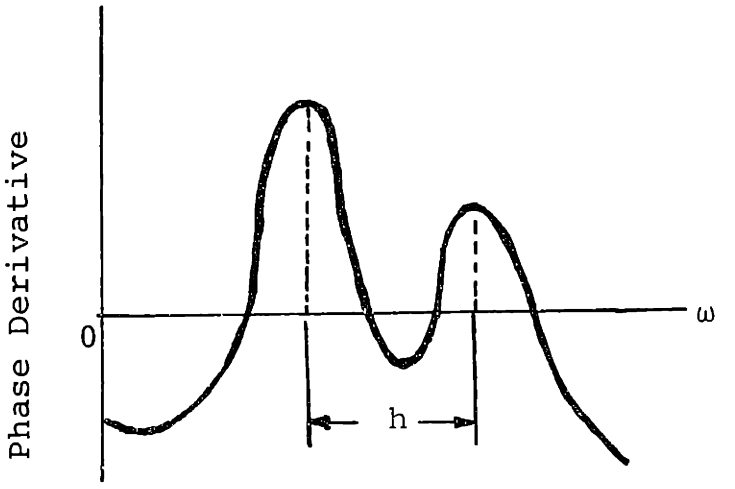

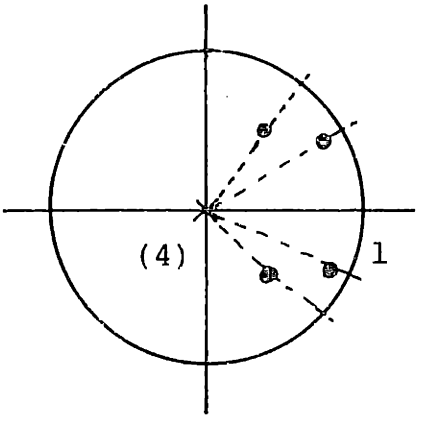

Fig. 4.13(a)

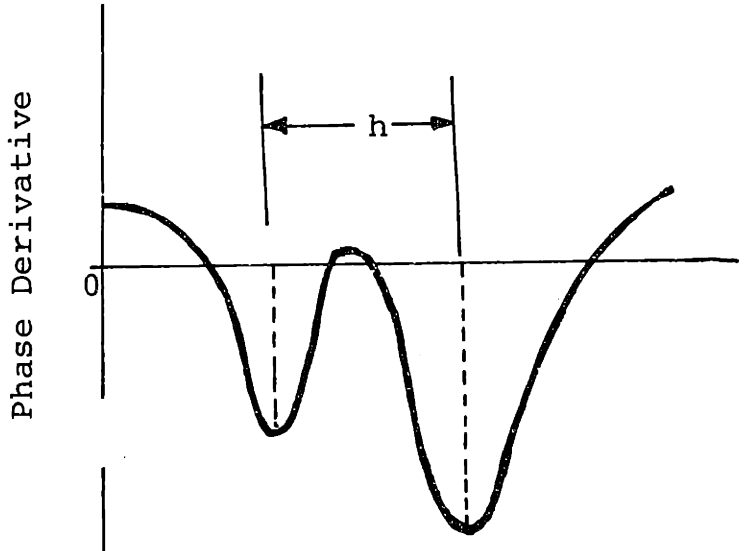

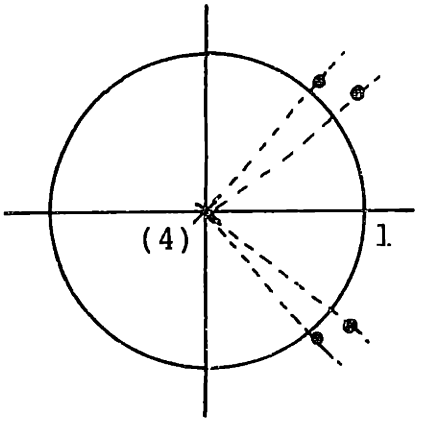

Fig. 4.13(b)

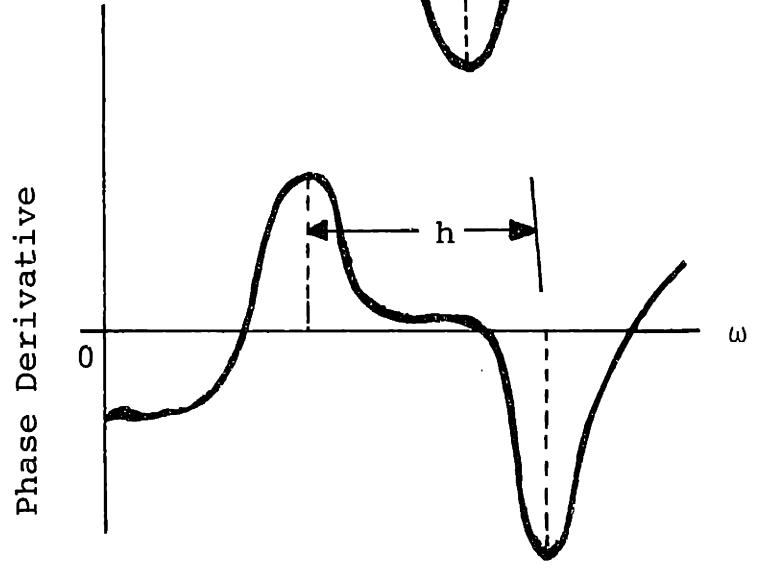

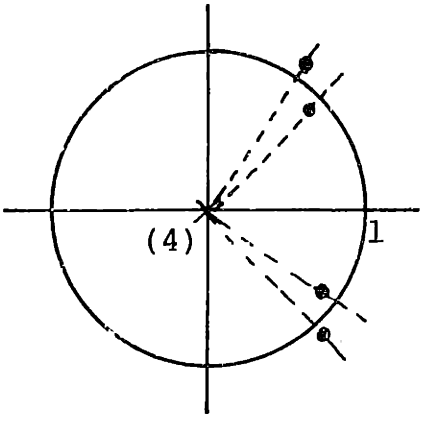

Fig. 4.13(c)

Fig. 4.13 Various Possibilities of 2 Peaks in Phase Derivative (Diagrams Are Not to Scale)

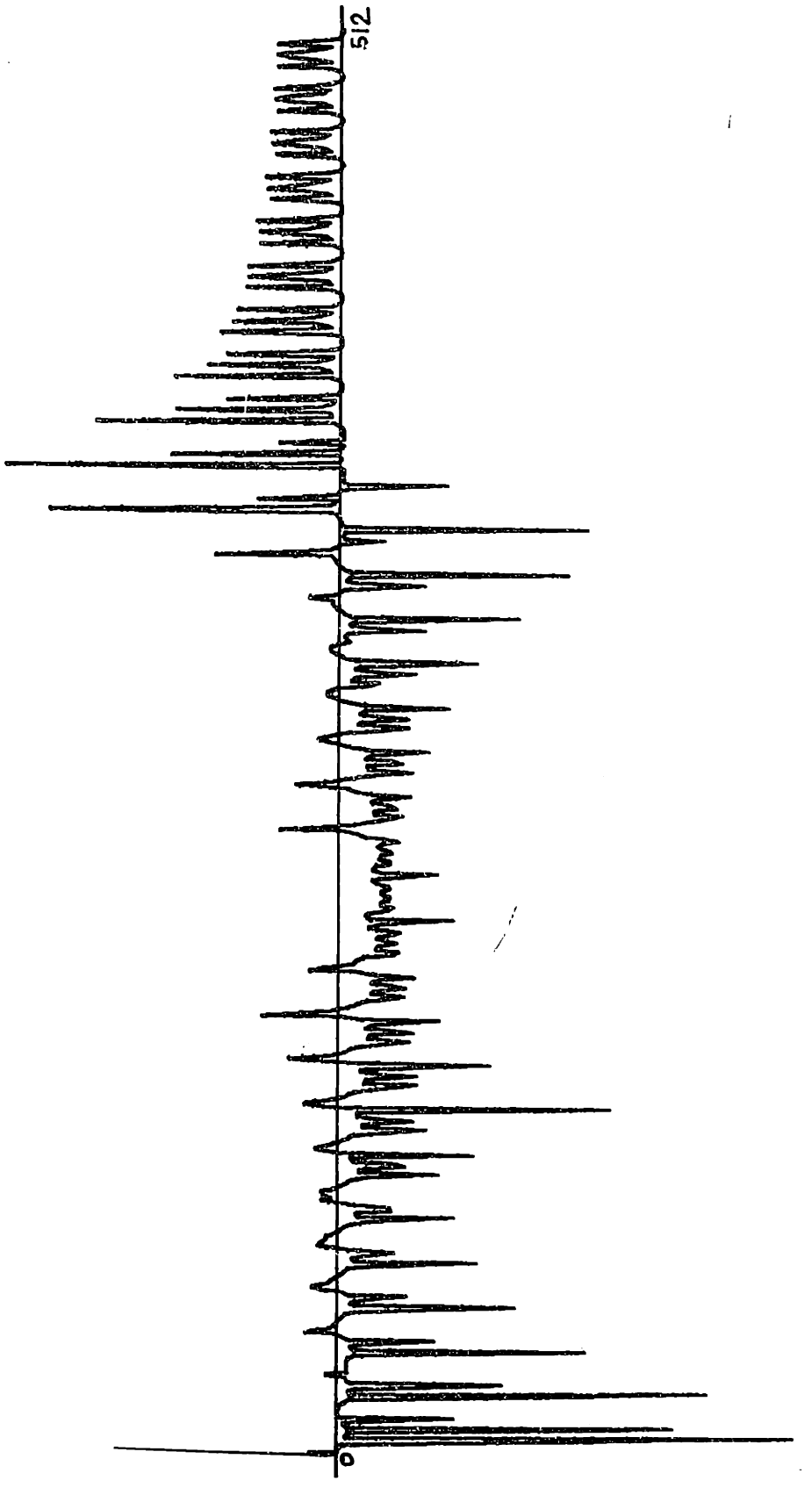

Fig 4.14 Typical 513 Points Phase Derivative Curve

Find the relative maxima or minima (location and value) of the phase derivative. Say in Fig. 4.13(a) we have found the absolute maxima or in Fig. 4.13(c) picked the absolute maxima or minima whichever is larger in absolute value. Corresponding to this we find the minimum FFT size, N from Table 4.4. Since we know the location of both the peaks we can find out the frequency spacing h between them. Then we obtain,

$$N1 = \frac{2\pi}{h} \tag{4.41}$$

If $N1 \leqslant N$, we select N as the size of FFT to be used for phase unwrapping and consider the two peaks as independent from each other. If however, $N1 > N$, we say that the two peaks are dependent and we use the following idea for obtaining the minimum FFT size for successful phase unwrapping.

Determine the width of the two peaks using eq. (4.40). Let the minimum of the two peaks be denoted as L. Then, the minimum FFT size equals

$$\frac{2\pi}{L} \tag{4.42}$$

The size so obtained conforms with the seventh column of Table 4.4.

In general an experiment similar to example 4.2 can always be carried out.

Now we give a stepwise procedure that can be used to answer the various questions mentioned at the beginning of this chapter for any sequence whose pole-zero plot is known.

(1) From the given pole-zero plot, determine the sequence.

(2) Obtain the expression for phase first and second derivatives.

(3) Obtain the exact relation for the unwrapped phase using eqs. (4.13) and (4.17).

(4) Obtain the relative and absolute maxima and minima (location and value) of the phase derivative.

(5) Determine the absolute maxima or absolute minima whichever is larger in absolute value. Hereafter referred to as the super peak.

(6) Apply the procedure similar to that of example 4.2 around the super peak picked up in step (5). Obtain the minimum FFT size, say N1.

(7) Obtain the frequency spacing between every two adjacent relative maximas or minimas in the phase derivative curve. Let the minimum spacing be denoted by h. Then $N = \frac{2\pi}{h}$.

(8) If $N < N1$, the minimum FFT size obtained in step (6) i.e., N1 is all right, otherwise the new minimum FFT size which should be used equals $\frac{2\pi}{L}$ where L = minimum width of all the relative maximas or minimas occurring in the phase derivative.

It has been found that if we are using 1024 points FFT with stack size of 13, we can do successful phase unwrapping when the three zeroes are close to the unit circle by a factor of 10^{-5} and separated from each other by $\pi/10^4$. In this case all the three zeroes lie between two DFT points.

Until now in this chapter we have considered the cases where it has been assumed that we know a priori the location of zeroes of the finite length sequence, but in practice this may not be the case. However, the above given results can be used if we, somehow, have an idea about the order of closeness of zero to the unit circle depending upon its generation, for example, whether it is a speech, seismic, image or milling machine signal. For example if the signal happens to be close to periodic, we expect zeroes very close to the unit circle and phase unwrapping becomes relatively more difficult. In practice using the incremental threshold of 2 and consistency threshold of 1, the FFT size given in Table 4.4 can be used.

In the next chapter we discuss the properties and computational strategies for the two-dimensional complex cepstrum.

CHAPTER V

COMPUTATION OF TWO DIMENSIONAL COMPLEX CEPSTRUM

V.1 Introduction

In the previous chapters we have discussed in detail the theoretical and practical issues related to the computation of the one-dimensional complex cepstrum. We considered several features such as the improvement of the integration rule, efficient computation of the DFT at a single frequency which is not on the DFT raster, the need for double precision for certain variables, determination of incremental and consistency thresholds and linear phase so as to obtain an efficient and reliable phase unwrapping algorithm. Now in this chapter we consider the computation of the two-dimensional complex cepstrum. The need for the efficient and reliable two dimensional phase unwrapping has been long felt. Various attempts were made to use the complex cepstrum in image processing for deblurring purposes and recently for checking the stability of two dimensional recursive digital filters. Filip [4] estimated the impulse response of linear, shift invariant image deblurring system using homomorphic filtering technique as opposed to using power spectral density and maximum likelihood techniques for modeling the image as a random field because homomorphic technique incorporates the information about the phase of the transform which is necessary in image restoration

[20]. He used the phase unwrapping algorithm based on the phase principle value (Schafer's algorithm) and this led to the poor estimate of the phase. Rom [18] considered the two dimensional real cepstrum. Stockham [19] found the major weakness of the solutions of blind deconvolution (both signals are unknown and the only data available is the convolution itself and the task is to estimate or eliminate one of the unknown signals) is the inability to correct for the unknown phase distortions in the general case as he makes no use of phase unwrapping. Ekstrom [21] considers the use of complex cepstrum for checking the stability of two dimensional recursive digital filters by taking the input of the characteristic system as the autocorrelation of the signal so as to avoid phase unwrapping. Ekstrom [22] has also considered the use of Schafer's phase unwrapping algorithm as it greatly simplifies the stability test. We have already mentioned that the use of a phase unwrapping algorithm based only on the principal value is not sufficient [2], so we seek better phase unwrapping methods.

In this chapter we consider two dimensional homomorphic systems for convolution, discuss some important properties of the 2-D cepstrum and consider several phase unwrapping computational strategies.

We shall restrict the use of complex cepstrum to checking the stability of one and two dimensional recursive digital filters and this application is considered in the next chapter.

V.2 Two-Dimensional Homomorphic System for Convolution

The definition of 2-D complex cepstrum is a straightforward extension from its one dimensional definition. It is given by

$$x[m,n] = Z^{-1} [\log z(x[m,n])] \qquad (5.1)$$

A 2-D homomorphic system for convolution is shown in Fig. 5.1.

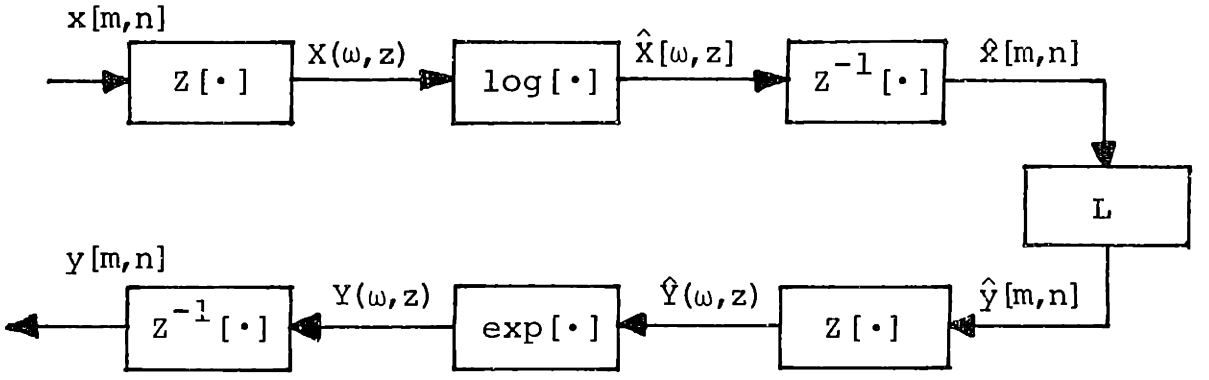

Fig. 5.1

Dudgeon [3] has given the necessary and sufficient conditions for the existence of 2-D cepstrum. These conditions are similar to those in the 1-D case. Specifically, any real two dimensional array whose Fourier transform has a log magnitude which is continuous, even and periodic, and whose phase is continuous, odd and periodic over the frequency plane will have a well defined two dimensional complex cepstrum which is real.

Various relations involved are:

$$\hat{x}[m,n] \leftrightarrow \hat{X}(w,z) = \log [X(w,z)] \tag{5.2}$$

$$= \sum_m \sum_n \hat{x}[m,n] w^{-m} z^{-n} \tag{5.3}$$

defined within its region of convergence that includes $|w| = |z| = 1$.

Evaluating

$$\hat{X}(w,z)\Big|_{\omega=e^{j\mu}, z=e^{j\nu}}$$

we get

$$\hat{X}(e^{j\mu},e^{j\nu}) = \log [X(e^{j\mu},e^{j\nu})]$$

$$= \hat{X}_R(e^{j\mu},e^{j\nu}) + j\hat{X}_I(e^{j\mu},e^{j\nu})$$

$$= \log |X(e^{j\mu},e^{j\nu})| + j \arg [X(e^{j\mu},e^{j\nu})]$$

So, $$\hat{X}_R(e^{j\mu},e^{j\nu}) = \log |X(e^{j\mu},e^{j\nu})| \tag{5.4}$$

and $$\hat{X}_I(e^{j\mu},e^{j\nu}) = \arg [X(e^{j\mu},e^{j\nu})] \tag{5.5}$$

Similar to the 1-D case, if we define the unwrapped phase as the integral of phase derivative, then the representation is not unique in the sense that we could integrate any of the three second partial derivatives. We define it as

$$\arg\,[X(e^{j\mu},e^{j\nu})] = \hat{X}_I(e^{j\mu},e^{j\nu})$$

$$= \int_0^{\mu}\int_0^{\nu} \frac{\partial^2}{\partial\mu_1\partial\nu_1}\,\hat{X}_I\,(e^{j\mu_1},e^{j\nu_1})\,d\mu_1 d\nu_1 \qquad (5.6)$$

and

$$\arg\,[X(e^{j\mu},e^{j\nu})]\Big|_{\mu=\nu=0} = 0 \qquad (5.7)$$

If the phase as defined in eqs. (5.6) and (5.7) is not periodic, it can be made so by subtracting off a linear phase component along the two axes which corresponds to a shift in the time origin of the original signal.

Since we have assumed that the complex log is well defined so its derivatives also represent the proper Fourier transform, we have

$$\frac{\partial}{\partial\mu}\,\hat{X}_I(e^{j\mu},e^{j\nu}) = \frac{X_R\,(\frac{\partial}{\partial\mu}X_I) - (\frac{\partial}{\partial\mu}X_R)\,X_I}{|x|^2} \qquad (5.8)$$

$$\frac{\partial^2}{\partial\mu^2}\,\hat{X}_I(e^{j\mu},e^{j\nu}) = \frac{1}{|x|^4}\Bigg(|x|^2[X_R(\frac{\partial^2}{\partial\mu^2}X_I) - X_I(\frac{\partial^2}{\partial\mu^2}X_R)]$$

$$+ 2X_RX_I[(\frac{\partial}{\partial\mu}X_R)^2 - (\frac{\partial}{\partial\mu}X_I)^2]$$

$$+ 2(\frac{\partial}{\partial\mu}X_R)(\frac{\partial}{\partial\mu}X_I)(X_I^2 - X_R^2)\Bigg) \qquad (5.9)$$

and

$$\frac{\partial^2}{\partial\mu\partial\nu}\hat{x}_I(e^{j\mu},e^{j\nu}) = \frac{1}{|x|^4}\Big(|x|^2[X_R(\frac{\partial^2}{\partial\mu\partial\nu}X_I) - (\frac{\partial^2}{\partial\mu\partial\nu}X_R)X_I]$$

$$+ 2X_RX_I[(\frac{\partial}{\partial\mu}X_R)(\frac{\partial}{\partial\nu}X_R) - (\frac{\partial}{\partial\mu}X_I)(\frac{\partial}{\partial\nu}X_I)]$$

$$+ (X_I^2 - X_R^2)\ [(\frac{\partial}{\partial\mu}X_R)(\frac{\partial}{\partial\nu}X_I) + (\frac{\partial}{\partial\mu}X_I)(\frac{\partial}{\partial\nu}X_R)]\Big) \tag{5.10}$$

In the above three equations we have avoided the argument notation for simplicity. Derivatives with respect to the ν variable can be obtained similarly. Note that the determination of first derivatives of the phase requires the calculation of the Fourier transforms of x[m,n], mx[m,n] and nx[m,n]. Second derivatives require the determination of Fourier transforms of x[m,n], mx[m,n], nx[m,n], m^2x[m,n], n^2[m,n], and mnx[m,n].

V.3 Properties of Two Dimensional Complex Cepstrum

Many of the properties of one dimensional complex cepstrum can be extended to two dimensions. In the following we discuss three properties which are somewhat different from the 1-D case and which we shall be using in the next chapter.

Property 1 For a separable sequence the complex cepstrum exists only on the axes, i.e., $\hat{x}[m,n] \neq 0$ only on the m and n axes for $x[m,n] = x_1[m]\ x_2[n]$.

Proof

Given x[m,n] is separable, i.e.,

$$x[m,n] = x_1[m]\ x_2[n] \tag{5.11}$$

Then $X(e^{j\mu},e^{j\nu}) = X_1(e^{j\mu})\ X_2(e^{j\nu})$ from the definition of the Fourier transform.

$$\log\ [X(e^{j\mu},e^{j\nu})] = \log\ [X_1(e^{j\mu})] + \log\ [X_2(e^{j\nu})]$$

$$= \log\ [X_1(e^{j\mu})] \cdot 1(\nu) + \log\ [X_2(e^{j\nu})] \cdot 1(\mu) \tag{5.12}$$

where, $1(\nu)$ is a function that has a unit value for all ν and $1(\mu)$ is a function that has a unit value for all μ.

Taking the inverse Fourier transform of the above equation we get

$$\hat{x}[m,n] = \hat{x}_1[m] \cdot \delta[n] + \hat{x}_2[n]\ \delta[m] \tag{5.13}$$

This shows that the cepstrum of a separable sequence exists only on the axes.

Before considering the next property, a few definitions (see Ekstrom [21]) follow:

Support of h[m,n] is the set $\{(m,n)\,|\,h(m,n) \neq 0\}$

Non-symmetric half plane (NSHP) is a region of the form $\{m\geq 0, n\geq 0\} \cup \{m>0, n<0\}$ or their rotations. There are total eight NSHPs.

Admissible region is a NSHP intersected with a sector.

Property 2 If the support of $\hat{h}[m,n]$ lies in an admissible region, then support of $h[m,n]$ lies in the same admissible region.

Proof

By definition of complex cepstrum

$$H(\omega,z) = \exp\ (\hat{H}(\omega,z))$$

$$= \sum_{k=0}^{\infty} \frac{[\hat{H}(w,z)]^k}{k!} \tag{5.14}$$

The above expression corresponds to a k-fold convolution,

$$\therefore\ h[m,n] = \sum_{k=0}^{\infty} \frac{1}{k!}\ [\hat{h} * \ldots * \hat{h}] \tag{5.15}$$

Using the fact that two functions with support on a sector will have the same support for their convolutions, we conclude that k-fold convolutions will have the same support s as that of $\hat{h}[m,n]$. And since $h[m,n]$ is the sum of such terms, so it also has the support s.

Property 3 Here we develop the recursive equations for the signal $x[m,n]$ which is known to be min-min phase i.e., has no poles or zeroes in the region $|\omega| \geq 1$, $|z| \geq 1$.

Assume log $X(\omega,z)$ is analytic.

$$X(\omega,z) = \sum_{m=0}^{\infty}\sum_{n=0}^{\infty} x[m,n]\omega^{-m}z^{-n}$$

$$\hat{X}(\omega,z) = \log\,[X(\omega,z)] \tag{5.16}$$

$$\frac{\partial}{\partial\omega}\hat{X}(\omega,z) = \frac{\frac{\partial}{\partial\omega}[X(\omega,z)]}{X(\omega,z)} \tag{5.17}$$

$$x[m,n] \leftrightarrow X(\omega,z)$$

$$\therefore \quad -mx[m,n] \leftrightarrow \omega\frac{\partial}{\partial\omega}X(\omega,z)$$

Multiplying by ω both sides of eq. (5.17), we have

$$[\omega\frac{\partial}{\partial\omega}\hat{X}(\omega,z)][X(\omega,z)] = \omega\frac{\partial}{\partial\omega}[X(\omega,z)]$$

Since multiplication in the z-domain is the convolution in the time domain, by taking the inverse z-transform, we have

$$-\sum_{k}\sum_{\ell} k\hat{x}[k,\ell]\,x[m-k,n-\ell] = -mx[m,n]$$

Since $\quad x[m,n] = 0 \qquad$ for $m < 0,\ n < 0$

$\therefore\ \hat{x}[m,n] = 0 \qquad$ for $m < 0,\ n < 0$

So, $\quad x[m,n] = \frac{1}{m}\sum_{k=0}^{m}\sum_{\ell=0}^{n} x[m-k,n-\ell]k\hat{x}[k,\ell],$

$m \neq 0$

or, $\quad x[m,n] = \frac{x[m,n]}{x[0,0]} - \frac{1}{mx[0,0]}\sum_{\substack{k=0\\k=m,\ell=n}}^{m}\sum_{\ell=0}^{n} x[m-k,n-\ell]k\hat{x}[k,\ell]$

$m \neq 0$
$x[0,0] \neq 0$

not simultaneously

In order to find x[0,0], we use the initial value theorem.

$$\hat{X}(\omega,z) = \sum_{m=0}^{\infty}\sum_{n=0}^{\infty} \hat{x}[m,n]\omega^{-m}z^{-n}$$

$$\therefore \quad \hat{x}[0,0] = \lim_{\substack{\omega\to\infty \\ z\to\infty}} [\log X(\omega,z)] = \log\left(\lim_{\substack{\omega\to\infty \\ z\to\infty}} X[\omega,z]\right)$$

$$= \log [x[0,0]]$$

So the following are the recursive equations for solving x[m,n],

$$\hat{x}[m,n] = \begin{cases} 0 & m < 0,\ n < 0 \\ \dfrac{x[m,n]}{x[0,0]} - \dfrac{1}{mx[0,0]} \sum_{\substack{k=0 \\ k=m,\ \ell=n \\ \text{not simultaneously}}}^{m}\sum_{\ell=0}^{n} x[m-k,n-\ell]k\hat{x}[k,\ell] & m > 0,\ n \geq 0 \\ & x[0,0] \neq 0 \end{cases} \quad (5.18)$$

$$\hat{x}[0,0] = \log [x[0,0]] \quad (5.19)$$

Eq. (5.18) cannot be used to find the value of complex cepstrum along n axis. However, if we integrate with respect to z in eq. (5.16) and carry out he simplification similar to that above, we get

$$\hat{x}[m,n] = \frac{x[m,n]}{x[0,0]} - \frac{1}{nx[0,0]} \sum_{\substack{k=0 \\ k=m,\ \ell=n \\ \text{not simultaneously}}}^{m}\sum_{\ell=0}^{n} x[m-k,n-\ell]\ell\hat{x}[k,\ell] \quad (5.20)$$

$$n > 0,\ m \geq 0$$

$$x[0,0] \neq 0$$

Thus eqs. (5.18) and (5.20) are to be used first to get the value of x[m,n] along the axes and then either of them can be used to get x[m,n] in the 2-D plane for $m > 0$, $n > 0$.

V.4 Various Strategies for Computation

In two dimensions because of the presence of two independent variables, there can be several approaches for phase unwrapping.

An integration of eq. 5.6 can be carried out. The mixed second partial derivative is computed using eq. (5.10). However, we are not interested in the integration alone because of the truncation error in the process of numerical integration. Also for the same reasons we are not interested in the algorithms which make use of the principal value alone. Efficient and reliable use of bicubic spline interpolation [23] does not seem feasible. So finally we would like to use an adaptive numerical integration scheme with all the added features as discussed in Chapter III. Some of the approaches are shown in Fig. 5.2, where for the sake of simplicity we have indicated phase arg $[X(e^{j\mu},e^{j\nu})]$ by f and μ and ν variables by x and y respectively.

The approach that we have used for phase unwrapping is shown in Fig. 5.2(a). Here we compute the partial derivatives with respect to x at each of the DFT points and partial derivative with respect to y along the first column only using eqs. (5.8) and (5.9). Now making use of eq. (5.7) we unwrap the

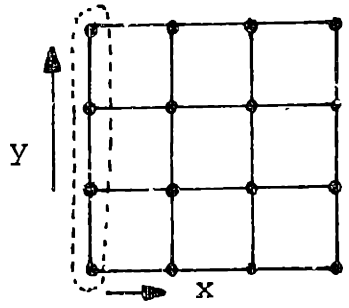

(a)

Computation – $\partial f/\partial x$, $\frac{\partial^2 f}{\partial x^2}$ at every point

$\partial f/\partial y$, $\frac{\partial^2 f}{\partial y^2}$ in the first column only

First along column wise and then r w wise

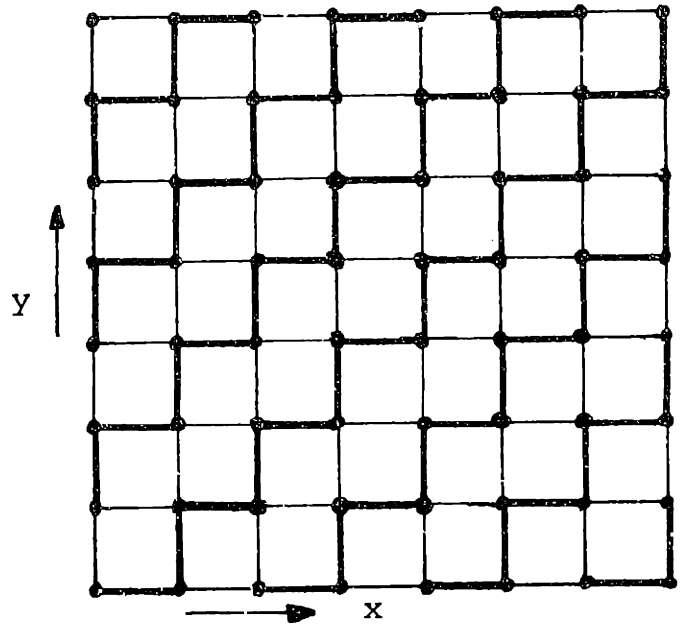

(b) Staircase pattern, alternate direction

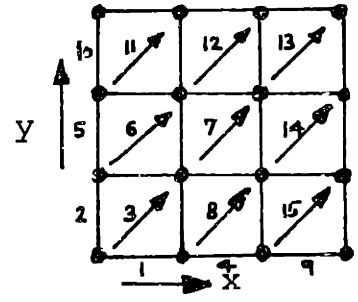

(c) Each time add one point diagonally and unwrap for the additional points of the square so formed.

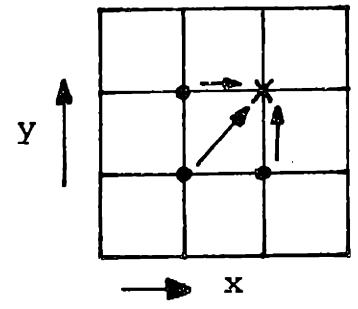

(d) First along the axes

× unknown
. known

Fig. 5.2

phase along the first column using the optimized adaptive phase unwrapping algorithm. Having computed the unwrapped phase along the first column, we compute the unwrapped phase for every row. Now we determine the linear phase along the two axes by looking at the value of the unwrapped phase at π along the two axes. Linear phase is subtracted from the unwrapped phase to make it periodic.

In the present implementation we have directly computed the 2-D DFT at a single frequency which is not on the DFT raster. However, it can be efficiently computed by extending the modified Goertzel Algorithm discussed in Chapter III. Specifically, consider a sequence x[m,n] of area (M,N) i.e., the sequence exists for $0 \leq m \leq M-1$ and $0 \leq n \leq N-1$. Suppose we want to compute DFT at frequency $\frac{k}{M_1}, \frac{\ell}{N_1}$ where $M_1 > M$ and $N_1 > N$. Then by definition of the 2-D DFT, we have,

$$X(k,\ell) = \sum_{m=0}^{M-1} \sum_{n=0}^{N-1} x[m,n] w_{M_1}^{km} w_{N_1}^{\ell n} \tag{5.21}$$

where $$w_{M_1} = e^{-j\frac{2\pi}{M_1}}, \quad w_{N_1} = e^{-j\frac{2\pi}{N_1}} \tag{5.22}$$

and,

$$k = 0, 1, \ldots, M-1$$

$$\ell = 0, 1, \ldots, N-1$$

Using the identity,

$$1 = e^{j \frac{2\pi}{M_1} k(M-M)} \; e^{j \frac{2\pi}{N_1} \ell(N-N)}$$

$$X(k,\ell) = e^{-j 2\pi(\frac{kM}{M_1} + \frac{\ell N}{N_1})} \sum_{m=0}^{M-1} \sum_{n=0}^{N-1} x[m,n] w_{M_1}^{-k(M-m)} w_{N_1}^{-\ell(N-n)}$$

Now exponential term outside the square brackets is the phase term and term inside the square brackets can be implemented using the approach of 1-D Goertzel Algorithm [7].

In this chapter we have discussed some of the properties of two-dimensional complex cepstrum and described the computational strategy that we have used for the computation of 2-D complex cepstrum. In the next chapter we consider the use of complex cepstrum for checking the stability of 1-D and 2-D recursive digital filters.

CHAPTER VI

APPLICATION TO TESTING THE STABILITY OF ONE AND TWO-DIMENSIONAL RECURSIVE DIGITAL FILTERS

VI.1 Introduction

In the last chapter we discussed the basic issues related to the computation of the two-dimensional complex cepstrum. We also considered some of its important properties. In this chapter we shall use the complex cepstrum to check the stability of recursive (infinite impulse response) digital filters.

The problem of testing an IIR filter for stability is of fundamental importance in the design and application of these filters. Particularly, in two-dimensions the stability problem becomes complicated because of the absence of a factorization theorem for two-dimensional polynomials. A number of attempts [24 - 27] have been made to develop stability theorems and to formulate algorithmic tests based on these theorems. However, the numerical implementation of these tests is usually inefficient. Moreover, these results are applicable only to the class of two-dimensional IIR filters which are quadrant causal, i.e., impulse response is non-zero only in one quadrant. The use of the complex cepstrum generalizes the concept of stability test in the sense that it not only includes quarter-plane filters, but also non-symmetric half plane filters. Furthermore, the implementation of the complex cepstrum is more efficient than existing

tests when the FFT is employed.

For testing the stability of 1-D linear discrete-time systems, we make use of the fact (which has not been emphasized because of the absence of an effective method of phase unwrapping) that the number of zeroes outside the unit circle is equal to the absolute value of the slope of the linear phase. In 2-D this concept does not apply, but it is known that if the system is stable, then the cepstrum is non-zero only where the impulse response is non-zero. So we shall make use of this fact to check the stability of quarter plane and non-symmetric half plane filters. A number of examples are presented including cases where the filter happens to be unstable.

This method of testing the stability is compared with existing methods on the basis of computational complexity, programming efficiency etc.

VI.2 Stability Testing in One Dimension

Once an IIR filter has been designed, the question of the stability of the resulting filter X(z) arises. Let $X(z) = \frac{N(z)}{D(z)}$. There are a number of stability tests in one dimension. The polynomial D(z) can always be factored to determine the poles of the filter, but this is a costly procedure that is best avoided. In the following we shall first discuss the use of the complex cepstrum for checking the stability of one-dimensional linear discrete-time systems and then we

shall compare it with the other methods which are bilinear transformation from z-to-s domain, Jury's method based on Schur-Cohn determinants [28] and Levinson's recursion for the autocorrelation method of linear prediction [29].

In Chapter II we mentioned the following two properties of the complex cepstrum:

(1) If $x[n]$ is minimum phase, then $\hat{x}[n] = 0$, $n < 0$

(2) If $x[n]$ is maximum phase, then $\hat{x}[n] = 0$, $n > 0$

These two properties follow in a straightforward manner from the definition of the complex cepstrum. Specifically, since

$$\hat{X}(z) = \log X(z)$$

Differentiating with respect to z, we get

$$\frac{d}{dz}\hat{X}(z) = \frac{1}{X(z)}\frac{d}{dz}X(z)$$

but $X(z) = \frac{N(z)}{D(z)}$, so we have

$$\frac{d}{dz}\hat{X}(z) = \frac{N(z)D'(z) - D(z)N'(z)}{N(z)D(z)} \qquad (6.1)$$

Also, $\hat{x}[n] \leftrightarrow \hat{X}(z)$ and $n\hat{x}[n] \leftrightarrow -z\frac{d}{dz}\hat{X}(z)$.

From the above expression it is clear that the poles of the z-transform of $n\hat{x}[n]$ occur at the poles and zeroes of the z-transform of $x[n]$. So, if all the poles and zeroes of $X(z)$

lie inside the unit circle (i.e., x[n] is minimum phase), then all poles of $-z \frac{d}{dz} \hat{X}(z)$ lie inside the unit circle and thus $n\hat{x}[n]$ or $\hat{x}[n]$ is zero for $n < 0$. A similar argument can be used to show the property for maximum phase case. From these properties it can be noted that $\hat{x}[n]$ is non-zero only where x[n] is non-zero.

Using the above properties the stability test using complex cepstrum becomes

(1) Find the complex cepstrum $\hat{d}[n]$ corresponding to the given D(z) (system function $X(z) = \frac{N(z)}{D(z)}$)

(2) Check whether $\hat{d}[n] = 0$ for $n < 0$ (causal case)

$= 0$ for $n > 0$ (anti-causal case)

and thus conclude about the stability. Note if $\hat{d}[n]$ happens to be mixed phase, then the system is unstable.

Now we develop an important result which could alternatively be used for checking the stability. It only requires the determination of the unwrapped phase and states that the number of zeroes outside the unit circle is equal to the slope of the linear phase evaluated at $\omega = \pi$.

For a finite length sequence which is non-zero only between $0 \leq n \leq M$, we have

$$X(z) = \sum_{n=0}^{M} x[n] z^{-n} \tag{6.2}$$

Obviously, X(z) is an M^{th} degree polynomial in z^{-1}, it has M zeroes and M poles. All these poles are located at the origin.

There are two possibilities for M zeroes. They may be inside or outside the unit circle. Let

m_i = number of zeroes inside the unit circle

and m_o = number of zeroes outside the unit circle

so that $M = m_i + m_o$.

These zeroes may be represented as $\prod_{k=1}^{m_i}(1-a_k z^{-1})$ and $\prod_{k=1}^{m_o}(1-b_k z)$, where $|a_k|, |b_k| < 1$. Now in order to get the valid z-transform X(z) we must divide the product of these zeroes by z^{m_o}. So within a constant factor A, we can write

$$X(z) = \frac{A \prod_{k=1}^{m_i}(1-a_k z^{-1}) \prod_{k=1}^{m_o}(1-b_k z)}{z^{m_o}}$$

$$\text{or } X(z)\Big|_{z=e^{j\omega}} = X(e^{j\omega}) = Ae^{-j\omega m_o} \prod_{k=1}^{m_i}(1-a_k e^{-j\omega}) \prod_{k=1}^{m_o}(1-b_k e^{j\omega}) \tag{6.3}$$

Assuming that the sign of A has already been made positive, we have

$$X(e^{j\omega})\Big|_{\omega=\pi} = Ae^{-j\pi m_o} \prod_{k=1}^{m_i}(1+a_k) \prod_{k=1}^{m_o}(1+b_k) \tag{6.4}$$

$$= |X(e^{j\pi})|\, e^{j \arg[X(e^{j\pi})]} \tag{6.5}$$

From eqs. (6.4) and (6.5),

$$\arg\ [X(e^{j\pi})] = -\ \pi m_o$$

$$\therefore\quad m_o = -\ \frac{\arg\ [X(e^{j\pi})]}{\pi} \qquad (6.6)$$

This shows that the number of zeroes outside the unit circle is equal to the absolute value of the slope of the linear phase. It can be noted that this result is in complete analogy to the Routh-Hurwitz criterion for stability in continuous time case, which makes it possible to find out exactly the number of roots of a polynomial lying in left half plane and right half plane without having to evaluate the actual roots. Thus we can give a binary answer (stable or unstable) about the stability of a linear discrete-time system.

So the procedure for checking the stability of linear discrete-time systems will be the following:

(1) Given the order of the system, we know the total number of zeroes of the denominator polynomial D(z) of the system function. In an attempt to find the complex cepstrum of D(z) we obtain the value of the slope of linear phase and thus determine the number of zeroes inside and outside the unit circle.

(2) Depending upon the slope of the linear phase conclude:

- For the causal stable system linear phase should be zero.
- For the anti-causal stable system, linear phase must be equal to the order of the system, i.e., all the zeroes of D(z) are outside the unit circle.
- If the slope of linear phase is greater than zero but not equal to the order of the system, then the system is unstable.

Computation required in the determination of complex cepstrum is proportional to N $\log_2$ N, where N is the FFT size used. Also we only approximate $\hat{x}[n]$ due to DFT as has been discussed in Chapter III.

Now let us consider the other methods for checking the stability of one-dimensional discrete time systems.

(1) Use of bilinear transformation $z = \frac{s+1}{s-1}$ to map the inside of the unit circle in the z-plane into the left half of the s-plane and then applying the Routh-Hurwitz criterion. This transformation involves two difficulties [28].

(a) Algebraic manipulations for higher-order systems become complicated.

(b) The final constraints on the coefficients in the z-plane become unwieldy and require algebraic reduction to yield the minimum number of terms.

Because of these limitations this criterion is not usually used for systems higher than second order.

A method suggested by Jury [28] is based on the evaluation of Schur-Cohn determinants computed directly from the system characteristic equation. For an n-th order system, the Schur-Cohn determinants consist of two first-order determinants, two second-order determinants and so on up to two n-th order determinants. The number of zeroes outside the unit circle is found by noting the number of sign changes in the sequence of determinants. Using Gaussian elimination total number of arithmetic operations (defining each division, and each multiplication-subtraction as a single operation) to evaluate an n-th order determinant equals

$$\frac{n^3-n}{3} + (n-1) \approx \frac{n^3+2n}{3}$$

$$\therefore \quad \text{total number of operations} = \frac{2}{3} \sum_{k=1}^{n} (k^3 + \frac{2}{3}k)$$

$$= \frac{n(n+1)}{18}(3n^2+3n+4) \qquad (6.7)$$

Thus the amount of computation is proportional to the fourth power of the order of the system.

One other method for testing the stability [29] is to solve the autocorrelation normal equations for predictor coefficients using Levinson recursion modified by Durbin. Now predictor parameters can be used to compute the reflection coefficients k_i by a backward recursion and the condition for

the stability of X(z) is that $|k_i| < 1$ for $1 \leq i \leq n$ where n is the order of predictor. This method of checking the stability is essentially the same as the Lehmer-Schur method [29]. The amount of computation is proportional to n^2.

Comparing the above methods with the use of complex cepstrum for checking the stability, on the basis of amount of computation, it can be seen that the method based on solving the autocorrelation normal equations is the most efficient. For high order systems use of complex cepstrum may be very efficient. For zeroes extremely close (by 10^{-6}) to the unit circle, as the phase unwrapping becomes difficult so are the ill-conditioning of Schur-Cohn matrix [4] and the autocorrelation matrix [29].

VI.3 Examples and Comments

In this section we present two examples.

Example 6.1 - 3rd order unstable system

Let the system function be

$$X(z) = \frac{N(z)}{D(z)} = \frac{1}{1+8z^{-1}+4z^{-2}+2z^{-3}} \qquad (6.8)$$

Corresponding to D(z), sequence is shown in Fig. 6.1.

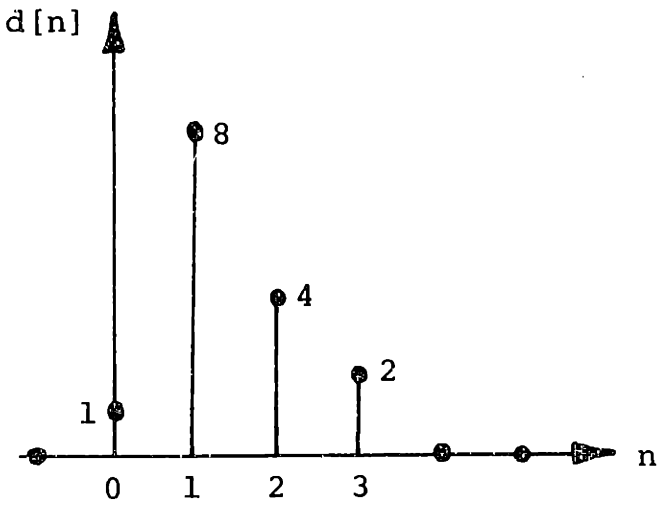

Fig. 6.1 Sequence Corresponding to D(z)

Looking at Fig. 6.1, we expect a linear phase of -1 (one zero should be outside the unit circle) and since the system is of 3rd order, we conclude that the system is unstable. Fig. 6.2 shows the phase derivatives, principal value, unwrapped phase and cepstrum of the signal. FFT size used is 512 points. From the cepstrum plot it can be seen that the cepstrum exists for low times and high times, hence the signal is mixed phase.

In this simple example, let us factor D(z) to find out the exact location of roots.

$$D(z) \approx 7.5z^{-1} \left(1 + \frac{1}{7.5} z\right)\left(1 + z_1 z^{-1}\right)\left(1 + z_1^{*} z^{-1}\right), \quad (6.9)$$

where $z_1 = -0.25 + j0.433$.

Thus we see that one real zero is at $z = -7.5$ and a complex pair of zeroes at $z_1 = -0.25 \pm j0.433$. So we expect

Linear phase = -1

$\hat{d}[0] = 2.0149$

EXAMPLE 6.1
Third order 1-D
unstable system

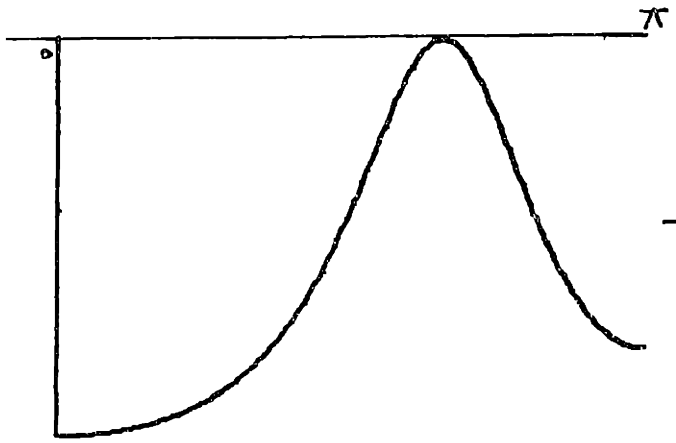

Phase Derivative

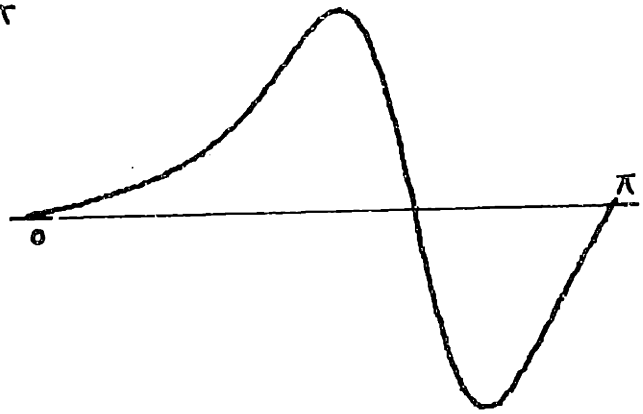

Phase Second Derivative

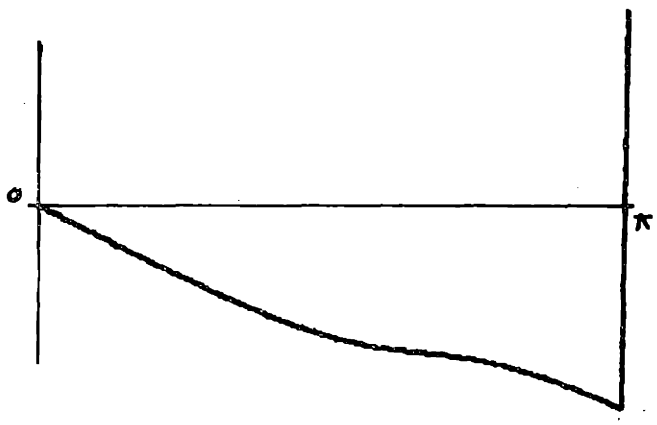

Phase Principal Value

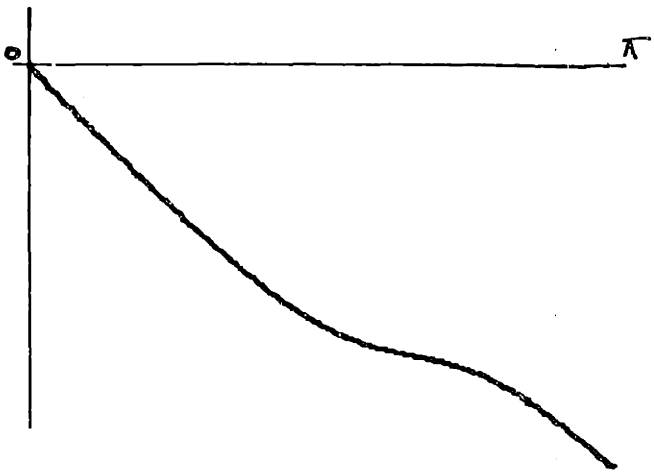

Unwrapped Phase before removal of linear phase

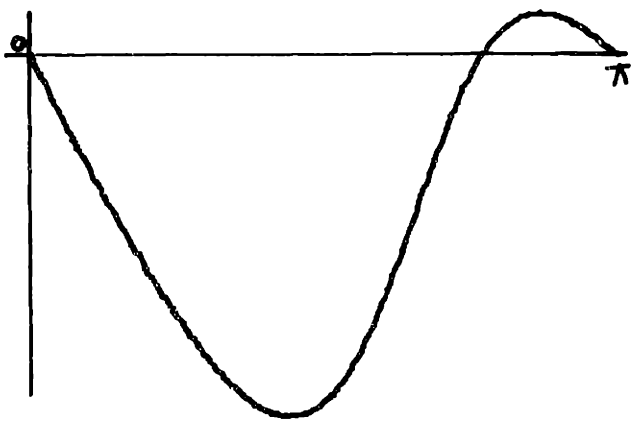

Unwrapped Phase after Removal of Linear Phase

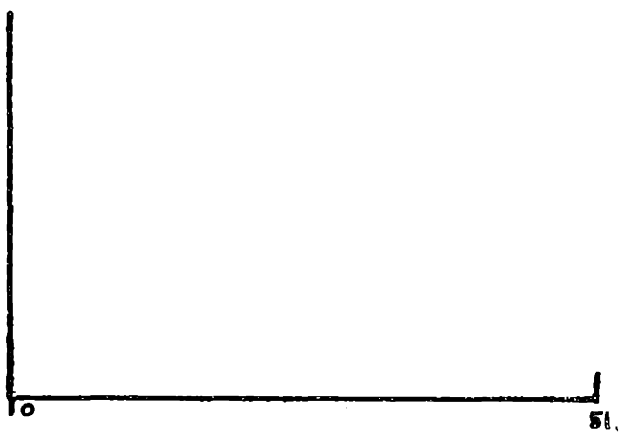

Complex Cepstrum

Fig. 6.2

$$\grave{d}[n] = \frac{(\frac{-1}{7.5})^n}{n} \quad , \; n < 0$$

$$\hat{d}[n] = -\left[\frac{(z_1)^n}{n} + \frac{(z_1^*)^n}{n}\right] \quad , \; n > 0$$

Example 6.2 - 8th order stable causal system

Let the system function be

$$X(z) = \frac{N(z)}{D(z)} = \frac{1}{1-\alpha_1 z^{-1}+\alpha_2 z^{-2}-\alpha_3 z^{-3}+\alpha_4 z^{-4}-\alpha_5 z^{-5}+\alpha_6 z^{-6}-\alpha_7 z^{-7}+\alpha_8 z^{-8}} \tag{6.10}$$

where $\alpha_1 = 0.137897$, $\alpha_2 = 0.0110411$, $\alpha_3 = -0.130083$, $\alpha_4 = 1.809621$,
$\alpha_2 = 0.138284$, $\alpha_6 = 0.011621$, $\alpha_7 = -0.129644$, $\alpha_8 = 0.809659$

Sequence corresponding to D(z) is shown in Fig. 6.3. We have generated this sequence corresponding to the pole zero plot shown in Fig. 6.4.

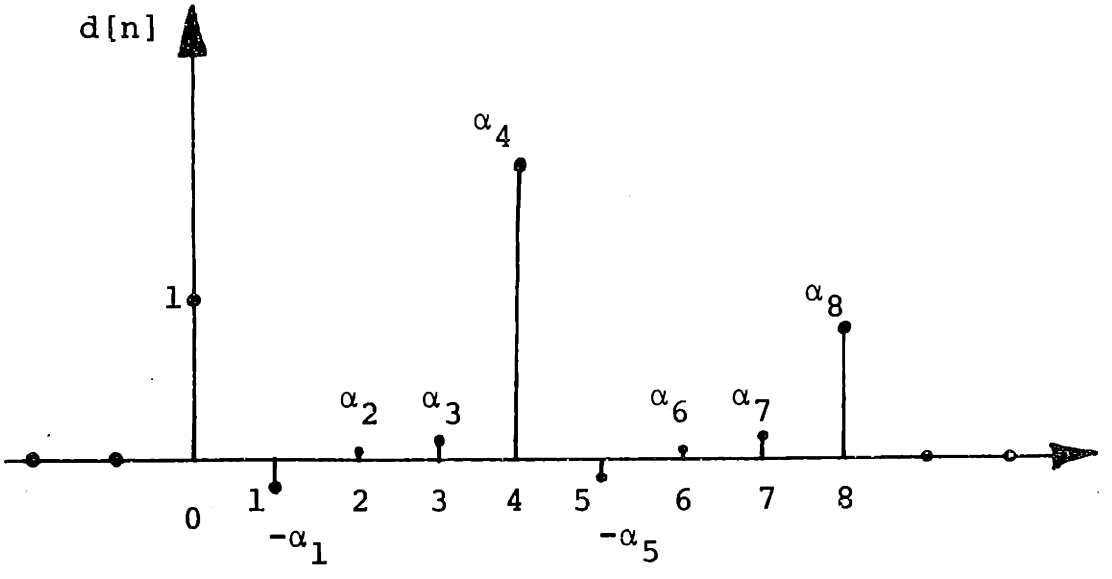

Fig. 6.3 Sequence Corresponding to D(z)

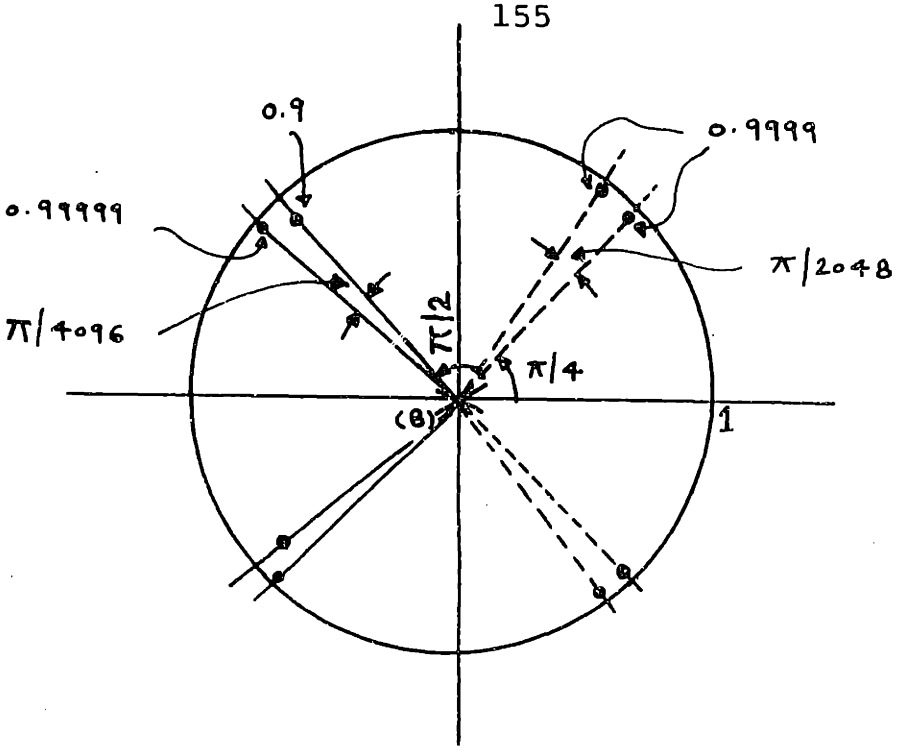

Fig. 6.4 Pole-Zero Plot for D(Z)

Since d[n] is minimum phase, we expect a linear phase of zero. Fig. 6.5 shows the phase derivatives, principal value, unwrapped phase and cepstrum. Cepstrum values can be checked using minimum phase recursive formula or summing the contributions to the cepstrum from each zero. Here we have considered zeroes very close to the unit circle and also quite close with each other.

VI.4 Stability Testing in Two Dimensions

The basic theorem for guaranteeing bounded input - bounded output stability of 2-D recursive digital filters was presented by Shanks [24] in 1972. Although this test is conceptually straightforward, it is computationally involved.

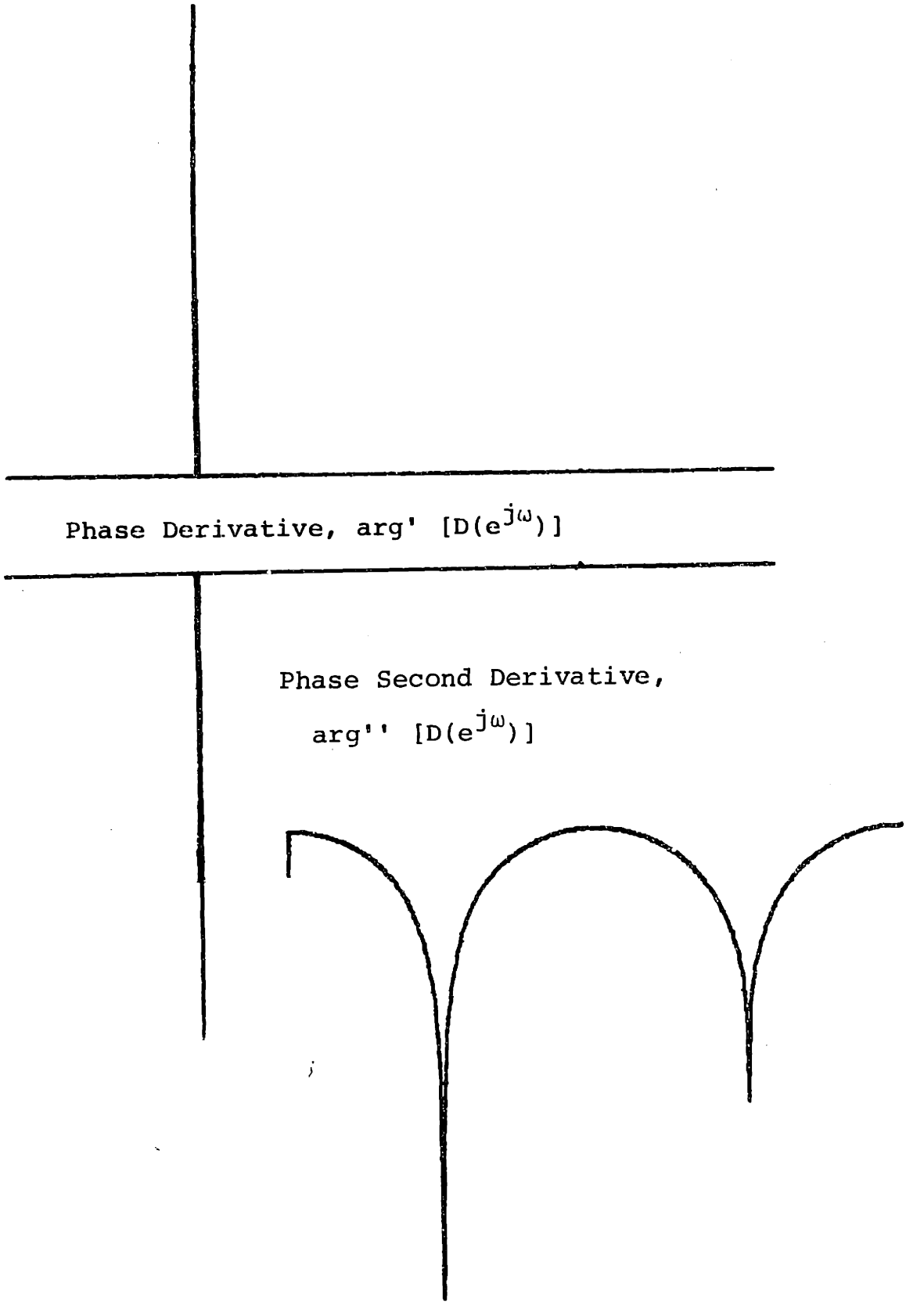
Phase Derivative, arg' [D(e^jω)]
Phase Second Derivative,
arg'' [D(e^jω)]
Log magnitude of frequency response,
log |D(e^jω)|

Fig. 6.5(a)

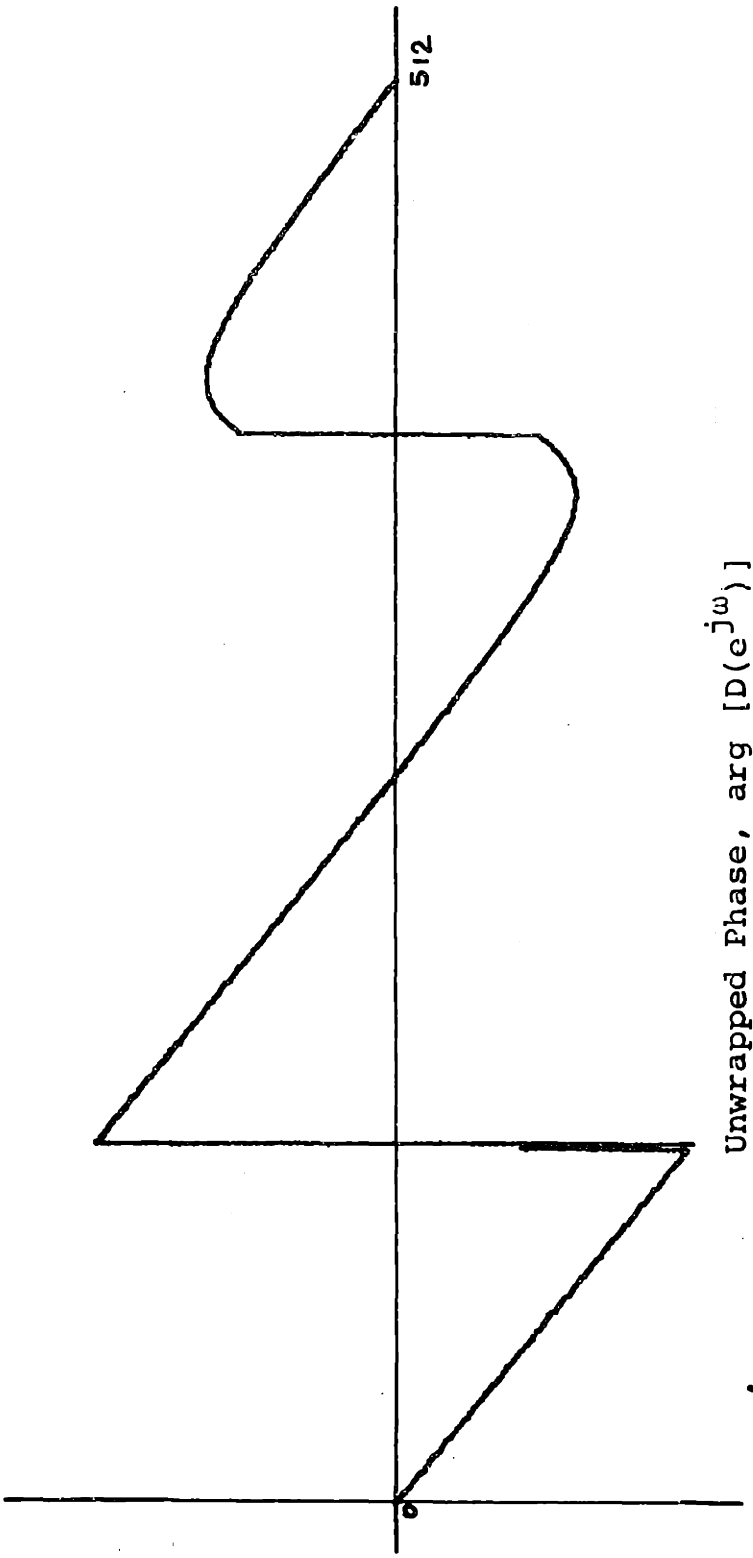

Unwrapped Phase, arg $[D(e^{j\omega})]$

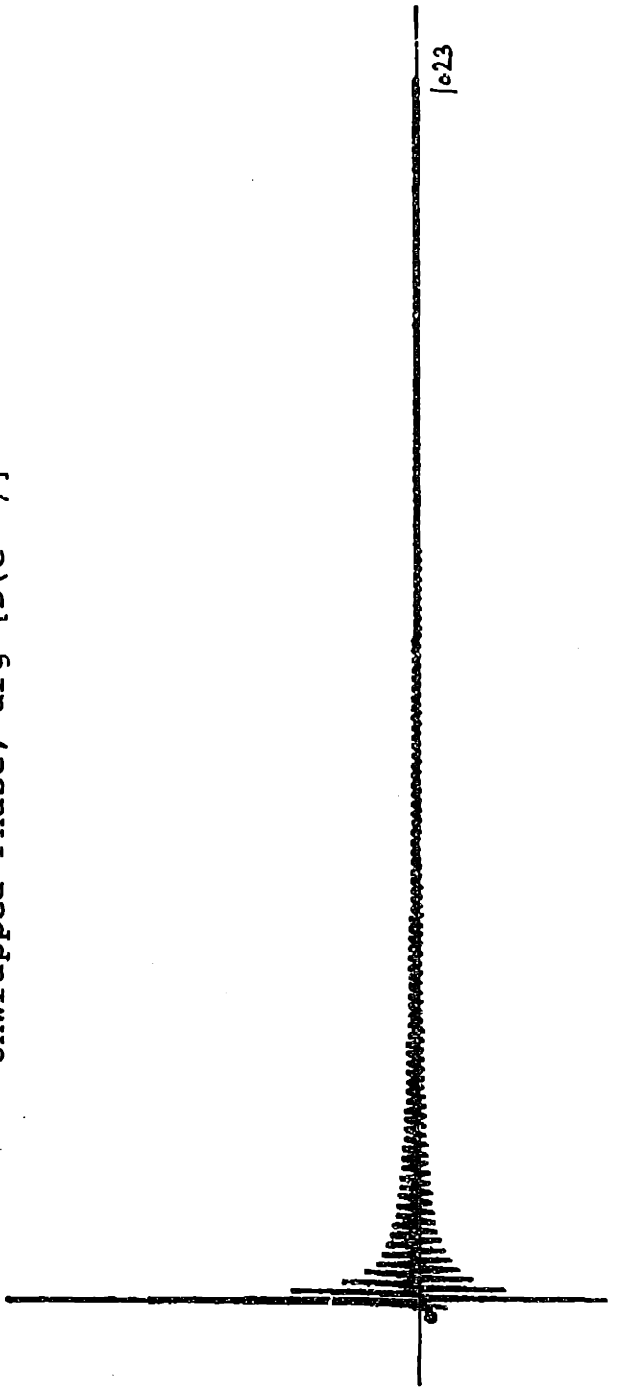

Complex cepstrum, $\hat{d}[n]$

Fig. 6.5(b)

The reason being that to test stability by ensuring that the denominator polynomial $D(\omega,z) \neq 0$ is impossible to do computationally, since we must check $D(\omega,z)$ at an infinite number of points. A simplified version of Shanks' stability theorem was given by Huang [25]. Various efforts have been made to find implementations of Huang's test which require only a finite amount of computation. Huang showed that his test could be reformulated in a form which only required a finite number of computational steps using a test of Ansell's for continuous system. Anderson & Jury [27] showed that the main component of Huang's test (bilinear transformation) could be accomplished using a Schur-Cohn matrix test and thus saving a substantial computational load for any but the simplest two-variable polynomials. Maria and Fahmy [26] have also proposed more efficient implementation of Huang's test. This method has the advantage that all the determinants used in the computation are of dimension two, while Huang's test uses determinants of an order up to the order of the filter. This test requires computations of $O(N^2\ 2^{2(N-1)})$ for an NxN filter. However, there are problems with this approach while implementing higher order filters.

Ekstrom and Woods [21] have described a method for checking the stability which requires computation of $O(N^2 \log N)$ and is based on the homomorphic signal processing approach. They avoid the problem of phase unwrapping by taking the input of a homomorphic system as the autocorrela-

tion of the sequence. After computing the cepstrum it is multiplied by a suitable window depending upon the choice of region in the 2-D plane and the resultant signal is taken as the input of the inverse characteristic system. Now the output of the inverse characteristic system is compared with the input sequence. If they happen to be the same, then the filter is stable, otherwise not. This procedure is computationally not as attractive as the method based on computing the complex cepstrum which requires phase unwrapping. Very recently Ekstrom and Twogood [22] have presented the stability test which uses the complex cepstrum and requires phase unwrapping. However, as we have described in the last chapter, the phase unwrapping which they employed is based on Schafer's [1] algorithm and is not reliable. Filip [4] got a very poor estimate of the phase while using homomorphic signal processing for estimating the phase angle of the degrading linear shift invariant system using Schafer's phase unwrapping approach. Our approach for testing the stability is similar to Ekstrom and Twogood [22] but the phase unwrapping technique that has been used is different from theirs. The technique that is used has been described in the last chapter.

It is to be noted that because we cannot factor 2-D polynomials, the concept of using linear phase (similar to that in the 1-D case) components along the two axes cannot be used to determine the stability in two dimensions. So we look at the first idea given in the 1-D case for checking the

stability, whose 2-D version is given below.

Let the system function of the 2-D recursive filter be given by

$$G(\omega,z) = \frac{N(\omega,z)}{D(\omega,z)} ,$$

where $N(\omega,z)$ and $D(\omega,z)$ are each 2-D polynomials.

In order to check the stability of this filter

(i) We take the denominator polynomial $D(\omega,z)$ and find its cepstrum $\hat{d}[m,n]$.

(ii) Check whether the support of $\hat{d}[m,n]$ is the same as that of $d[m,n]$. If yes, then the filter is stable, otherwise it is unstable. (Proof of this theorem has been given in the last chapter.)

Similar to that of the one-dimensional case, the DFT implementation of the characteristic system will give $\hat{d}_a[m,n]$ which is an aliased version of $\hat{d}[m,n]$. But since the cepstrum decays faster than an exponential, $\hat{d}_a[m,n]$ will be a reasonable approximation of $\hat{d}[m,n]$ for the modest size of 2-D FFT's.

One advantage of using the method based on computing the 2-D complex cepstrum for checking the stability is that the concept of checking the stability in two dimensions is generalized in the sense that we do not care whether the filter belongs to the quarter-plane or non-symmetric half-plane classes etc. All that we need is to check the support of $d[m,n]$ and $\hat{d}[m,n]$. Furthermore, this method requires less computation than any other method of checking the stability

of 2-D recursive digital filters. Also the order of filter can be very high. We have just to take the sufficiently large size of 2-D FFT so as to minimize the aliasing.

In the next section we present a number of examples for testing the stability of 2-D recursive digital filters. We also consider the unstable examples and comment on the phase unwrapping for such cases.

VI.5 Examples and Comments

In this section we present several examples for testing the stability of 2-D recursive digital filters using the method of computing the complex cepstrum discussed in Chapters V and VI. We have divided the examples to be discussed in the following three categories:

(1) Quarter-plane filters involving
    (a) separable sequences
    (b) nonseparable sequences
(2) Non-symmetric half-plane filters
and (3) Unstable quarter-plane filters.

Quarter-plane filters involving separable sequences

In this category we consider two examples.

Example 6.3 Separable sequence exponentials

Let the denominator array of the 2-D recursive filter be given by

$$\alpha[m,n] = \left(\frac{1}{2}\right)^{m} \left(\frac{1}{2}\right)^{n}, \qquad \begin{matrix} 0 \leq m \leq 3 \\ 0 \leq n \leq 3 \end{matrix}$$

i.e.,

$$\hat{d}[m,n] = \begin{array}{c} \begin{matrix} 0 & \text{---} & m \end{matrix} \\ \Big| \\ n \end{array} \begin{matrix} 1 & \frac{1}{2} & \frac{1}{4} & \frac{1}{8} \\ \frac{1}{2} & \frac{1}{4} & \frac{1}{8} & \frac{1}{16} \\ \frac{1}{4} & \frac{1}{8} & \frac{1}{16} & \frac{1}{32} \\ \frac{1}{8} & \frac{1}{16} & \frac{1}{32} & \frac{1}{64} \end{matrix} \qquad (6.11)$$

The z-transform corresponding to this 2-D array is

$$D(\omega,z) = \left(\frac{1-\frac{1}{16}\omega^{-4}}{1-\frac{1}{2}\omega^{-1}}\right)\left(\frac{1-\frac{1}{16}z^{-4}}{1-\frac{1}{2}z^{-1}}\right) \qquad (6.12)$$

$$D(\omega,z) = \log D(\omega,z)$$

$$= \log\left[1-\frac{1}{16}\omega^{-4}\right] - \log\left[1-\frac{1}{2}\omega^{-1}\right]$$

$$+ \log\left[1-\frac{1}{16}z^{-4}\right] - \log\left[1-\frac{1}{2}z^{-1}\right]$$

Using the series expansion for log, we get

$$\hat{d}[m,n] = \frac{(\frac{1}{2})^m}{m} u[m-1] + \frac{(\frac{1}{2})^n}{n} u[n-1] - \frac{1}{16}\delta[m-4]$$

$$- \frac{1}{16}\delta[n-4] - (\frac{1}{16})^2 \cdot \frac{1}{2} \cdot \delta[m-8] - (\frac{1}{16})^2 \cdot \frac{1}{2} \cdot \delta[n-8]$$

$$- (\frac{1}{16})^3 \cdot \frac{1}{3}\delta[m-12] - (\frac{1}{16})^3 \cdot \frac{1}{3}\delta[n-12]$$

$$- (\frac{1}{16})^4 \cdot \frac{1}{4}\delta[m-16) - (\frac{1}{16})^4 \cdot \frac{1}{4}\delta[n-16] - \ldots$$

(6.13)

From eq. (6.13) or Fig. 6.7 it can be observed that the complex cepstrum exists only on the axes as was expected from the Property 1 of Chapter 5. Fig. 6.6 shows $|D(e^{j\mu},e^{j\nu})|$, log $|D(e^{j\mu},e^{j\nu})|$, phase first derivative and second derivative. FFT size taken was 32x32. From the derivative curves the separable nature of the sequence can be observed. Fig. 6.7 shows the principal value of the phase, the complex cepstrum and the sequence as obtained from the inverse characteristic system. In this case the plot for the unwrapped phase is the same as for the principal value. The support of $d[m,n]$ and $\hat{d}[m,n]$ are the same as can be clearly observed, hence the system has got to be stable.

EXAMPLE 6.3
Separable Sequence
Exponentials
FFT size 32x32

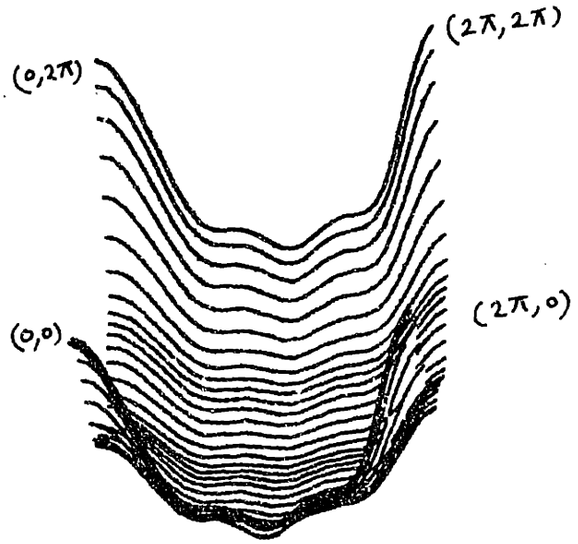

Absolute value of frequency response,

$$|D(e^{j\mu}, e^{j\nu})|$$

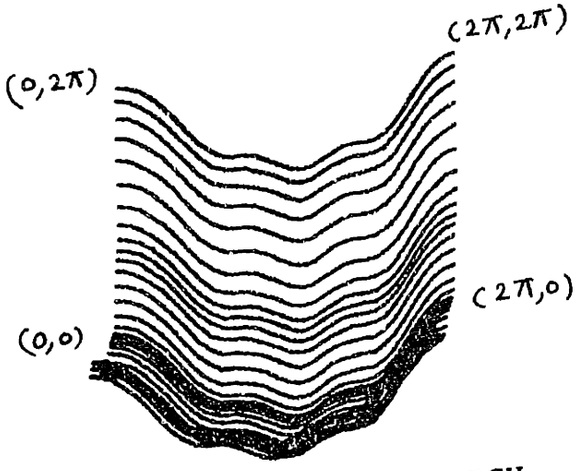

Log magnitude of frequency response,

$$\log |D(e^{j\mu}, e^{j\nu})|$$

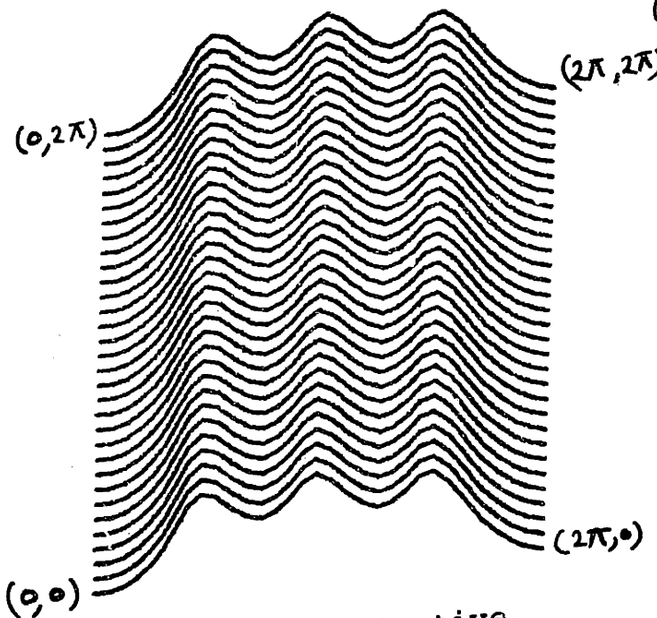

Phase first derivative,

$$\arg' [D(e^{j\mu}, e^{j\nu})]$$

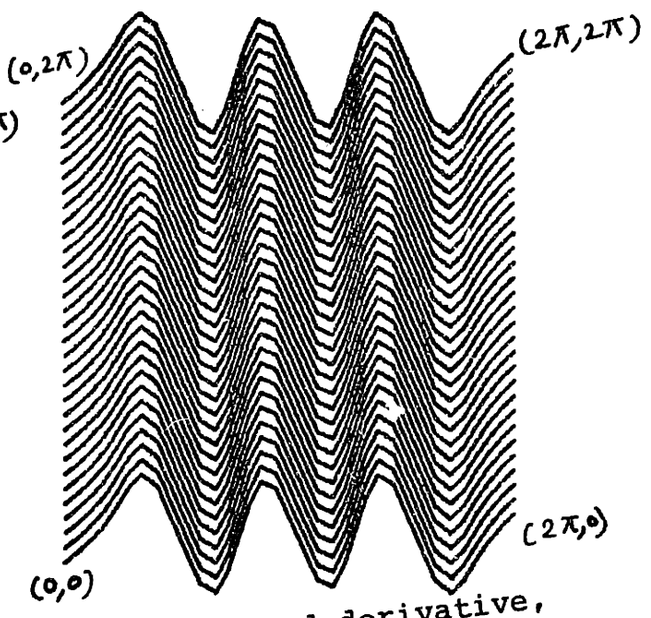

Phase second derivative,

$$\arg'' [D(e^{j\mu}, e^{j\nu})]$$

Fig. 6.6

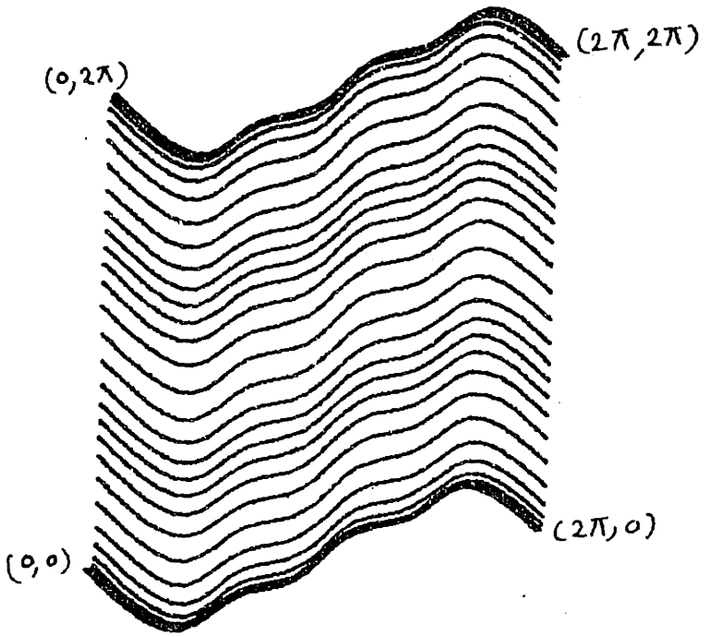

Principal value or unwrapped phase,

$$\arg\,[D(e^{j\mu}, e^{j\nu})]$$

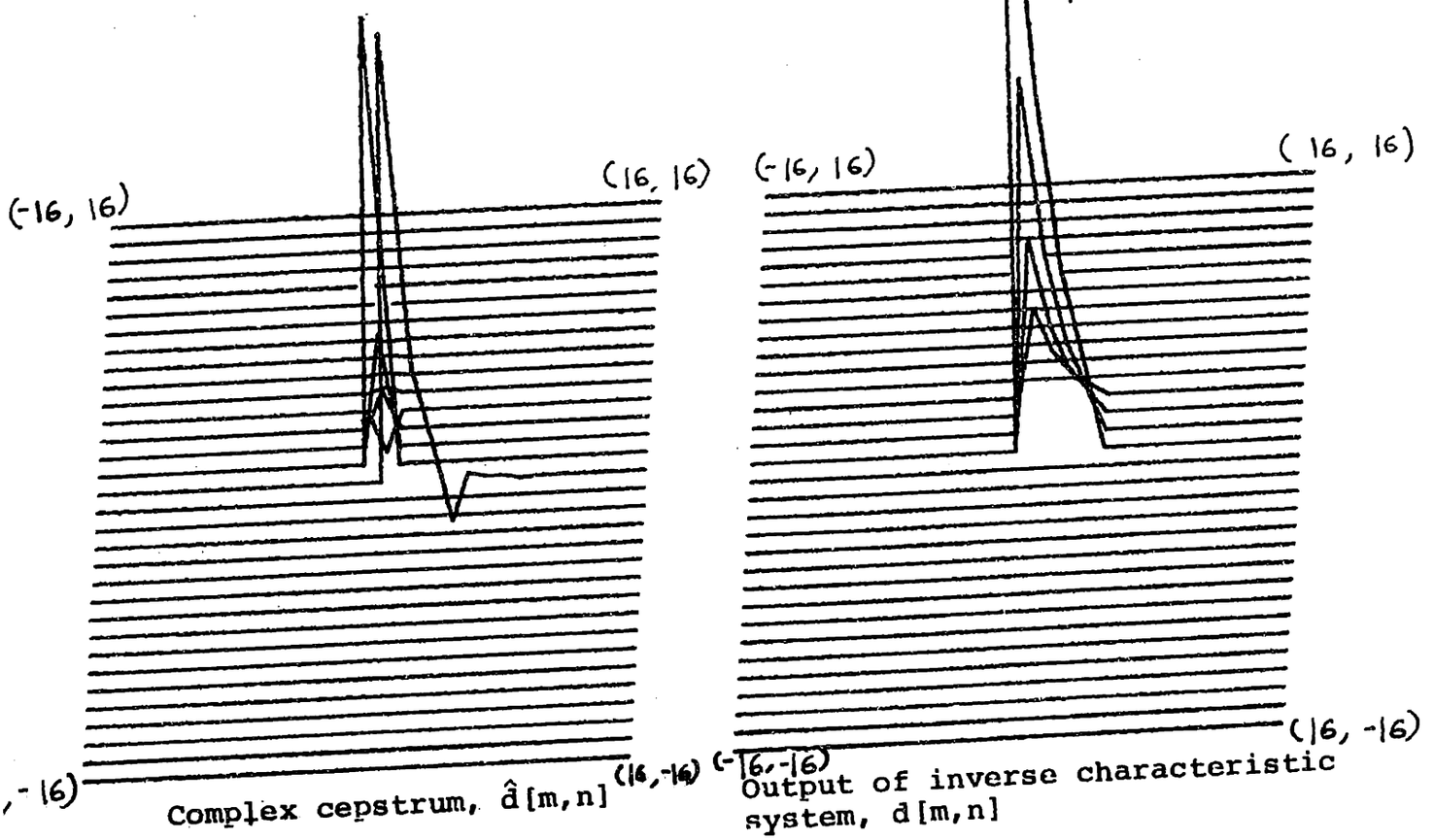

Complex cepstrum, $\hat{d}[m,n]$

Output of inverse characteristic system, $d[m,n]$

Fig. 6.7

Example 6.4

This is another example of a separable sequence which has been examined by Anderson & Jury [27]. The 2-D denominator array of the filter is given by

$$d[m,n] = \begin{array}{c} n \\ | \\ 0 \end{array} \begin{array}{ccc} 6 & 5 & 1 \\ 12 & 10 & 2 \\ \multicolumn{3}{c}{\text{———}} \\ \multicolumn{3}{c}{m} \end{array} \qquad (6.14)$$

Since one row is the multiple of the other, the separable nature of sequence d[m,n] can be identified. The z-transform is,

$$X(\omega,z) = (3+\omega^{-1})(2+\omega^{-1})(2+z^{-1}) \qquad (6.15)$$

The complex cepstrum can be easily obtained from eq. (6.15) as

$$d[m,n] = [\log 12]\delta[m,n] - \frac{1}{m}[(-\tfrac{1}{3})^{m} + (-\tfrac{1}{2})^{m}]\, u[m-1]$$

$$- \frac{(-\frac{1}{2})^{n}}{n}\, u[n-1] \qquad (6.16)$$

Figure 6.8 shows $|D(e^{j\mu},e^{j\nu})|$ and log $|D(e^{j\mu},e^{j\nu})|$. Fig. 6.9 shows phase first and second derivatives. Separable nature of the sequence is evident from these plots. Fig. 6.10 shows the unwrapped phase (it is the same as principal value plot), complex cepstrum sequence and

(Anderson & Jury)
FFT size 64x64

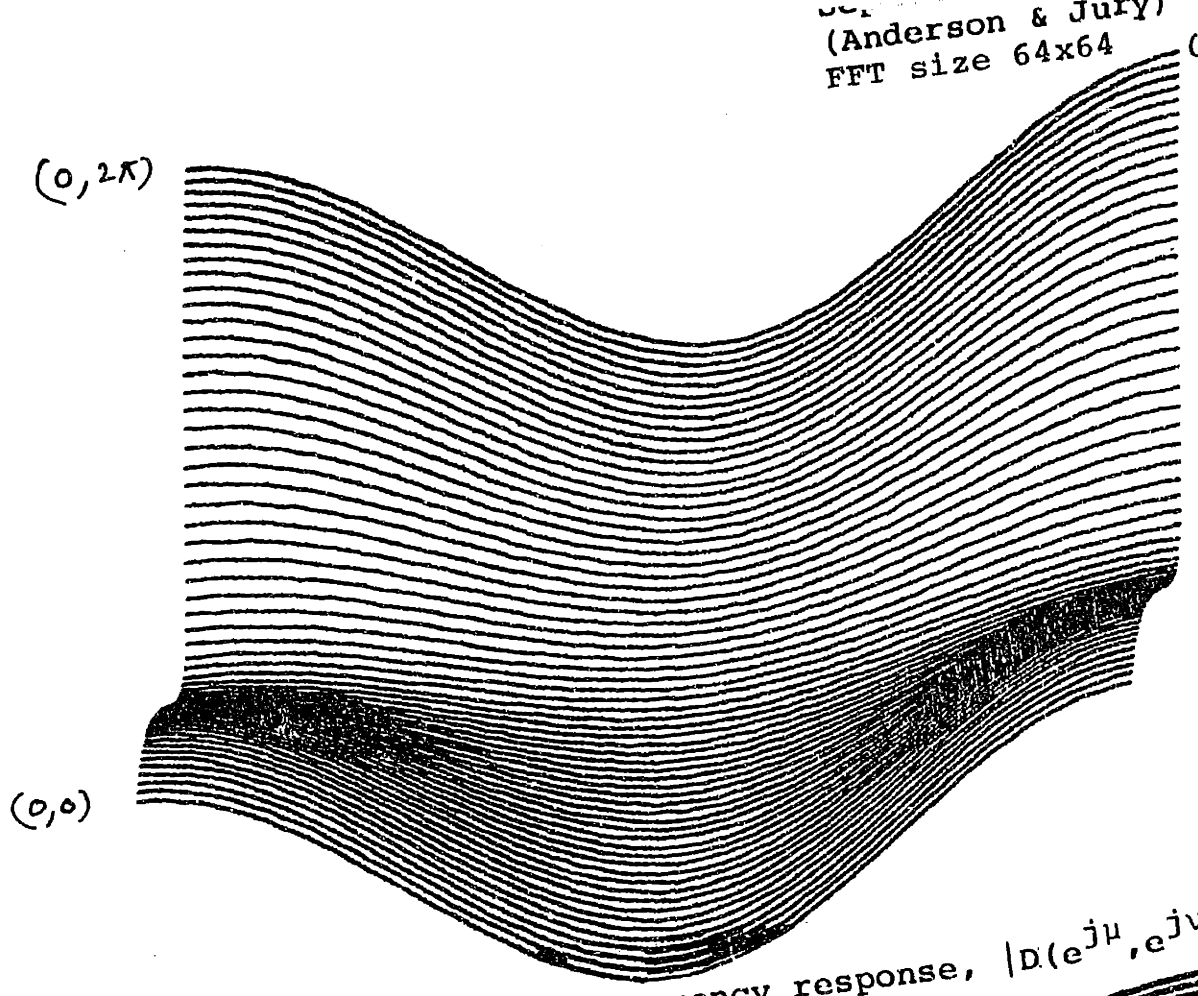

Absolute value of frequency response, $|D(e^{j\mu}, e^{j\nu})|$

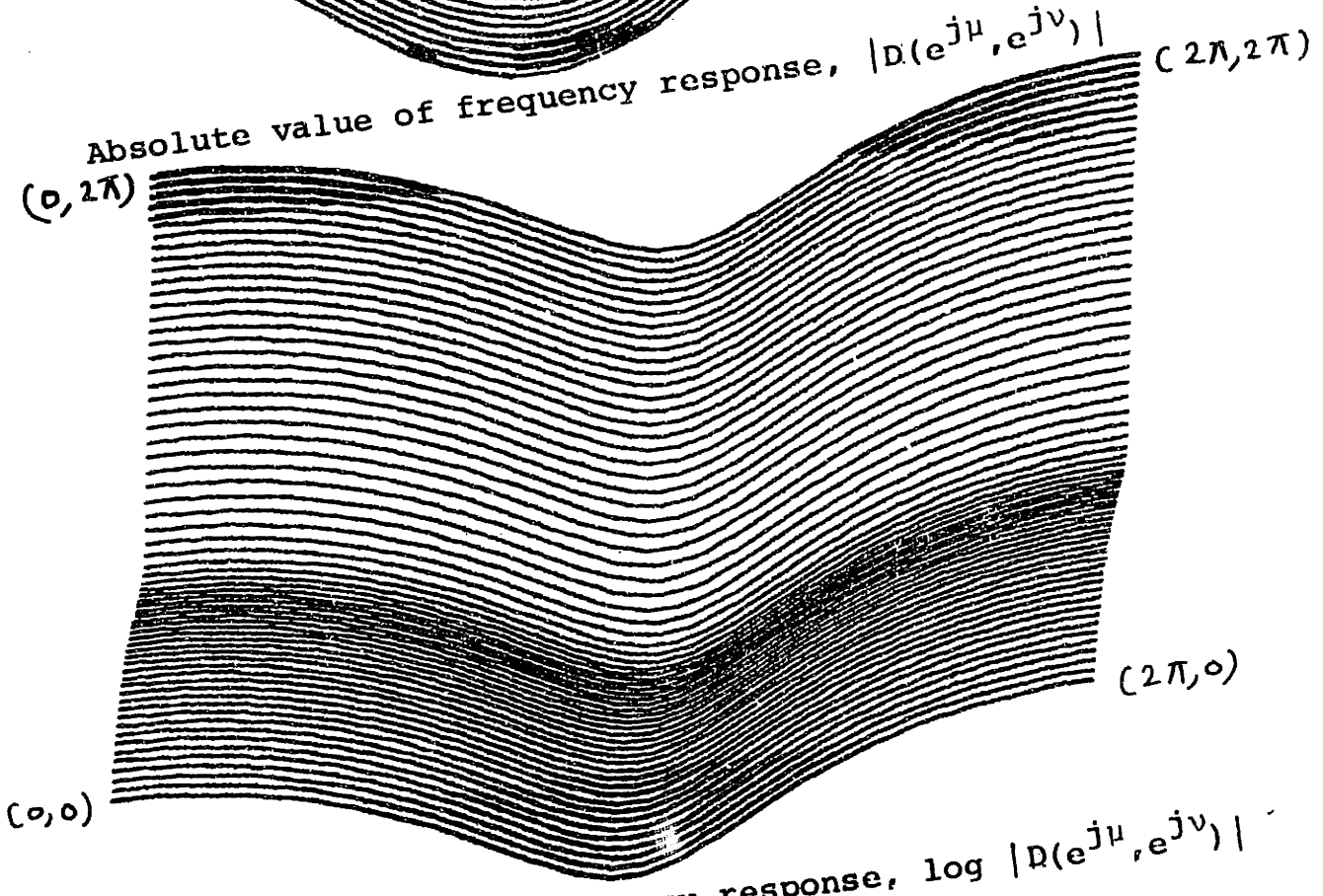

Log magnitude of frequency response, $\log |D(e^{j\mu}, e^{j\nu})|$

Fig. 6.8

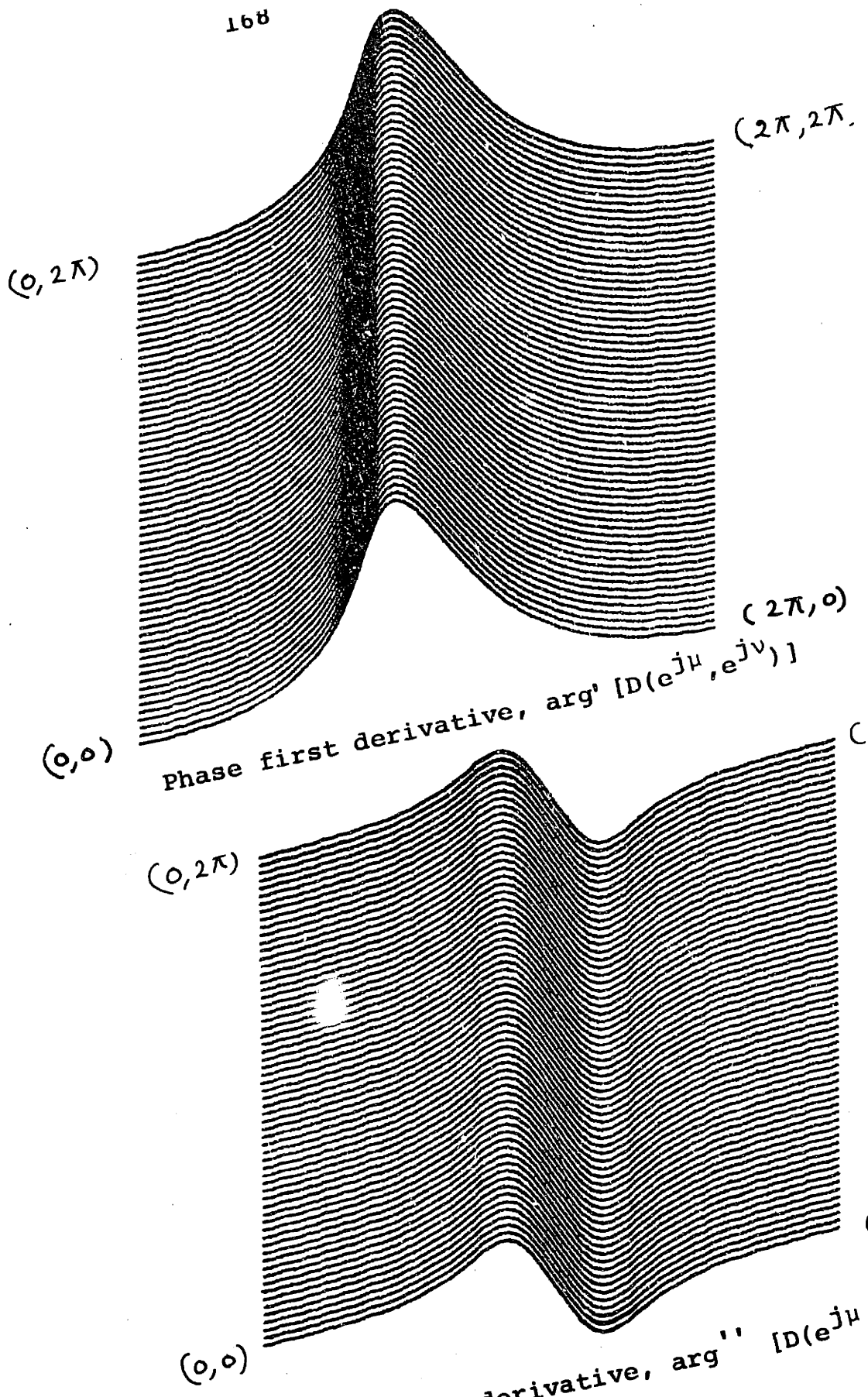
(0,2π)
(2π,2π)
(2π,0)
(0,0)
Phase first derivative, arg' [D(e^jμ, e^jν)]
(0,2π)
(2π,2π)
(2π,0)
(0,0)
Phase second derivative, arg'' [D(e^jμ, e^jν)]

Fig. 6.9

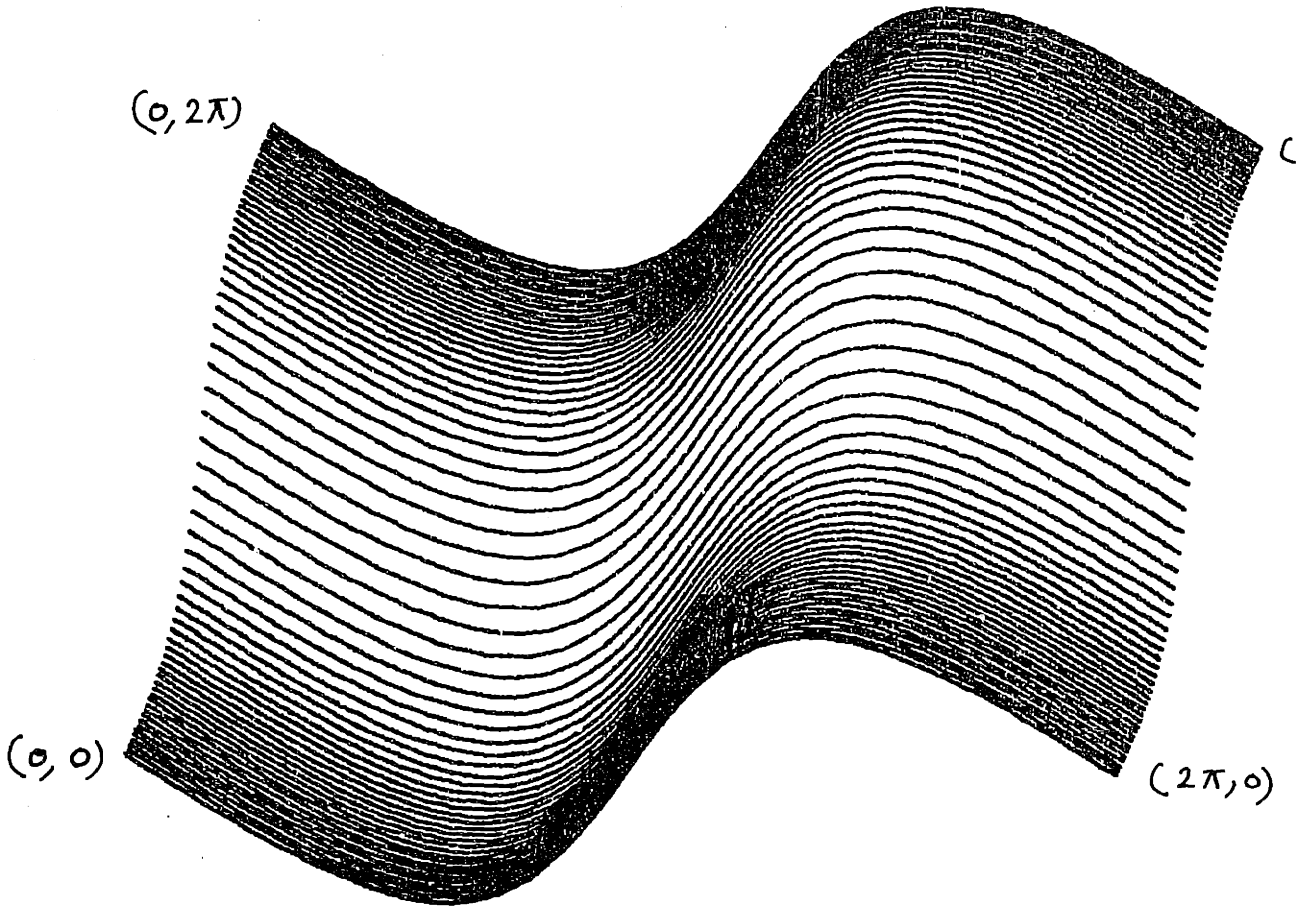

Principal value or unwrapped phase, arg $[D(e^{j\mu}, e^{j\nu})]$

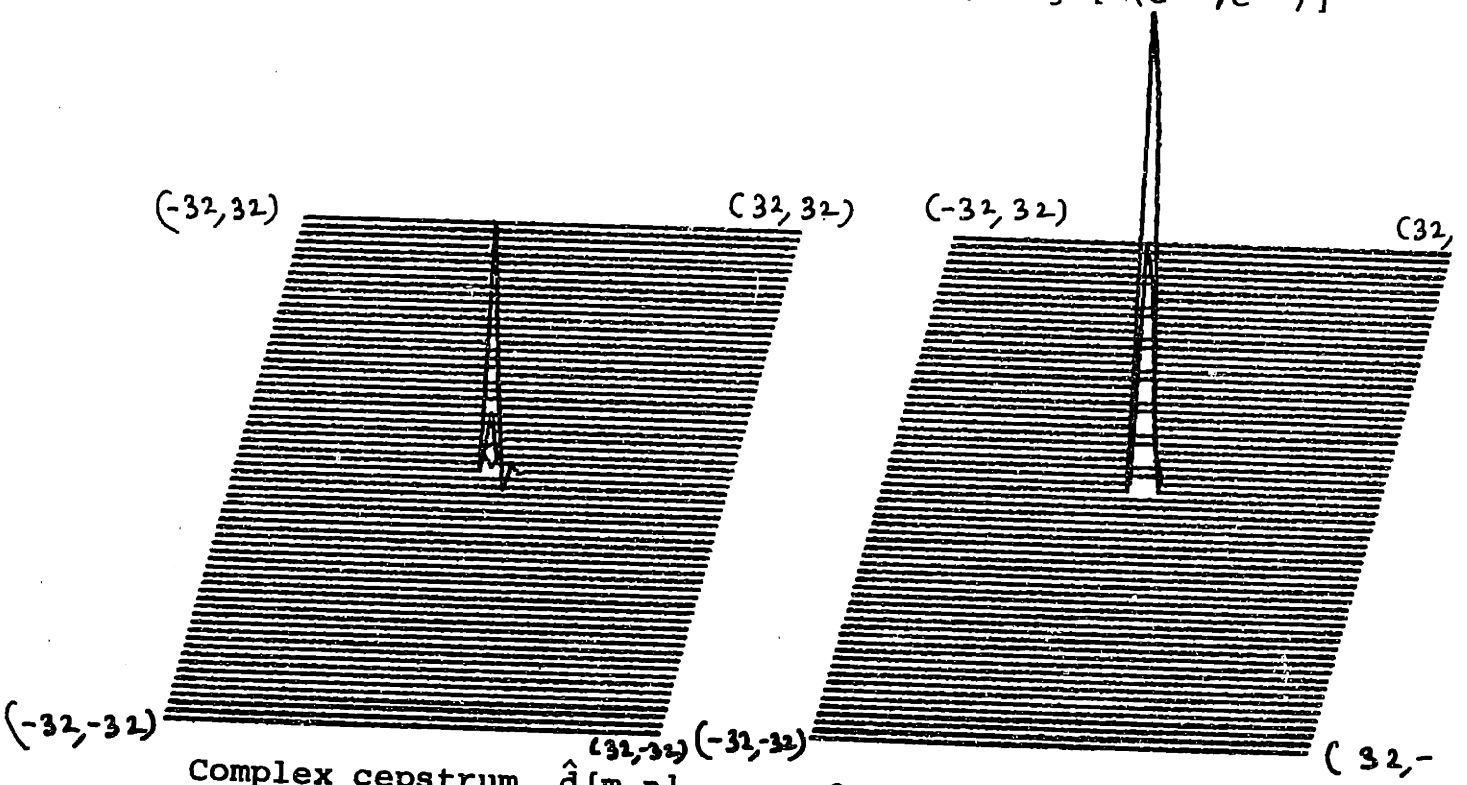

Complex cepstrum, $\hat{d}[m,n]$

Output of inverse characteristic system, $d[m,n]$

Fig. 6.10

and sequence d[m,n]. Note the same support for d[m,n] and $\hat{d}$[m,n] and stability is guaranteed. Also observe that $\hat{d}$[m,n] exists on the axes. The FFT size used was 64x64.

Quarter-plane filters involving non-separable sequences

In this category we consider two examples.

Example 6.5 Quarter-plane filter examined by Huang [25]

This example is a test of a filter examined by Huang and Ekstrom and Woods [21] using autocorrelation approach. Also this is the example about which Huang incorrectly concludes that it is unstable. The 2-D denominator array of the filter is given by

$$d[m,n] = \begin{array}{ccccc} & & \frac{1}{4} & & \\ & & \frac{1}{2} & \frac{1}{4} & \\ n & & & & \\ | & & 1 & \frac{1}{2} & \frac{1}{4} \\ | & & & & \\ 0 & \text{———} & & & \\ & & m & & \end{array}$$

In this case it may be little difficult to find the closed form formula for the cepstrum. However, using the recursion equations obtained in Property 3 of the last chapter, we list some values of the cepstrum.

$$\hat{x}[0,0] = 0,\ \hat{x}[1,0] = \frac{1}{2},\ \hat{x}[2,0] = \frac{1}{8},$$

$$\hat{x}[3,0] = -\frac{1}{12},\ \hat{x}[4,0] = \frac{1}{64}$$

Fig. 6.11 shows the absolute value of the frequency response and log of absolute value of the frequency response. Fig. 6.12 shows the phase first and second derivatives. Looking at these derivatives plot we expect that the sequence should be non-separable as it is. Finally Fig. 6.13 shows the unwrapped phase plot (same as the principal value plot, no jump), the complex cepstrum plot and the sequence plot. Note the same supports for $d[m,n]$ and $\hat{d}[m,n]$ and hence conclude that the filter has got to be stable. FFT size used was 64x64.

Example 6.6 Quarter-plane 6th order bandpass filter examined by Ekstrom and Twogood [22].

The denominator array is given by

$$d[m,n] = \begin{array}{c|ccccccc} n & & & & & & & \\ & 0.015626 & & & & & & \\ & 0.09375 & 0.046875 & & & & & \\ & 0.375 & 0.28125 & 0.09375 & & & & \\ & 0.875 & 0.09375 & 0.46875 & 0.109375 & & & \\ & 1.5 & 1.875 & 1.3125 & 0.46875 & 0.09375 & & \\ & 1.5 & 2.25 & 1.875 & 0.09375 & 0.28125 & 0.046875 & \\ & 1 & 1.5 & 1.5 & 0.875 & 0.375 & 0.09375 & 0.015625 \\ 0 & \multicolumn{7}{c}{\text{---------- } m} \end{array} \qquad (6.17)$$

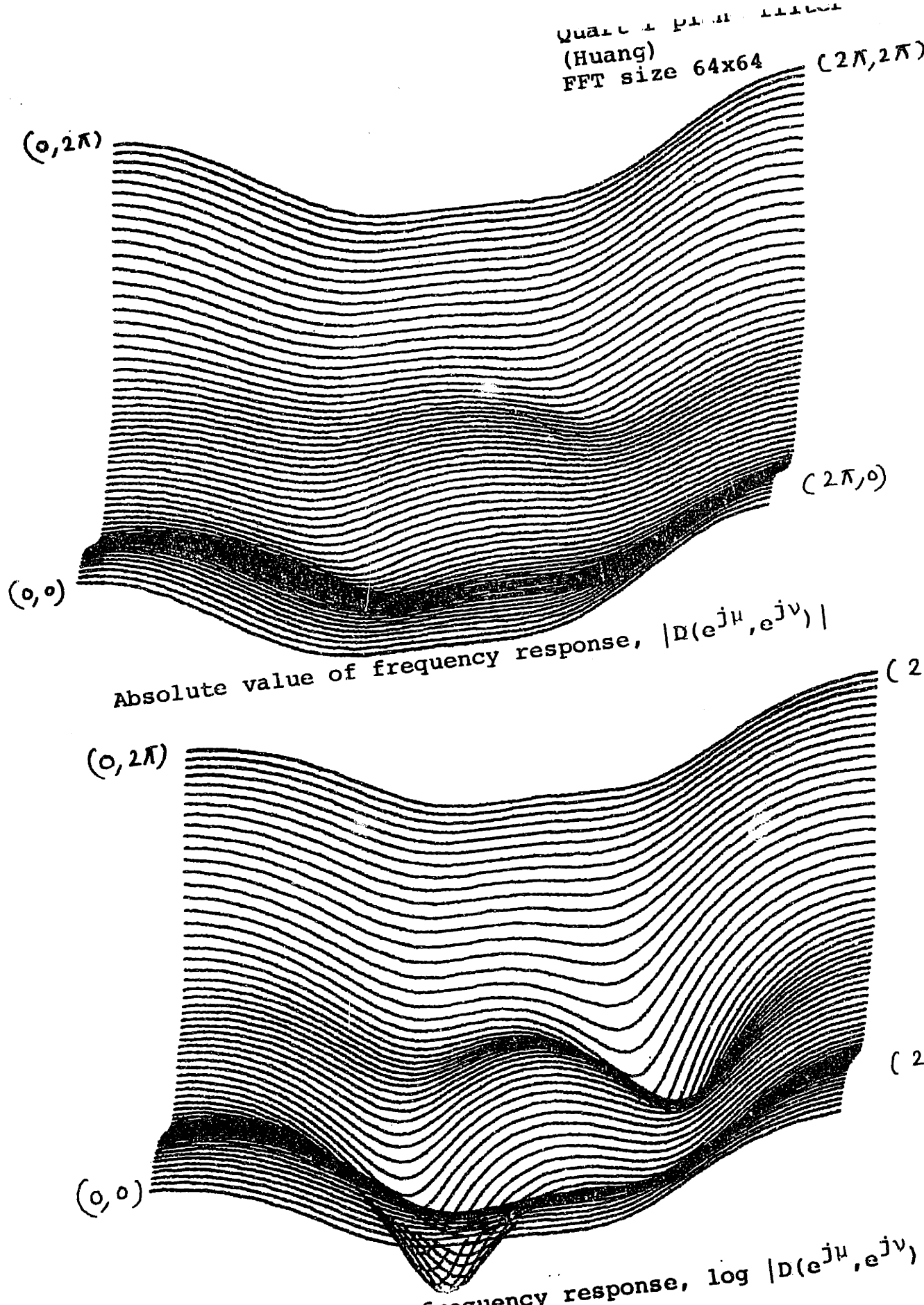
Quarter plane filter
(Huang)
FFT size 64x64
(2π,2π)
(0,2π)
(2π,0)
(0,0)
Absolute value of frequency response, $|D(e^{j\mu},e^{j\nu})|$
(2π,2π)
(0,2π)
(2π,0)
(0,0)
Log magnitude of frequency response, $\log |D(e^{j\mu},e^{j\nu})|$

Fig. 6.11

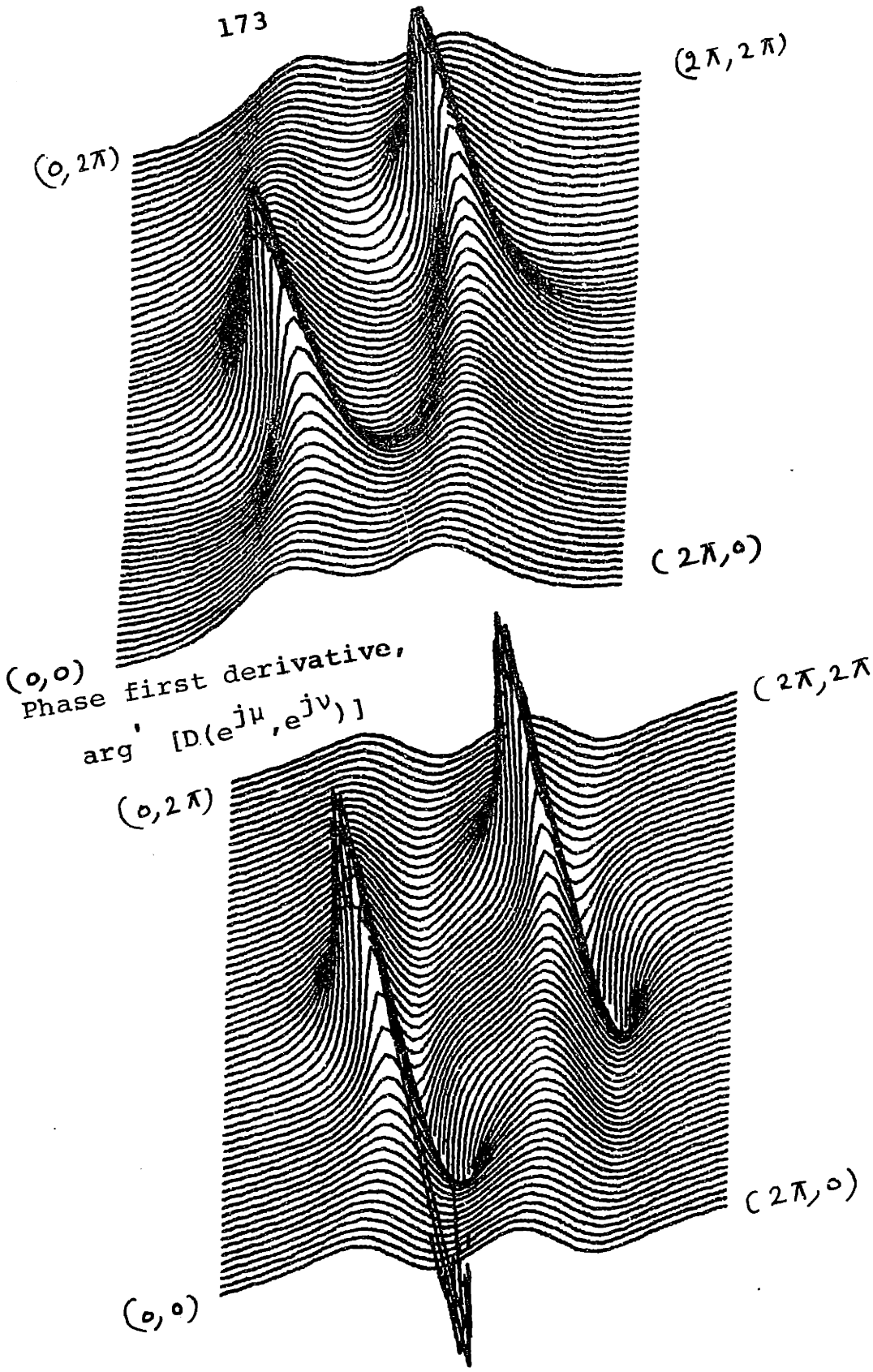

Phase first derivative,
$\arg' [D(e^{j\mu}, e^{j\nu})]$

Phase second derivative,
$\arg'' [D(e^{j\mu}, e^{j\nu})]$

Fig. 6.12

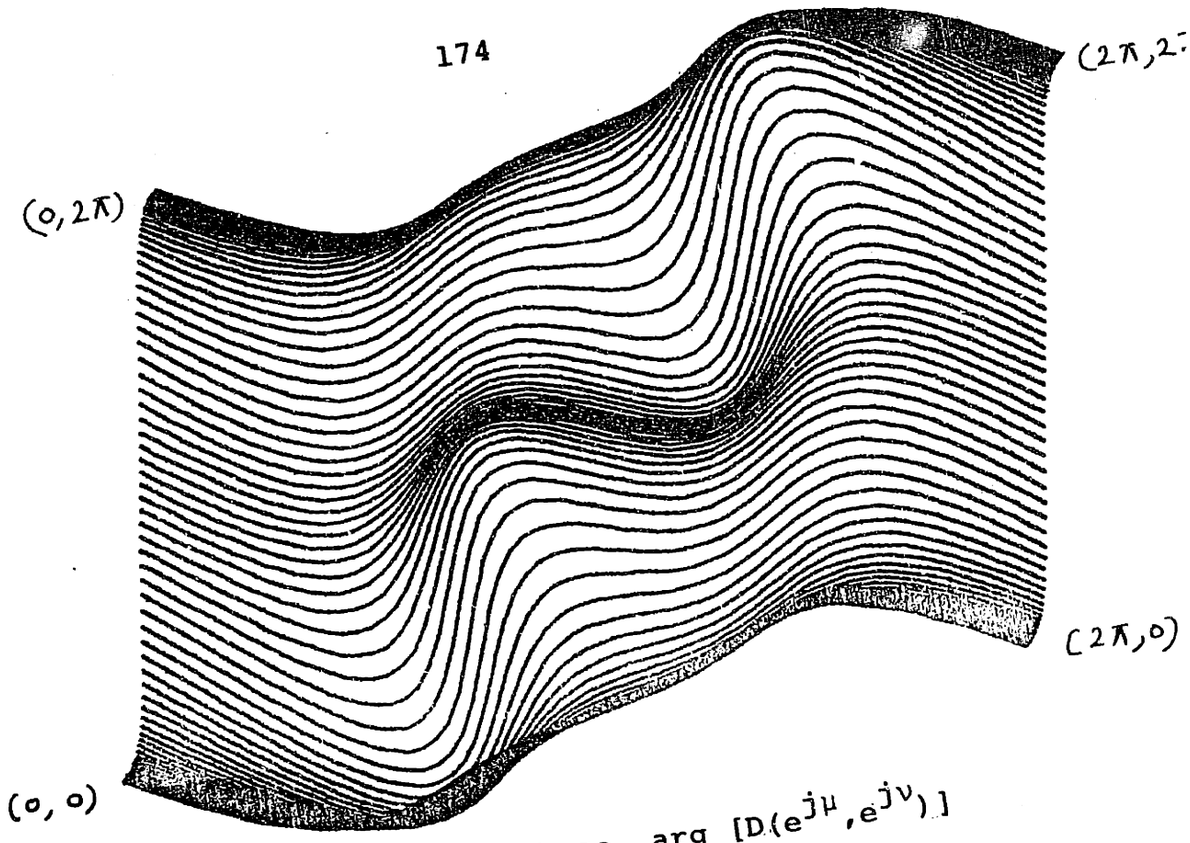

Unwrapped phase, arg $[D(e^{j\mu}, e^{j\nu})]$

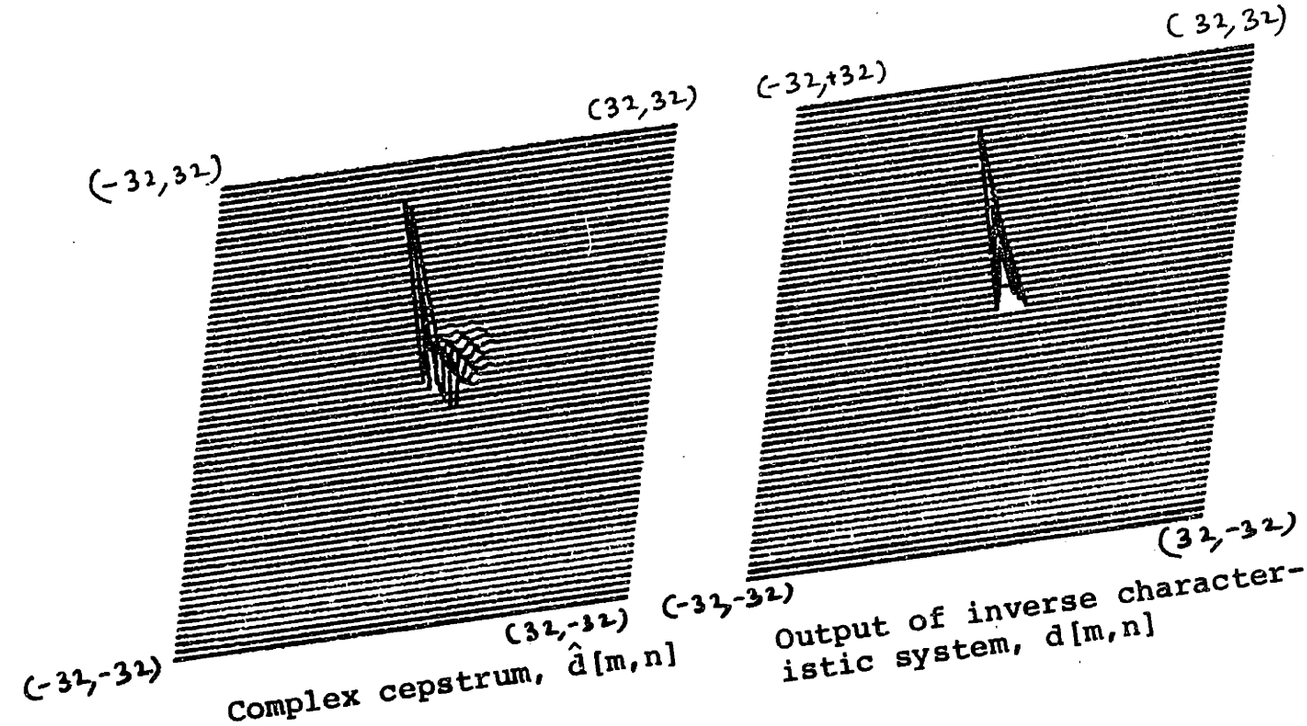

Complex cepstrum, $\hat{d}[m,n]$

Output of inverse characteristic system, $d[m,n]$

Fig. 6.13

EXAMPLE 6.3
Separable Sequence
Exponentials
FFT size 32x32

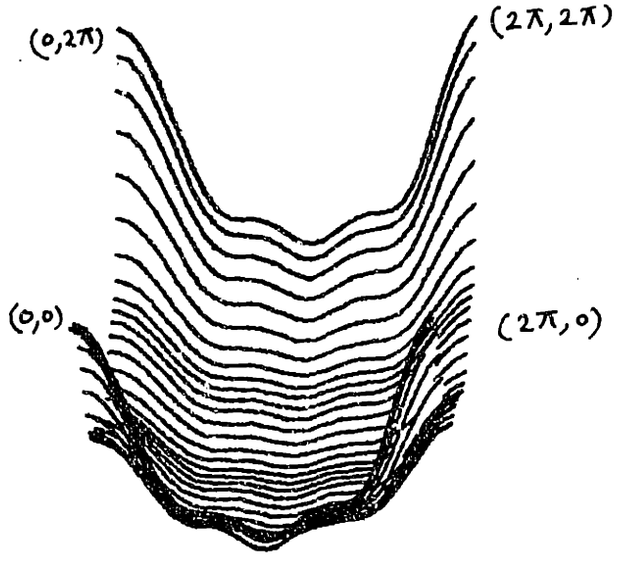

Absolute value of frequency response,

$$|D(e^{j\mu},e^{j\nu})|$$

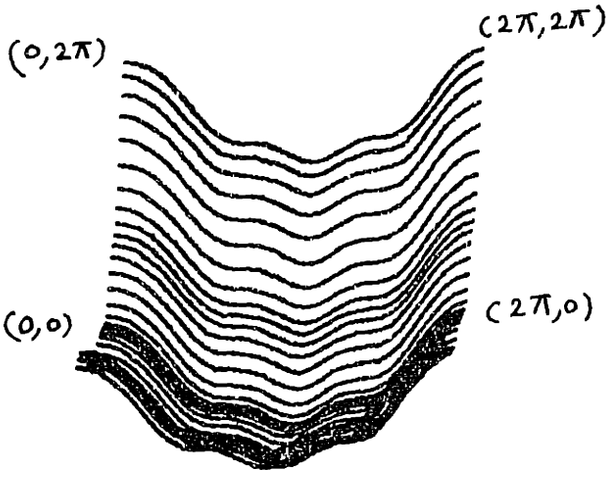

Log magnitude of frequency response,

$$\log |D(e^{j\mu},e^{j\nu})|$$

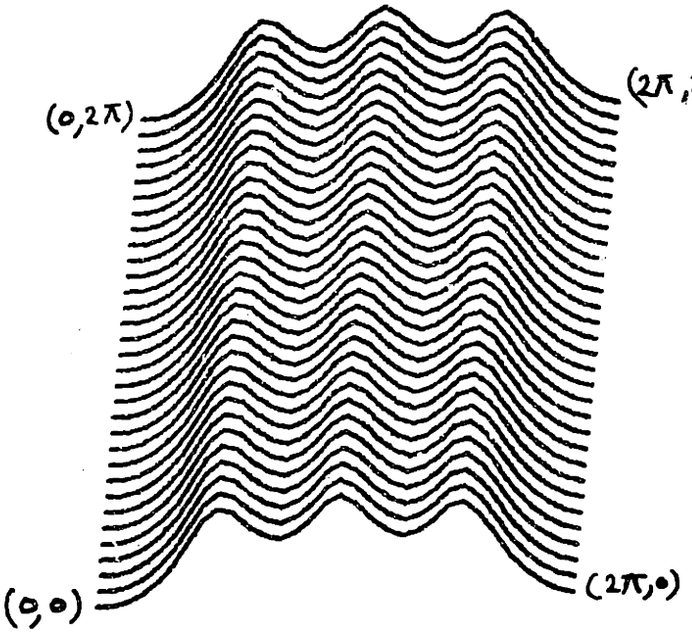

Phase first derivative,

$$\arg' [D(e^{j\mu},e^{j\nu})]$$

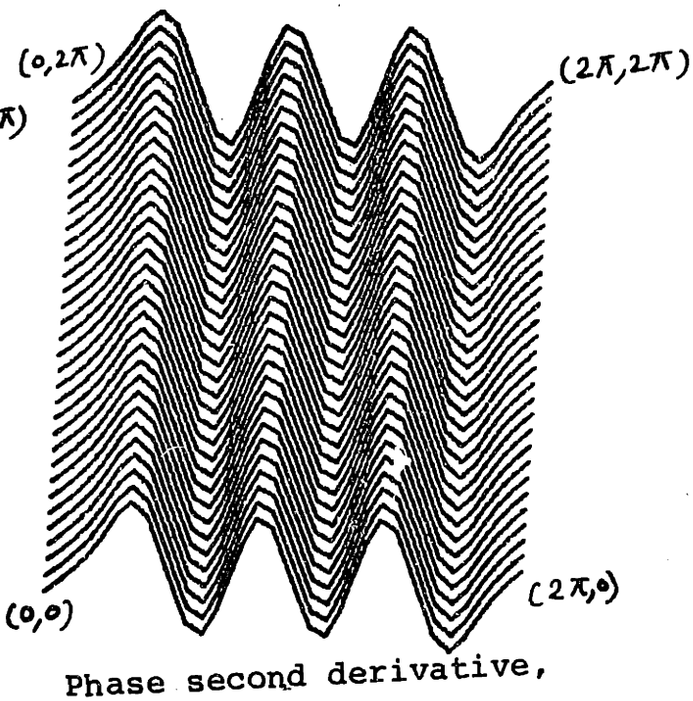

Phase second derivative,

$$\arg'' [D(e^{j\mu},e^{j\nu})]$$

Fig. 6.6

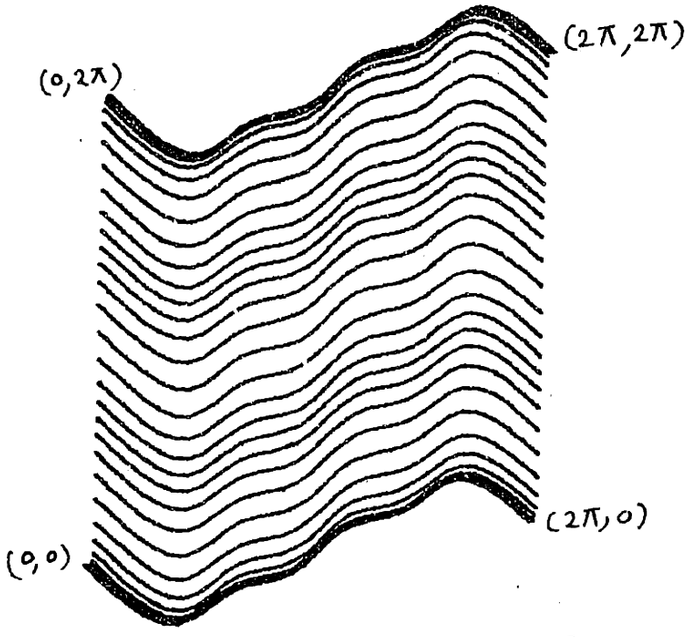

Principal value or unwrapped phase,

$$\arg\,[D(e^{j\mu}, e^{j\nu})]$$

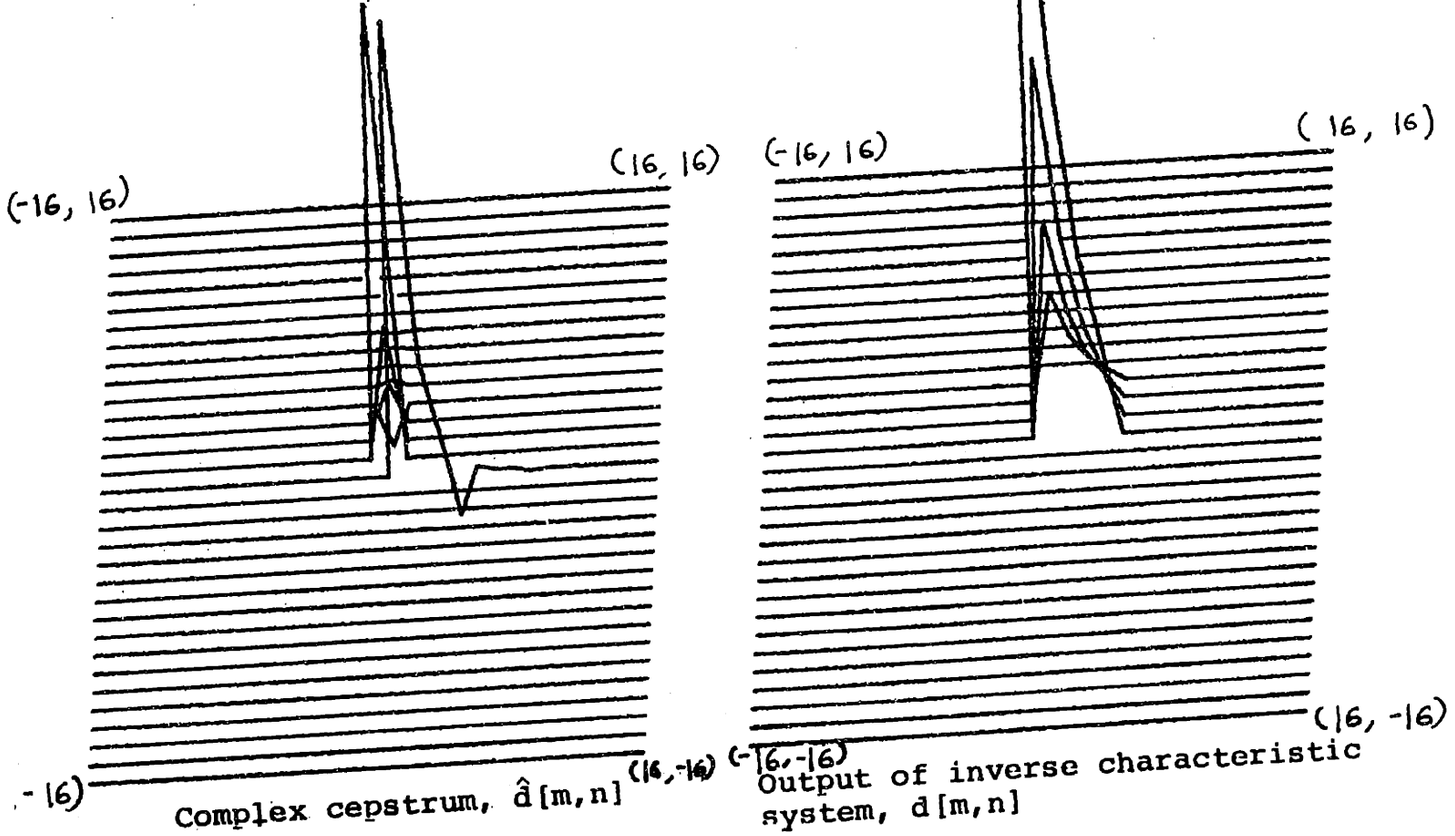

Complex cepstrum, $\hat{d}[m,n]$

Output of inverse characteristic system, $d[m,n]$

Fig. 6.7

Example 6.4

This is another example of a separable sequence which has been examined by Anderson & Jury [27]. The 2-D denominator array of the filter is given by

$$d[m,n] = \begin{array}{c|ccc} & 6 & 5 & 1 \\ n & & & \\ & 12 & 10 & 2 \\ 0 & & & \\ \hline & & & m \end{array} \qquad (6.14)$$

Since one row is the multiple of the other, the separable nature of sequence d[m,n] can be identified. The z-transform is,

$$X(\omega,z) = (3+\omega^{-1})(2+\omega^{-1})(2+z^{-1}) \qquad (6.15)$$

The complex cepstrum can be easily obtained from eq. (6.15) as

$$d[m,n] = [\log 12]\delta[m,n] - \frac{1}{m}[(-\tfrac{1}{3})^{m} + (-\tfrac{1}{2})^{m}]\, u[m-1]$$

$$- \frac{(-\frac{1}{2})^{n}}{n}\, u[n-1] \qquad (6.16)$$

Figure 6.8 shows $|D(e^{j\mu},e^{j\nu})|$ and log $|D(e^{j\mu},e^{j\nu})|$. Fig. 6.9 shows phase first and second derivatives. Separable nature of the sequence is evident from these plots. Fig. 6.10 shows the unwrapped phase (it is the same as principal value plot), complex cepstrum sequence and

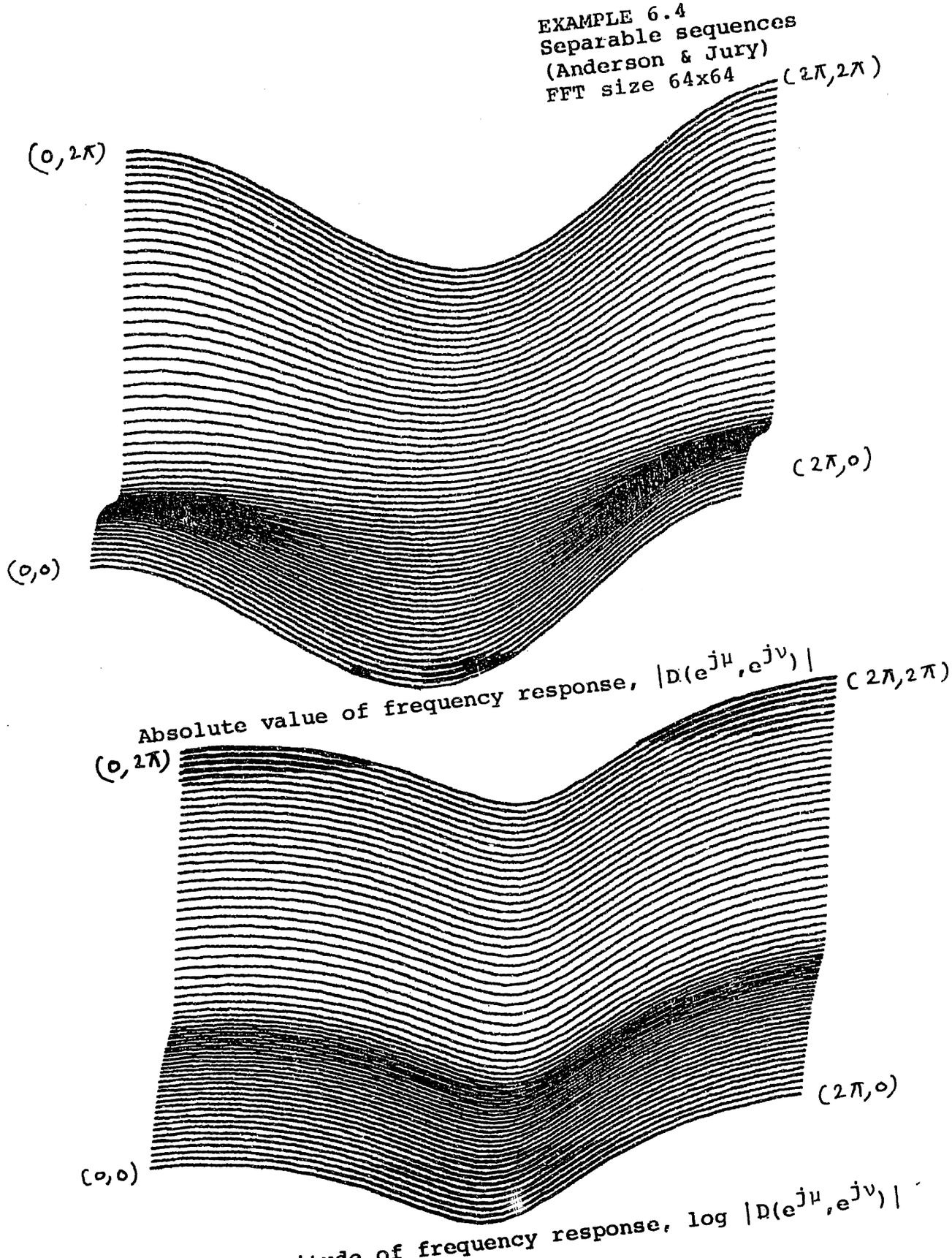
EXAMPLE 6.4
Separable sequences
(Anderson & Jury)
FFT size 64x64
(2π,2π)
(0,2π)
(2π,0)
(0,0)
Absolute value of frequency response, |D(e^jμ, e^jν)|
(2π,2π)
(0,2π)
(2π,0)
(0,0)
Log magnitude of frequency response, log |D(e^jμ, e^jν)|

Fig. 6.8

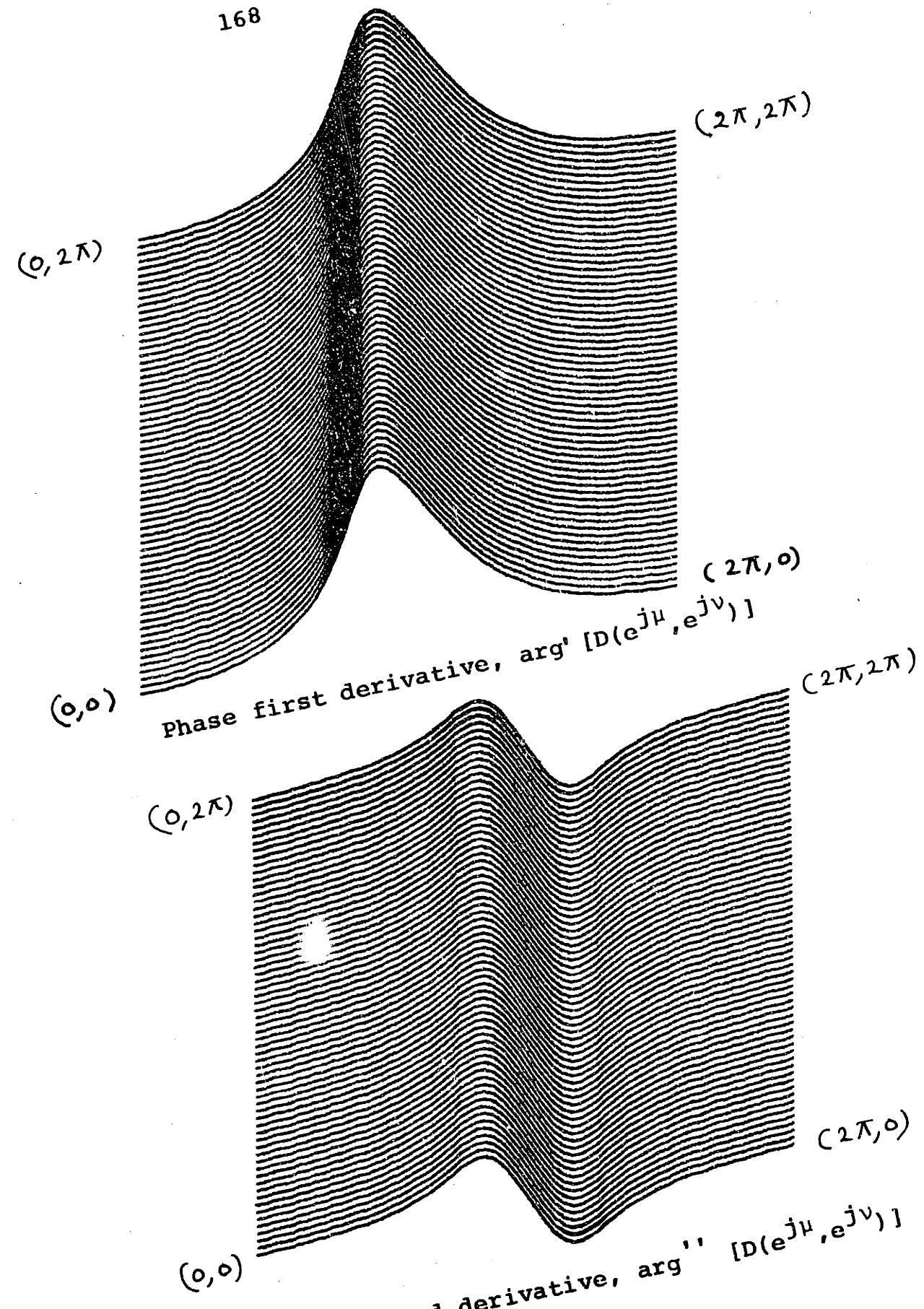
(0,2π)
(2π,2π)
(2π,0)
(0,0)
Phase first derivative, arg' [D(e^jμ, e^jν)]
(0,2π)
(2π,2π)
(2π,0)
(0,0)
Phase second derivative, arg'' [D(e^jμ, e^jν)]

Fig. 6.9

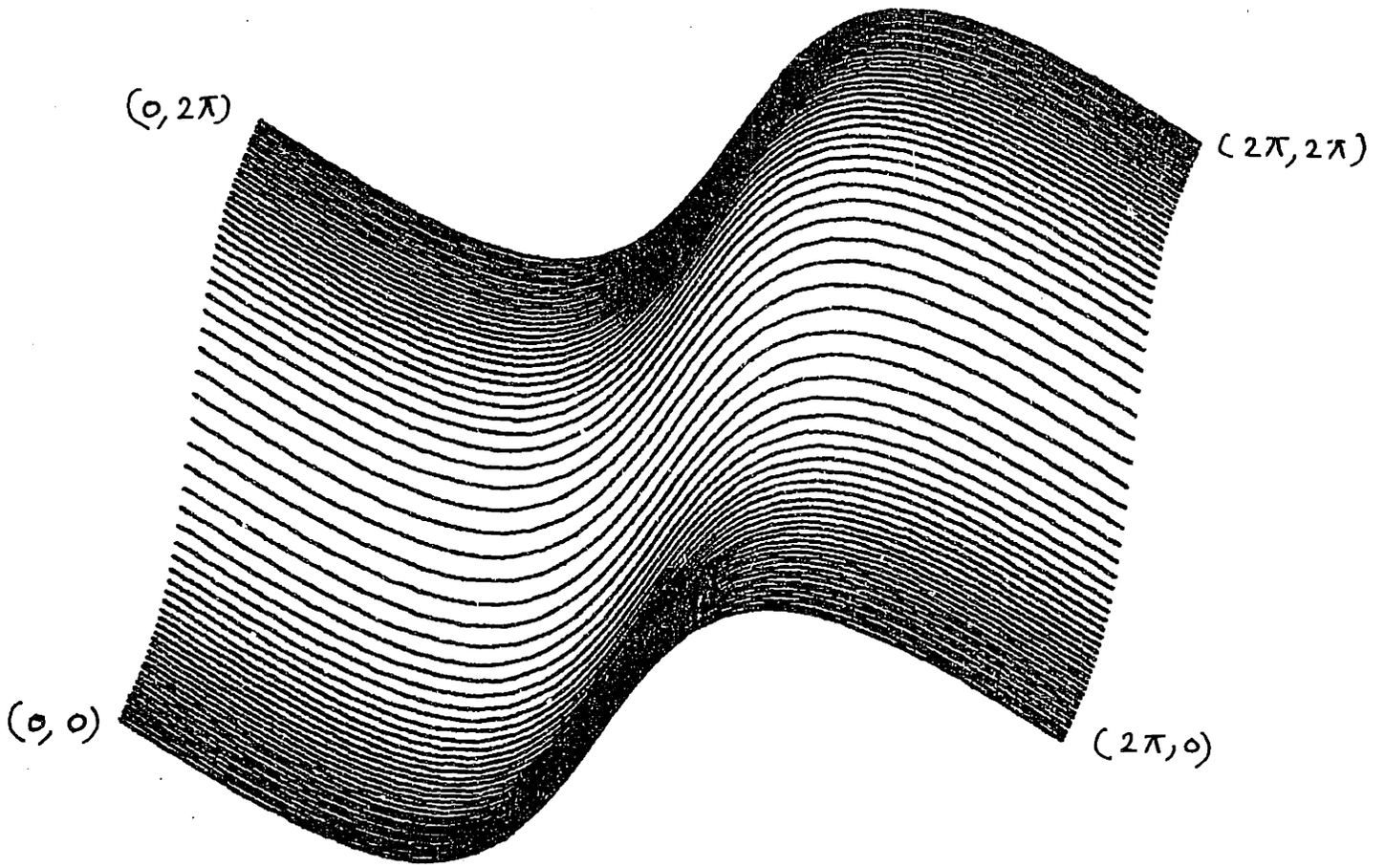

Principal value or unwrapped phase, arg $[D(e^{j\mu}, e^{j\nu})]$

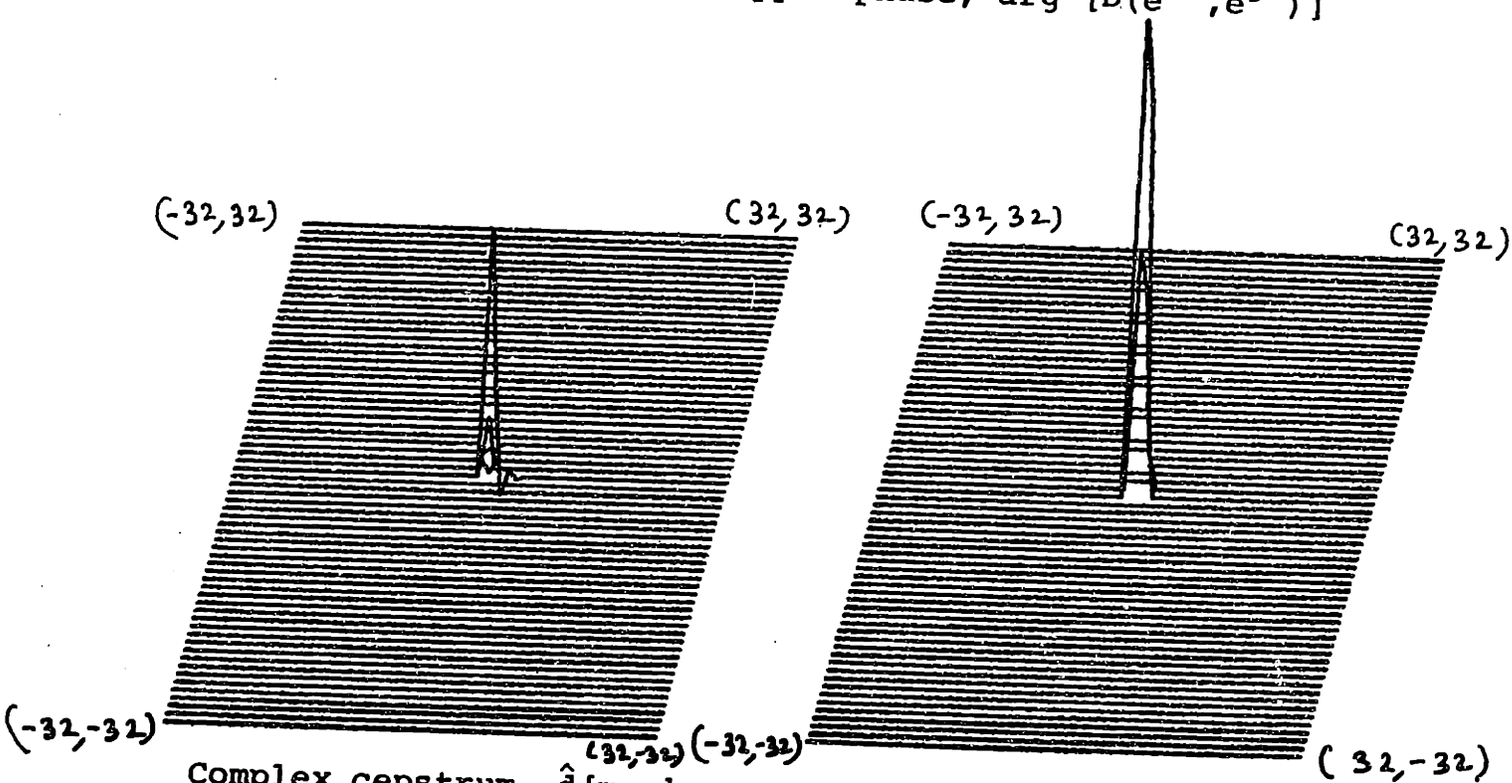

Complex cepstrum, $\hat{d}[m,n]$

Output of inverse characteristic system, $d[m,n]$

Fig. 6.10

and sequence d[m,n]. Note the same support for d[m,n] and $\hat{d}$[m,n] and stability is guaranteed. Also observe that $\hat{d}$[m,n] exists on the axes. The FFT size used was 64x64.

Quarter-plane filters involving non-separable sequences

In this category we consider two examples.

Example 6.5 Quarter-plane filter examined by Huang [25]

This example is a test of a filter examined by Huang and Ekstrom and Woods [21] using autocorrelation approach. Also this is the example about which Huang incorrectly concludes that it is unstable. The 2-D denominator array of the filter is given by

$$d[m,n] = \begin{array}{ccccc} & & \frac{1}{4} & & \\ & & \frac{1}{2} & \frac{1}{4} & \\ n & & & & \\ | & & 1 & \frac{1}{2} & \frac{1}{4} \\ 0 & \text{———} & & & \\ & & m & & \end{array}$$

In this case it may be little difficult to find the closed form formula for the cepstrum. However, using the recursion equations obtained in Property 3 of the last chapter, we list some values of the cepstrum.

$$\hat{x}[0,0] = 0,\ \hat{x}[1,0] = \frac{1}{2},\ \hat{x}[2,0] = \frac{1}{8},$$

$$\hat{x}[3,0] = -\frac{1}{12},\ \hat{x}[4,0] = \frac{1}{64}$$

Fig. 6.11 shows the absolute value of the frequency response and log of absolute value of the frequency response. Fig. 6.12 shows the phase first and second derivatives. Looking at these derivatives plot we expect that the sequence should be non-separable as it is. Finally Fig. 6.13 shows the unwrapped phase plot (same as the principal value plot, no jump), the complex cepstrum plot and the sequence plot. Note the same supports for $d[m,n]$ and $\hat{d}[m,n]$ and hence conclude that the filter has got to be stable. FFT size used was 64x64.

Example 6.6 Quarter-plane 6^{th} order bandpass filter examined by Ekstrom and Twogood[22].

The denominator array is given by

$$d[m,n] = \begin{array}{l} n \\ \vdots \\ 0 \end{array} \begin{array}{|ccccccc} 0.015626 & & & & & & \\ 0.09375 & 0.046875 & & & & & \\ 0.375 & 0.28125 & 0.09375 & & & & \\ 0.875 & 0.09375 & 0.46875 & 0.109375 & & & \\ 1.5 & 1.875 & 1.3125 & 0.46875 & 0.09375 & & \\ 1.5 & 2.25 & 1.875 & 0.09375 & 0.28125 & 0.046875 & \\ 1 & 1.5 & 1.5 & 0.875 & 0.375 & 0.09375 & 0.015625 \end{array} \quad \begin{array}{l} \\ \\ \\ \\ \\ \\ \\ \\ m \end{array} \qquad (6.17)$$

EXAMPLE 6.5
Quarter plane filter
(Huang)
FFT size 64x64

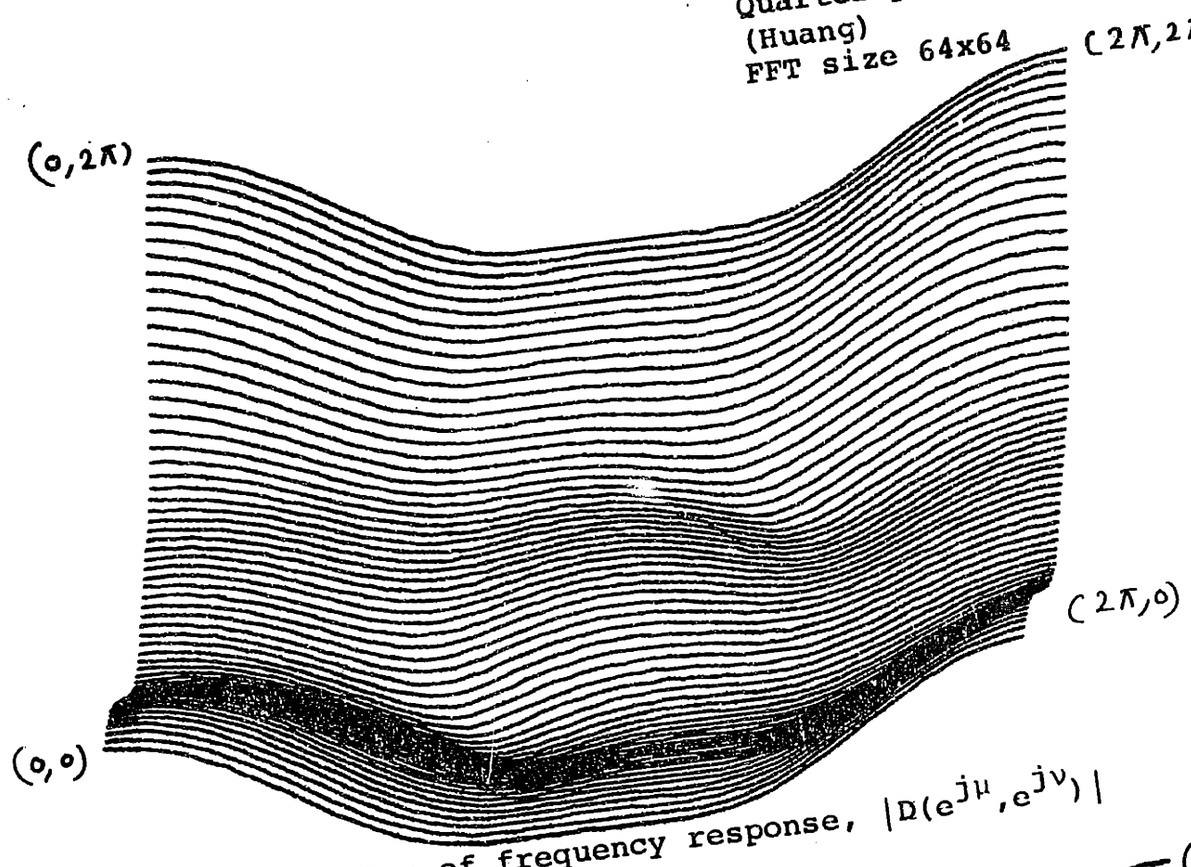

Absolute value of frequency response, $|D(e^{j\mu}, e^{j\nu})|$

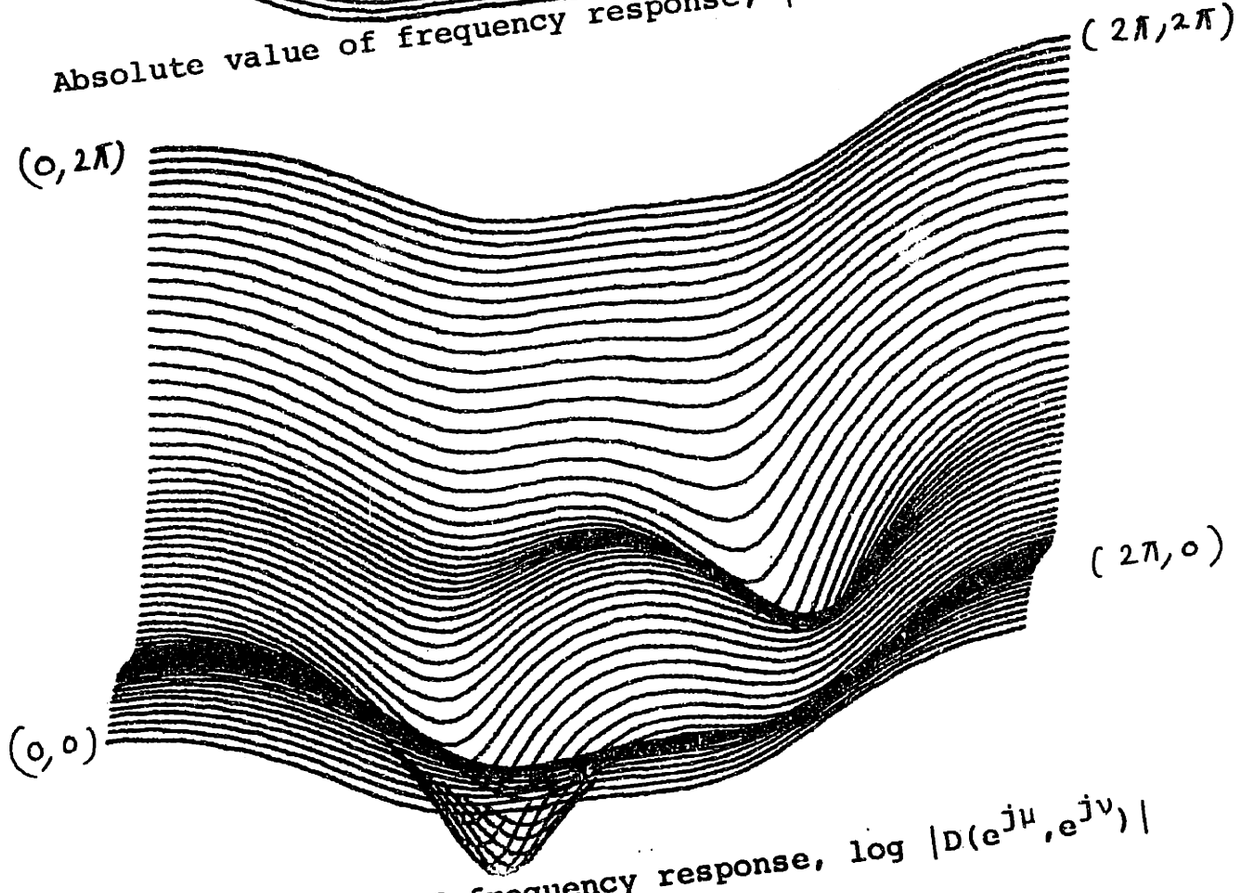

Log magnitude of frequency response, $\log |D(e^{j\mu}, e^{j\nu})|$

Fig. 6.11

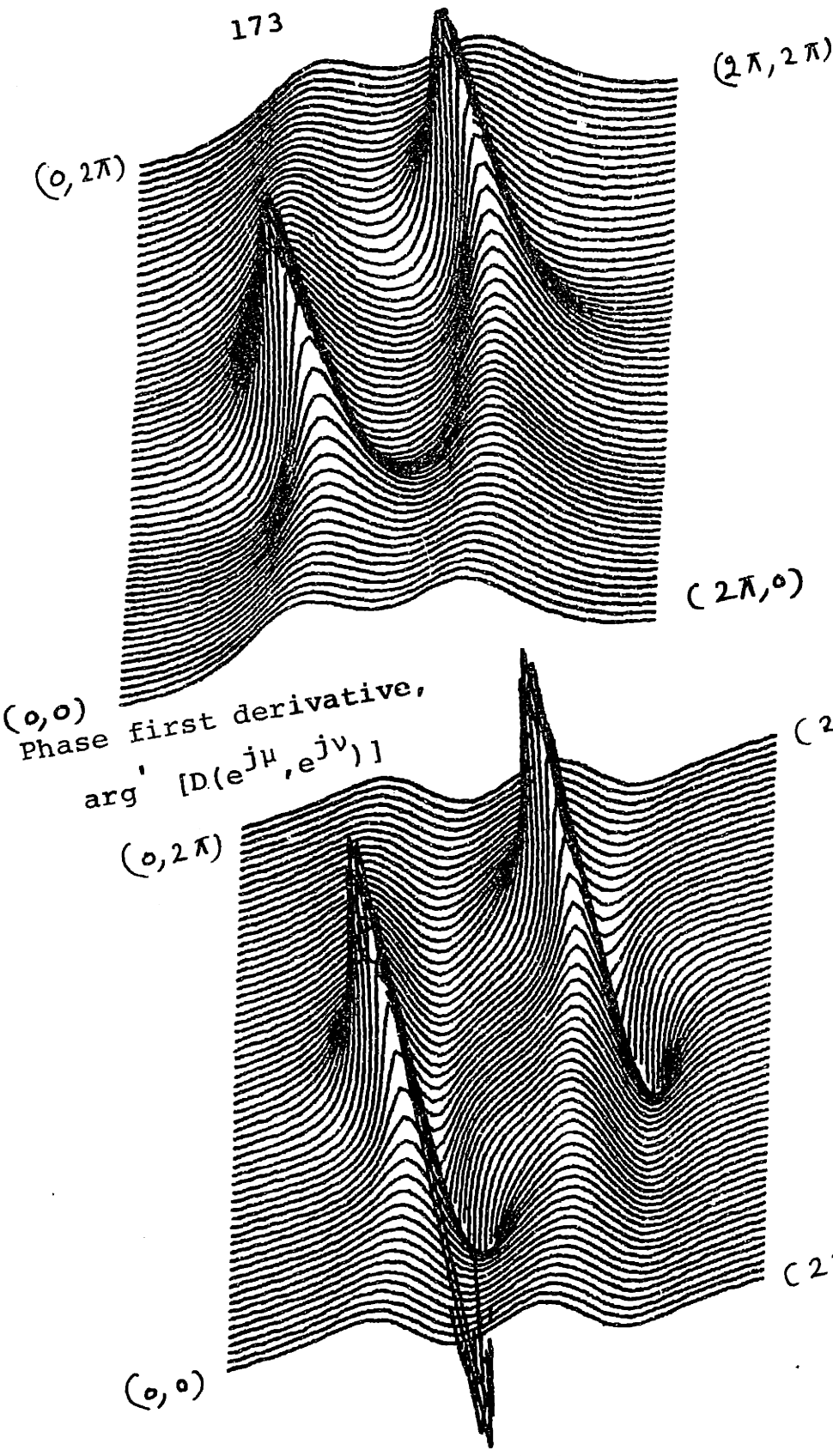

Phase first derivative,

$\arg' [D(e^{j\mu}, e^{j\nu})]$

Phase second derivative,

$\arg'' [D(e^{j\mu}, e^{j\nu})]$

Fig. 6.12

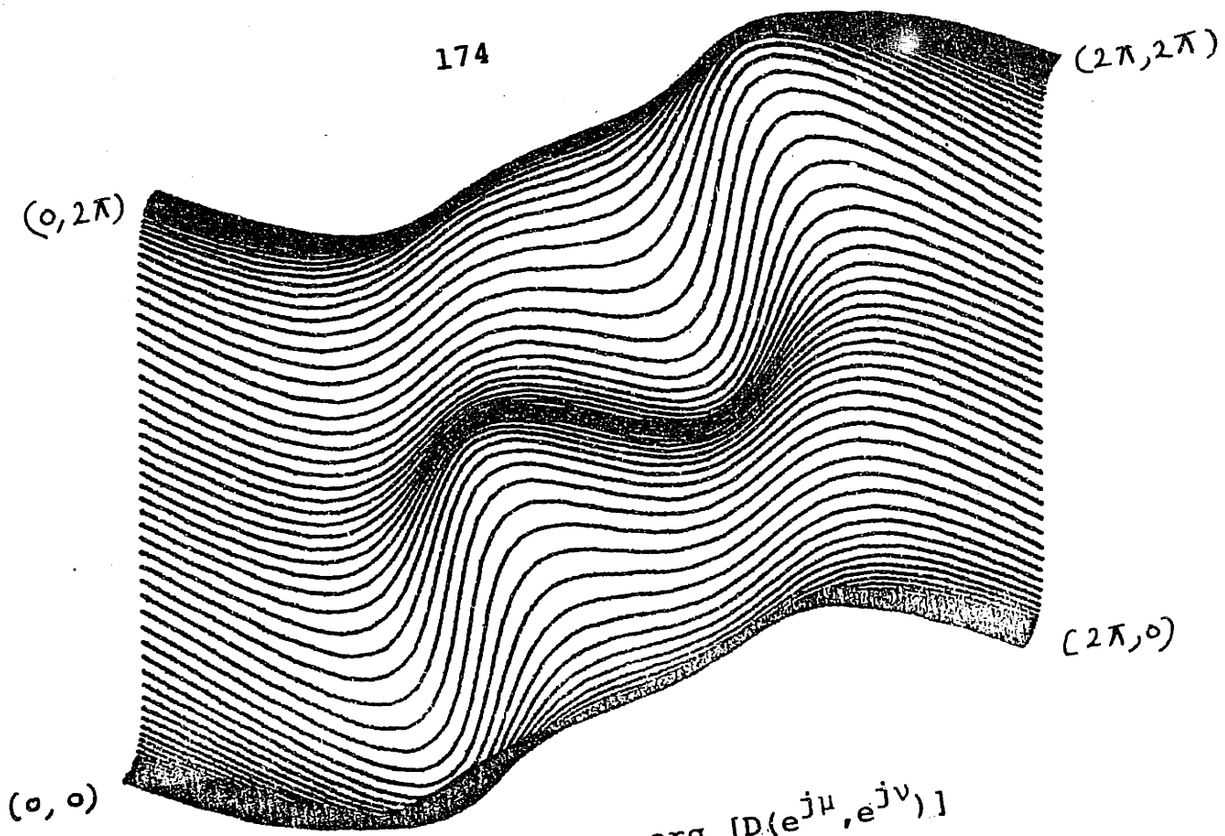

Unwrapped phase, arg $[D(e^{j\mu}, e^{j\nu})]$

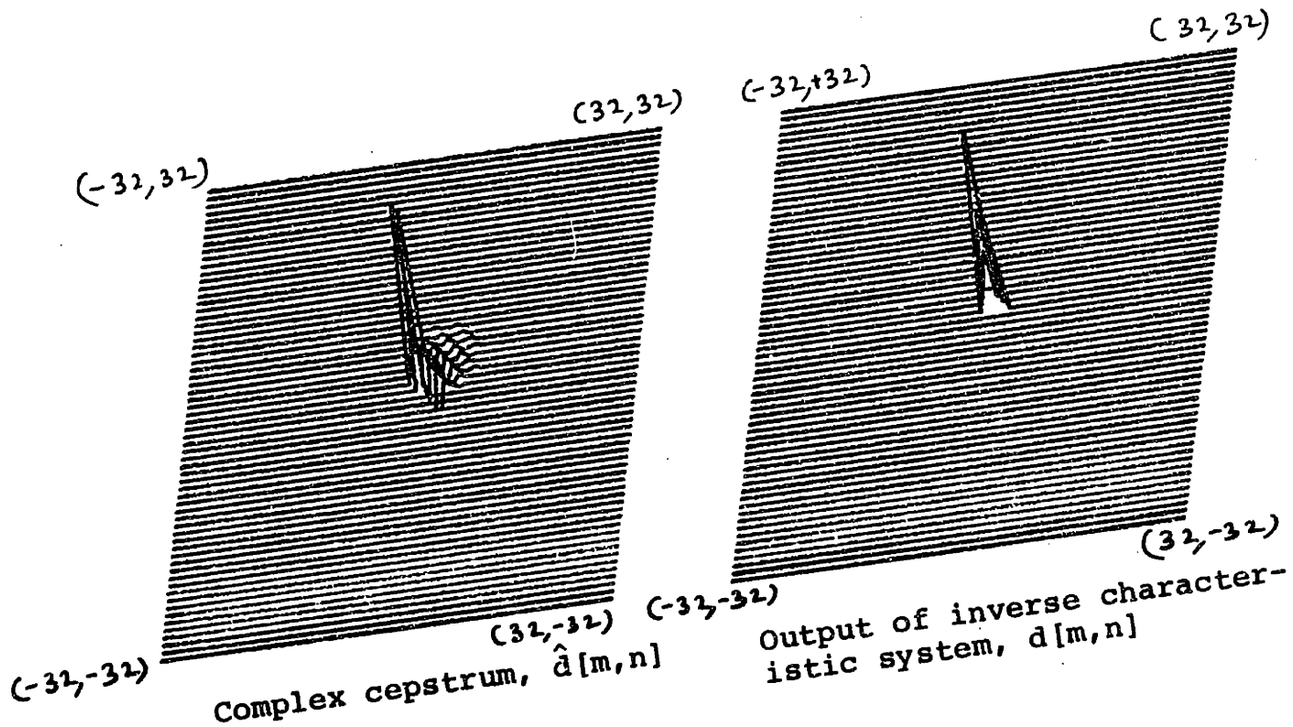

Complex cepstrum, $\hat{d}[m,n]$

Output of inverse characteristic system, $d[m,n]$

Fig. 6.13

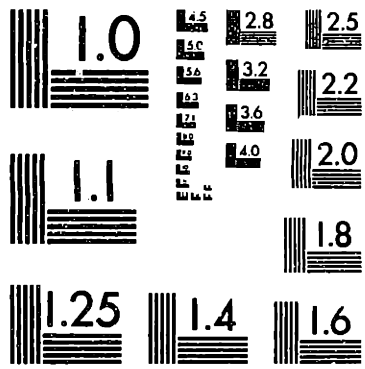

20X

The first few values of the complex cepstrum using recursion equations are given by

$$\hat{x}[0,0] = 0,\ \hat{x}[1,0] = 1.5,\ \hat{x}[2,0] = 0.375,$$

$$\hat{x}[3,0] = -0.25,\ \hat{x}[4,0] = 0.046875 \qquad (6.18)$$

Fig. 6.14 shows the absolute value of the frequency response and its logarithmic. Fig. 6.15 shows the phase first and second derivatives. Fig. 6.16 shows the principal value and unwrapped phase plot. Note that the discontinuities because of modulo 2π operation have been removed. Fig. 6.17 shows the complex cepstrum and signal. Observe that both of these lie in the first quadrant and hence we conclude that the filter is stable. The FFT size taken was 64x64.

Non-symmetric half-plane filters

Having discussed the quarter-plane filters we now consider non-symmetric half-plane filters. We shall present two examples for these filters.

Example 6.7

Let the system function of the filter be

$$G(\omega,z) = \frac{1}{1-\frac{1}{3}z^{-1}-\frac{1}{3}\omega^{-1}z} \qquad (6.19)$$

so,
$$D(\omega,z) = 1-\frac{1}{3}z^{-1}-\frac{1}{3}\omega^{-1}z \qquad (6.20)$$

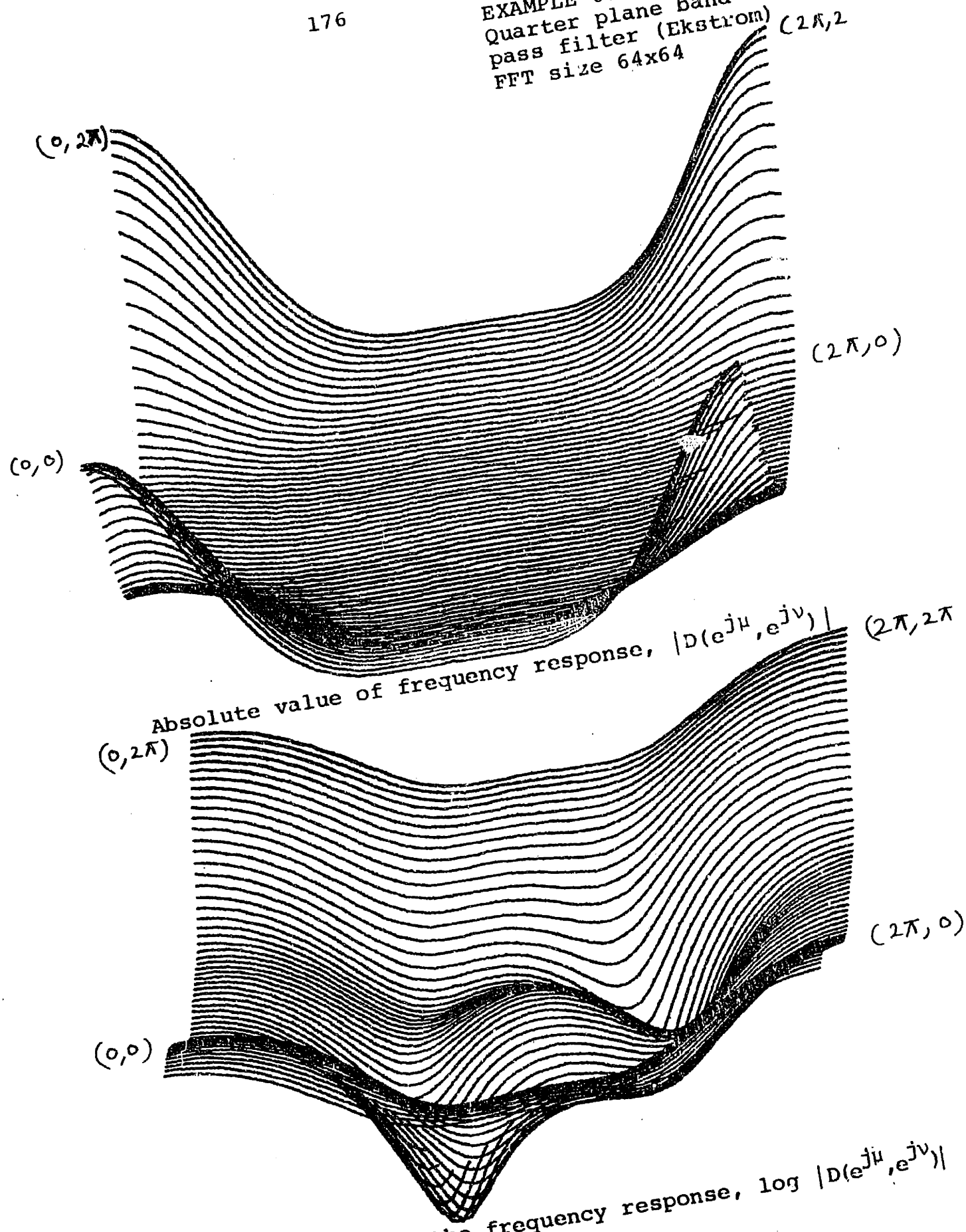
EXAMPLE 6.6
Quarter plane band-pass filter (Ekstrom)
FFT size 64x64
(0, 2π)
(2π, 2
(2π, 0)
(0, 0)
Absolute value of frequency response, |D(e^jμ, e^jν)|
(0, 2π)
(2π, 2π
(2π, 0)
(0, 0)
Log magnitude of the frequency response, log |D(e^jμ, e^jν)|

Fig. 6.14

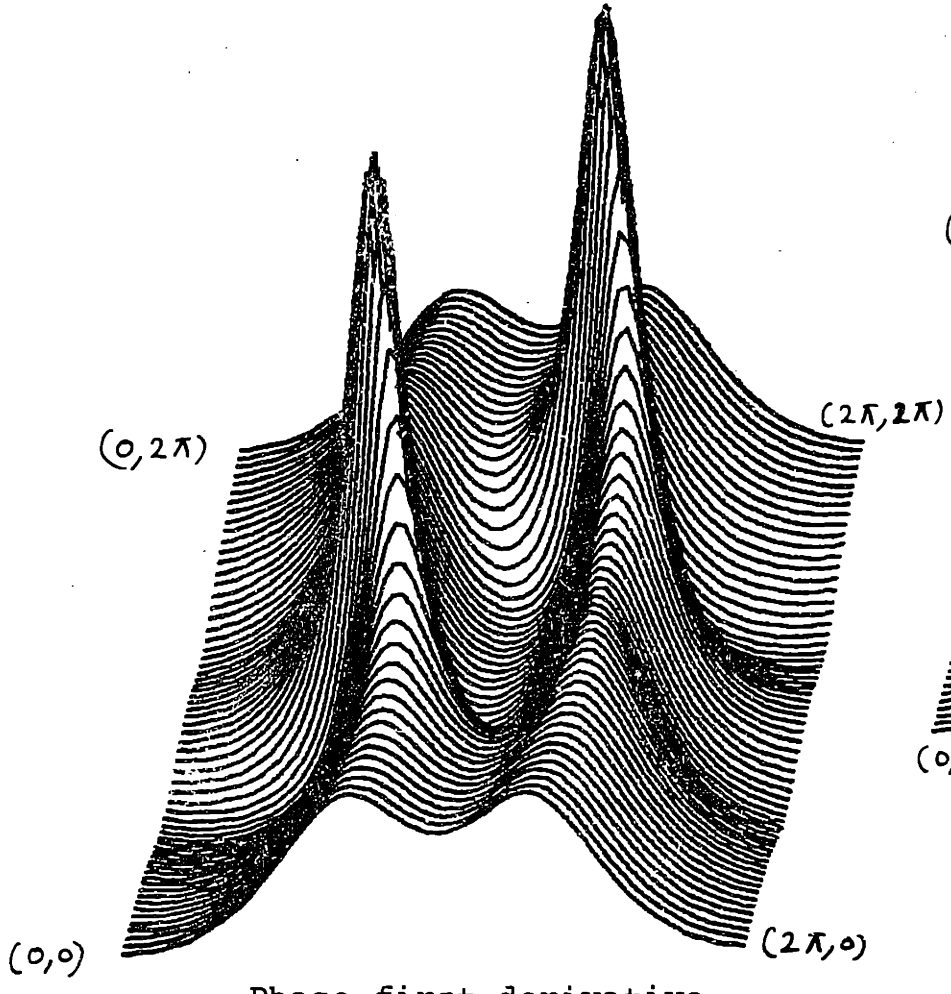

Phase first derivative,

$\arg' [D(e^{j\mu}, e^{j\nu})]$

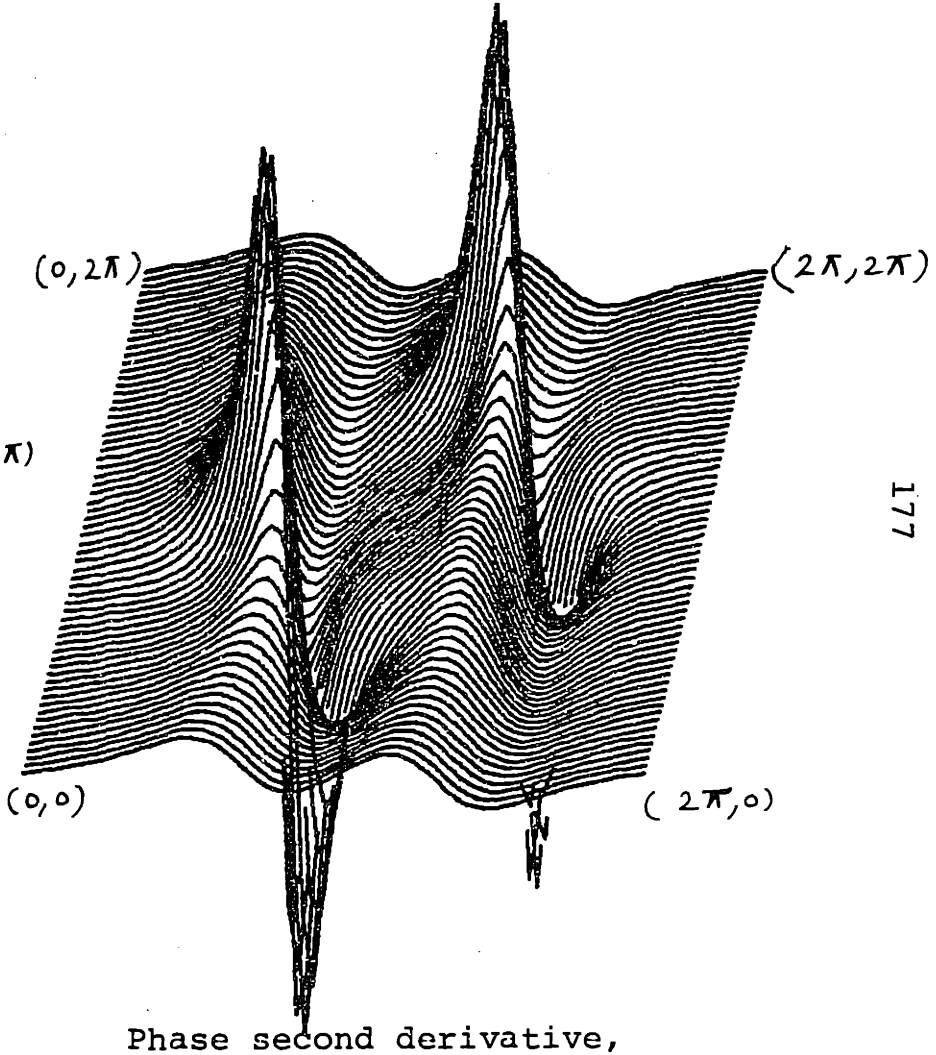

Phase second derivative,

$\arg'' [D(e^{j\mu}, e^{j\nu})]$

Fig. 6.15

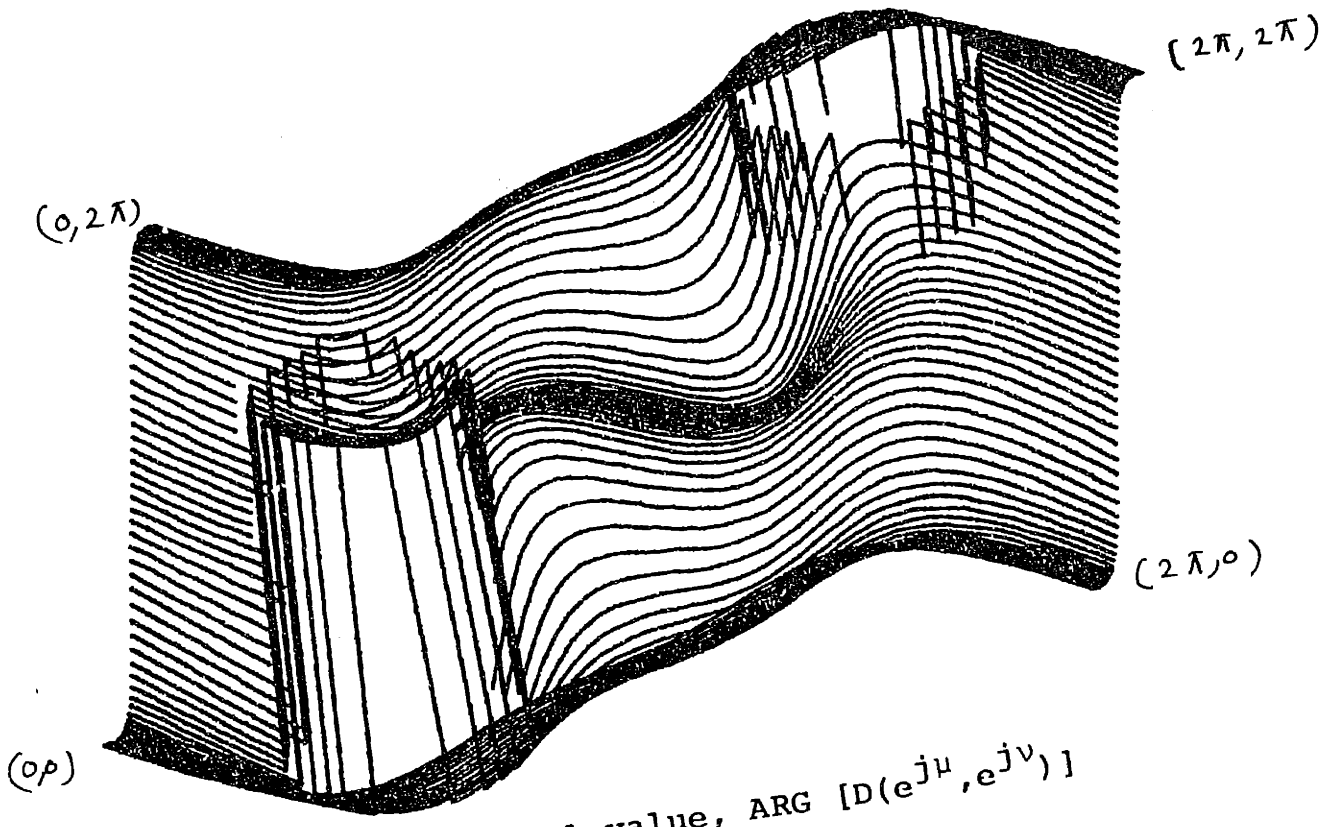

Phase principal value, ARG $[D(e^{j\mu}, e^{j\nu})]$

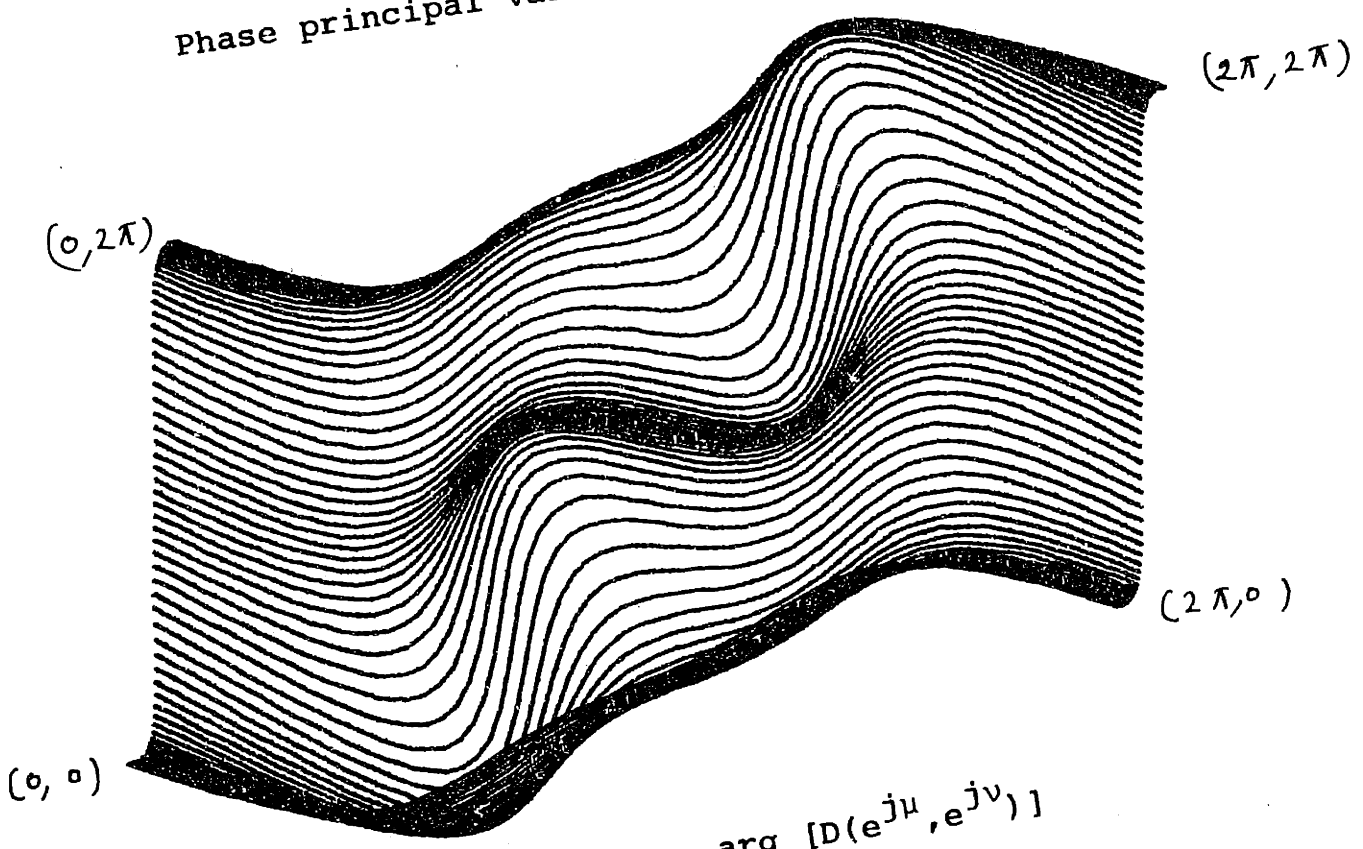

Unwrapped phase, arg $[D(e^{j\mu}, e^{j\nu})]$

Fig. 6.16

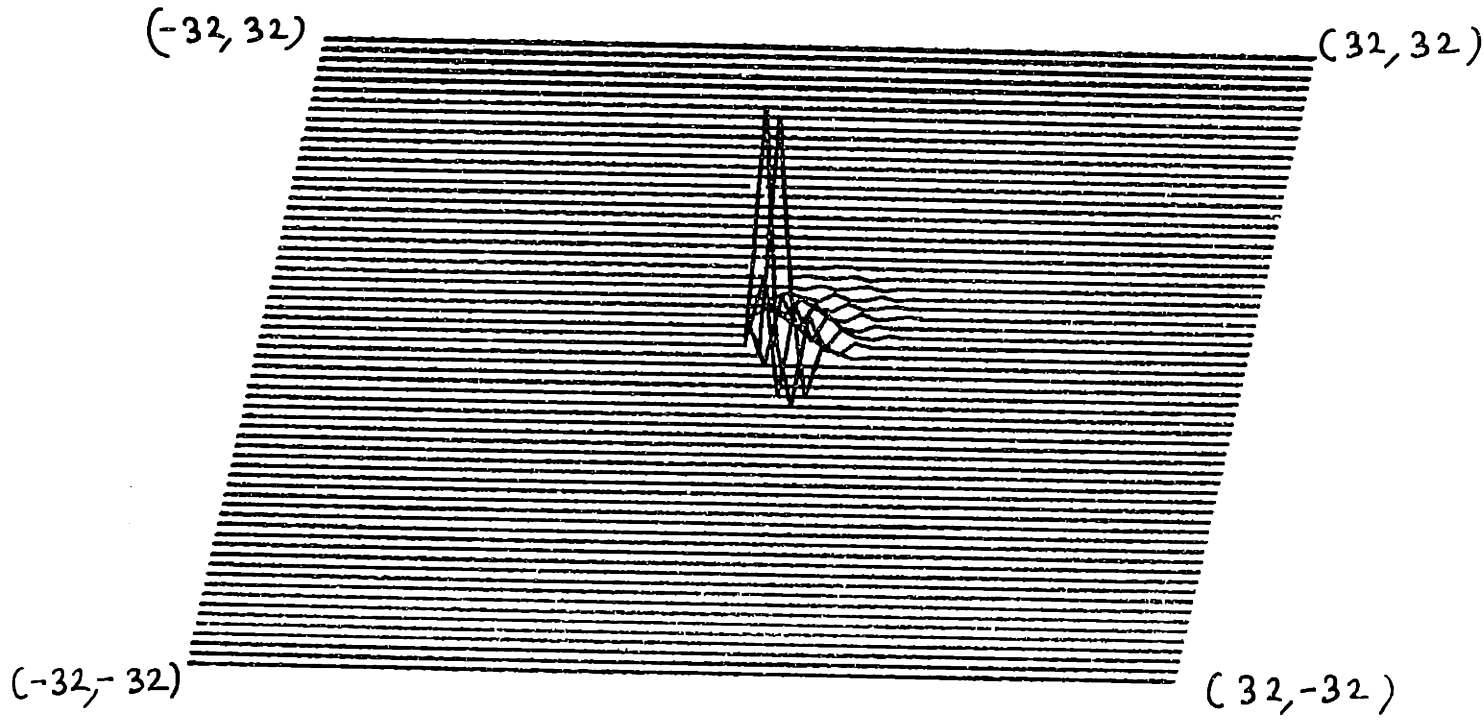

Complex cepstrum, $\hat{d}[m,n]$

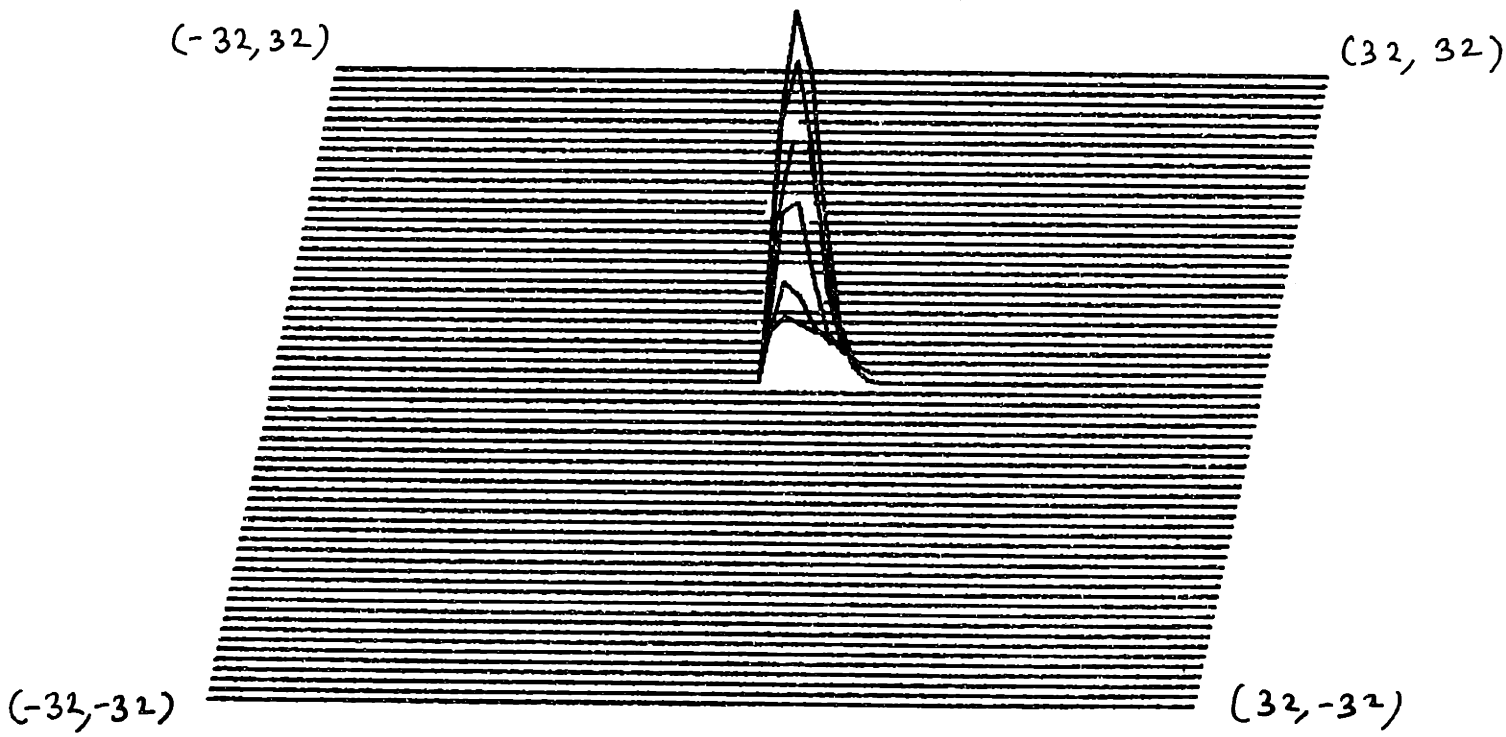

Output of inverse characteristic system, $d[m,n]$

Fig. 6.17

The complex cepstrum corresponding to the above equation can be found out by taking the logarithmic of the above equation and using a power series expansion. The complex cepstrum in closed form is given by

$$\hat{d}[m,n] = -\begin{pmatrix} 2m+n \\ m \end{pmatrix} \frac{(\frac{1}{3})^{2m+n}}{2m+n} \qquad \begin{matrix} 2m+n \geq 1 \\ 0 \leq m \leq 2m+n \end{matrix} \tag{6.21}$$

which lies in the first and fourth quadrants. The input array which we used for computing the complex cepstrum is

$$d[m,n] = \begin{array}{c|cccc} & -\frac{1}{3} & 0 & 0 & 0 \\ & 1 & 0 & 0 & 0 \\ n & 0 & -\frac{1}{3} & 0 & 0 \\ & 0 & 0 & 0 & 0 \\ 0 & \multicolumn{4}{c}{\underbrace{\qquad\qquad\qquad\qquad}_{m}} \end{array} \tag{6.22}$$

and thus we have introduced a linear phase of 2 along the n-axis. Fig. 6.18 shows the absolute value of the frequency response, its log and phase first and second derivatives. Fig. 6.19 shows the principal value and the unwrapped phase plot. Note that the jumps introduced by the modulo 2π operation have been removed. Fig. 6.20 shows the unwrapped after we have removed the linear phase along the n-axis. It also shows the complex cep-

EXAMPLE 6.7
Non-symmetric half-plane filter
FFT size 64x64

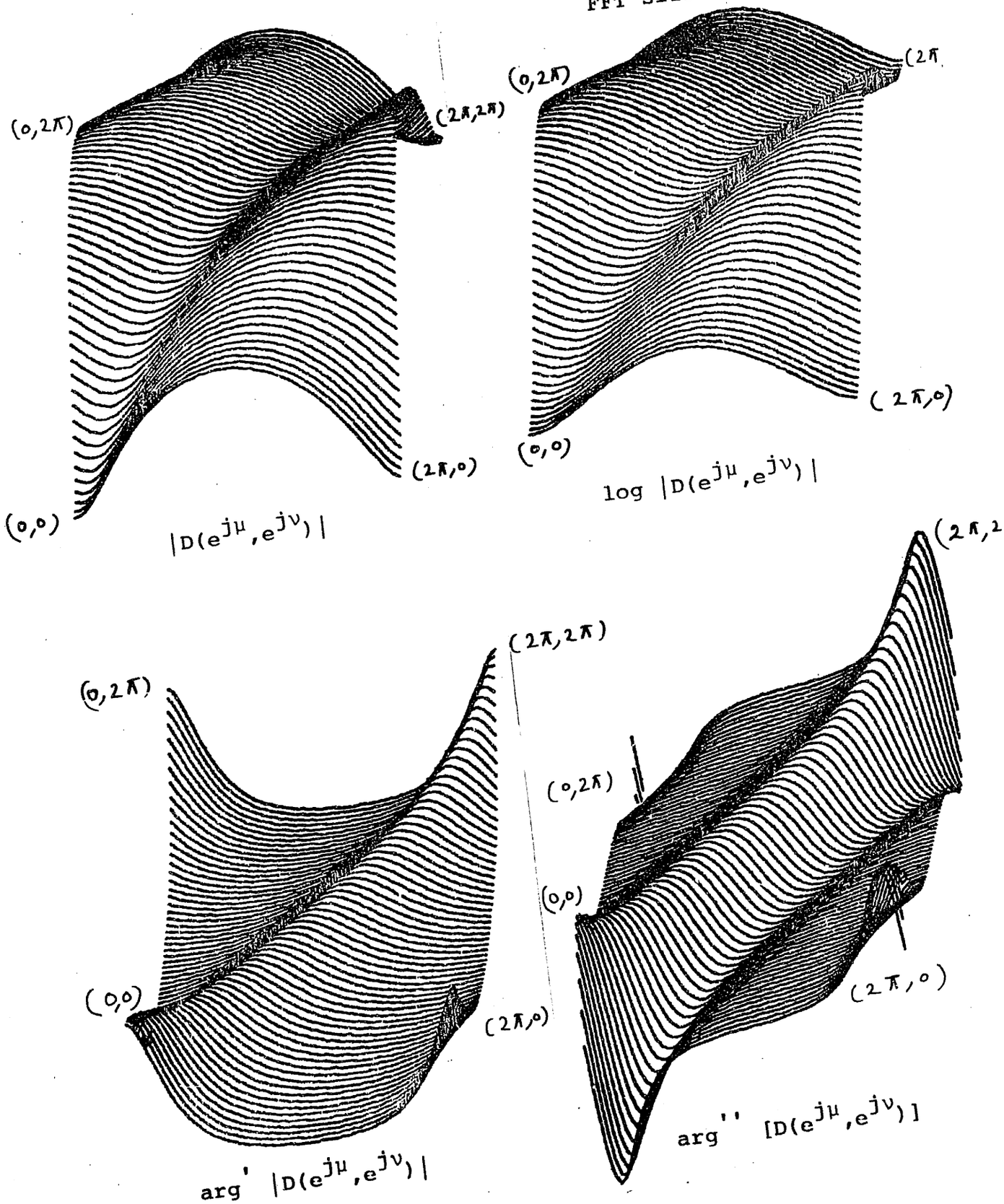

Fig. 6.18

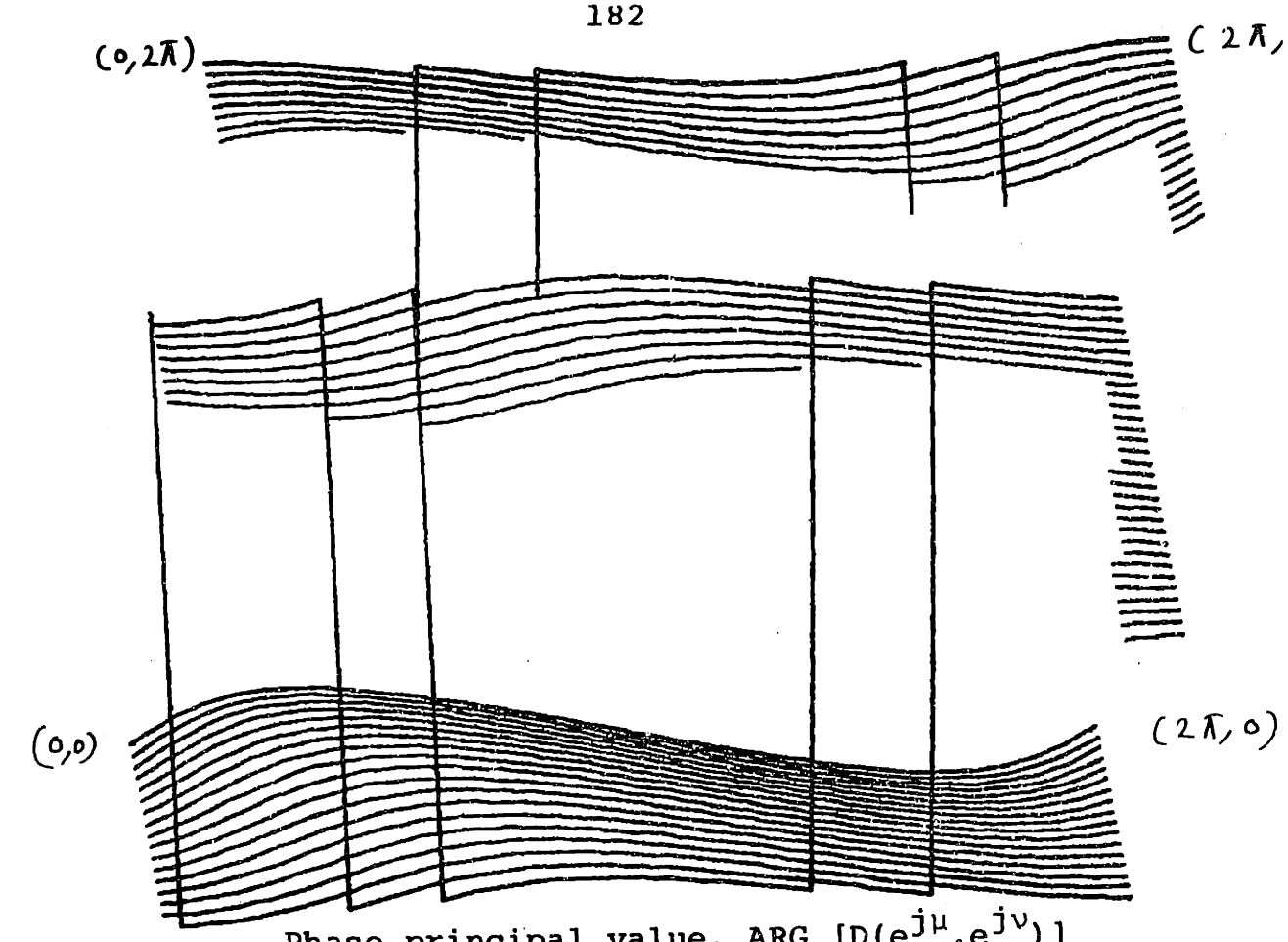

Phase principal value, ARG $[D(e^{j\mu}, e^{j\nu})]$

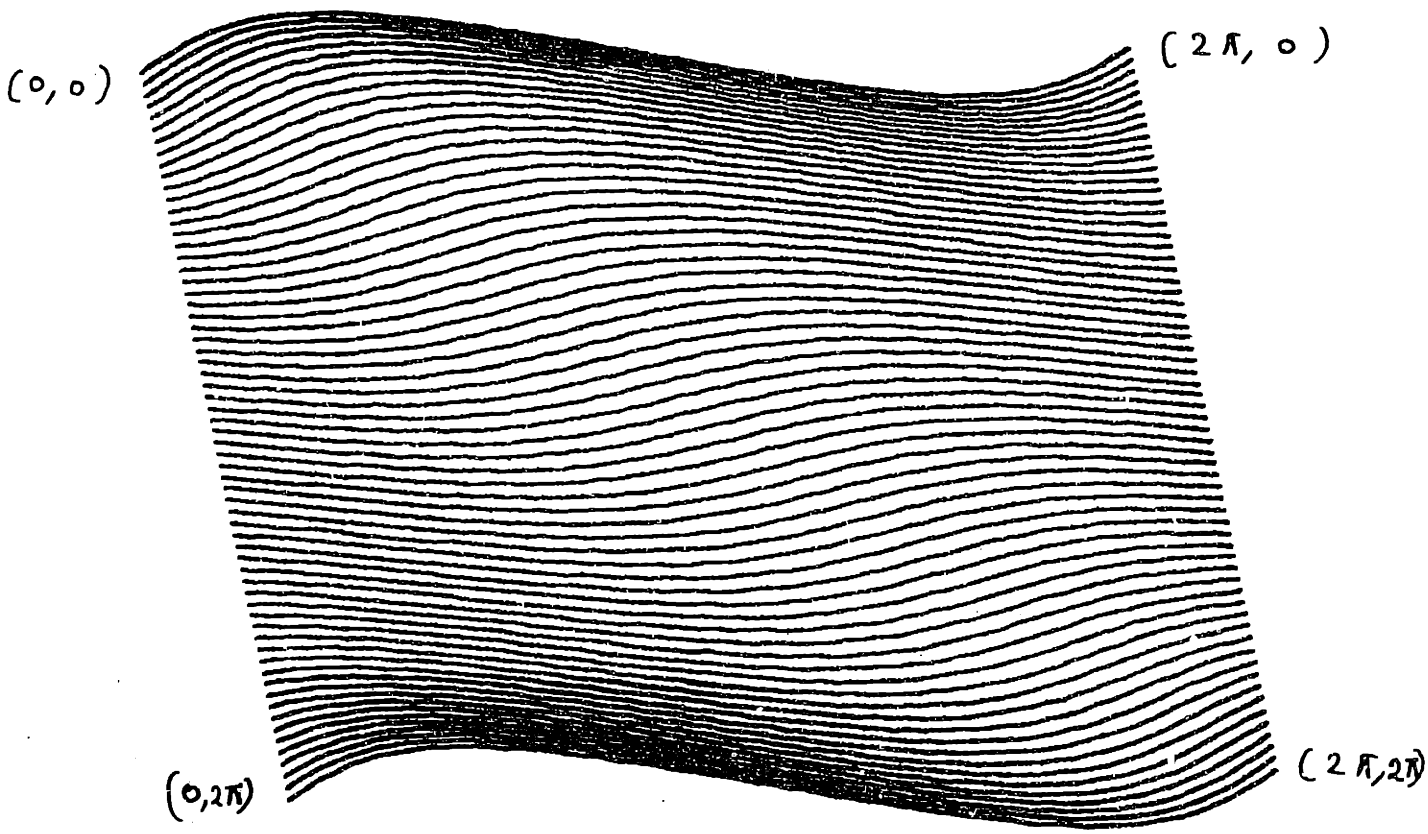

Unwrapped phase before removal of linear phase

Fig. 6.19

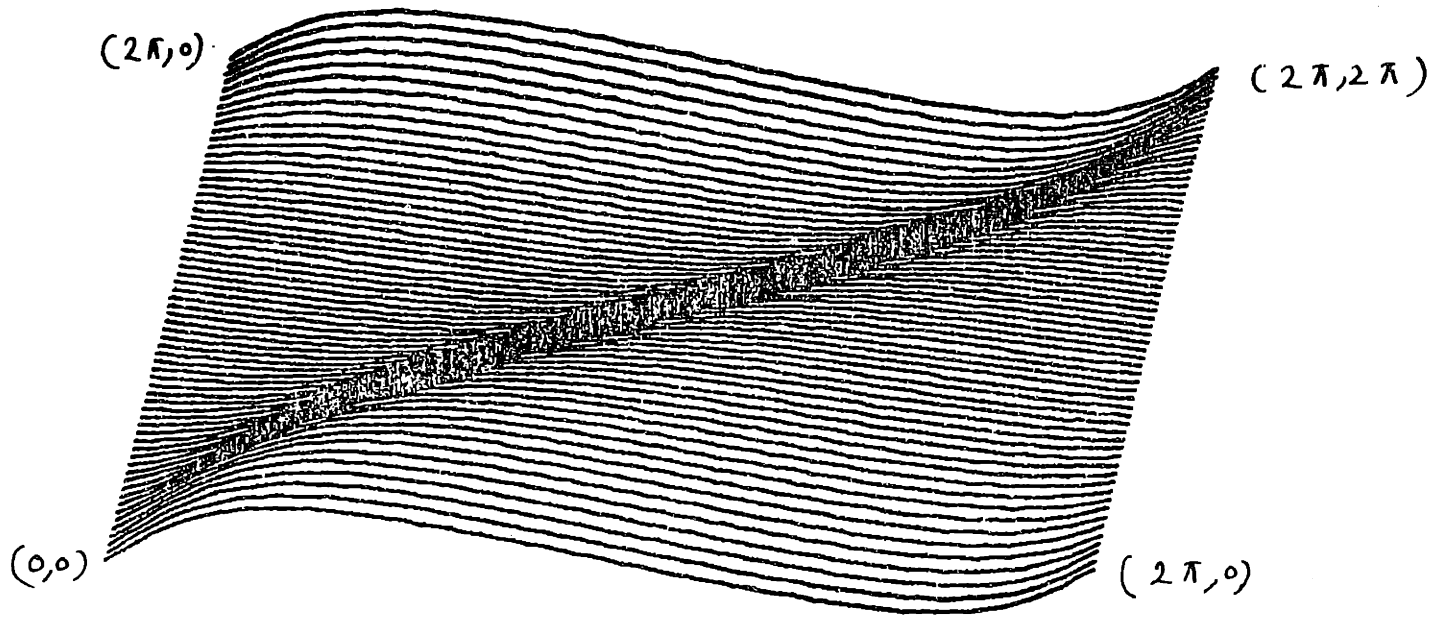

Unwrapped phase, arg $[D(e^{j\mu},e^{j\nu})]$ after removal of linear phase

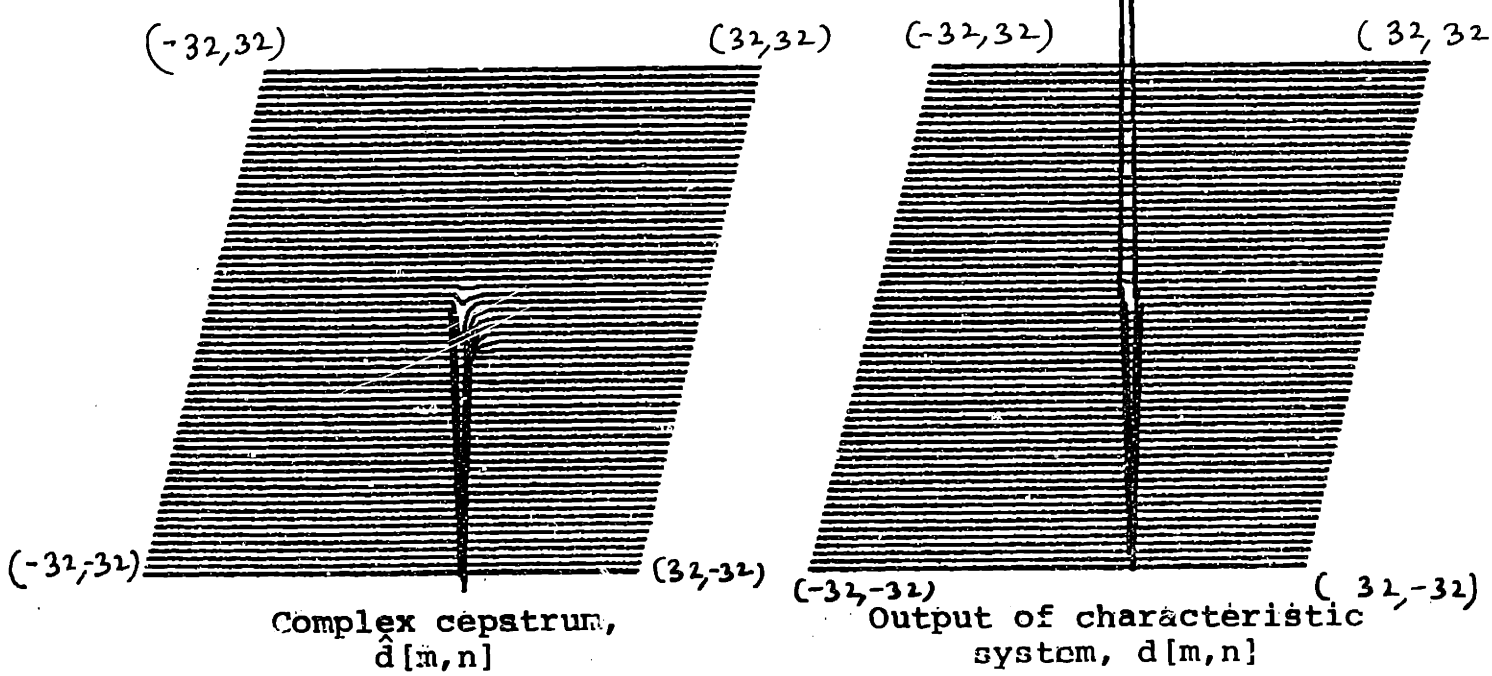

Complex cepstrum, $\hat{d}[m,n]$

Output of characteristic system, $d[m,n]$

Fig. 6.20

strum and the sequence obtained at the output of the inverse characteristic system.

It is to be noted (Fig. 6.20)that both the cepstrum and the sequence occupy the same support and we conclude that the filter is stable. FFT size used was 64x64.

Example 6.8 Non-symmetric half-plane fan filter examined by Ekstrom and Twogood [22].

The denominator array of the filter is,

$$
d[m,n] = \begin{array}{c|ccccc}
n & & & & & \\
\vdots & 0.001 & -0.001 & & & \\
 & -0.010 & 0.004 & -0.025 & -0.002 & \\
 & 0.051 & 0.002 & 0.025 & -0.002 & \\
 & -0.227 & -0.152 & 0.004 & 0.003 & 0.001 \\
 & 0.355 & 0.218 & 0.026 & 0.007 & 0.001 \\
 & 0. & 0.040 & 0.050 & 0.005 & 0.001 \\
 & 0. & -0.037 & -0.009 & 0.005 & \\
 & 0. & 0.003 & -0.004 & -0.002 & \\
 & 0. & -0.001 & & & \\
0 & \multicolumn{5}{l}{\text{———————— } m}
\end{array} \qquad (6.23)
$$

Setting the origin in the (m,n) plane as shown above we have introduced a linear phase of 4 along the n-axis. Fig. 6.21 shows the absolute value of the frequency response, its magnitude and the phase first and second derivatives. Fig. 6.22 shows the principal value, the unwrapped phase before and after the removal of the

EXAMPLE 6.8
Non-symmetric half-plane fan filter
FFT size 32x32

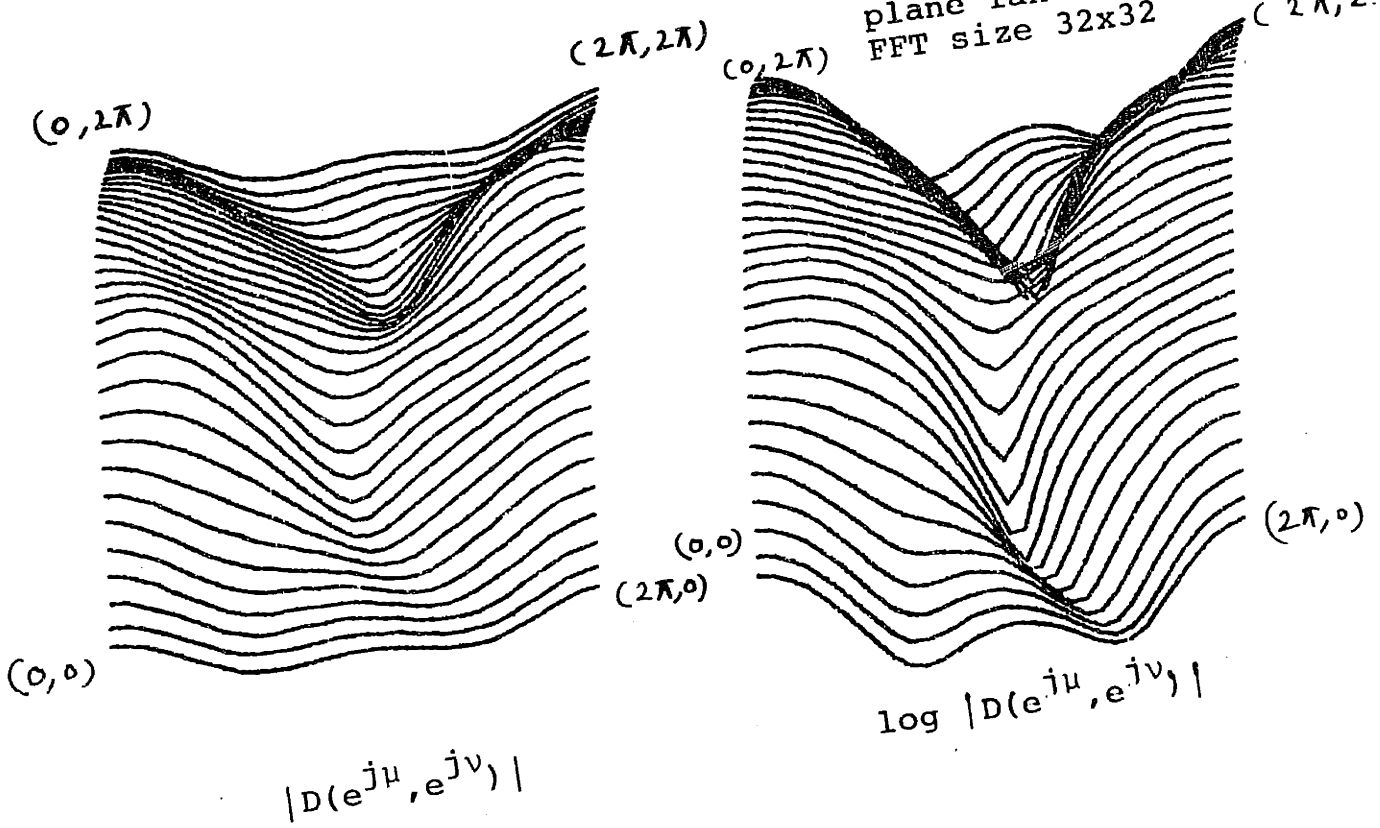

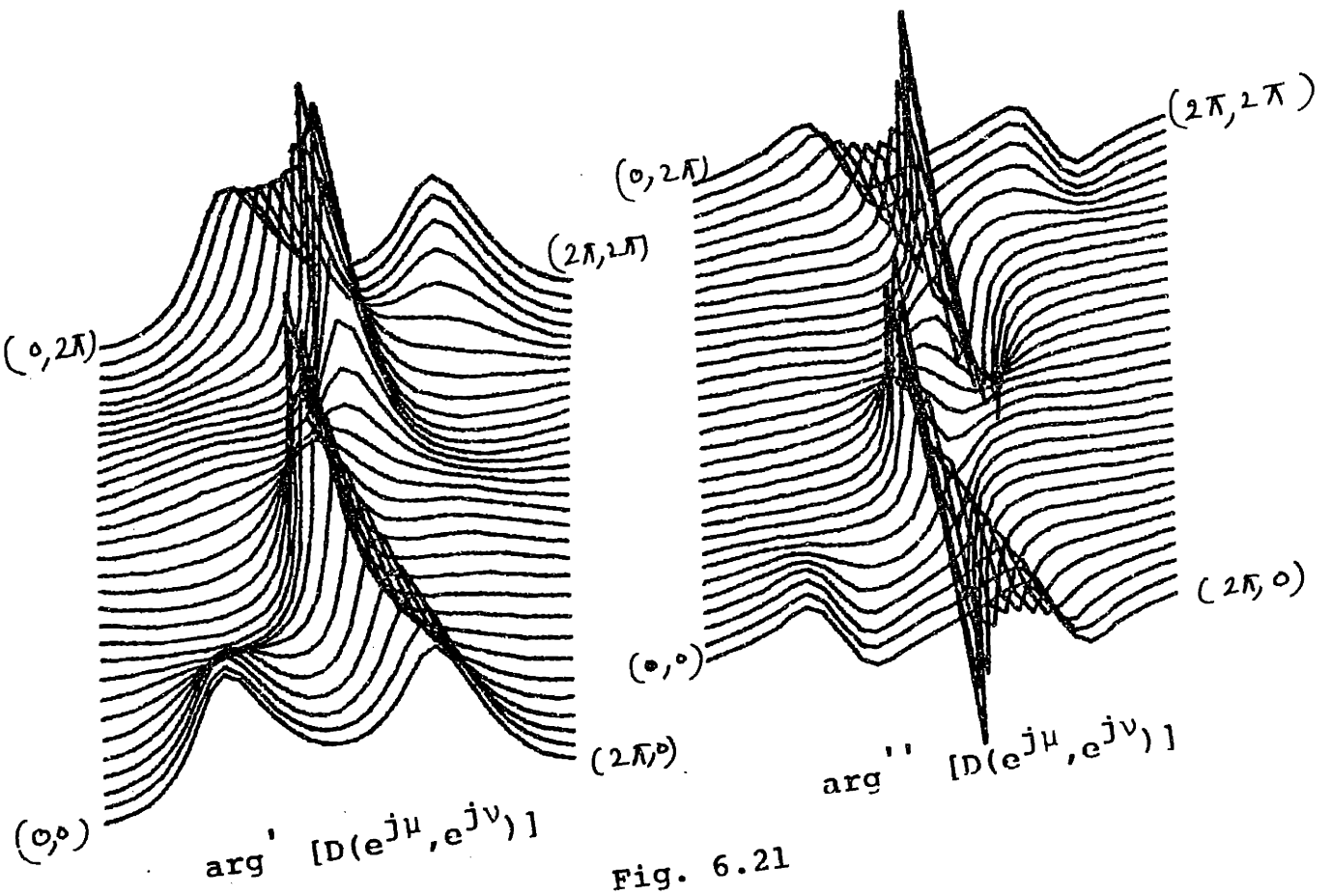

Fig. 6.21

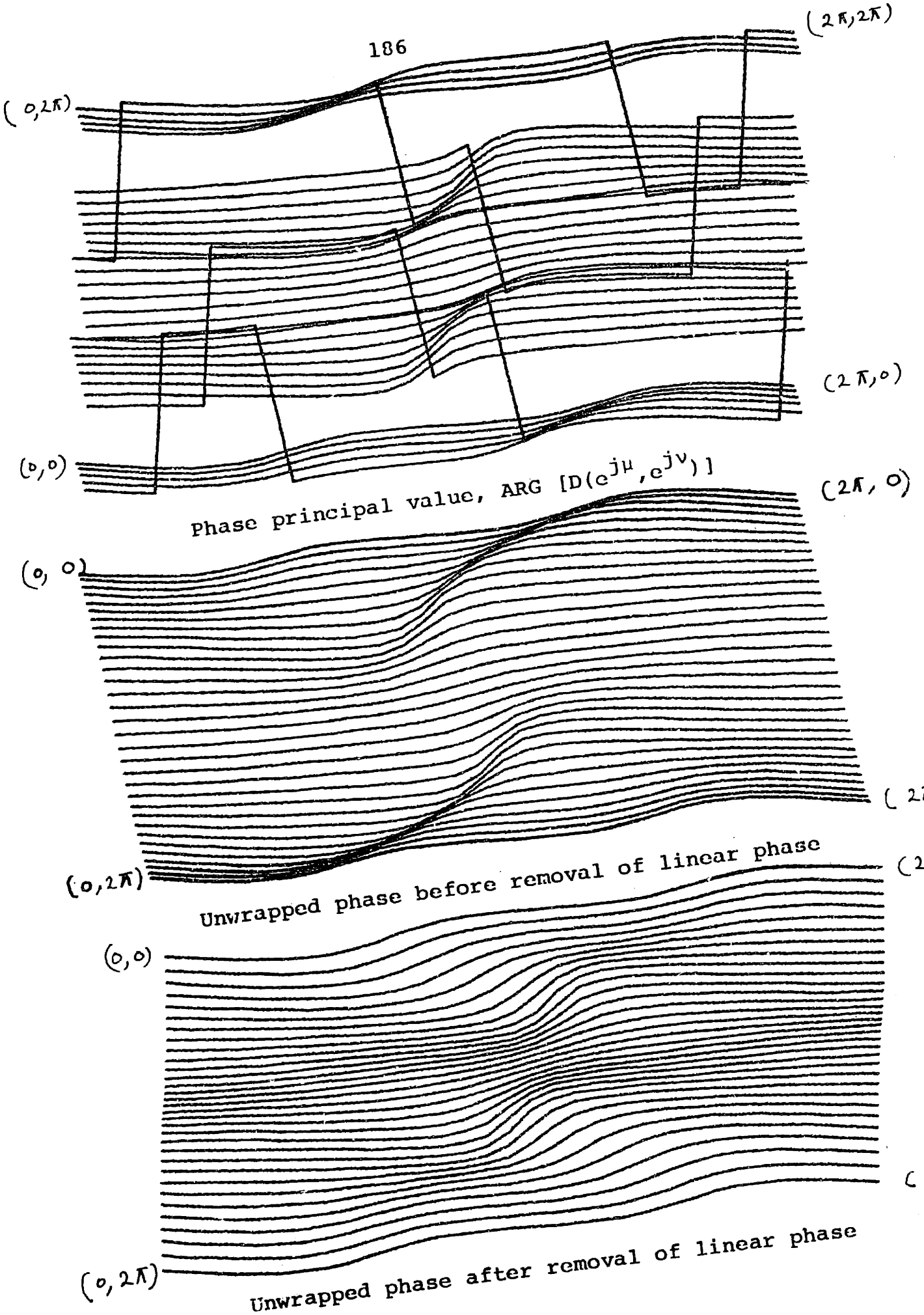
(0,2π)
(2π,2π)
(2π,0)
(0,0)
Phase principal value, ARG [D(e^jμ,e^jν)]
(0, 0)
(2π, 0)
(2π, 2π)
(0,2π)
Unwrapped phase before removal of linear phase
(0,0)
(2π,0)
(2π,2π)
(0,2π)
Unwrapped phase after removal of linear phase

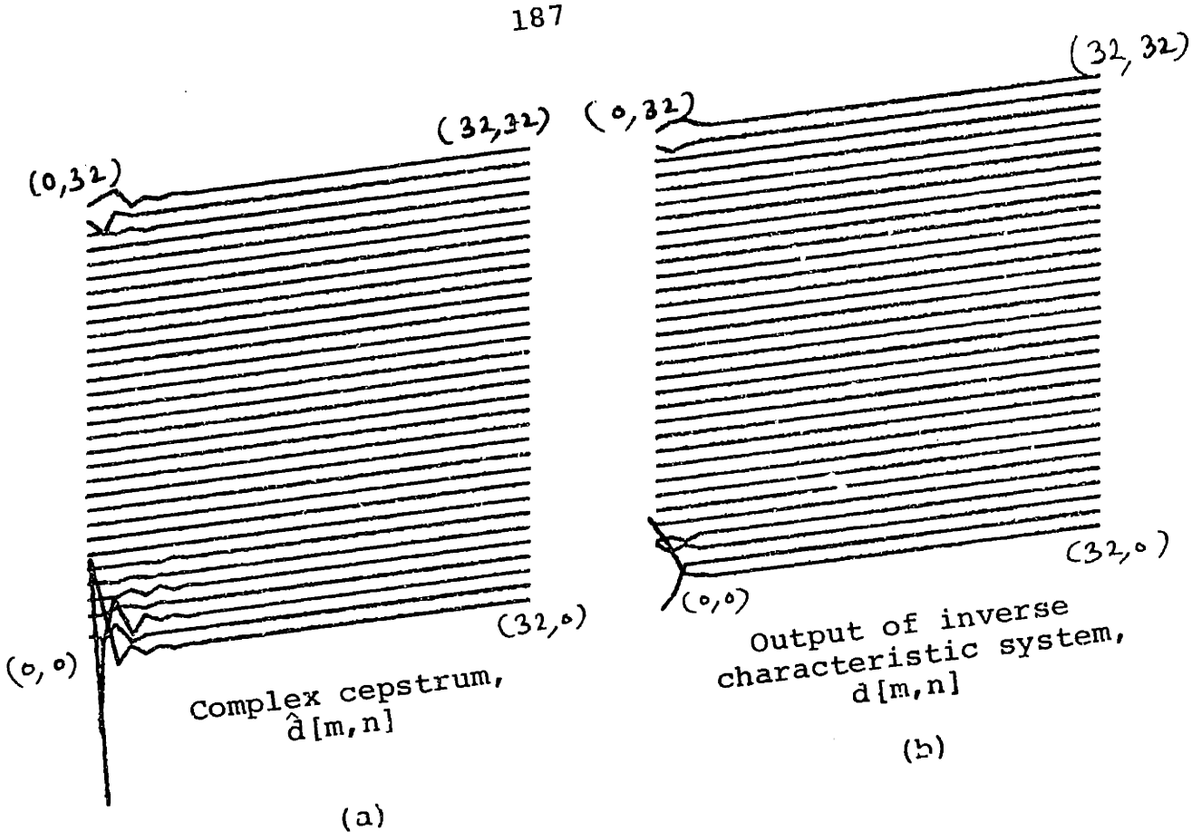
(32,32)
(0,32)
(0,0)
(32,0)
Complex cepstrum,
$\hat{d}[m,n]$
(a)
(32,32)
(0,32)
(32,0)
(0,0)
Output of inverse
characteristic system,
d[m,n]
(b)

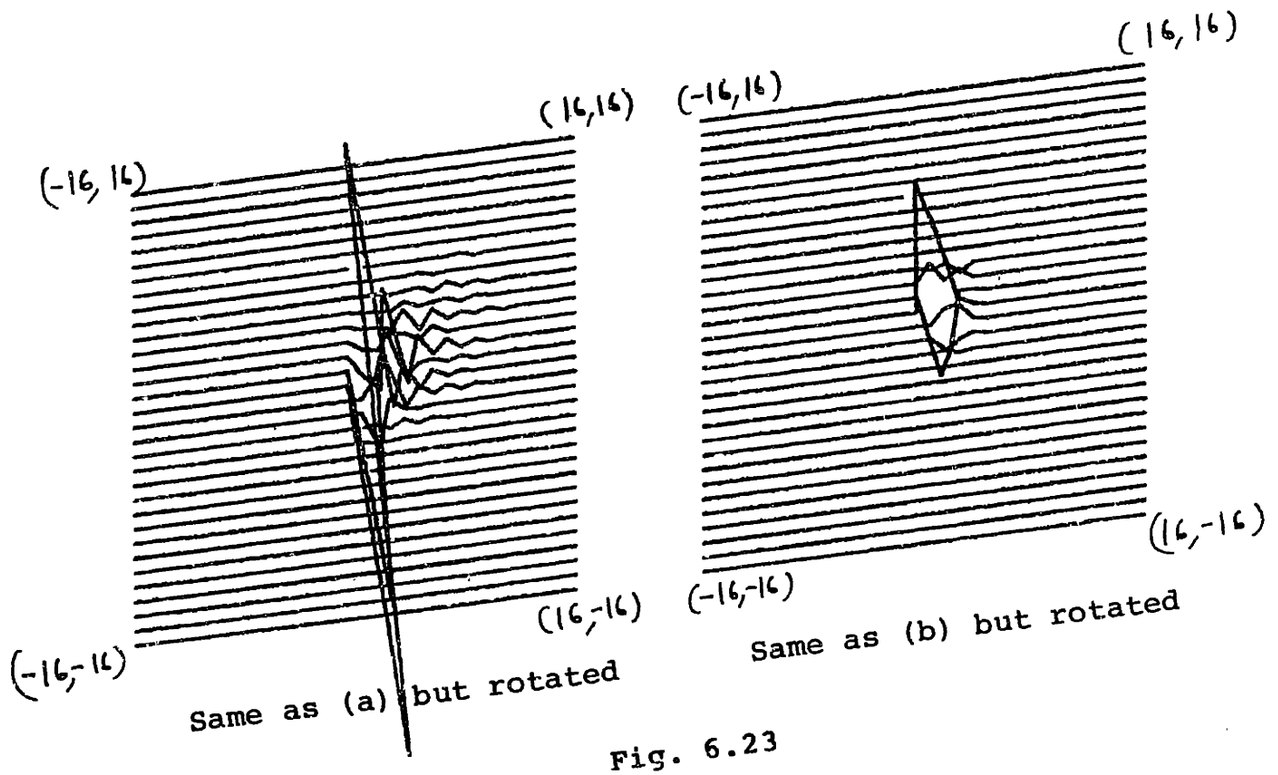
(16,16)
(-16,16)
(-16,-16)
(16,-16)
Same as (a) but rotated
(16,16)
(-16,16)
(-16,-16)
(16,-16)
Same as (b) but rotated

Fig. 6.23

linear phase. Since we have introduced the linear phase, we observe jumps in the principal value plot. Actually we would like to feed our input array such that (settting origin properly using the periodicity of 2-D DFT) no linear phase is introduced, because it makes the unwrapping more difficult. Fig. 6.23 shows the cepstrum and the sequence. We have rotated the upper two plots so as to get the lower two figures. It is clear that the sequence (output of the inverse characteristic system) and cepstrum have the same support, hence the filter is stable. FFT size used was 32x32. It also worked for 16x16.

Unstable quarter-plane filters

Having considered the stable quarter-plane and half-plane filters, we are interested in the behavior of phase unwrapping or the complex cepstrum when the filter happens to be unstable.

Example 6.9

First we tried the counter example of Shank's conjecture by Genin & Kamp [30]. In this case the denominator array is

$$\begin{array}{c|cccc} 0 \;\backslash\; m & & & & \\ n & & & & \\ & 1 & -1.15 & -0.902 & 1.75 \\ & -1.15 & 3.72 & -2.23 & -0.902 \\ & -0.902 & -2.23 & 3.72 & -1.15 \\ & 1.75 & -0.902 & -1.15 & 1 \end{array} \qquad (6.24)$$

EXAMPLE 6.9
Counter example of
Shank's conjecture
FFT size 64x64

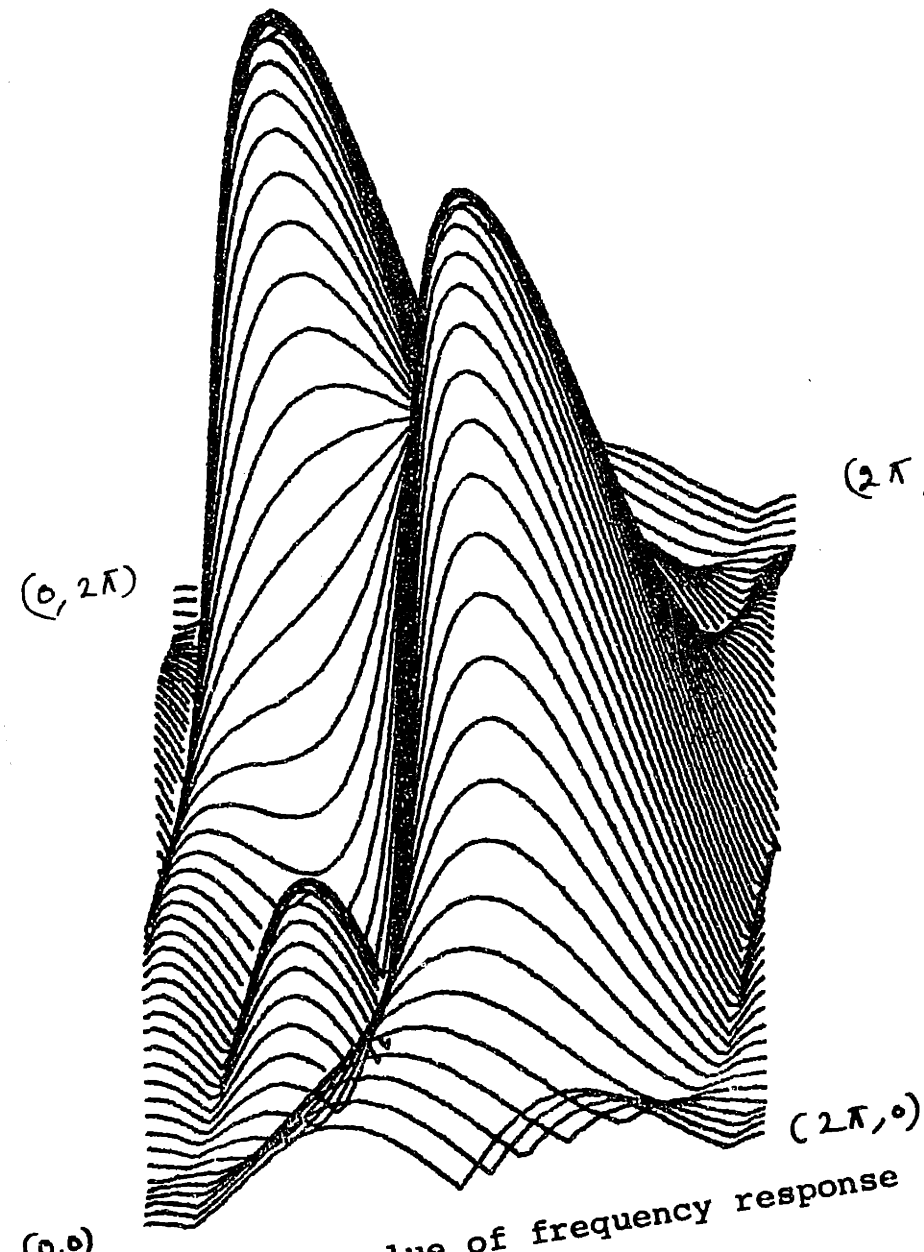

Absolute value of frequency response
$[D(e^{j\mu}, e^{j\nu})]$

Fig. 6.24

It is found that the magnitude of the frequency response (shown in Fig. 6.24) becomes zero at a certain DFT point and hence the cepstrum cannot be calculated. The filter is unstable. The planar least square inverse [24] of the above array is also unstable.

Example 6.10 Unstable filter examined by Shanks [24].

The denominator array is given by

$$d[m,n] = \begin{array}{c|cc} n & & \\ & -0.9 & 0.05 \\ & 1 & -0.95 \\ 0 & \multicolumn{2}{c}{\overline{\qquad\qquad}} \\ & \multicolumn{2}{c}{m} \end{array} \qquad (6.25)$$

Using Huang's test filter can be shown to be unstable. Fig. 6.25 shows the magnitude of the frequency response, its log and phase first and second derivatives. Fig. 6.26 shows the principal value plot and the unwrapped phase. We got the linear phase of -1 along the two axes. Fig. 6.27 shows the unwrapped phase after the removal of linear phase. The unwrapped phase before and after the removal of linear phase appears to be discontinuous. Finally Fig. 6.28 shows the complex cepstrum and the sequence as obtained at the output of the inverse characteristic system. These two do not occupy the same support, hence the filter is unstable. FFT size used was 32x32.

EXAMPLE 6.10
Unstable quarter plane Shank's filter
FFT size 32x32

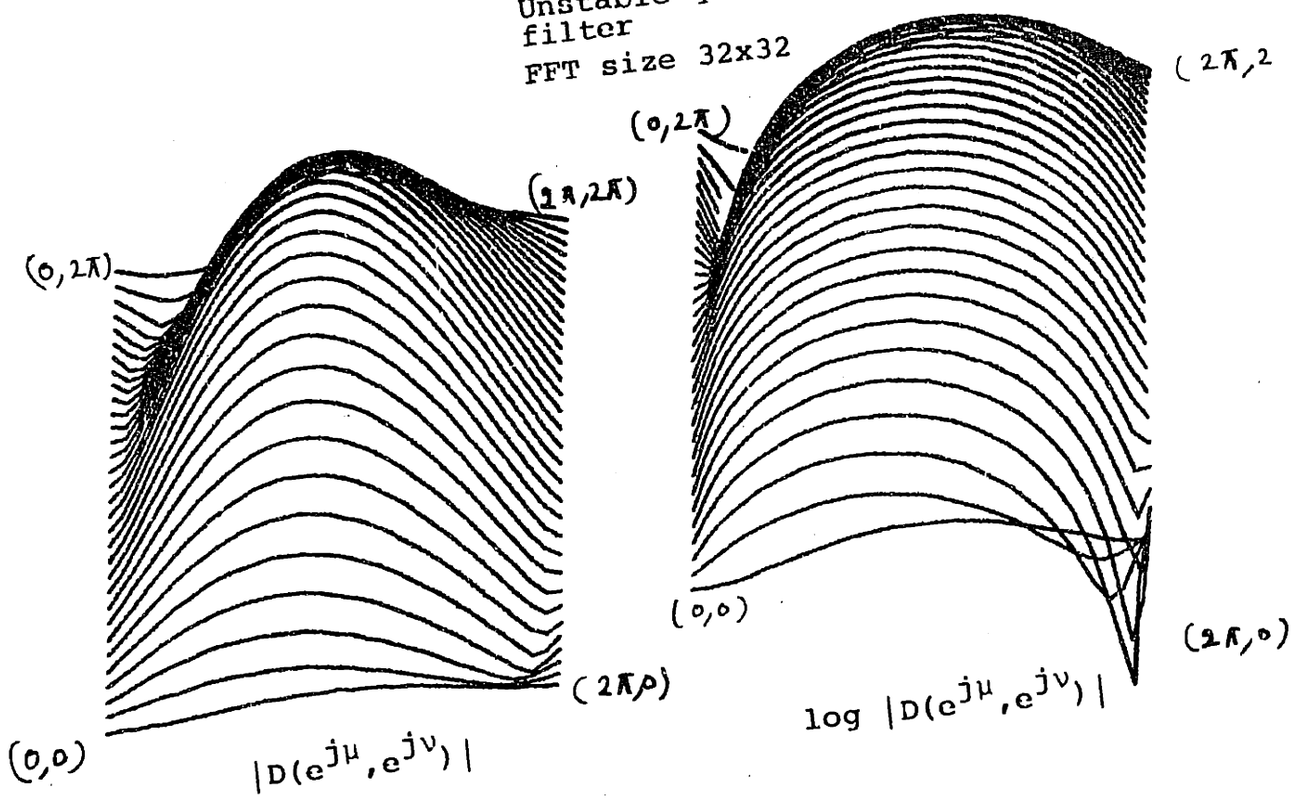

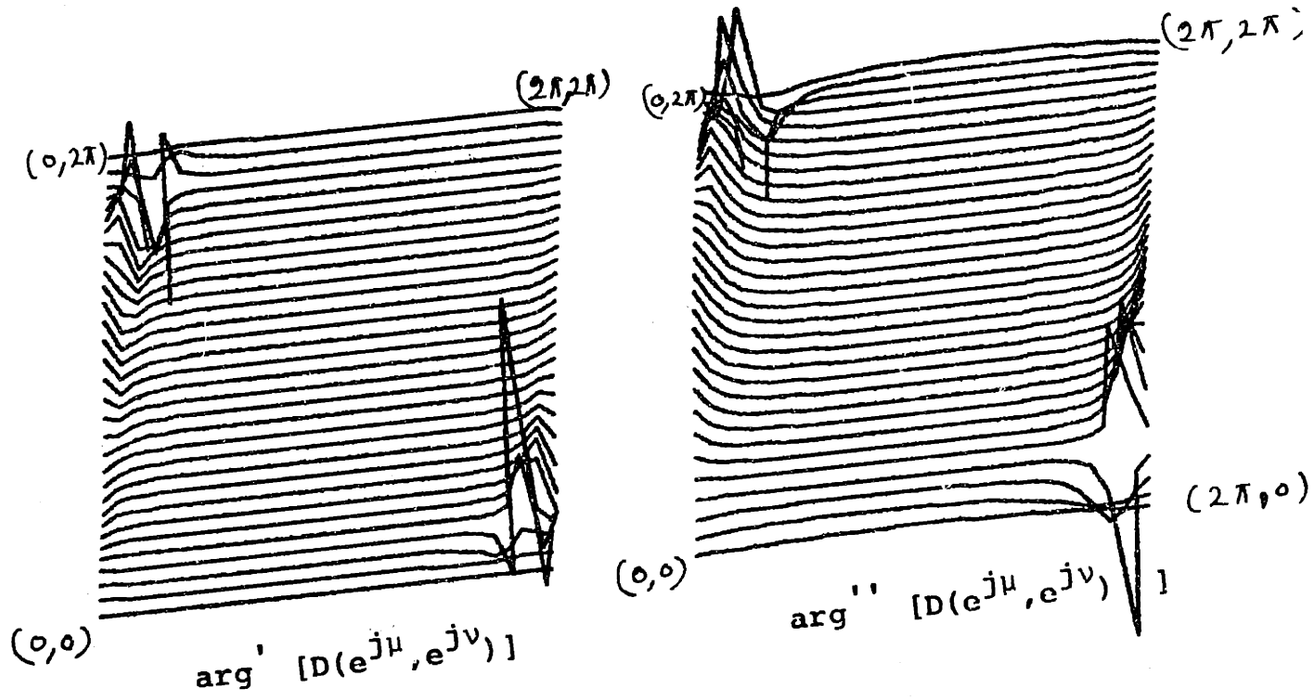

Fig. 6.25

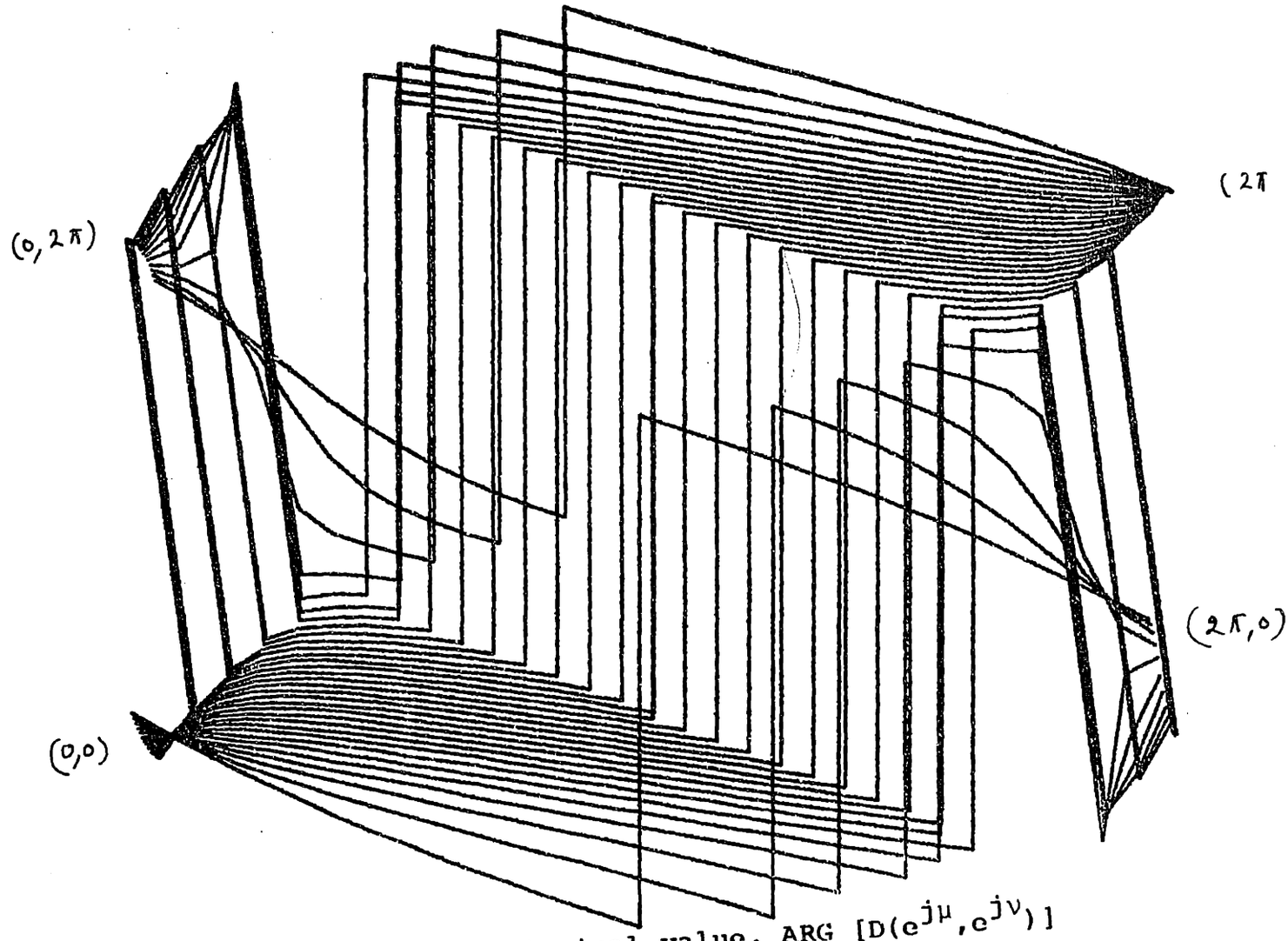

Phase principal value, ARG $[D(e^{j\mu}, e^{j\nu})]$

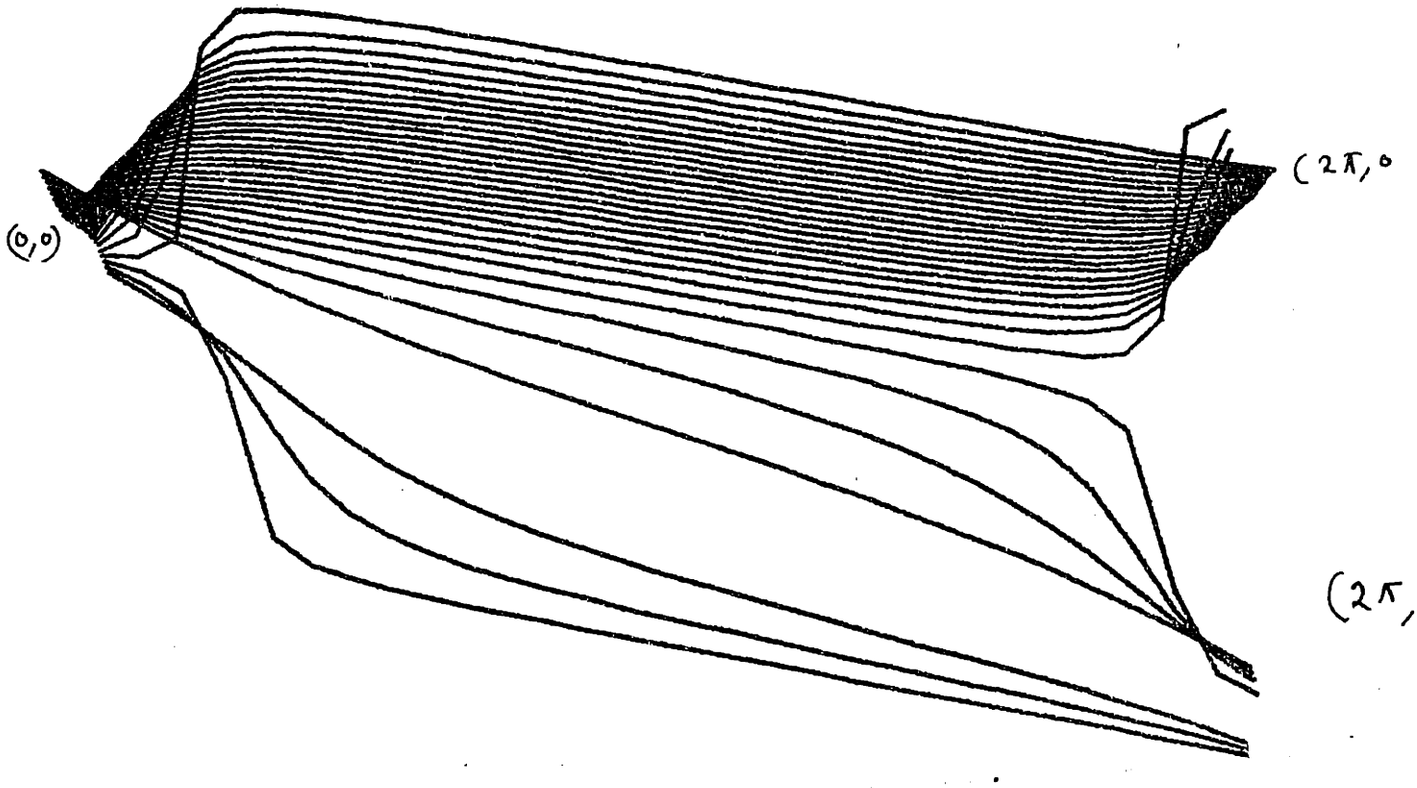

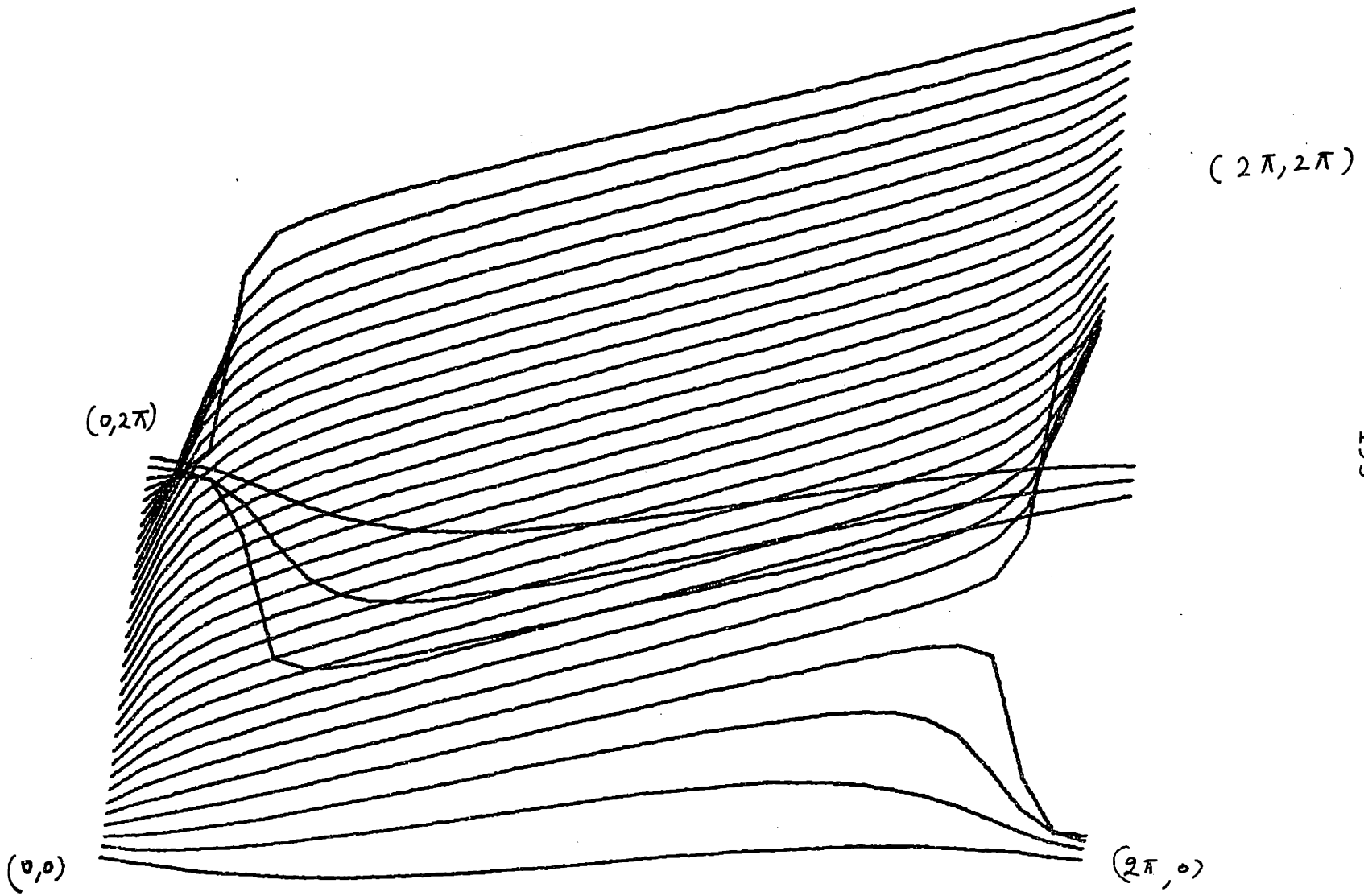

Unwrapped phase after removal of linear phase, arg $[D(e^{j\mu}, e^{j\nu})]$

Fig. 6.27

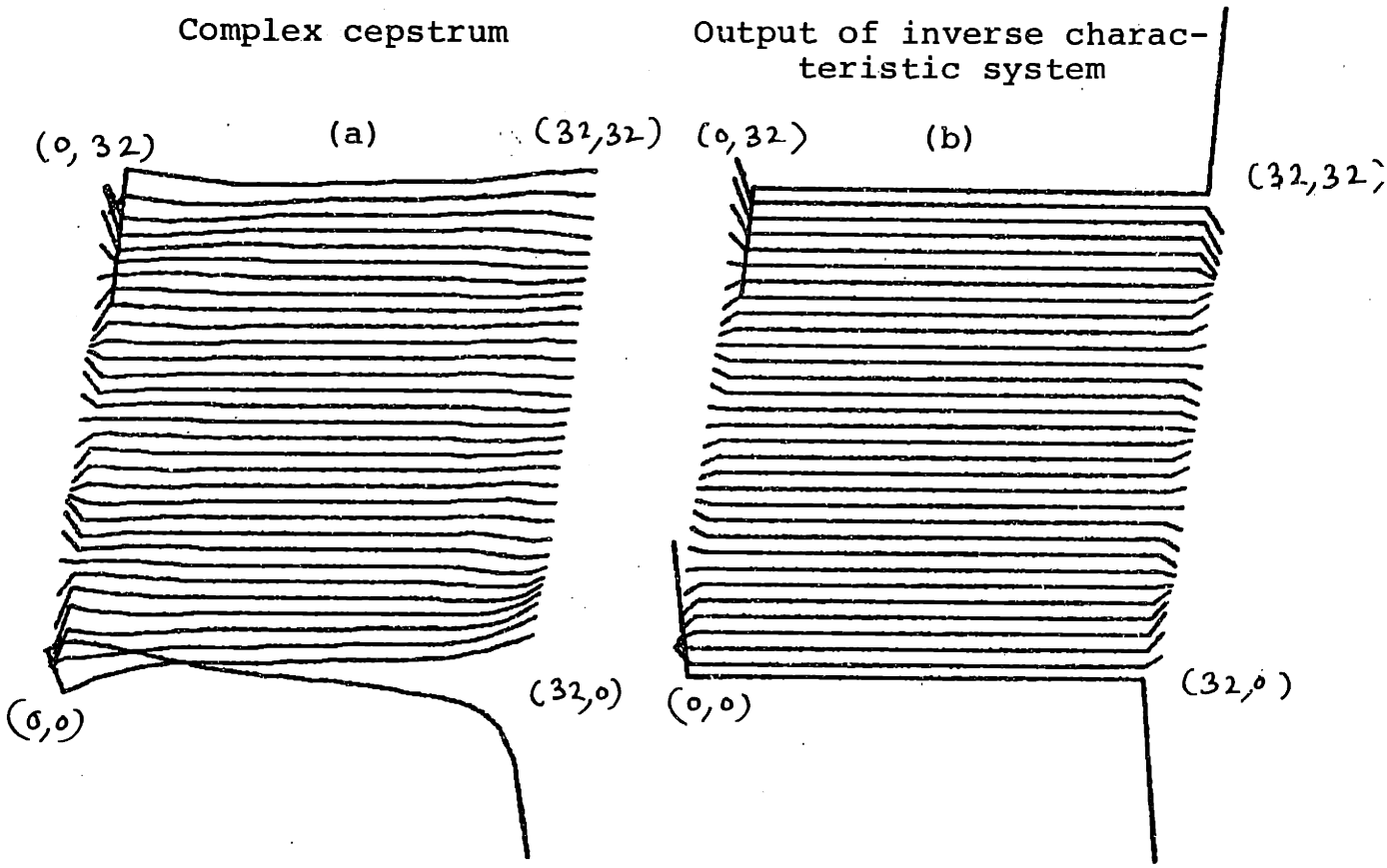
Complex cepstrum
Output of inverse characteristic system
(0, 32)
(a)
(32,32)
(0,32)
(b)
(32,32)
(32,0)
(0,0)
(0,0)
(32,0)
Same as (a) but rotated
Same as (b) but rotated
(-16,16)
(16,16)
(-16,16)
(16,16)
(-16,-16)
(16,-16)
(-16,-16)
(16,-16)

Fig. 6.28

Example 6.11 Unstable filter examined by Shanks [24].

The denominator array is given by

$$d[m,n] = \begin{array}{c} n \\ | \\ 0 \end{array} \begin{array}{ccc} 0.5 & -0.75 & 0.25 \\ -1.2 & 1.8 & -0.72 \\ 1 & -1.5 & 0.6 \\ \hline & m & \end{array} \qquad (6.26)$$

Figs. 6.29 to 6.32 shows the magnitude of the frequency response, its log, two derivatives, principal value plot, unwrapped phase before and after the removal of linear phase and the complex cepstrum and the sequence. FFT size used was 64x64.

Comments similar to Example 6.10 apply here. Using contour plots Shanks shows that zeroes lie right on the unit circle and the stability theorem is not satisfied.

In the above two unstable examples, we observe the discontinuity in the phase plots and the cepstrum and the output of the inverse characteristic system do not occupy the same support. These are the characteristics of the complex cepstrum for the unstable cases.

In an attempt to observe how the computation of the complex cepstrum is susceptible to the slight changes in the values of the 2-D denominator array, we changed the value of x[2,2] in eq. (6.26) from 0.25 to 0.29. Thus getting the array as,

EXAMPLE 6.11
Unstable Shanks
quarter plane filter
FFT size 64x64

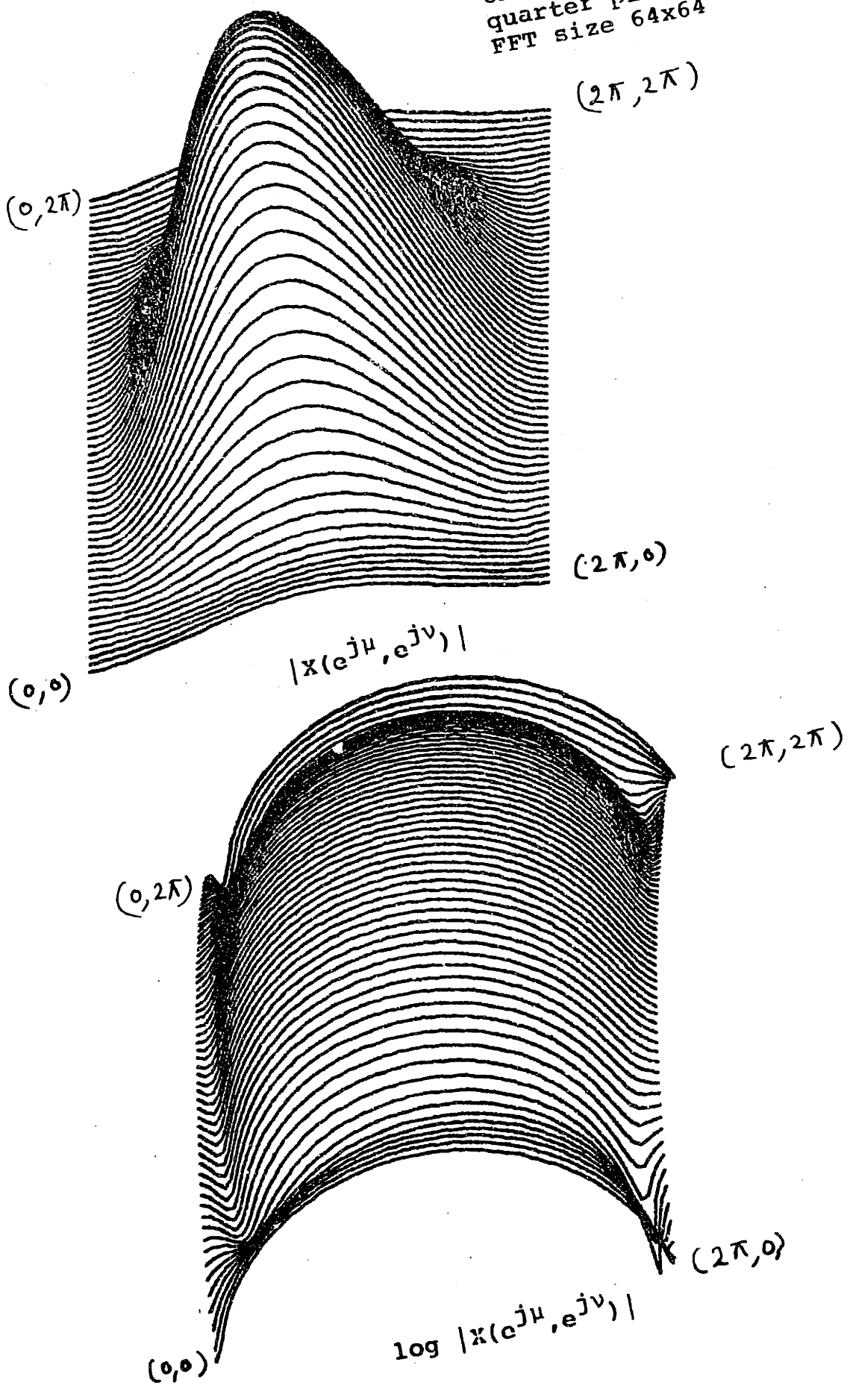

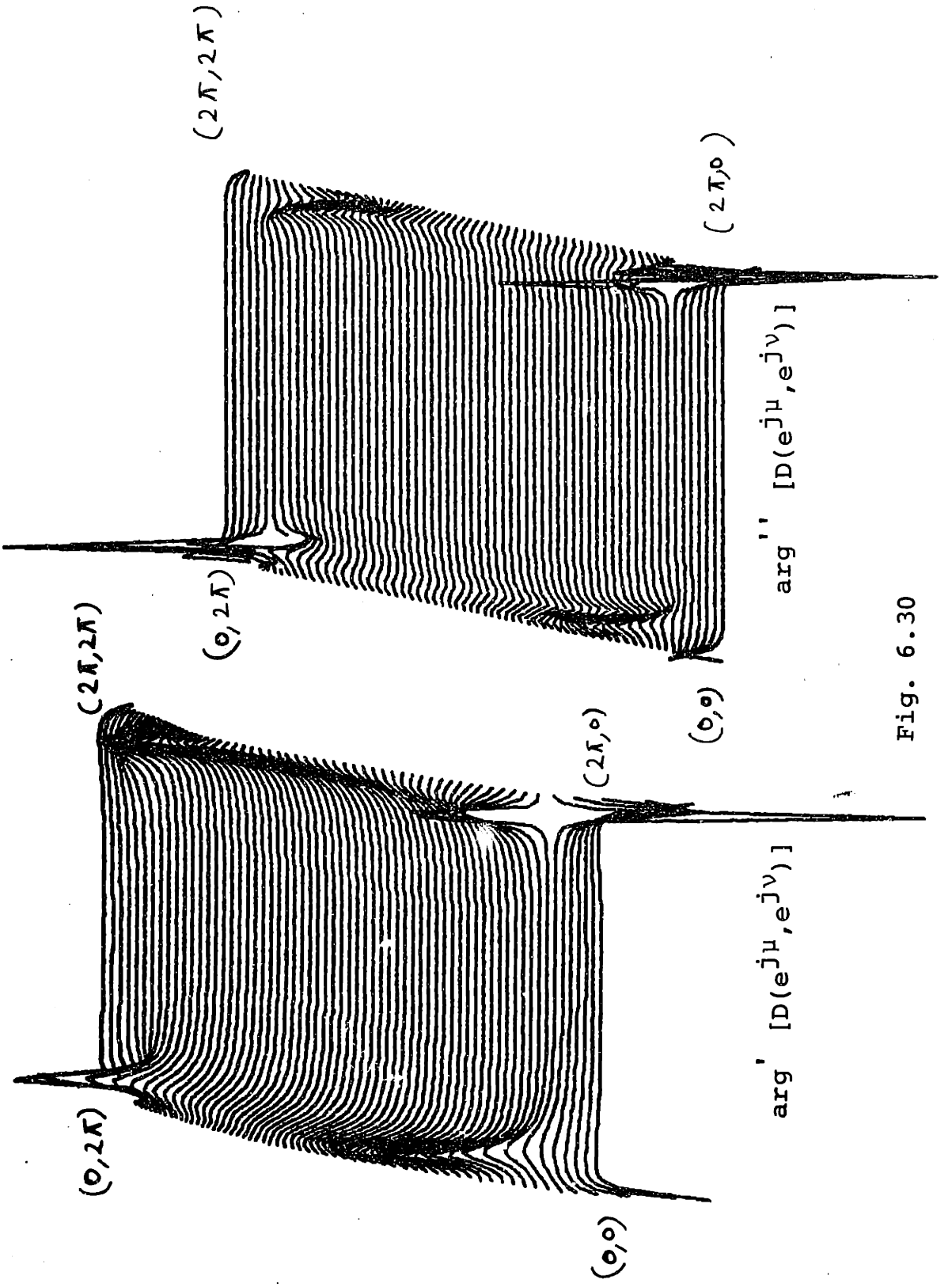

Fig. 6.30

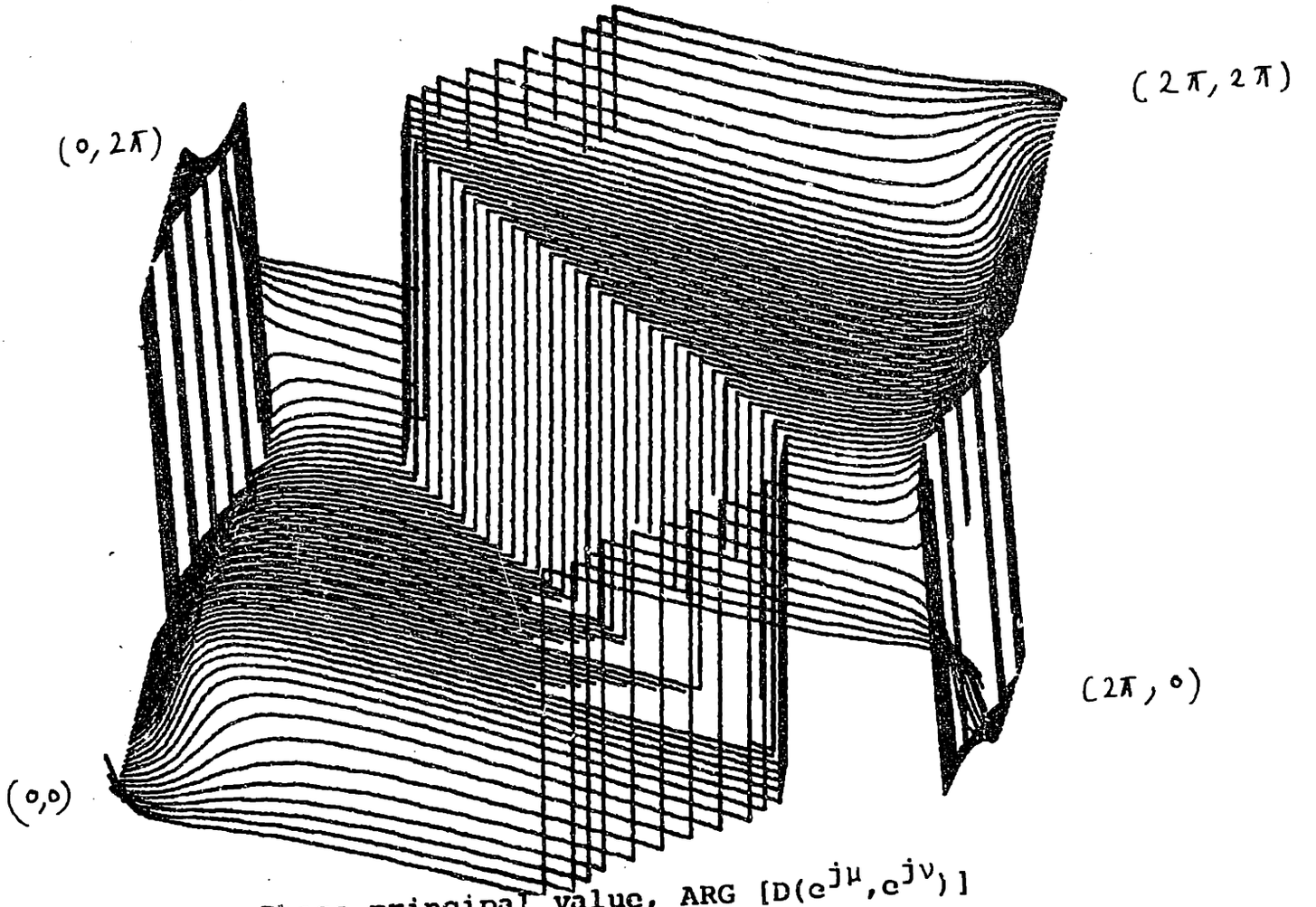

Phase principal value, ARG $[D(e^{j\mu}, e^{j\nu})]$

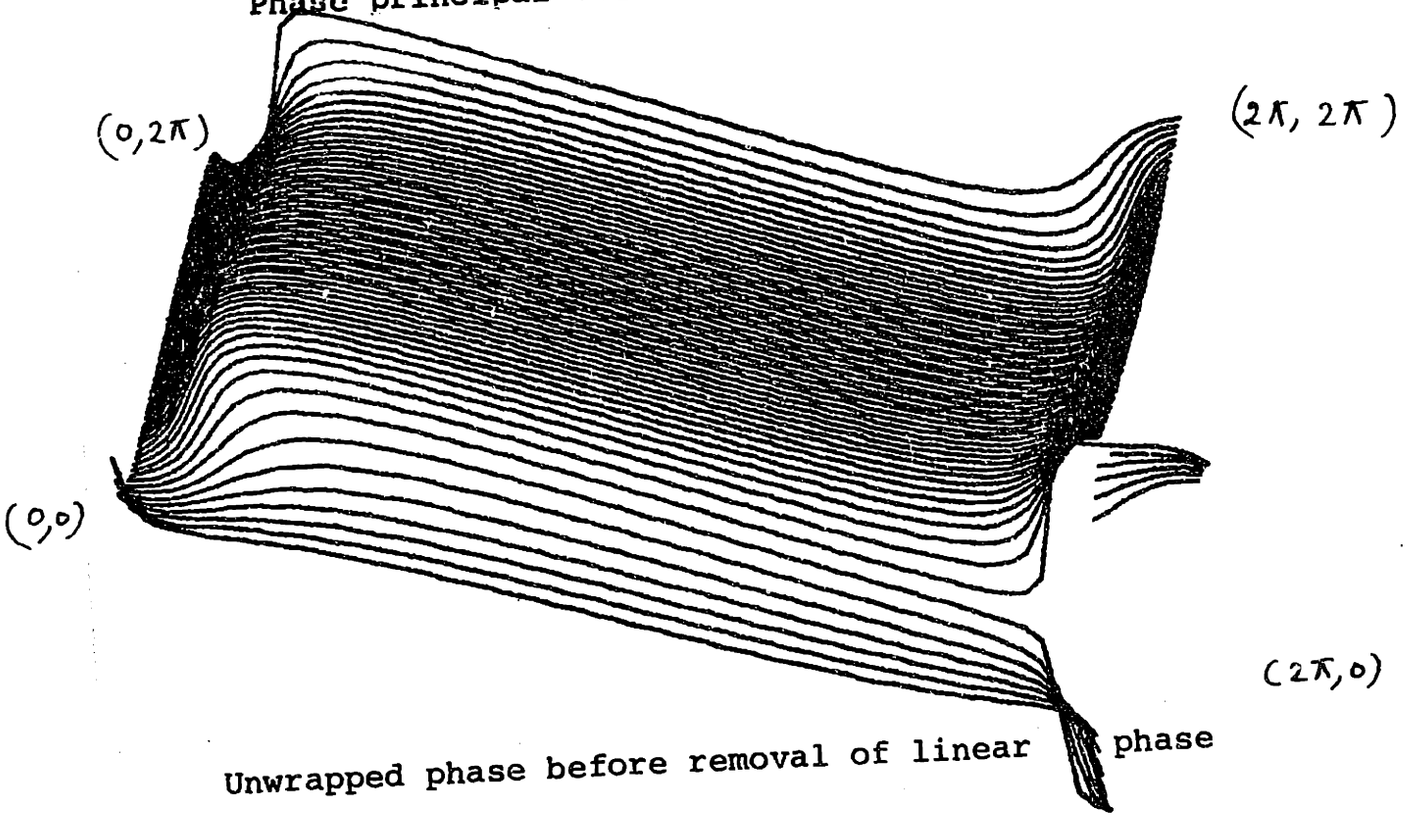

Unwrapped phase before removal of linear phase

Fig. 6.31

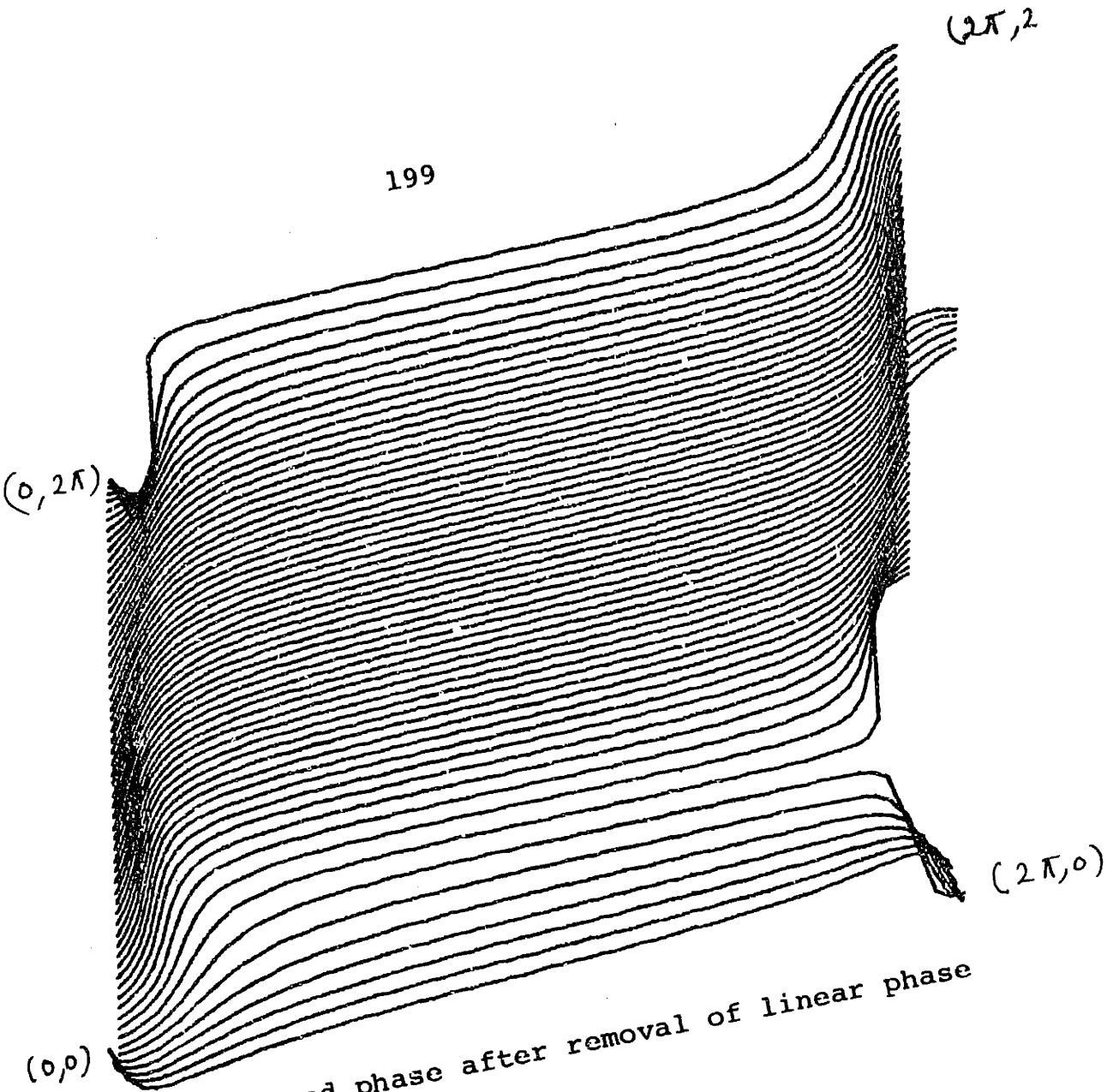

Unwrapped phase after removal of linear phase

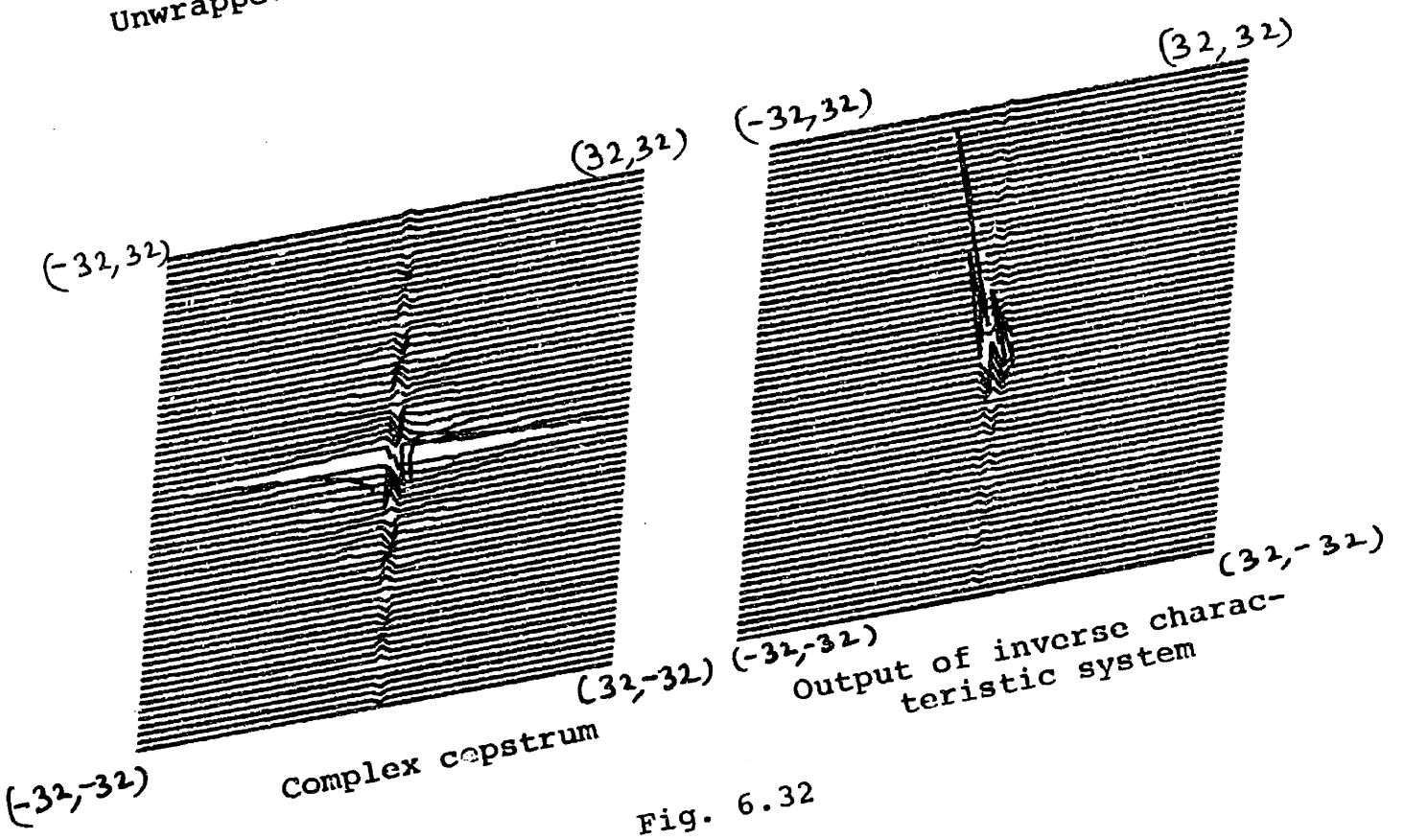

Complex cepstrum

Output of inverse characteristic system

Fig. 6.32

$$d[m,n] = \begin{array}{c|ccc} & 0.5 & -0.75 & 0.29 \\ n & -1.2 & 1.8 & -0.72 \\ & 1 & -1.5 & 0.6 \\ 0 & \multicolumn{3}{c}{\overline{\qquad\qquad\qquad}\ m} \end{array} \tag{6.27}$$

This case has also been examined by Shanks using contour mapping and has been shown to be stable. We are interested in the behavior of cepstrum. Fig. 6.33 shows the absolute value of the frequency response, its log magnitude, phase first and second derivatives. This figure can be compared with Figs. 6.29 and 6.30 and it can be noted that in Fig. 6.33 there are no discontinuities in the phase derivatives whereas they seem to be present in Fig. 6.30. Fig. 6.34 shows the unwrapped phase (which happened to be the same as the principal value) and cepstrum and the output of the inverse characteristic system. It can be noted that both cepstrum and the output of the inverse system have the same support which lies in the first quadrant, hence we conclude that the phase unwrapping worked successfully and the computed values of the complex cepstrum are right and they were checked using min. phase formulae. FFT size used was 32x32.

In this chapter we discussed the use of the complex cepstrum for checking the stability of 1-D and 2-D recursive digital filters. Quadrant and non-symmetric half-plane filters were considered. It is found that the computation of the cepstrum is quite sensitive to the stable and unstable

MODIFICATION OF
EXAMPLE 6.11

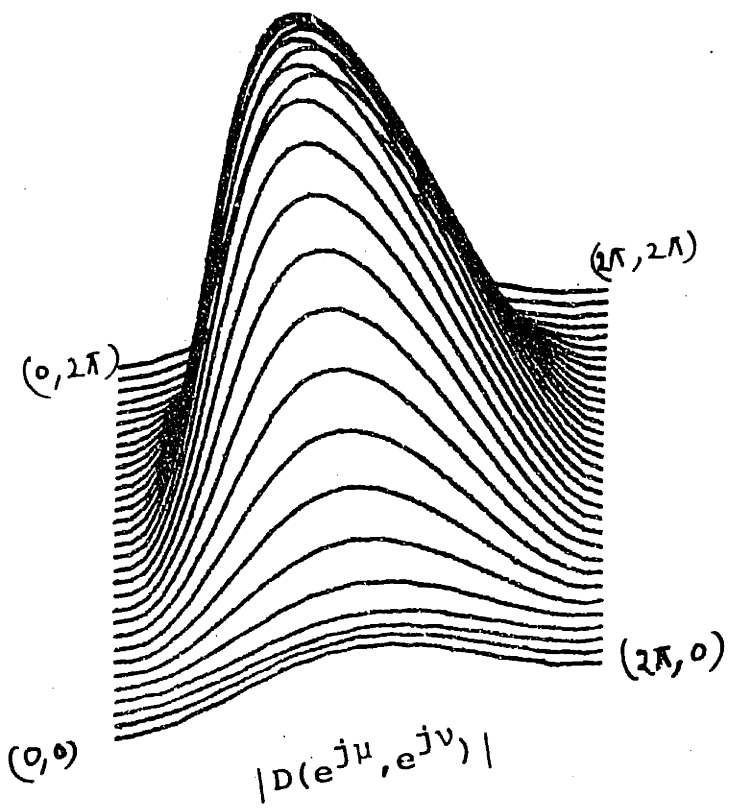

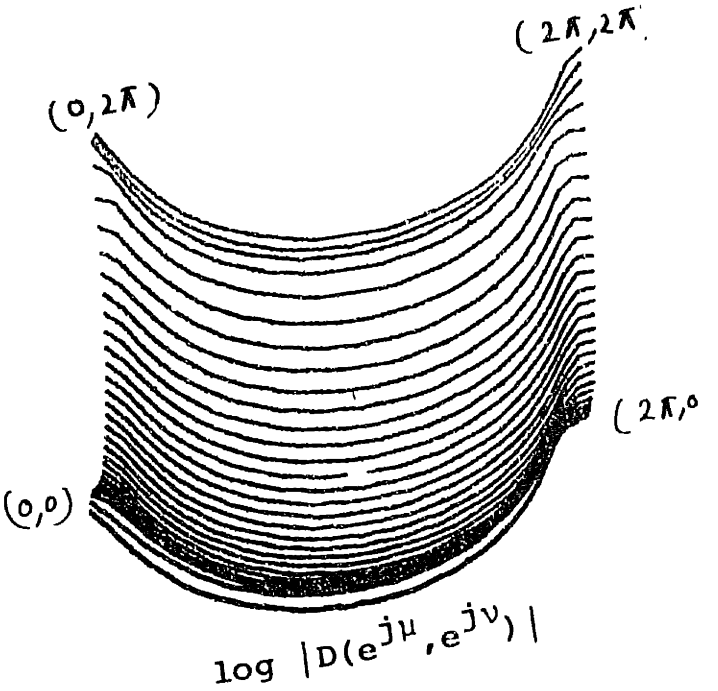

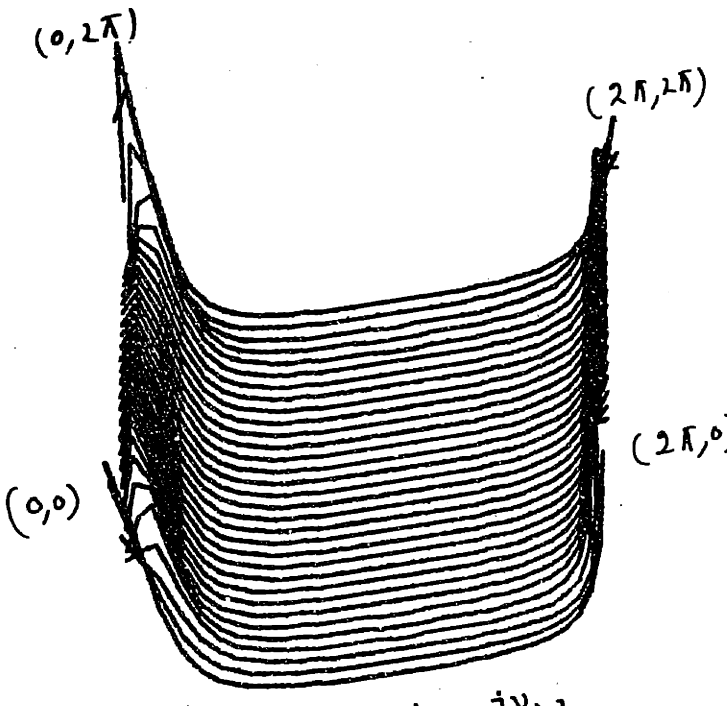

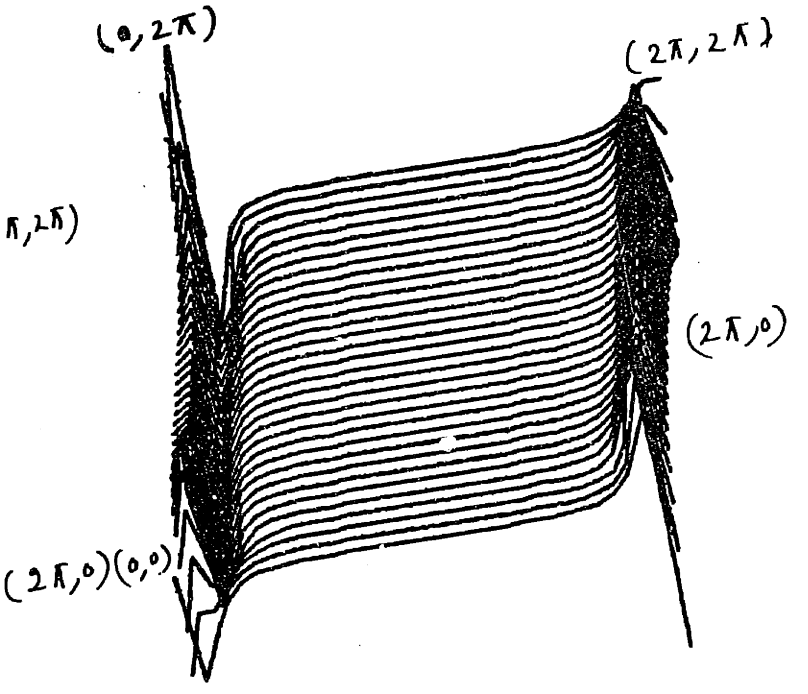

Fig. 6.33

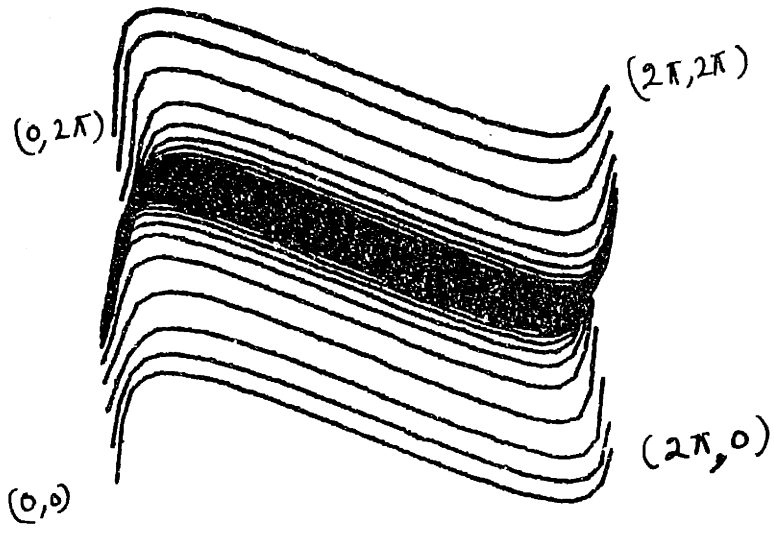
(0,2π)
(2π,2π)
(0,0)
(2π,0)
arg [D(e^jμ, e^jν)]

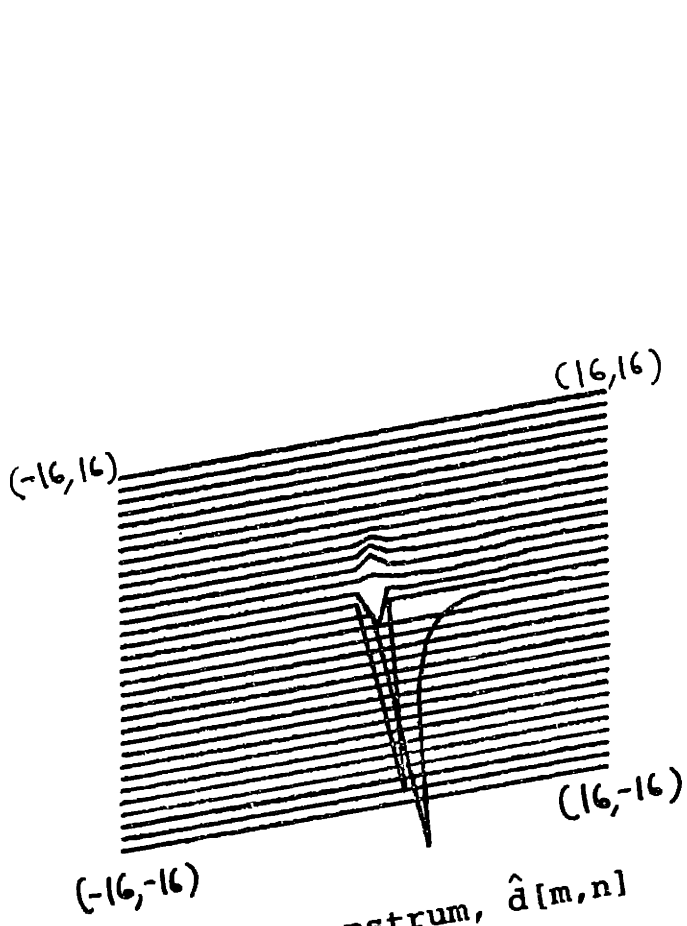
(16,16)
(-16,16)
(16,-16)
(-16,-16)
Complex cepstrum, d̂[m,n]

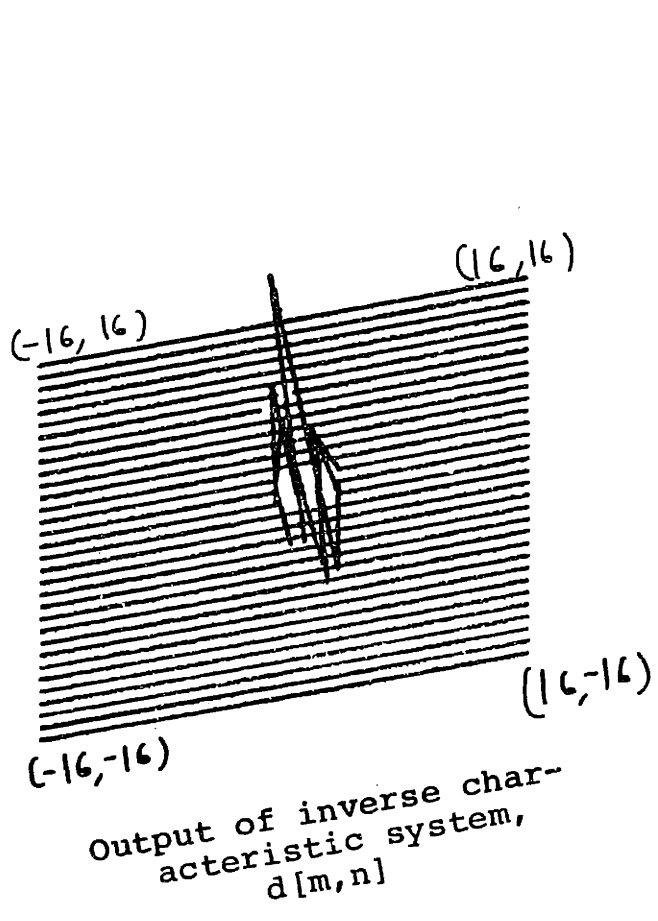
(16,16)
(-16,16)
(16,-16)
(-16,-16)
Output of inverse characteristic system, d[m,n]

Fig. 6.34

cases and phase unwrapping works very well. For unstable cases we do not get the output of the inverse characteristic system as that of the sequence. However, if we change the parameters slightly to make the unstable filter as stable, phase unwrapping works correctly and the cepstrum values are right.

CHAPTER VII

CONCLUSION

VII.1 Summary

In this thesis we have considered the various strategies to make the computation of one- and two-dimensional complex cepstrum more efficient and reliable. In one dimension we investigated the use of piecewise polynomial interpolation methods as they give rise to better rules for integration. We showed that the use of splines leads to a very reliable phase unwrapping algorithm when the zeroes of the sequence are quite close to the unit circle. The computation time required for phase unwrapping with this added feature is comparable to that obtained by adaptive numerical integration scheme [2]. Other features such as the need for double precision for certain variables, efficient computation of the DFT at a single frequency and a more reasonable estimate of the linear phase component were considered. The incorporation of all the above features in a phase unwrapping algorithm leads to a very reliable and efficient phase unwrapping.

In one dimension, analytic relations have been obtained which allow us to obtain the unwrapped phase for any combination of known zeroes of a sequence. Using these relations an analysis has been carried out relating the closeness of the zeroes of a finite length sequence to the frequency sampling

rate in order to determine the minimum FFT size required for successful phase unwrapping. It has been found that for zeroes very close to the unit circle, the minimum FFT size, N, varies inversely with the closeness to the unit circle, ε, as εN = constant.

The above ideas of phase unwrapping have also been implemented in two dimensions. The solution (unwrapped phase as the integral of phase derivative) is not unique because of the presence of two independent variables. The approach that we have adopted for phase unwrapping is to first unwrap the phase along the first column and then we unwrap the phase along every row. We found that this method of 2-D phase unwrapping works very well for zeroes very close to the unit circle.

Finally, an application of complex cepstrum in testing the stability of one- and two-dimensional recursive digital filters is considered. In one dimension use is made of the fact that the number of zeroes outside the unit circle is equal to the absolute value of linear phase component. We have considered cases where the zeroes are as close as 10^{-4} to the unit circle and separated from each other by 10^{-4}. It is shown that the use of the complex cepstrum for checking the stability of one-dimensional discrete-time systems is quite efficient when the order of the system is high.

In two dimensions, because there is no factorization theorem, we use the fact that if the system is stable, then the system impulse response and the cepstrum occupy the same

support. This approach is similar to that of Ekstrom [22]. However, the technique of phase unwrapping that is employed is different from theirs. A number of examples have been carried out both for stable and unstable filters and quarter-plane as well as non-symmetric half-plane filters.

VII.2 Suggestions for Further Research

In this thesis we have mainly concentrated on the techniques of computing the complex cepstrum, which not only employs the integration, but also the information about the principal value of the phase, i.e., it is an adaptive numerical integration scheme. Although we have got a very reliable and efficient phase unwrapping algorithm, yet there can be some more significant methods which can be investigated.

(1) Rather than using the DFT implementation of the Fourier transform, it is possible to approximate the Fourier transform using equidistant splines interpolation [33].

(2) It is possible to fit splines to a curve which involves infinite derivatives at certain samples [32]. It seems possible to develop an adaptive algorithm such that it efficiently fits the splines into the phase derivative curve, making use of the information about the location of the peaks in the phase derivative curve.

(3) A direct method of computation of complex cepstrum which avoids aliasing will be of much interest in general and checking the stability of recursive digital filters in particular.

APPENDIX - 1

In this appendix a proof is given for the unwrapped phase when the sequence is as shown in Fig. A.1(a). The corresponding pole-zero diagram is shown in Fig. A.1(b)

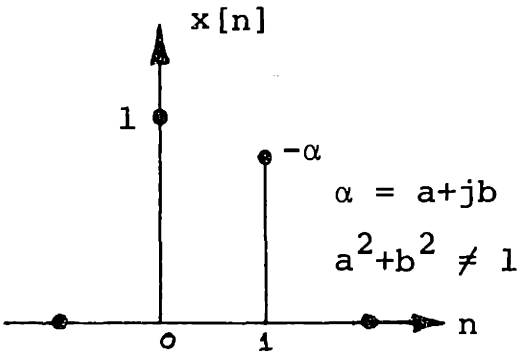

Fig. A.1(a)

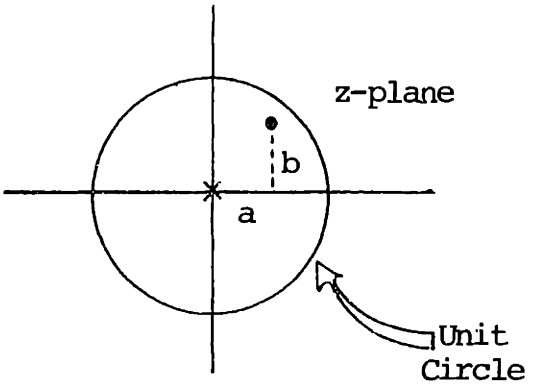

Fig. A.1(b)

Fig. A.1 Two Point Sequence and Its Pole-Zero Plot

The z-transform of the signal shown in Fig. A.1(a) is, $X(z) = 1 - \alpha z^{-1}$, where α is a complex number given by $\alpha = a + jb$.

Now $$X(z)\Big|_{z=e^{j\omega}} = X(e^{j\omega}) = 1 - \alpha e^{-j\omega}$$

or $$X(e^{j\omega}) = 1 - a\cos\omega - b\sin\omega + j(a\sin\omega - b\cos\omega) \quad (A.1)$$

The Fourier transform of the signal nx[n] is,

$$X_1(e^{j\omega}) = -\alpha e^{-j\omega}$$

$$= -a\cos\omega - b\sin\omega + j(a\sin\omega - b\cos\omega) \quad (A.2)$$

Denoting,

$$A_1 = 1 - a \cos \omega - b \sin \omega$$

$$B_1 = a \sin \omega - b \cos \omega$$

$$C_1 = -a \cos \omega - b \sin \omega$$

$$D_1 = a \sin \omega - b \cos \omega$$

The phase derivative,

$$\arg' [X(e^{j\omega})] = - \left(\frac{A_1C_1+B_1D_1}{A_1^2+B_1^2}\right)$$

$$\text{or,} \quad \arg' [X(e^{j\omega})] = \frac{-(a^2+b^2)+a \cos \omega + b \sin \omega}{1+a^2+b^2-2a \cos \omega - 2b \sin \omega} \qquad (A.3)$$

Therefore, the unwrapped phase at $\omega = \omega_1$ is,

$$\arg [X(e^{j\omega_1})] = \int_0^{\omega_1} \arg' [X(e^{j\omega})] \, d\omega \qquad (A.4)$$

$$\text{or, } \arg [X(e^{j\omega_1})] = \int_0^{\omega_1} \frac{-(a^2+b^2)+a \cos \omega +b \sin \omega}{(1+a^2+b^2)-2a \cos \omega - 2b \sin \omega} \, d\omega \qquad (A.5)$$

Representing,

$$I1 = -(a^2+b^2) \int_0^{\omega_1} \frac{d\omega}{(1+a^2+b^2)-2a\cos\omega-2b\sin\omega} \qquad (A.6)$$

$$I2 = a \int_0^{\omega_1} \frac{\cos\omega\, d\omega}{(1+a^2+b^2)-2a\cos\omega-2b\sin\omega} \qquad (A.7)$$

and

$$I3 = b \int_0^{\omega_1} \frac{\sin\omega\, d\omega}{(1+a^2+b^2)-2a\cos\omega-2b\sin\omega} \qquad (A.8)$$

we have

$$\arg [X(e^{j\omega_1})] = I1 + I2 + I3 \qquad (A.9)$$

We shall evaluate the above three integrals for only the interested case, when a^2+b^2-1 is different from zero, i.e., any zero of the finite length sequence does not lie on the unit circle (If a^2+b^2-1 happens to be zero, then the complex cepstrum does not exist.).

Each of the above integrals has a common denominator and requires a substitution of the form $y = \tan\frac{\omega}{2}$.

Then, $$d\omega = \frac{2dy}{1+y^2}, \quad \cos\omega = \frac{1-y^2}{1+y^2}, \quad \text{and} \quad \sin\omega = \frac{2y}{1+y^2} \qquad (A.10)$$

Using (A.10), we have

$$I1 = \frac{-2(a^2+b^2)}{[(1+a)^2+b^2]} \int_0^{\tan -\frac{\omega_1}{}} \frac{dy}{y^2 - \frac{4by}{(1+a)^2+b^2} + \frac{(1-a)^2+b^2}{(1+a)^2+b^2}}$$

$$= \frac{-2(a^2+b^2)}{[(1+a)^2+b^2]} \int_0^{\tan \frac{\omega_1}{2}} \frac{dy}{[y - (\frac{2b}{(1+a)^2+b^2})^2]^2 + [\frac{(b^2+a^2-1)}{(1+a)^2+b^2}]^2}$$

$$= \frac{-2(a^2+b^2)}{b^2+a^2-1} \tan^{-1} \left[\frac{-2b + [(1+a)^2+b^2]y}{b^2+a^2-1} \right]_0^{\tan \frac{\omega_1}{2}},$$

$$b^2+a^2-1 \neq 0$$

(A.11)

Now using (A.10) in (A.7), we get

$$I2 = \frac{2a}{[(1+a)^2+b^2]} \int_0^{\tan \frac{\omega_1}{2}} \frac{(1-y^2)\,dy}{(1+y^2)(y^2-2py+q)}$$

where, $p = \frac{2b}{(1+a)^2+b^2}$, $q = \frac{(1-a)^2+b^2}{(1+a)^2+b^2}$

Now the integrand can be written as

$$\frac{1-y^2}{(1+y^2)(y^2-2py+q)} = \frac{Ay+B}{y^2-2py+q} + \frac{Cy+D}{1+y^2} ,$$

where

$$A = \frac{-4p}{(q-1)^2+4p^2} , \quad B = \frac{1+4p^2-q^2}{(q-1)^2+4p^2} ,$$

$$C = -A, \text{ and } D = \frac{2(q-1)}{(q-1)^2+4p^2}$$

Making use of standard integral formulae,

$$I2 = \frac{2a}{[(1+a)^2+b^2]} \left[0.5A \ \ell n(y^2-2py+q) + 0.5C \ \ell n(y^2+1) + D \tan^{-1} y \right.$$

$$\left. + \frac{(B+Ap)}{\sqrt{q-p^2}} \tan^{-1} \left(\frac{y-p}{\sqrt{q-p^2}}\right) \right]_0^{\tan \frac{\omega_1}{2}}$$

where, $q > p^2$ or, $a^2+b^2-1 \neq 0$

Substituting for A, B, C and D we get

$$I2 = \frac{2a}{[(1+a)^2+b^2][(q-1)^2+4p^2]} \left[-2p \ \ell n \left(\frac{y^2-2py+q}{y^2+1}\right) + 2(q-1) \tan^{-1} y \right.$$

$$\left. + \frac{(1-q^2)}{\sqrt{q-p^2}} \tan^{-1} \left(\frac{y-p}{\sqrt{q-p^2}}\right) \right]_0^{\tan \frac{\omega_1}{2}} \qquad (A.12)$$

Now substituting (A.10) in (A.8), we get

$$I3 = \frac{4b}{[(1+a)^2+b^2]} \int_0^{\tan \frac{\omega_1}{2}} \frac{ydy}{(1+y^2)(y^2-2py+q)} ,$$

where p and q are the same as defined above.

Proceeding similar to the I2 case, we get

$$I3 = \frac{4b}{[(1+a)^2+b^2]} \left[0.5A' \ell n (y^2-2py+q) + 0.5C' \ell n (y^2+1) + D' \tan^{-1} y \right.$$

$$\left. + (B'+A'p) \tan^{-1} \left(\frac{y-p}{\sqrt{q-p^2}}\right) \right]_0^{\tan \frac{\omega_1}{2}}$$

where $q > p^2$ or, $a^2+b^2-1 \neq 0$, and

$$A' = \frac{1-q}{(1-q)^2+4p^2} , \quad B' = \frac{2pq}{(1-q)^2+4p^2}$$

$$C' = -A' , \text{ and } D' = \frac{2p}{(1-q)^2+4p^2}$$

Substituting for A', B', C' and D' we get

$$I3 = \frac{4b}{[(1+a)^2+b^2][(q-1)^2+4p^2]} \left[0.5(1-q) \ell n \left(\frac{y^2-2py+q}{y^2+1}\right) - 2p \tan^{-1} y \right.$$

$$\left. + \frac{p(q+1)}{\sqrt{q-p^2}} \tan^{-1} \left(\frac{y-p}{\sqrt{q-p^2}}\right) \right]_0^{\tan \frac{\omega_1}{2}} \qquad (A.13)$$

Now substituting for y, p and q in (A.11), (A.12) and (A.13), we get the unwrapped phase in terms of a, b, and ω.

$$\arg\,[X(e^{j\omega_1})] = I1 + I2 + I3,$$

$$\text{where } I1 = \frac{-2(a^2+b^2)}{(a^2+b^2-1)} \tan^{-1}\left\{\frac{-2b+[(1+a)^2+b^2]y}{a^2+b^2-1}\right\}_0^{\tan\frac{\omega_1}{2}} \tag{A.14}$$

$$I2 = \frac{a}{(a^2+b^2)}\Bigg\{-0.5b\ \ln\{[(a+1)^2+b^2]y^2 - 4by + b^2 + (a-1)^2\}$$

$$+ 0.5b\ \ln\{y^2+1\} + \frac{(ab^2+a+a^3)}{(a^2+b^2-1)} \tan^{-1}\left\{\frac{[(a+1)^2+b^2]y-2b}{(a^2+b^2-1)}\right\}$$

$$- a\ \tan^{-1}(y)\Bigg\}_0^{\tan\frac{\omega_1}{2}} \tag{A.15}$$

$$I3 = \frac{b}{(a^2+b^2)}\Bigg\{0.5a\ \ln\{[(a+1)^2+b^2]y^2 - 4by + b^2 + (a-1)^2\}$$

$$- 0.5a\ \ln\{y^2+1\} + \frac{(ba^2+b+b^3)}{(a^2+b^2-1)} \tan^{-1}\left\{\frac{[(a+1)^2+b^2]y-2b}{(a^2+b^2-1)}\right\}$$

$$- b\ \tan^{-1}(y)\Bigg\}_0^{\tan\frac{\omega_1}{2}} \tag{A.16}$$

where, $a^2+b^2-1 \neq 0$ for (A.14), (A.15) and (A.16).

Summing (A.14), (A.15) and (A.16), we get a simplified form of unwrapped phase,

$$\arg\,[X(e^{j\omega_1})] = -\frac{\omega_1}{2} - \tan^{-1}\left(\frac{-2b+[(1+a)^2+b^2]\tan\frac{\omega_1}{2}}{a^2+b^2-1}\right) + \tan^{-1}\left[\frac{-2b}{a^2+b^2-1}\right],$$

$$a^2+b^2-1 \neq 0 \qquad \text{(A.17)}$$

Therefore, for a complex pair of zeroes at $a \pm jb$, the expression for unwrapped phase is

$$\arg_c\,[X(e^{j\omega_1})] = -\omega_1 - \tan^{-1}\left(\frac{-2b+[(1+a)^2+b^2]\tan\frac{\omega_1}{2}}{a^2+b^2-1}\right) - \tan^{-1}\left(\frac{+2b+[(1+a)^2+b^2]\tan\frac{\omega_1}{2}}{a^2+b^2-1}\right),$$

$$a^2+b^2-1 \neq 0 \qquad \text{(A.18)}$$

REFERENCES

1. R. W. Schafer, "Echo Removal by Discrete Generalized Linear Filtering", Tech. Rept. 466, MIT Research Laboratory of Electronics, MIT, Cambridge, Mass., Feb. 1969, Also Ph.D. Thesis, Dept. of Elec. Engg. & Comp. Sc., MIT, Feb. 1968.

2. J. M. Tribolet, "A New Phase Unwrapping Algorithm", IEEE Trans. on Acoust., Speech and Signal Processing, vol. 25, no. 2, pp. 170-177, April 1977.

3. D. E. Dudgeon, "The existence of cepstrum for two-dimensional rational polynomials", IEEE Trans. on Acoust., Speech and Signal Processing (Correspondence), vol. 23, pp. 242-243, April 1975.

4. A. E. Filip, "Estimating the impulse response of linear, shift-invariant image deblurring system", Ph.D. Thesis, Dept. of Elec. Engg. & Comp. Sc., MIT, 1972.

5. G. Birkhoff and C. R. Deboor, "Piecewise polynomial interpolation and approximation" in "Approximation of Functions", Edited by H. L. Garabedian, Elsevier Publishing Company, 1965.

6. A. V. Oppenheim, "Superposition in a class of non-linear systems", Tech. Rept. 432, Research Laboratory of Electronics, MIT, Cambridge, Mass., March 1965.

7. A. V. Oppenheim and R. W. Schafer, "Digital Signal Processing", Prentice Hall, 1975.

8. J. M. Tribolet, "Seismic applications of homomorphic signal processing", Sc.D. Thesis, Dept. of Elec. Engg. & Comp. Sc., MIT, May 1977.

9. B. P. Bogert, M. J. Healy and J. W. Tukey, "The quefrency analysis of time series for echoes: cepstrum, pseudo-autocovariance, cross-spectrum, and saphe cracking", in M. Rosenblatt (Ed.), Time Series Analysis, John Wiley, pp. 209-243, Chapter 15, 1963.

10. F. Bonzanigo, "An improvement of Tribolet's phase unwrapping algorithm", To be published in IEEE Trans. on Acoust., Speech and Signal Processing.

11. J. H. Ahlberg, E. N. Nilson and J. L. Walsh, "The Theory of Splines and Their Approximation", Academic Press, 1967.

12. A. R. Curtis, "The approximation of function of one variable by cubic splines", in "Numerical Approximation to Function and Data", edited by J. G. Hayes, University of London, The Athlone Press, 1970.

13. J. C. Holladay, "A Smoothest Curve Approximation", Mathematical Tables and Other Aids to Computation 11, 1957.

14. M. J. D. Powell, "A comparison of Spline approximations with classical interpolation methods", pp. 95-98 of Information Processing 68, Proceedings IFIP Congress, Edinburgh, 1968, Mathematics, Software, North-Holland, Amsterdam, 1969.

15. F. B. Hildebrand, "Introduction to Numerical Analysis", McGraw-Hill, 1974.

16. T. N. E. Greville, "Theory and Applications of Spline Functions", Academic Press, 1969.

17. D. Secrest, "Best approximate integration formulas and best error bounds", Mathematics of Computation, 19, 1965.

18. R. Rom, "On the cepstrum of two-dimensional functions", IEEE Trans. on Information Theory (Correspondence) vol. 21, no. 2, March 1975.

19. T. G. Stockham, T. M. Cannon, and R. B. Ingebretsen, "Blind convolution through digital signal processing", Proc. IEEE, vol. 63, pp. 678-692, April 1975.

20. T. S. Huang, J. W. Burnett, and A. G. Deczky, "The importance of phase in image processing filters", IEEE Trans. on Acoust., Speech and Signal Processing, vol. 23, no. 6, Dec. 1975.

21. M. P. Ekstrom and J. W. Woods, "Two-dimensional spectral factorization with applications in recursive filtering", IEEE Trans. on Acoust., Speech and Signal Processing, vol. 24, pp. 115-128, April 1976.

22. M. P. Ekstrom and R. E. Twogood, "A stability test for 2-D recursive digital filters using the complex cepstrum", Proc. of the Int. Conference of Acoust., Speech and Signal Processing, Hartford, Conn., May 9-11, 1977.

23. C. Deboor, "Bicubic spline interpolation", Journal of Math and Physics, 41, pp. 212-218, 1962.

24. J. L. Shanks, S. Treitel, and J. H. Justice, "Stability and synthesis of two-dimensional recursive filters", IEEE Trans. on Audio Electroacoust., vol. 20, pp. 115-128, June 1972.

25. T. S. Huang, "Stability of two-dimensional recursive filters", IEEE Trans. on Audio Electroacoust., vol. 20, pp. 158-163, June 1972.

26. G. A. Maria and M. M. Fahmy, "On the stability of two-dimensional digital filters", IEEE Trans. Audio Electroacoust., vol. 21, pp. 470-472, Oct. 1973.

27. B. D. O. Anderson and E. I. Jury, "Stability of multidimensional digital filters", IEEE Trans. Circuits and Syst., vol. 21, pp. 300-304, March 1974.

28. E. I. Jury, "A simplified stability criterion for linear discrete systems", Proc. IRE, vol. 50, pp. 1493-1500, June 1962.

29. J. Makhoul, "Linear prediction: a tutorial review", Proc. IEEE, vol. 63, pp. 561-580, April 1975.

30. Y. Genin and Y. Kamp, "Counterexample in the least-squares inverse stabilization of 2-D recursive filters", Electronic Letters, vol. 11, no. 15, pp. 330-331, July 24, 1975.

31. R. M. Mersereau and D. E. Dudgeon, "The representation of two-dimensional sequences as one-dimensional sequences", IEEE Trans. on Acoust., Speech and Signal Processing, vol. 22, pp. 320-325, Oct. 1974.

32. A. Inselberg, "Cubic splines with infinite derivatives, at some knots", IBM J. Res. Develop., September 1976.

33. I. J. Schoenberg, "Cardinal spline interpolation," Regional Conference Series in Applied Math, Math. Res. Center, University of Wisconsin, Madison.